Biosensors for drug discovery applications

Bhalla, Nikhil

Award date:
2016

Awarding institution:
University of Bath

Biosensors for drug discovery applications

Submitted by

Nikhil Bhalla

For the degree of Doctor of Philosophy

University of Bath

Department of Electronic and Electrical Engineering

2015

COPYRIGHT

Signature of Author……..

Nikhil Bhalla

Dedicated in the memory of my grandfather

Tule Ram Bhalla

Abstract

This research developed a biosensor for kinase drug discovery applications. In particular it combined electronic techniques with optical techniques to understand the phosphorylation of proteins. There are two major electronic characteristics of phosphorylation that aid in its detection and subsequently biosensor development: first is the release of a proton upon phosphorylation of a protein (change in pH) and second is the addition of negative charge to the protein upon its phosphorylation. The work in this thesis reports an electrolyte–insulator–semiconductor sensing structures to detect the pH changes associated with phosphorylation and metal–insulator–semiconductor structures to detect the charge change upon phosphorylation of proteins. Major application of the developed devices would be to screen inhibitors of kinase that mediate phosphorylation of proteins. Inhibitors of kinase act as drugs to prevent or cure diseases due to the phosphorylation of proteins. With the advancements in VLSI and microfluidics technology this method can be extended into arrays for high throughput screening for discovering drugs.

Acknowledgements

I express my sincere gratitude to my supervisor, Dr. Pedro Estrela, under whose esteemed guidance and supervision, this work has been completed. This project work would have been impossible to carry out without his motivation and support throughout. I also thank Dr. Mirella Di Lorenzo and Dr. Giordano Pula, my co-supervisors, for their valuable support. In particular, Dr. Di Lorenzo has been very encouraging right from the day I applied for PhD program and Dr. Pula has imparted hands-on experience in learning bio-analytical tools.

Special thanks are giving to the authorities of University of Bath for providing financial support in form of University Research Student-Overseas fellowship. My colleagues and friends Dr. Anna Miodek, Dr. Ed Regan, Dr. Zhugen Yang, Dr. Dina Vara, Dr Jonathan Storey, Nello Formisano, Pawan Jolly, Jules Hammond, Benjamin Metcalfe, Pavel Zhurauski, Aleksandrs Sergejevs, Tiago Fortunato and Caleb Wong for the time spent both in fruitful and trivial discussions.

I must thank Prof. Danny Wen-Yaw Chung in Taiwan and Liu Heru in China/USA for their moral boost and cheering my confidence up. Last, but not least, my parents, lovely little sister Kritika and grandmother, who are continuously supporting and encouraging my study in every moment despite the distance.

Table of contents

List of figures

List of tables

List of abbreviations

MBP – Myelin Basic Protein

EIS – Electrolyte Insulator Semiconductor

MIS – Metal Insulator Semiconductor

LSPR – Localized Surface Plasmon Resonance

SPR – Surface Plasmon Resonance

QCM – Quartz Crystal Microbalance

CV – Capacitance Voltage

PKC – Protein Kinase C

ATP – Adenosine Triphosphate

ATP-S – Adenosine Thiotriphosphate

GOPTS – 3-Glycidyloxypropyl-trimethoxysilane

APTES – 3-Aminopropyl-triethoxysilane

MPTS – 3-Mercaptopropyl-trimethoxysilane

AHS – 1-Hydroxyallyltrimethylsilane

AuNP/s – Gold nanoparticle/s

EDX –Energy Dispersive X-ray spectroscopy

SEM – Scanning Electron Microscopy

TEM –Transmission Electron Microscopy

XRD – X Ray Diffraction

PDMS – Polydimethylsiloxane

CMOS – Complementary Metal Oxide Semiconductor

VLSI – Very Large Scale Integration

SDS – Sodium Dodecyl Sulphate

PAGE – Polyacrylamide Gel Electrophoresis

PVDF – Polyvinylidene Fluorid

Chapter 1 Introduction

The work in this project developed electrochemical and optical biosensing techniques for drug discovery applications. For successful drug discovery it is important to understand the fundamentals of the underlying causes and consequences of the diseases for which the drug is being developed. One such physiological process in eukaryotic cells is protein phosphorylation, which is the main post-translational modification of proteins responsible for the onset or progression of Alzheimer's disease, diabetes and various cancers. Protein phosphorylation is facilitated by kinases, inhibitors of kinases act as drugs in controlling or curing these diseases by reducing protein phosphorylation. Therefore, this project developed proof of concepts for biosensors capable of detecting kinase activity and screening candidate compounds to identify novel inhibitors of protein kinases.

The aim of this chapter is to introduce the fundamentals of protein phosphorylation and kinases, and characteristics of phosphorylation reaction that allows detection of phosphorylated proteins. The chapter also discusses the urgent need of developing kinase biosensors by highlighting the current kinase drug discovery market.

1.1 Protein phosphorylation

One of the prime fundamentals of biology is the transcription of deoxyribonucleic acid (DNA) into ribonucleic acid (RNA) and translation of RNA into proteins [1]. To regulate various cellular activities, proteins then undergo post-translational modification. Post-translational modification is a chemical modification of the proteins usually caused by covalent bonding with molecules containing phosphate, methyl, acetyl, lipids or carbohydrates. The addition of a phosphate group to a protein is commonly defined as protein phosphorylation. It is catalysed by kinases, which transfer a phosphate group from a phosphate donor to the protein [2]. This modifies the biological activity of the proteins by generating protein dependent functional cell aberrations [3]. It is the proteins with serine, threonine, tyrosine or histidine amino acid residues that undergo this post-translational modification, which brings conformational changes in their structure [4]. Phosphorylation of proteins is a

reversible chemical reaction and the opposite of it is called protein dephosphorylation, which is the removal of phosphate from the protein and is catalysed by the enzymes called protein phosphatases [5].

Phosphate groups play an important part in various cell mechanisms, acting as building blocks for DNA and RNA. Phosphates are also significant components of the energy generating molecules (e.g. ATP) in all metabolic processes [6]. The role of phosphorylation is significant in the regulation of many processes such as mitosis and carbohydrate metabolism [3] and acts as a switch that turns on and off various cellular mechanisms. Its impact on cellular processes depends on how different proteins behave in their phosphorylated and dephosphorylated states.

Phosphorylation was originally discovered by Carl and Getry Cori in late 1930s as a control mechanism while studying glycogenolysis [1]. However, Fisher and Kerb understood the true nature of glycogenolysis many years later while working on the enzyme phosphorylase kinase, which led to authentic discovery of the protein phosphorylation mechanism [3]. This is because glycogenolysis involved several secondary messengers and other factors, which were discovered between 1930 to early 1950s [3]. Finally, protein kinase activity was understood when Gene Kennedy in 1954 and Earl Sutherland discovered the secondary messengers which trigger phosphorylation in response to certain cellular stimuli. For instance when the body is in need of energy, phosphorylase kinase becomes phosphorylated switching from its inactive-b to active-a form, which converts the stored glycogen into glucose [7].

1.2 Role of Protein Phosphorylation

In this section the role of protein phosphorylation in cellular metabolism will be explained with two different examples before explaining how it can then lead to disease. One essential metabolic process which is regulated specifically by protein phosphorylation is glycogenolysis, i.e. conversion of glucose into energy [7]. In this process, when blood sugar levels are low, the glucagon hormone is released into the blood and binds to the surface of liver cells. This activates the cyclic adenosine monophosphate (cAMP) that binds to the regulatory receptors of glycogen phosphorylase kinase, turning it on, leading it to become phosphorylated. This phosphorylated state of glycogen phosphorylase kinase leads to phosphorylation of

glycogen phosphorylase and activates it to convert glycogen into glucose. The resultant energy is then used by the cells to perform various physiological processes.

There are over 500 protein kinases and about 30% of the human proteins undergo phosphorylation to perform essential cellular activities [8]. Therefore it is not surprising that abnormal phosphorylation should turn out to be a cause of human disease [9]. There are over 400 diseases that are linked with the phosphorylation of proteins, with most of the diseases caused by mutations in the genes that regulate kinases that alter the phosphorylation sites in a protein. For instance in Alzheimer disease, Tau proteins are the major constituents of intra-neuronal and glial fibrillar lesions and are referred to as 'tauopathies' [10,11]. Molecular analysis has revealed that an abnormal phosphorylation is one of the important events in the process leading to the disorder. Similarly, mutations in somatic cells have been reported to encourage phosphorylation of proteins which induces malignancy in the cells [12]. Figure 1.1 shows a schematic where phosphorylation of proteins activates the cells and makes them cancerous. It also depicts how an inhibitor can stop the cell from being cancerous.

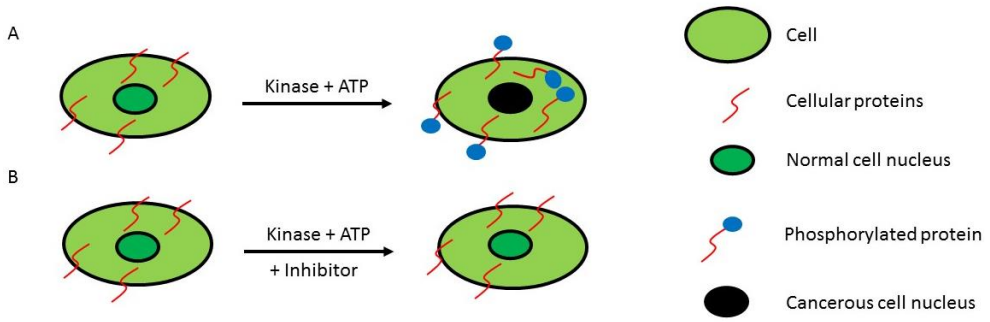

Figure 1-1 schematic of protein phosphorylation A) damage to the cell upon phosphorylation of proteins B) No phosphorylation in the presence of inhibitor

1.4 Kinase inhibitors

Kinase inhibitors are the most funded target in the drug discovery market [13]. Kinase inhibitors are a special kind of enzyme inhibitors that slow or impede the activity of the enzymes called kinases. The most important use of kinase inhibitors is in cancer cure therapy [14]. In this therapy, the patient is injected with a specific kinase inhibitor as a form of chemotherapy. The kinase inhibitors are given as a single therapy or as a

combinatorial cancer treatment with radiation therapy [15]. Kinase inhibitors usually work by binding covalently or non-covalently to the kinases [16]. Inhibitors that bind covalently block kinase activity by binding to the Cysteine (Cys) residue either on the ATP active site or around the active site. For instance in epidermal growth factor receptor (EGFR) kinase the Cys residue is on the ATP active site and the extracellular signal-regulated kinase 2 (ERK2) kinase Cys residue is on the d… f… g… -motif (DFG-motif) around the active site. DFG-motif is a combination of three amino acids: aspartic acid, phenylalanine and glycine (Asp-Phe-Gly) [17]. Non-covalently binding inhibitors bind to the hinge region of the kinase. These can further be classified into ATP-competitive or non-ATP-competitive inhibitors. Competitive inhibitors compete with the high concentrations of intracellular ATP to attach on the kinase. The non-ATP-competitive inhibitors act by inducing a conformational shift in the kinase such that it is no longer able to function [18].

1.5 Characteristics of protein phosphorylation reaction

This section describes the protein phosphorylation characteristics that can be explored to develop a 'phosphorylation biosensor'. The protein phosphorylation reaction involves the release of a proton (H^+) and the transfer of a phosphate group from a donor (e.g. ATP), facilitated by kinase, resulting in an increase in negative charge on the protein. Measuring the change in the charge of the protein after phosphorylation is one method of identifying protein phosphorylation. Another method could be to detect the release of protons. ATP consists of three phosphoryl groups with the terminal phosphoryl (called as gamma (γ) phosphoryl) group being the one that is transferred to the proteins upon phosphorylation (Figure 1-2) [17,19]. Therefore a modification at the γ-phosphoryl group that generates either an optical or electrical response can be incorporated. For instance modifying γ-phosphoryl with a sulphide bond can allow attachment of gold nanoparticles (AuNPs) after transfer to the proteins. Presence of AuNPs can then be analysed using biosensing techniques such as the localized surface plasmon resonance technique.

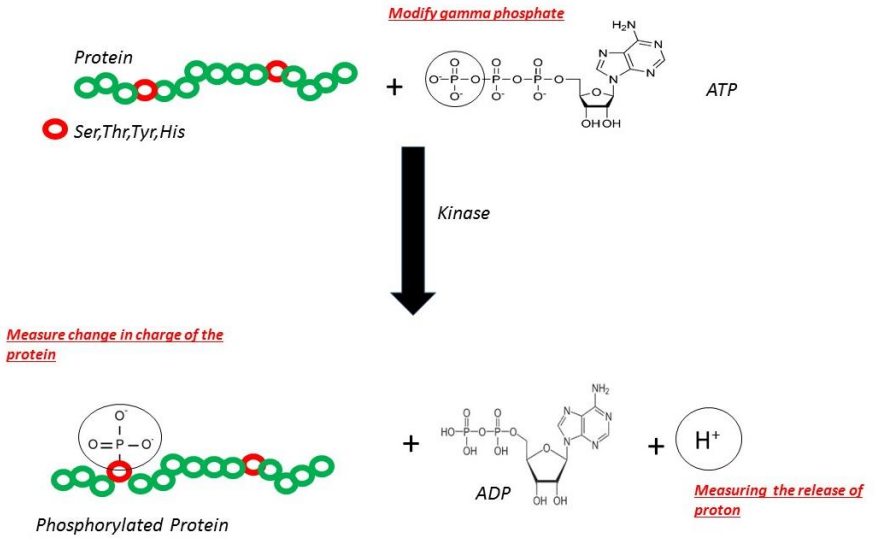

Figure 1-2 Scheme showing phosphorylation reaction

1.6 Methodology

The methodology of this research is primarily experimental. Based on the previous findings by various research groups protocols for different types of experiments are identified and explored. For example: choice of material, immobilization protocols, wafer cleaning procedures, device dimensions and deposition process are chosen from the relevant literature. Electrochemical measurements were made using a potentiostat and recorded using specialist data acquisition software. Direct biochemical analytical techniques like western blot were also a requisite. The work included use of a clean room facility for fabrication of microfluidic structures. Other experimental procedures involved the use of quartz crystal microbalance (QCM), infrared spectroscopy and other absorption-based spectroscopy techniques. Theoretical modelling of the concept using finite element analysis was essential to support our experiments and further understanding. Statistical analysis of data was carried out with MATLAB, Origin and Prism Graphpad software.

In earlier stages, the project primarily focused on developing highly-selective and sensitive pH-sensing structures in order to better understand protein phosphorylation. Later stages of the project explored a combination of electrochemical and optical techniques to measure both pH and charge changes occurring after protein phosphorylation. To start with electrolyte-insulator-semiconductor (EIS) structures

(Si_3N_4-SiO_2-Si) were used to validate the detection of protein phosphorylation. Protein was immobilised on the silicon nitride (Si_3N_4) surface before introducing the kinase and a source of phosphate to initiate the reaction. Protein was immobilized by silanising the silicon nitride surface. Different silanisation protocols were explored to optimise biofunctionalisation of the silicon nitride surface for the protein phosphorylation application. The response from the Si_3N_4-SiO_2-Si structure was measured by analysing the change in charge of the depletion region at the oxide-semiconductor interface due to the adsorption of H^+ ions on the surface of the insulator. This system was also integrated with the localized surface plasmon resonance (LSPR) detection technique with the use gold nanoparticles (AuNPs).

The change in the charge of the myelin basic protein (MBP) upon phosphorylation was identified with the use of gold based metal–insulator–semiconductor (MIS) capacitor structures. Similar to the EIS sensors, MIS structures were also integrated with AuNPs to allow plasmonic detection. Surface plasmon resonance (SPR) was conducted to analyse all reaction steps in real-time. Quartz crystal microbalance (QCM) measurements were also conducted to quantify the nanoparticles, correlating it with the thiophosphorylated sites estimated by SPR detection on the gold surface.

Preliminary studies were done on the development of a prototype microfluidic system for the EIS sensor that could potentially be used for future studies. In addition, phosphorylation studies were also conducted on commercial MOSFETs (metal-oxide-semiconductor field-effect transistors) with nanoporous aluminium oxide as extended gate structures. Microfluidic integration and MOSFET studies were carried out to demonstrate the potential of the system for future commercialisation

1.7 Scope and Limitations

Phosphorylation is the main post-translational modification of proteins in mammalian cells and plays a key role in cell physiology regulation and tissue homeostasis. Protein kinases are the enzymes capable of catalysing the protein phosphorylation reaction in physiological conditions, whilst protein phosphatases catalyse the opposite reaction resulting in protein dephosphorylarion. The balance between protein phosphorylation and dephosphorylation is critical for the regulation of physiological processes and its unbalance is the cause of several diseases, including Alzheimer’s disease and cancer.

Therefore there is a considerable interest in biomedical research and drug discovery in developing a convenient and reliable technology to analyse protein kinase activity.

At present protein kinase activity is investigated by 32-phosphorus (^{32}P) labelling of a target substrate with ^{32}P-ADP acting as a radionuclide donor or by using phosphor-specific antibodies, that rely on antibodies recognising a protein only after phosphorylation [20,21]. Neither technique is truly suitable for high-throughput screening of potential inhibitors, which is hindering the discovery of new therapeutic molecules for several important human diseases. The work in this project allows direct assessment of protein kinase activity and modulation by different biomolecules will become easily assessable. The independence of this technique from the use of specific detecting reagents (i.e. phosphor-specific antibodies or ^{32}P-ADP) makes this technique significantly more resource-effective than existing approaches. Another significant advantage of the techniques discussed in this work is its compatibility with high-throughput microplate-based platforms, which will make this approach particularly appealing for testing high numbers of compounds for drug discovery purposes.

As emphasised earlier, kinase inhibitors are one of the most important targets for drug development. However, to date there are very few kinase inhibitors that are available on the market (Table 1.1) > Most of these inhibitors are used in chemotherapy for cancer treatment. Given, the continuous need for development of kinase inhibitors in the pharmaceutical research, the scope of the work primarily focused on:

- Real time study of phosphorylation kinetics.
- Developing a proof of concept for a device that can screen inhibitors of kinase
- Developing a device that will speed up the kinase drug discovery in pharmaceutics.
- Towards a cost effective device for drug screening
- Discovering new protein-kinase activity pairs. For instance if whole proteome is exposed to one type of kinase, one can see which proteins get phosphorylated by that particular kinase.

Table 1-1 Registered kinase inhibitors

(Reproduced with permission from Springer protocol publishers, Table 1 from reference [17])

Compound	**Kinase target**	**Cancer target**	**Company**
Imatinib (Glivec, Gleevec, STI571)	ABL 1–2, PDGFR, KIT	CML, Ph+ B-ALL, MML, CEL, GIST	Novartis
Gefitinib (Iressa, ZD1839)	EGFR	NSCLC	AstraZeneca
Erlotinib (Tarceva, OSI-774)	EGFR	NSCLC, pancreatic cancer	OSI, Genentech Inc, Roche
Lapatinib (Tykerb, GW2016)	EGFR, ERBB2	Breast cancer	Glaxo SmithKline
Dasatinib (Sprycel, BM-354825)	ABL1–2, PDGFR, KIT, SRC	CML	Bristol Myers
Nilotinib (Tasigna, AMN107)	ABL1–2, PDGFR, KIT	CML	Novartis
Sunitinib (Sutent, SU11248)	VEGFR1–3, KIT, PDGFR, RET, CSF1R, FLT3	RCC, GIST	Pfizer
Sorafenib (Nexavar, Bay 43-9006)	VEGFR2, PDGFR, KIT, FLT3, BRAF	RCC	Onyx and Bayer Pharmaceuticals
Pazopanib (Votrient, GW-786034)	VEGFR1–3, PDGFR, KIT,	RCC	GlaxoSmithKline

Everolimus (Afinitor, Rad001)	mTOR	RCC	Novartis
Temsirolimus (Torisel, CCI-779)	mTOR	RCC	Wyeth
Afatinib	EGFR/eRB2	Lung cancer	Boehringer Ingelheim
Axitinib	VEGFR1/VEGFR2/PDGFEB/c-KIT	Renal cell carcinoma	Pfizer
Bosutinib	BcrABl/SRC	Chronic myelogenous leukemia	Pfizer
Cetuximab	ErbB1	SCCHN	BMS
Ruxolitinib	JAK	Myelofibrosis	Incyte

As with any research project, there were some unavoidable limitations. Finances and time were the most crucial factors; the project was funded by University of Bath for 3 years and given the high cost of consumables (kinase, protein, semiconductor materials, clean room charges, etc.), testing large number of proteins/kinase pairs was not feasible. In addition, it would be presumptuous to expect clinical results or validation at industrial scale of the devices or technology produced from this work.

1.4 Preview of thesis

This is a thesis submitted at the end of project as a fulfilment of requirements for the PhD degree in Electronic and Electrical Engineering at the University of Bath. Beside the overview and introduction of the project in chapter 1, chapter 2 provides a detailed literature review of the related work accomplished by various researchers across the

globe. Chapter 3 outlines the experimental work accomplished to characterise biochemistry on silicon nitride based surfaces. Chapter 4 discusses the field effect and nanoplasmonic studies on silicon nitride-based devices for the detection of phosphorylation. In addition it also describes the use of commercial micro-pH sensors to measure pH changes associated with the phosphorylation of proteins. Chapter 5 covers the studies on gold-based field effect devices for the detection of charge changes associated with phosphorylation of proteins. The results on gold sensors are then validated using SPR and QCM techniques. Chapter 6 focusses on microfluidic integration of the field effect devices and phosphorylation studies using commercial field effect devices. Finally, chapter 7 provides insight on future prospects, significance and expected commercial outcome of the project.

References

[1] G. Walsh and R. Jefferis, "Post-translational modifications in the context of therapeutic proteins" *Nature Biotechnology* vol. 24, pp. 1241–1252, 2006.

[2] M. Mann and O. N. Jensen, "Proteomic analysis of post-translational modifications" *Nature Biotechnology* vol. 21, pp. 255–261, 2003.

[3] P. Cohen, "The origins of protein phosphorylation" *Nature Cell Biology*, vol. 4, no. 5, pp. 127–130, 2002.

[4] D. Caballero, E. Martinez, J. Bausells, A. Errachid, and J. Samitier, "Impedimetric immunosensor for human serum albumin detection on a direct aldehyde-functionalized silicon nitride surface" *Analytica Chimica Acta*, vol. 720, pp. 43–8, 2012.

[5] R. A. Merrill, S. Strack and M. Zhuo, "Protein Kinases and Phosphatases" *Molecular Pain*, pp. 187–205, 2007

[6] C. Bagshaw, "ATP analogues at a glance" *Journal of Cell Science*, vol. 114, pp. 459–460, 2001.

[7] R. H. Unger, “Glucagon physiology and pathophysiology in the light of new advances” *Diabetologia*, vol. 28, pp. 574–578, 1985.

[8] P. Cohen, “Protein kinases--the major drug targets of the twenty-first century?” *Nature Reviews Drug Discovery*, vol. 1, pp. 309–315, 2002.

[9] W. J. Israelsen and M. G. Vander Heiden, “ATP consumption promotes cancer metabolism” *Cell*, vol. 143. pp. 669–671, 2010.

[10] K. Iqbal, A. Del C. Alonso, S. Chen, M. O. Chohan, E. El-Akkad, C. X. Gong, S. Khatoon, B. Li, F. Liu, A. Rahman, H. Tanimukai, and I. Grundke-Iqbal, “Tau pathology in Alzheimer disease and other tauopathies” *Biochimica et Biophysica Acta - Molecular Basis of Disease*, vol. 1739. pp. 198–210, 2005.

[11] K. Iqbal, F. Liu, C.-X. Gong, and I. Grundke-Iqbal, “Tau in Alzheimer disease and related tauopathies” *Current Alzheimer Reserach*, vol. 7, pp. 656–664, 2010.

[12] G. I. Evan and K. H. Vousden, “Proliferation, cell cycle and apoptosis in cancer” *Nature*, vol. 411, pp. 342–348, 2001.

[13] J. Zhang, P. L. Yang, and N. S. Gray, “Targeting cancer with small molecule kinase inhibitors” *Nature Reviews Cancer*, vol. 9, pp. 28–39, 2009.

[14] P. A. Jänne, N. Gray, and J. Settleman, “Factors underlying sensitivity of cancers to small-molecule kinase inhibitors” *Nature Reviews Drug Discovery*, vol. 8, pp. 709–723, 2009.

[15] M. A. Fabian, W. H. Biggs, D. K. Treiber, C. E. Atteridge, M. D. Azimioara, M. G. Benedetti, T. A. Carter, P. Ciceri, P. T. Edeen, M. Floyd, J. M. Ford, M. Galvin, J. L. Gerlach, R. M. Grotzfeld, S. Herrgard, D. E. Insko, M. A. Insko, A. G. Lai, J.-M. Lélias, S. A. Mehta, Z. V Milanov, A. M. Velasco, L. M. Wodicka, H. K. Patel, P. P. Zarrinkar, and D. J. Lockhart, “A small molecule-kinase interaction map for clinical kinase inhibitors” *Nature Biotechnology*, vol. 23, pp. 329–336, 2005.

[16] D. Fabbro, S. W. Cowan-Jacob, H. Möbitz, and G. Martiny-Baron, "Targeting cancer with small-molecular-weight kinase inhibitors" *Methods in Molecular Biology*, vol. 795, pp. 1–34, 2012.

[17] B. Kuster, *Kinase Inhibitors*, vol. 795. Totowa, NJ: Humana Press, 2012, p. 256.

[18] J. Zhang, P. L. Yang, and N. S. Gray, "Targeting cancer with small molecule kinase inhibitors," *Nature Reviews Cancer*, vol. 9, pp. 28–39, 2009.

[19] C. Bagshaw, "ATP analogues at a glance," *Journal of Cell Science*, vol. 114, pp. 459–460, 2001.

[20] P. Dalbon, G. Brandolin, F. Boulay, J. Hoppe, and P. V Vignais, "Mapping of the nucleotide-binding sites in the ADP/ATP carrier of beef heart mitochondria by photolabeling with 2-azido[alpha-32P]adenosine diphosphate," *Biochemistry*, vol. 27, pp. 5141–5149, 1988.

[21] A. M. Aponte, D. Phillips, R. A. Harris, K. Blinova, S. French, D. T. Johnson, and R. S. Balaban, "Chapter 4 32P Labeling of Protein Phosphorylation and Metabolite Association in the Mitochondria Matrix," *Methods in Enzymology*, vol. 457. pp. 63–80, 2009.

Chapter 2 Literature Review

This chapter mainly discusses the methods used to detect protein phosphorylation. Described approaches include conventional assays (ELISA, western blot), nanoparticle based assays, mass spectroscopy, electrochemical techniques, MEMS based devices and other modern optical and electronic systems. These methods that detect the kinase activity serve as drug discovery tools for the diseases caused by the abnormal protein phosphorylation.

2.1 Introduction

The discovery of 'protein kinase activity' in 1954, by Gene Kennedy, intrigued scientists to understand the role of kinases at the intracellular level [1]. Ever since then, over 500 kinases have been discovered that play a critical role in cellular regulation and transduction. Under pathological conditions, the dysfunction of kinases alters the phosphorylation states of the proteins [2]. As emphasised in the previous chapter, the cause of this abnormal 'protein phosphorylation' is responsible for more than 400 diseases including cancer, diabetes, Alzheimer's, cardiac and central nervous system disorders. This has led a number of researchers in both academia and industry, to develop novel kinase inhibitors, as potential drugs, to treat protein phosphorylated moderated diseases.

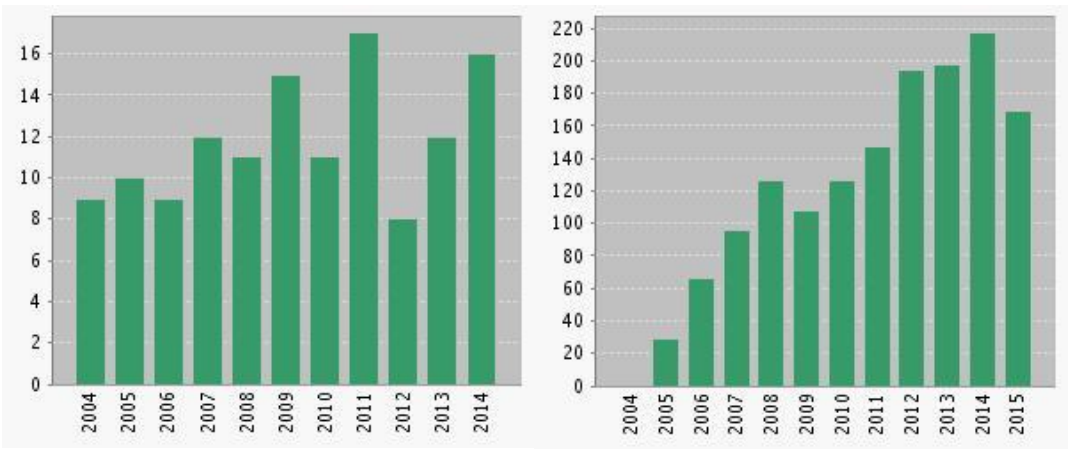

Figure 2-1 Number of: A) articles indexed from 2004-2014 B) citations received by 2005-2015 for the title 'phosphorylation' and 'detection' (data accessed in August 2015 from web of science).

Therefore, it is not surprising that 130 publications have been indexed by ISI web of science in the last decade (2004-2014), which received an average of over 11 citations per article for the title ‘phosphorylation’ and ‘detection’[3] , Figure 2-1. On the other hand, only 40 patents are available on the Espacenet patent search (August 2014) for the phrase ‘phosphorylation and detection’ [4]. Consequently the development of technologies to detect ‘protein phosphorylation’ for screening the kinase inhibitors is still premature both academia and industry. Thus, the upshot of commercial biosensors that are capable of scrutinizing the kinase inhibitors is the need of the hour.

Methods that have been reported to assess kinase activity include colorimetric, fluorescence, optical, electrochemical, radioactive and spectroscopic techniques. The detection mechanism of most of these usually involves either phospho-specific recognition of proteins or quantifying the phosphorylation product. Recent developments have encouraged the use of nano-scale materials, for example gold and silver nanostructures, quantum dots, graphene oxide, carbon nanotubes, magnetic beads and semiconductor materials to analyse kinase activity. The implementation of these nano hunks has greatly improved the detection limits and selectivity of protein phosphorylation reaction. Yet, there are bottlenecks that have hindered the potential of these advancements to transform into high throughput drug screening tools.

The following sections aim at presenting the bibliography of kinase drug discovery tools developed in academia and industry. In brief, it will contextualize the need to develop technologies for protein phosphorylation analysis by presenting progresses from past to present in the kinase biosensor development.

2.2 Conventional biochemical assay

Conventional biochemical assay uses a label, for instance an antibody, to detect the analyte of interest. Based on the label, analysis tools that are employed to detect the phosphorylation of proteins can be categorised into phospho-specific antibody and radioactive-labelled techniques. These assays are carried out using western blots or on a microtiter plate based ELISA platforms.

2.2.1 Western blot

In pharmaceutical research western blot is a standard method used to assess the post-translational modification of proteins. This is because the technique does not require

expensive laboratory equipment necessary to perform the experiments and the assay steps are user friendly to carry out. The first step of the assay involves passing the sample through a polyacrylamide gel. The process consists of using sodium dodecyl sulphate (SDS) to impart negative charge on the proteins which assists size dependent movement of proteins through the sample. This whole process of separating protein samples according to their size is called Polyacrylamide gel electrophoresis (PAGE). Next step involves transfer of the sample from the gel to a membrane, usually made of polyvinylidene fluoride (PVDF) or nitrocellulose. From the membrane the analyte of interest is detected using antibodies that produces a chemo-luminescent signal to detect the analyte of interest. Detection of phosphorylated protein and screening of inhibitors of kinase has been demonstrated using this method by in several studies [5–13]. While antibody based western blot eliminates the use and waste disposal requirements of radioisotopes, it is a very laborious technique and is not suitable for high throughput screening of inhibitors. The usual time for the assay varies from 24 to 72 hours so it may take a week to screen for instance 3-5 inhibitors. In addition, this technique provides limited information on the kinetics of the reaction therefore it is only suitable as a validating tool to observe the presence of phosphorylated proteins in an unknown solution [14].

2.2.2Enzyme-linked immunosorbent assay (ELISA)

ELISA is another conventional method in pharmaceutical research that is frequently used for measuring protein phosphorylation [15–19]. ELISA is usually carried out in a high throughput reaction platform (96 well plate). These ELISA plates are either made up of glass or polystyrene that facilitates immobilisation of enzymes and proteins easily. The technique is more quantitative than western blot because the calibration of the detection mechanisms is standardised. This means that the interpretation of the change in the signal is quantifiable by utilizing a calibrated standard [20]. The detection mechanisms usually involve colorimetric or fluorometric detections [21–30]. The analyte of interested for instance the phosphorylated proteins are captured by antibodies that are generally tagged with enzyme which generate fluorescence or colour change signal. There are some loopholes of ELISA that has temporised the use of ELISA plates as trademark drug screening device. One of them is that it doesn’t allow detection of the analyte in real-time and therefore obtaining

information of kinetics and binding specificities of the inhibitor is limited. In addition the coloured or fluorescent product is prone to quenching effects that may cause the system to give false negative signals. Lastly, since it involves labelling the phosphorylation event, there is always a possibility of non-specific attachment of the labels that again may provide unreliable signals.

2.2.3 Radioactive labelled assays

The γ-phosphoryl group of ATP, which is transferred to the protein upon phosphorylation, is modified with radioactive a isotope (^{32}P, ^{33}P) or radioactive orthophosphates [31]. The phosphorylated proteins are then detected using autoradiography. Autoradiography is a technique of measuring the distribution of radioactivity on a surface. The amount of radioactivity is qualitatively proportional to the amount of phosphorylation. Although radioactive assays are quite sensitive in detecting the amount of phosphorylation in a given sample however it has a major disadvantage of not being environmental friendly. Radioactive isotope can damage the cells of the human body and can induce carcinogenic mutations. Therefore carrying out a radioactive assay may cause life-threatening complications. Since radioisotopes has also the potential to damages the proteins, there is a high probability that inhibitor of kinase under test looses its function. Hence, radioactive assays for screening inhibitors of kinases are discouraged to use.

2.3 Mass spectroscopy

The addition of phosphate group adds a negative charge to the protein, in addition to the increase in its mass. Therefore it is not surprising that mass spectroscopy (MS) has been regarded as a comprehensive tool in the detection of phosphorylated proteins. In this technique the sample to be analysed is ionized to cations, which are separated according to their mass and charge in a magnetic field. The separated ions are then detected to produce a record of ions as a function of mass/charge. Although MS is a very sensitive technique with high resolution in identifying a single proton, it is not efficient in distinguishing a non-phosphorylated protein from a phosphorylated one. This is mainly attributed to the trade off with the MS principle that comes in when there is a mass and charge change in protein upon phosphorylation. There is poor

ionization of phospho-proteins since they are negatively charged and the ion source that ionises them in positive mode makes them loose their negative charge. This generates a very weak signal from phosphopeptides especially in the presence of high abundance of non-phosphorylated proteins. Secondly, stoichiometric levels of phosphoprotein may be very low and phosphopeptides have relatively low ion abundance in the presence of non-phosphorylated peptides. Lastly, improper sample preparation or peptide fragmentation may cause phosphate groups on phosphoserine and phosphothreonine to decompose. To overcome these drawbacks, several strategies have been proposed to analyse phospho proteins with MS techniques. This includes antibody enrichment, chemical modification and affinity tag based chromatography methods [32].

2.4 Quartz crystal microbalance

Quartz crystal microbalance (QCM) is a sensor that measures mass per unit area as a change in the resonance frequency of an oscillating quartz crystal. The addition of mass upon addition of phosphate group or attachment of functional kinase to its substrate in the presence/absence of a kinase inhibitor can be monitored by QCM to develop drug screening devices. Xu *et al.* [33,34] described one-step detection strategy for kinases using QCM. An aptameric peptide (IP_{20}) was used to attach PKA kinase via RRNAI motif of the kinase. A change of over -250 Hz was observed on the QCM upon attachment of kinase. These changes were observed in the real-time and the reaction was completed in 4 minutes. QCM has also been used to distinguish phosphorylated protein from the dephosphorylated ones [35]. In this work, the authors monitored the attachment of 3 biotinylated phospho-tags on the phosphorylation/dephosphorylated proteins using QCM. The attachment of their most sensitive phosphor-tag (monobiotinylated) at a concentration of 0.1 µg/ml revealed a change of around -40 Hz. Other phosphorylation studies using QCM are that of DNA phosphorylation by polynucleotide kinase [36] and the phosphorylation of polycystin-2 to obtain the binding affinities and kinetic constants of the reaction [37]. The advantages of using QCM for kinase assays is that the real-time monitoring of the reaction can be achieved in addition to the detection of mass binding events. This may provide useful information of the kinase inhibitor under screening trials. For instance, the kinetics of an inhibitor can provide information on how fast the drug would work

or information on its non-specificity could be extracted. However there are few loopholes in the QCM detection which make researchers cautious while using QCM.

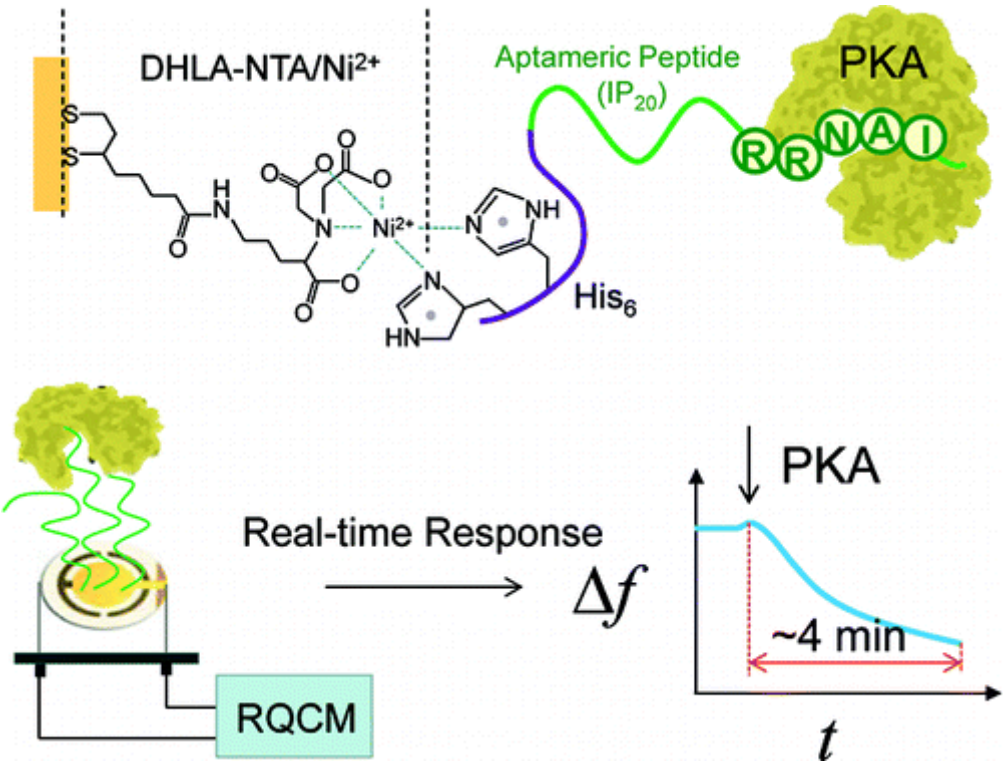

Figure 2-2 Xu el al. approach to detect kinase using Aptameric sensor on QCM produced from [34] *with permission from publisher*

The main disadvantages are the over estimation of the mass binding events and an approximate detection limit of 1 ng/cm^2. Another drawback is that it is difficult to use quartz crystal as a multiple channel platform. In addition since most of the measurements done on QCM are preferable in a liquid flow, there is a requirement of a steady flow over the sensor surface with at least 50 µl of buffer required [38]. These complexities have limited the use of QCM as an independent validating tool and often a confirmation tool is required to support the inferences from QCM.

2.5 Nanoparticle based technologies

Nanoparticles have been widely used in biosensing applications either to detect the presence of an analyte or enhance the detection signal. For the analysis of kinase assay or the detection of phosphorylated proteins, the use of magnetic particles and gold nanoparticles (AuNPs) with optical properties has been reported by several research

groups [39]. Recently Su *at el.* induced crosslinking in AuNPs using phosphorylated proteins and quantified it via a colorimetric assay [40]. They exploited the negative charge imparted on the proteins upon phosphorylation to aggregate the AuNPs. AuNPs are usually reddish pink in colour (the colour becomes lighter when the size of the nanoparticle is increase) and upon aggregation the colour turns blue. Different shades of blue colour can be obtained with different amounts of aggregation. The authors claim that different amounts of phosphorylation generates varied amounts of aggregation. In this way naked eye distinction of phosphorylated proteins from the dephosphorylated can be achieved [41]. Other approaches using AuNPs have also been used to enhance the electrochemical signals from the phosphorylated proteins [42] and employed to either enable optical detection like LSPR [43] or enhance SPR signal [44] [45].

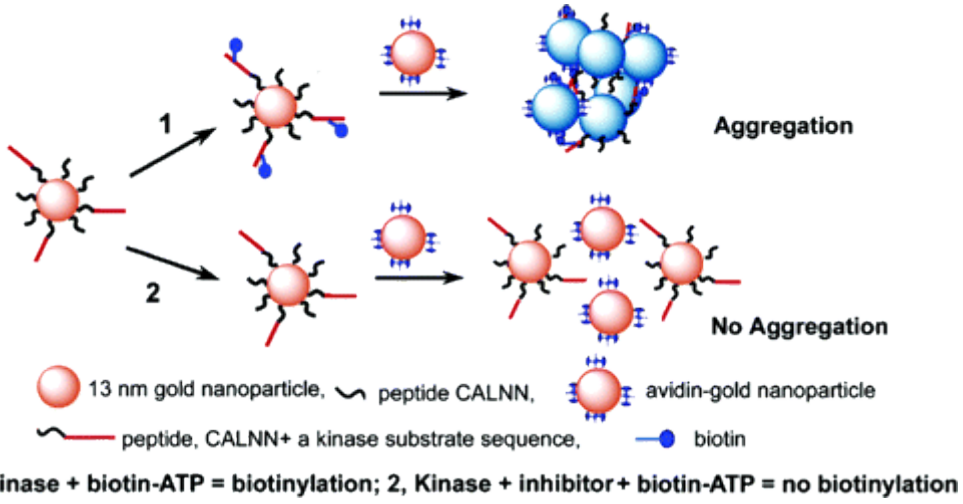

Figure 2-3 Kinase assay using AuNPs produced from [41] with permission from publisher

Metal oxide nanoparticles have been reported to have specificity for phosphoryl-groups and has therefore been used to detect phosphorylation [46,47]. Chen *et al.* carried out separation of phosphorylated α and β-caseins mixed in non-fat milk and egg white in the presence/absence of phosphatase inhibitor using alumina coated magnetic particles [48]. The phosphatase inhibitor avoids the removal of phosphate group from the proteins and allows the phosphorylated protein to attach on the alumina coated magnetic particles. The magnetic particles were then extracted using magnet and analysed using mass spectroscopy to confirm the attachment of phosphoprotein on them. Similarly Wang *et al.* recently purified phosphorylated peptides using

zirconium oxide coated iron-oxide magnetic particles [49]. An approach where phosphorylated peptides were extracted from a solution using zirconium magnetic particles and analysed using a portable glucose sensor was also recently demonstrated by Yang *at el.* [50].

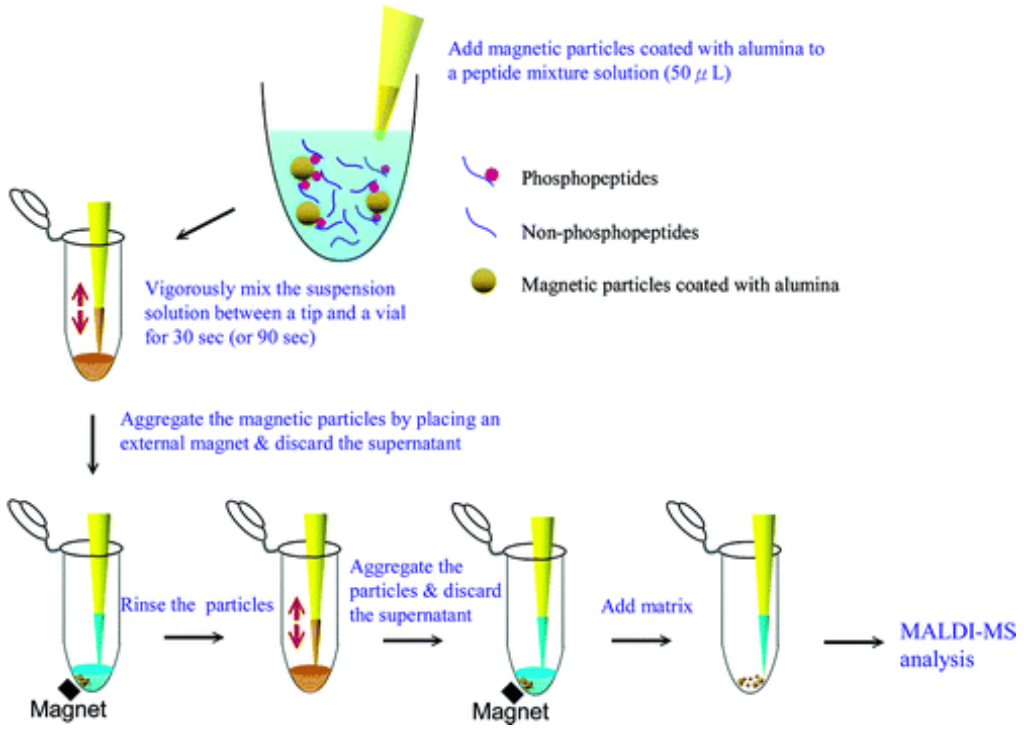

Figure 2-4 Separation of phosphoproteins using magnetic particles [48]; produced with permission from the publisher

While the detection methodologies using nanoparticles have an advantage of making the system smaller and simple to use, it might have low impact for screening inhibitors of kinase. One reason for this is that inhibitors containing phosphoryl group that have non-specific attachment on the nanoparticles may give a false signal. Secondly it is not easy to produce homogenous nanoparticles of same shape and size therefore the signal may vary from sample to sample. In addition it is not a trivial task to detect real-time changes from nanoparticle based detection system. For instance, complex phenomenon like plasmonic coupling or magneto plasmonic coupling occurs when AuNPs or magnetic particles are coupled on real-time detection systems like SPR and QCM. This makes the detection of the analytical more qualitative than quantitative.

2.6 Electrochemical Biosensors

Electrochemical detection involves commingling of electronics and reaction chemistry. The principle is based on the measurement of change in the surface charge of the electrode due to the activity of analyte in contact with electrode. This change in charge as a function of time is amplified and recorded as current. When a protein gets phosphorylated, it becomes negatively charged and therefore this change in charge makes the electrochemical detection feasible. Electrochemical methods involving potentiometry and amperometry are some of the techniques used to detect protein phosphorylation [51]–[55]. In potentiometry systems the measure of potential difference at zero current detects the analyte. Most commonly used potentiometric biosensor is an ion-sensitive field effect transistor (ISFET) or an open circuit potential (OCP) biosensor.

Formisano *et al.* reported a multimode electrochemical biosensor where OCP was used to detect phosphorylation of proteins in the absence and presence of kinase inhibitor [56]. A real-time detection of the kinase that gives an insight of enzymatic kinetics was achieved using this system. In the same work amperometric detection of kinase was achieved using differential pulse voltammetry (DPV). Voltammetry is a type of amperometric technique where the analyte gets oxidized or reduced by the application of a varying voltage between reference and working electrode. The measure of the analyte is given by measuring the changes in the current. In another work Song *et al.* used adenosine-59-[γ-ferrocene] triphosphate to carry out phosphorylation of proteins, Figure 2-5. In their approach phosphorylated proteins had the presence of ferrocene that was detected using cyclic voltammetry. The corresponding current was the measure of phosphorylation activity [52][57].

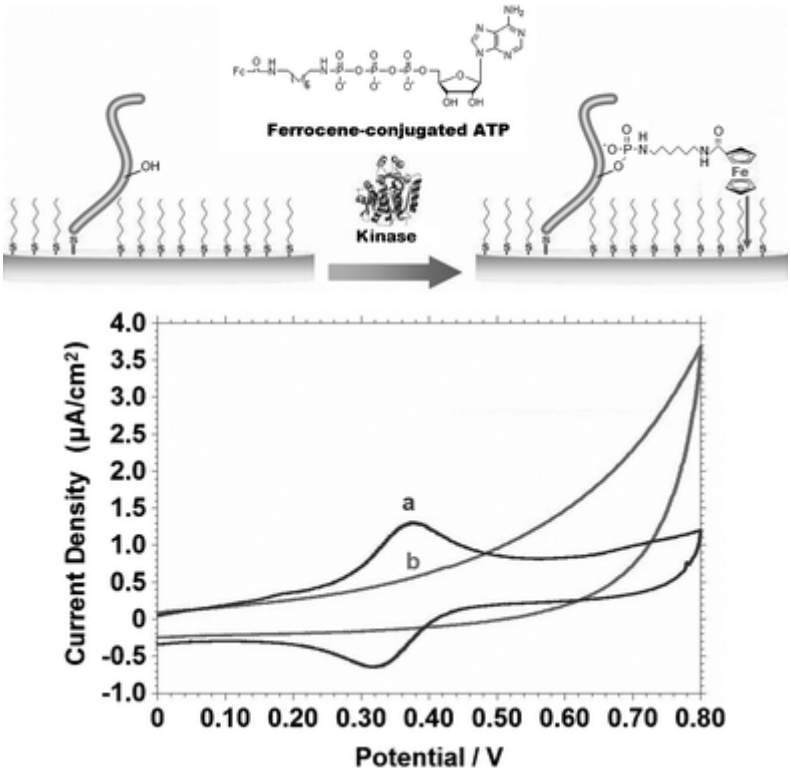

Figure 2-5 Detection of phosphorylation using cyclic voltammetry: Curve (a) phosphorylation (b) control; [52] produced with permission from publisher

The interface of electrochemistry with nanoparticles has made the electrochemical detection techniques more sensitive and robust. [58]. For instance Kerman *et al.* demonstrated the application of AuNPs in the detection of protein phosphorylation [51][53]. They immobilized the kinase substrate on screen-printed electrodes and coupled the phosphorylation reaction with biotinylation of it. The biotinylated-phosphorylated kinase binds to the Au nanoparticles coated with streptavidin. In another report they measured differential pulse voltammetry response of AuNPs to monitor the activity of kinase and its substrate [53]. In addition Wang *et al.* proposed a strategy based on HRP linked catalysis where AuNPs were used for the signal amplification [55]. Impedimetric tools like impedance spectroscopy, voltage–current and charge-transfer characteristics have also been reported to be useful in determination of protein phosphorylation events. For instance, change in charge of self-assembled monolayer of peptides upon phosphorylation was also seen by Wang *et al* [55]. Another example with label-free phosphorylation detection was demonstrated by Yitzchaik *et al.* [54]. They immobilized substrate and kinase in monolayers and saw a decrease in the electrochemical impedance of gold electrodes

and a negative shift in gate voltage of field effect transistor upon phosphorylation [54].

One of the great advantages of using electrochemical techniques for the phosphorylation detection is its high sensitivity. Secondly the electrodes are simple to use, time saving and large amount of data can be acquired within short duration. In addition electrochemical detection techniques have the capacity of monitoring binding events that happen during a chemical reactions. However achieving high throughput using these techniques is extremely challenging that limits its use in drug discovery applications.

2.7 MEMS based tools

Micro electro mechanical systems (MEMS) based cantilevers have been very useful in performing label-free biochemical assays. The cantilevers work on the principle of converting mechanical deformation into an electrical signal upon addition of mass. These structures are usually comprised of a transducing element in the form of a capacitive, piezoelectric or piezoresistive actuator integrated to respond to the changes in mechanical structures. Eun Yang's group developed a peptide inhibitor-based cantilever sensor assay for cyclic adenosine monophosphate-dependent protein kinase [59]. They immobilized the kinase on the bottom surface of the cantilever made up of gold layer. The addition of phosphate group on the immobilized protein resonated the piezoelectric crystal embedded on the top of the cantilever. Figure 2-6 shows the scheme of the Yang *et al's* system.

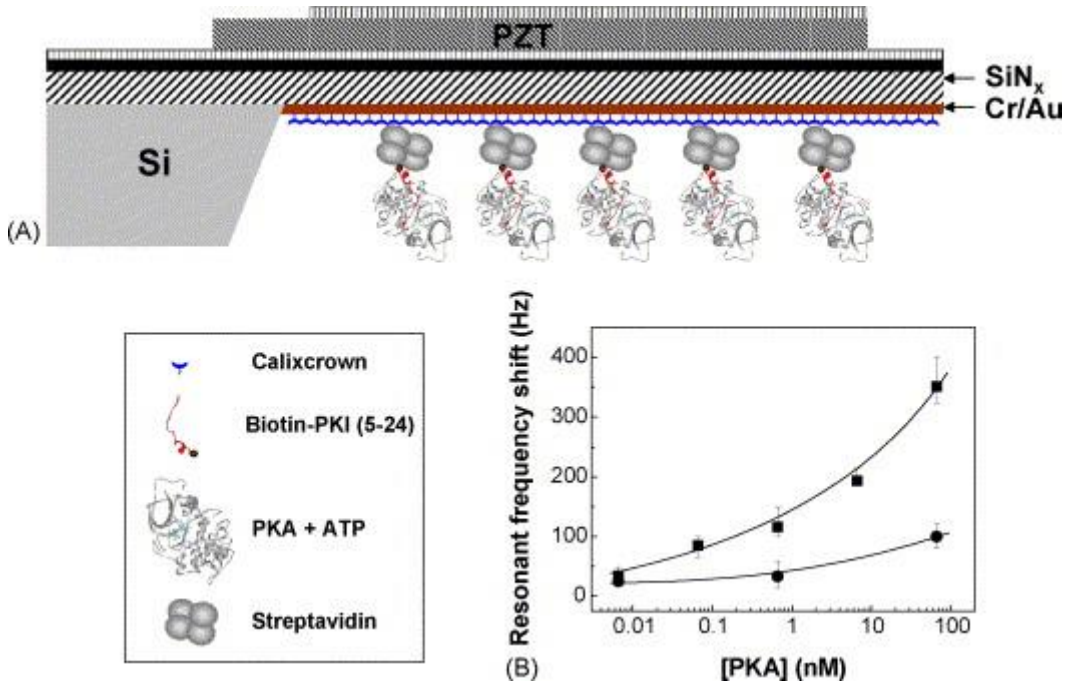

Figure 2-6 Nanomechanical detection of PKA catalytic subunit on a functionalised cantilever. (A) Schematic representation of the binding of on the Au surface of the PZT cantilever functionalised (B) Results of kinase assay test on cantilever [59]. Produced with permission from publisher.

They exploited the high throughput capabilities of standard MEMS foundry process and produced a device with an array of 12 cantilevers. While MEMS has the ability to produce high throughput drug screening devices, the standard foundry process that enables these processes are immature for biosensing application. For instance, it is challenging to independently expose electrodes in an array to a flow of fluid. The choice of material is also limited to silicon and gold in most processes (e.g. TSMC-BioMEMS, UMC-MEMS) so it is not trivial to interface nanomaterials to enhance sensitivity of the sensor. Interfacing MEMS with standard complementary metal oxide semiconductor (CMOS) technology and nanostructures presents an exploratory task for researchers to enable development of ultimate drug screening devices.

2.8 Atomic Force Microscopy

Since the protein monolayers on a surface get distorted upon phosphorylation, roughness changes seen under atomic force microscopic (AFM) could be used to determine the phosphorylation. Snir *et al.* [54] reported a change of 9.6 Å in the roughness of the sensor after phosphorylation of peptides. AFM uses a probe on the

cantilever structure. Mechanical deflection of the cantilever is the measures the roughness of the surface. The advantage of using AFM is that it is relatively simple to use. However, it is too presumptuous to confirm reaction by just measuring the change in the roughness of sensor as the technique does not provide information on the unwanted or non-specific interactions of the biomolecules on the surface. Therefore it has limited scope in drug discovery applications. Although it may be used as an extra validation tool to observe changes on the sensor surface upon phosphorylation.

2.9 Infrared Spectroscopy

Infrared spectroscopy is based on the principle that molecules absorb energies at certain frequencies that are characteristic of their structure. Attenuated total reflection Fourier transform infrared spectroscopy (ATR–FTIR) was employed by Goldsztein *et al*. to study phosphorylation of proteins [60]. They found major changes between the wavenumber 1300–1000 cm^{-1}, a region where phosphate vibration occurs. Strongest peak was observed at 1077 cm^{-1}. While an authentic conformation of presence of phosphate can be achieved using FTIR [61], it is difficult to associate the changes with phosphorylation. This is attributed to the fact that any non-specific attachment of the ATP will show presence of phosphate peaks in the sample and asserting these peaks to phosphorylated protein would be misleading. In addition this technique also requires expensive instrumentation. All these loopholes limit its use for drug screening applications.

2.10 Quantum dots

Quantum dots (QDs) are semiconductor based nanoparticles with fluorescence properties. These nanoparticles typically consist of 10 to 100 atoms. A simple assay to detect phosphorylation of proteins was demonstrated by Shiosaki *et al*. using QDs [62]. They demonstrated that QDs interact with the negative charge on peptides upon phosphorylation. The interaction was quantified using fluorescence resonance energy transfer (FRET). FRET is a technique in which there is distance dependent energy transfer between two fluorophores. As shown in Figure 2-7 the peptides were tagged with fluorophores and the negative charge of the phosphorylated peptides increased the distance between the QDs and fluorophore that caused a change in the resonance

properties of the system. The authors studied the activity of PKC kinases in the presence and absence of a known inhibitor of PKC. There are few other reports in literature that have explored the properties of QDs to study phosphorylation of proteins [63], [64]. Although FRET provides remarkable sensitivity to detect the phosphorylated proteins and subsequently screen inhibitors of kinase, they are subjected to fluorescence quenching effects. This may occasionally lead to a false signal of detection.

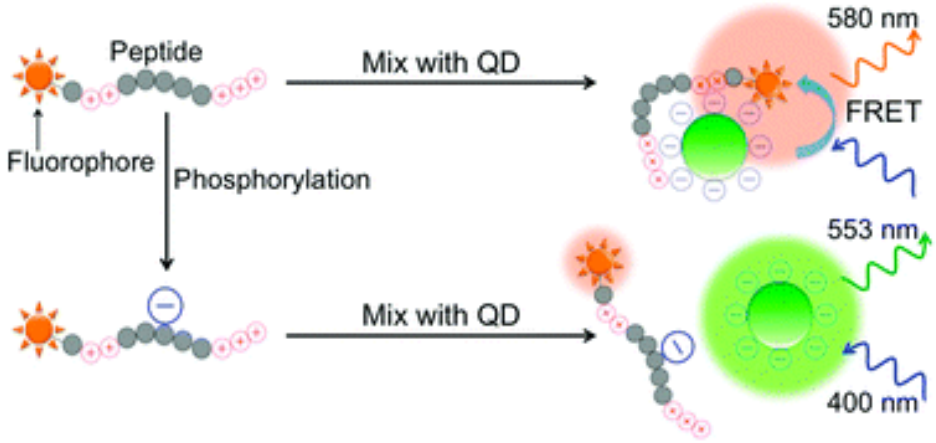

Figure 2-7 Scheme for using quantum dots for the detection of kinase activity [62]*; produced with permission*

2.11 Photonic crystal

A photonic crystal biosensor was developed by MacConagy *et al.* to obtain dose and time dependent response of phosphorylation of peptides [65, 66]. The device consisted of a crystalline colloidal array (CCA) polymerized into a hydrogel matrix. Diffraction measurements from the hydrogel matrix revealed that upon phosphorylation of peptides there is a redshift in the diffraction wavelength of the gel. This is due to the fact that the negative charge of the phosphorylated protein encourages repulsion of crystals in CCA. This was revealed by observation of expansion in the gel upon phosphorylation. Figure 2-8 shows the expansion of the hydrogen upon activity of kinase.

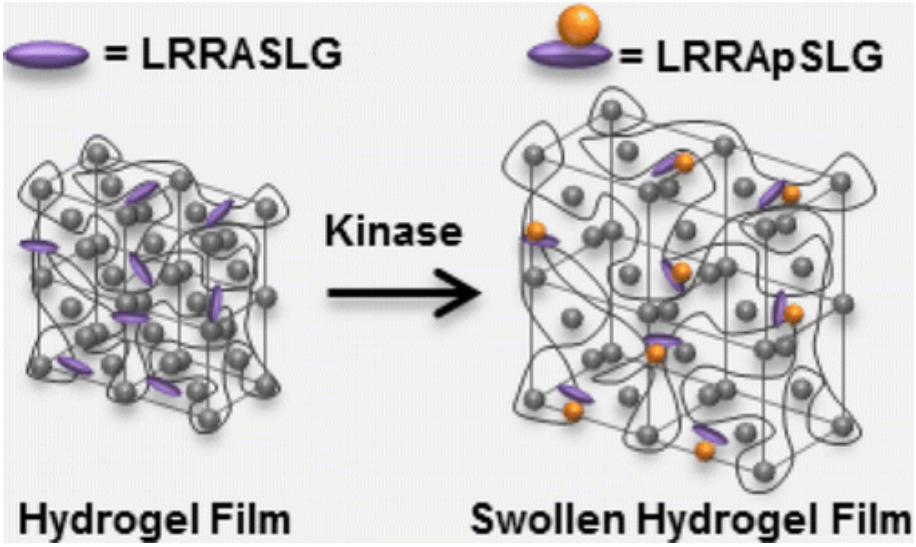

Figure 2-8 Expansion of hydrogen upon activity of kinase; Obtained from open access article [65]

2.13 Contact angle

Contact angle systems measure the wetting properties of the surface. Every surface has a characteristic surface tension that makes it either hydrophobic or hydrophilic in nature. Upon binding of biomolecules to a sensor surface, there are changes in the surface tension of the material that is measured by observing the spread of water on it. The angle that water makes on the sensor surface while it spreads is known as contact angle. Wieckowska *et al* studied phosphorylation of proteins using contact angle [67]. The negative charge of the phosphorylated proteins makes the sensor surface hydrophilic and a reduction of the contact from 67.5º to 36.8º was observed on the gold based surfaces [68]. Usually the measurement system is simple and it requires a camera, optical lens and a source of light to give the right contrast to the droplet. However, contact angle does not provide any significant information on kinetics of the reaction. Therefore it is an addition validation tool to confirm changes on the surface of the sensor. Whether the changes are due to the specific or non-specific interactions of the molecules is asserted by other detection mechanisms.

2.14 Field effect devices

Field effect transistor (FET) measures the changes of potential on the surface of an electrode. This research has explored the prospects of using field effect devices has drug screening tool. The potential is usually changed due to change in change upon a

chemical reaction in which case a charge sensitive electrodes, for instance gold electrodes, are used for the measurement of the analyte. The potential change on the FETs may also be due to the change in the pH upon chemical reaction in which case pH sensitive material such as silicon nitride is used as an electrode. Freeman *et al*. first studied the degree of charging of the gate surface due to kinase activity [69]. They used aluminium oxide gated field effect transistor to follow the phosphorylation of proteins. They carried out simultaneous phosphorylation and dephosphorylation on their sensor and achieved a 40 mV change in the signal upon phosphorylation of proteins. Real-time monitoring of the kinetics of the reaction was also followed. Another study that demonstrated phosphorylation/dephosphorylation of peptides using silicon nitride based FETs reported a change of 118 mV [54]. Detection of the release of pH associated with phosphorylation of protein, changes in charge upon phosphorylation and demonstration of how kinase inhibitors could be screened was first demonstrated by this research [43, 45, 70].

Major advantage of using FET based devices is their high throughput capabilities. Potential of very large scale integration technology (VLSI) to form an array of FETs to monitor biocatalytic transformation was explored by Ion Torrent on their DNA sequencing chip [71]. Whole genome sequencing was performed on that chip whereby the protons were produced by adding a nucleotide to each of the several molecules in a clonal colony of DNA [72]. This release of protons was measured by an array of FETs. Similarly if entire human proteome is printed on an array of ISFETs such that there is one type of protein above each FET, then it will be possible to address the whole human proteome and study which protein was phosphorylated with a given kinase [73]. This would also make it possible to know how various inhibitors (drugs) of kinase affect that particular protein phosphorylation [73]. Therefore its application in development of miniaturized rapid drug discovery platform is of prime significance.

2.15 Plasmonic biosensors

The quantum associated with collective oscillations of electrons that takes place when light is shinned on a material with specific dielectric constant is known as plasmon. Materials that satisfy the large negative real dielectric constant and small imaginary dielectric constant refractive index show the presence of plasmons and are generally

called plasmonic material [74]. The concept of plasmonic biosensor is based on the interaction of surface plasmon wave produced at the interface of the plasmonic material and an isotropic media for light. Plasmonic biosensors can be categorised into surface plasmon resonance (SPR) and localized surface plasmon resonance (LSPR) based detection systems.

Thin planar films of gold (< 100 nm) are one of the materials that satisfy the requirements for the formation of plasmons. To excite surface plasmons on the gold the most common configuration is the Kretschmann configuration where the light is shinned through a prism at 'just near' to the critical angle of incidence. At angles near to critical angle of incidence, there is total internal reflection of the light and it is allowed to pass through the other media (gold film). The variations in the light that passes through the other media can be measured as a change in the angle of the total internal reflected light. These variations are usually brought in by the interactions of plasmonic evanescent wave with the biomolecules attach on the surface. On the other hand LSPR works with the similar physics except that the formation of plasmons is on nanoscale materials.

Nordin *et al.* is the only exclusive report that demonstrated the use of SPR biosensors to screen inhibitors of kinase [75]. The work successfully demonstrated the use of SPR to study direct binding of inhibitors to the kinases and a detailed kinetic analyses of their binding events. On the other hand use of LSPR to screen inhibitors of the kinase was first demonstrated by the work reported in the thesis. The LSPR was combined with the field effect devices as complementary biosensors to confirm phosphorylation of proteins [43]. Detailed description of the technique is demonstrated in the following chapters.

2.15 Gel Proteomics

In quantitative gel proteomics, 2-D gel electrophoresis is a common technique used to analysis protein mixtures. The first step is the separation of proteins based on their isoelectric point. Isoelectric point is a pH in which net charge of protein is zero. Proteins having similar isoelectric point are found in the same band. The second step separates the proteins based on their charges using SDS-PAGE. In addition to the change in isoelectric point, the negative charge of phosphorylation proteins move them

towards the anode plate of the applied electric field [76, 77]. Schematic in the figure 2.9 shows a classic example of where phosphorylated proteins would be present in the gel.

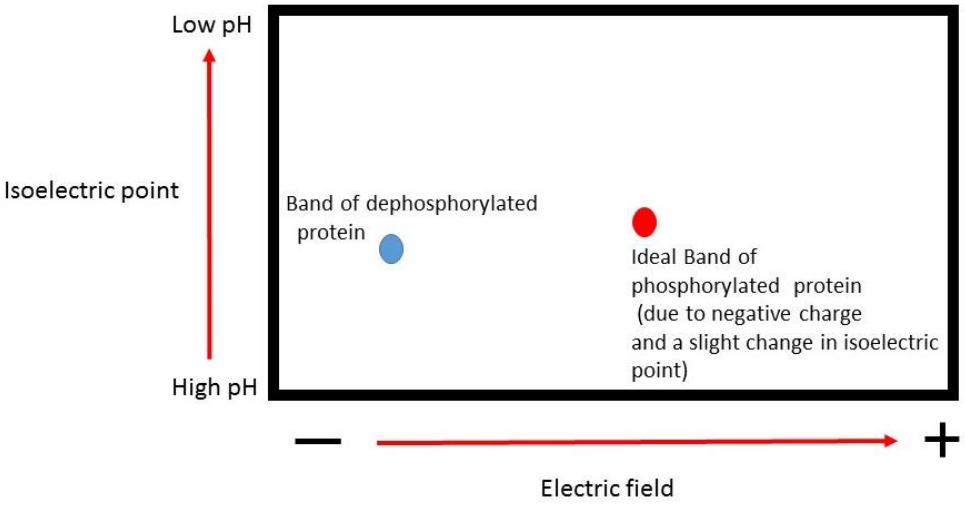

Figure 2-9 Schematic of 2-D gel electrophoresis of a mixture containing phosphorylated and dephosphorylated proteins

2.16 Conclusions

This chapter reported a survey of techniques used by the researchers to study phosphorylation of proteins for the development of kinase inhibitor screening devices.

While highly sophisticated assays and devices have been reported in literature to study kinase activity, the research is still pre-mature to develop a high throughput drug screening device.

Highlights of the above mentioned techniques are provided in table 2.1 below.

Table 2-1 Pros and Cons of the techniques used for kinase assays (a) High throughput (b) Cost of setup per assay less than 1 £ (c) monitoring kinetics of phosphorylation activity (d) time consumption less than 1 hour (e) ease of use and analysis ; '✓' symbol indicates the attribute of the technique in the table below

Techniques	**a**	**b**	**c**	**d**	**e**
Conventional assays					
Western blots					✓
96-well ELISA					✓
2-D gel electrophoresis					✓
Radioactive labelled assays					
Mass spectroscopy				✓	
QCM			✓	✓	✓
Nanoparticle based technologies		✓		✓	✓
Electrochemical Biosensors					
Electrochemical Impedance Spectroscopy		✓	✓		✓
Voltammetry		✓	✓		✓
Field effect sensing	✓	✓	✓	✓	✓
MEMS devices		✓	✓		✓
AFM				✓	✓
FTIR				✓	✓
Quantum dots		✓		✓	✓
Photonic crystal biosensors		✓		✓	✓
Optical angle systems				✓	✓
Plasmonic biosensors					
SPR	✓		✓		✓
LSPR	✓	✓	✓	✓	✓

Therefore there is considerable scope to develop simple biosensors to study phosphorylation of proteins. To overcome this there is a need for the researchers from chemistry/biology and other basic sciences to closely work with the researchers in the

field of nano/micro-engineering and electronics as biosensors is a highly interdisciplinary area of research.

References

[1] P. Cohen, "The origins of protein phosphorylation" *Nature Cell Biololgy*, vol. 4, no. 5, pp. E127–30, 2002.

[2] P. Cohen, "Protein kinases--the major drug targets of the twenty-first century?" *Nature Reviews Drug Discovery*, vol. 1, pp. 309–315, 2002.

[3] Citation Report, "Web of Science" [Online]. Available: http://apps.webofknowledge.com/CitationReport.do?product=UA&search_mode=CitationReport&SID=W2YmNBCmNdU2jnOzVzb&page=1&cr_pqid=4&viewType=summary.

[4] "Espacenet patent search." [Online]. Available: http://worldwide.espacenet.com/searchResults?submitted=true&locale=en_EP&DB=EPODOC&ST=advanced&TI=phosphorylation+and+detection&AB=&PN=&AP=&PR=&PD=&PA=&IN=&CPC=&IC=&Submit=Search.

[5] B. J. Druker, M. Talpaz, D. J. Resta, B. Peng, E. Buchdunger, J. M. Ford, N. B. Lydon, H. Kantarjian, R. Capdeville, S. Ohno-Jones, and C. L. Sawyers, "Efficacy and safety of a specific inhibitor of the BCR-ABL tyrosine kinase in chronic myeloid leukemia" *New England Journal of Medicine*, vol. 344, no. 14, pp. 1031–7, 2001.

[6] J. P. MacKeigan, L. O. Murphy, and J. Blenis, "Sensitized RNAi screen of human kinases and phosphatases identifies new regulators of apoptosis and chemoresistance" *Nature Cell Biololgy*, vol. 7, no. 6, pp. 591–600, 2005.

[7] C. J. Vlahos, W. F. Matter, K. Y. Hui, and R. F. Brown, "A specific inhibitor of phosphatidylinositol 3-kinase, 2-(4-morpholinyl)-8-phenyl-4H-1-benzopyran-4-one (LY294002)" *Journal of Biological Chemistry*, vol. 269, no. 7, pp. 5241–8, 1994.

[8] D. Toullec, P. Pianetti, H. Coste, P. Bellevergue, T. Grand-Perret, M. Ajakane, V. Baudet, P. Boissin, E. Boursier, and F. Loriolle, “The bisindolylmaleimide GF 109203X is a potent and selective inhibitor of protein kinase C” *Journal of Biological Chemistry*, vol. 266, no. 24, pp. 15771–81, 1991.

[9] J. Xu, L. Sun, I. Ghosh, and M. Xu, “Western blot analysis of Src kinase assays using peptide substrates ligated to a carrier protein” *Biotechniques*, vol. 36, no. 6, pp. 976–8, 980–1, 2004.

[10] S. Sawasdikosol, “Detecting tyrosine-phosphorylated proteins by Western blot analysis” *Curr. Protoc. Immunol. Ed. by John E Coligan al*, vol. Chapter 11, p. Unit 11.3.1–11, 2010.

[11] M. Hashiguchi, “Characteristic of tau phosphorylation by multiple kinases,” in *JPS 札幌第81*, 2004.

[12] A. Martiny, J. R. Meyer-Fernandes, W. De Souza, and M. A. Vannier-Santos, “Altered tyrosine phosphorylation of ERK1 MAP kinase and other macrophage molecules caused by Leishmania amastigotes” *Molecular Biochemical Parasitology*, vol. 102, pp. 1–12, 1999.

[13] I. Sugimoto and E. Hashimoto, “Modulation of protein phosphorylation by Mr 25,000 protein partially overlapping phosvitin and lipovitellin 2 in Xenopus laevis vitellogenin B1 protein” *Protein Journal*, vol. 25, pp. 109–115, 2006.

[14] B. E. M. Schaefer and B. W. Jarvis, “A Comparison of Western Blotting Techniques Using Phospho-Specific Antibody Detection of Protein Kinase Activation,” no. 64, pp. 26–32, 1997. https://www.promega.co.uk/resources/pubhub/promega-notes-1997/a-comparison-of-western-blotting-techniques-using-phosphospecific-antibody-detection/

[15] M. J. Khosravi, A. Diamandi, and J. Mistry, “Immunoassay of insulin-like growth factor binding protein-1” *Clinical Chemistry*, vol. 43, pp. 523–32, 1997.

[16] E. Schremmer-Danninger, E. Toepfer-Petersen, H. Fritz, and A. A. Roscher, “Bradykinin-induced tyrosine phosphorylation of proteins in cultured human keratinocytes” *Biological Ressearch*, vol. 31, pp. 189–198, 1998.

[17] A. Diamandi, J. Mistry, R. G. Krishna, and J. Khosravi, “Immunoassay of insulin-like growth factor-binding protein-3 (IGFBP-3): new means to quantifying IGFBP-3 proteolysis” *Journal of Clinical Endocrinology Metabolism*, vol. 85, pp. 2327–2333, 2000.

[18] J.-M. Kee, R. C. Oslund, D. H. Perlman, and T. W. Muir, “A pan-specific antibody for direct detection of protein histidine phosphorylation” *Nature Chemical Biology*, 2013.

[19] L. Delbroek, K. Van Kolen, L. Steegmans, R. Da Cunha, W. Mandemakers, G. Daneels, P.-J. De Bock, J. Zhang, K. Gevaert, B. De Strooper, D. R. Alessi, P. Verstreken, and D. W. Moechars, “Development of an enzyme-linked immunosorbent assay for detection of cellular and in vivo LRRK2 S935 phosphorylation” *Journal of Pharmaceutical and Biomedical Analysis*, vol. 76, pp. 49–58, 2013.

[20] “Methods for Detecting Protein Phosphorylation.” [Online]. Available: https://www.rndsystems.com/resources/articles/methods-detecting-protein-phosphorylation.

[21] Z. H. Zhao, D. A. Malencik, and S. R. Anderson, “Characterization of a new substrate for protein kinase C: assay by continuous fluorometric monitoring and high performance liquid chromatography” *Biochemical and Biophysicsal Research Communication*, vol. 176, pp. 1454–1461, 1991.

[22] K. Viht, A. Vaasa, G. Raidaru, E. Enkvist, and A. Uri, “Fluorometric TLC assay for evaluation of protein kinase inhibitors” *Analytical Biochemistry*, vol. 340, pp. 165–170, 2005.

[23] M. Seville, A. B. West, M. G. Cull, and C. S. McHenry, “Fluorometric assay for DNA polymerases and reverse transcriptase” *Biotechniques*, vol. 21, pp. 664, 666, 668, 670, 672, 1996.

[24] K. Tomizaki and H. Mihara, “Rational design of homogenous protein kinase assay platforms that allow both fluorometric and colorimetric signal readouts” *Molecular Biosystems*, vol. 2, pp. 580–589, 2006.

[25] P. R. Harvey, G. A. Upadhya, J. L. Toth, and S. M. Strasberg, “Fluorometric assay of protein in native human bile” *Clinical Chimica acta* vol. 183, pp. 147–154, 1989.

[26] H. Ebrahim and K. Dakshinamurti, “A fluorometric assay for biotinidase” *Analytical Biochemistry*, vol. 154, pp. 282–286, 1986.

[27] T. A. Bennett, T. D. Foutz, V. V Gurevich, L. A. Sklar, and E. R. Prossnitz, “Partial phosphorylation of the N-formyl peptide receptor inhibits G protein association independent of arrestin binding” *Journal of Biological Chemistry*, vol. 276, pp. 49195–49203, 2001.

[28] L. B. Daniels, R. H. Glew, N. S. Radin, and R. R. Vunnam, “A revised fluorometric assay for Gaucher’s disease using conduritol-beta-epoxide with liver as the source of Beta-glucosidase” *Clinica Chimica acta* vol. 106, pp. 155–163, 1980.

[29] E.-K. Song, H.-J. Park, J.-S. Kim, H.-H. Lee, U.-H. Kim, and M.-K. Han, “A novel fluorometric assay for ADP-ribose pyrophosphatase activity” *Journal of Biochemical and Biophysical Methods*, vol. 63, pp. 161–169, 2005.

[30] B. E. Pape, “Enzyme immunoassay and two fluorometric methods compared for the determination of quinidine in serum” *Therapeutic Drug Monitoring*, vol. 3, pp. 357–363, 1981.

[31] J. X. Yan, N. H. Packer, A. A. Gooley, and K. L. Williams, “Protein phosphorylation: Technologies for the identification of phosphoamino acids,” *Journal of Chromatography A*, vol. 808. pp. 23–41, 1998.

[32] “Methods for Detection Protein Phosphorylation.” [Online]. Available: https://www.rndsystems.com/resources/articles/methods-detecting-protein-phosphorylation.

[33] X. Xu, Y. Li, J. Zhou, Z. Nie, and S. Yao, “Peptide inhibitor based QCM biosensor for rapidly detecting protein kinase activity,” in *2012 IEEE Sensors*, 2012, pp. 1–4.

[34] X. Xu, J. Zhou, X. Liu, Z. Nie, M. Qing, M. Guo, and S. Yao, “Aptameric peptide for one-step detection of protein kinase” *Analalytical Chemistry*, vol. 84, no. 11, pp. 4746–53, 2012.

[35] E. Kinoshita, E. Kinoshita-Kikuta, Y. Sugiyama, Y. Fukada, T. Ozeki, and T. Koike, “Highly sensitive detection of protein phosphorylation by using improved Phos-tag Biotin” *Proteomics*, vol. 12, no. 7, pp. 932–7, 2012.

[36] H. Furusawa, K. Uemura, H. Yoshimine, and Y. Okahata, “In situ monitoring of a trace intermediate during DNA phosphorylation by T4 polynucleotide kinase for transient kinetic studies” *Analyst*, vol. 137, no. 6, pp. 1334–7, 2012.

[37] D. Morick, M. Schatz, R. Hubrich, H. Hoffmeister, A. Krefft, R. Witzgall, and C. Steinem, “Phosphorylation of C-terminal polycystin-2 influences the interaction with PIGEA14: a QCM study based on solid supported membranes” *Biochemical and Biophysical Research Communications*, vol. 437, no. 4, pp. 532–7, 2013.

[38] B. Instrument, “Technical Note: Surface plasmon resonance v. quartz crystal microbalance.” [Online]. Available: http://biosensingusa.com/technical-notes/technical-note-103-surface-plasmon-resonance-v-quartz-crystal-microbalance/.

[39] M. C. . K. K. Vestergaard, I.-M. Hsing, and E. Tamiya, *Nanobiosensors and Nanobioanalyses*, pp. 251–267, 2015

[40] S. Sun, H. Shen, C. Liu, and Z. Li, “Phosphorylation-regulated crosslinking of gold nanoparticles: a new strategy for colorimetric detection of protein kinase activity” *Analyst*, vol. 140, no. 16, pp. 5685–91, 2015.

[41] Z. Wang, R. Lévy, D. G. Fernig, and M. Brust, "Kinase-catalyzed modification of gold nanoparticles: a new approach to colorimetric kinase activity screening" *Journal of American Chemical Soceity*, vol. 128, pp. 2214–2215, 2006.

[42] R. Chand, D. Han, I.-S. Shin, J.-I. Hong, and Y.-S. Kim, "Gold Nanoparticle Enhanced Electrochemical Assay for Protein Kinase Activity Using a Synthetic Chemosensor on a Microchip," *Journal of Electrochemical Soceity*, vol. 162, no. 4, pp. B89–B93, 2015.

[43] N. Bhalla, M. Di Lorenzo, G. Pula, and P. Estrela, "Protein phosphorylation detection using dual-mode field-effect devices and nanoplasmonic sensors" *Scientific Reports*, vol. 5, p. 8687, 2015.

[44] Y.-P. Kim, Y.-H. Oh, and H.-S. Kim, "Protein kinase assay on peptide-conjugated gold nanoparticles" *Biosensensors and Bioelectronics*, vol. 23, no. 7, pp. 980–6, 2008.

[45] N. Bhalla, N. Formisano, A. Miodek, A. Jain, M. Di Lorenzo, G. Pula, and P. Estrela, "Plasmonic ruler on field-effect devices for kinase drug discovery applications" *Biosensensors and Bioelectronics* vol. 71, pp. 121–8, 2015.

[46] C.-T. Chen and Y. Chen, "Fe3O4/TiO2 core/shell nanoparticles as affinity probes for the analysis of phosphopeptides using TiO2 surface-assisted laser desorption/ionization mass spectrometry" *Analytical Chemistry*, vol. 77, no. 18, pp. 5912–9, 2005.

[47] O. Yildirim, T. Gang, S. Kinge, D. N. Reinhoudt, D. H. Blank, W. G. van der Wiel, G. Rijnders, and J. Huskens, "Monolayer-directed assembly and magnetic properties of FePt nanoparticles on patterned aluminum oxide" *International Journal of Molecular Science*, vol. 11, no. 3, pp. 1162–79, 2010.

[48] C.-T. Chen, W.-Y. Chen, P. Tsai, K. Chien, J. Yu, and Y. Chen, "Rapid enrichment of phosphopeptides and phosphoproteins from complex samples using magnetic particles coated with alumina as the concentrating probes for MALDI MS analysis" *Journal of Proteome Research*, vol. 6, no. 1, pp. 316–25, 2007.

[49] J. Wang, F. Niu, Y. Su, and Y. Yang, “Facile Synthesis of Zirconia-Modified Magnetic Nanoparticles for Purification of Phosphopeptides,” *Journal of Food Process Engineering*, pp. 1–10, 2015.

[50] W. Yang, X. Lu, Y. Wang, S. Sun, C. Liu, and Z. Li, “Portable and sensitive detection of protein kinase activity by using commercial personal glucose meter,” *Sensors and Actuators B Chemical*, vol. 210, pp. 508–512, 2015.

[51] K. Kerman, M. Chikae, S. Yamamura, and E. Tamiya, “Gold nanoparticle-based electrochemical detection of protein phosphorylation” *Analytical Chimica Acta*, vol. 588, no. 1, pp. 26–33, 2007.

[52] H. Song, K. Kerman, and H.-B. Kraatz, “Electrochemical detection of kinase-catalyzed phosphorylation using ferrocene-conjugated ATP” *Chemical Communication*, vol. 4, no. 4, pp. 502–4,2008.

[53] K. Kerman and H.-B. Kraatz, “Electrochemical detection of protein tyrosine kinase-catalysed phosphorylation using gold nanoparticles” *Biosensensors and Bioelectronics* vol. 24, no. 5, pp. 1484–9, 2009.

[54] E. Snir, J. Joore, P. Timmerman, and S. Yitzchaik, “Monitoring selectivity in kinase-promoted phosphorylation of densely packed peptide monolayers using label-free electrochemical detection” *Langmuir*, vol. 27, no. 17, pp. 11212–21, 2011.

[55] J. Wang, Y. Cao, Y. Li, Z. Liang, and G. Li, “Electrochemical strategy for detection of phosphorylation based on enzyme-linked electrocatalysis,” *Journal of Electroanalytical Chemistry*, vol. 656, no. 1–2, pp. 274–278, 2011.

[56] N. Formisano, N. Bhalla, L. C. Caleb Wong, M. Di Lorenzo, G. Pula, and P. Estrela, “Multimodal electrochemical and nanoplasmonic biosensors using ferrocene-crowned nanoparticles for kinase drug discovery applications,” *Electrochemistry communication*, vol. 57, pp. 70–73, 2015.

[57] G. Hanrahan, D. G. Patil, and J. Wang, "Electrochemical sensors for environmental monitoring: design, development and applications" *Journal of Environmental Monitoring*, vol. 6, no. 8, pp. 657–64, 2004.

[58] J. Wang, M. Shen, Y. Cao, and G. Li, "Switchable 'On-Off' electrochemical technique for detection of phosphorylation" *Biosensensors and Bioelectronics* vol. 26, no. 2, pp. 638–42, 2010.

[59] H.-S. Kwon, K.-C. Han, K. S. Hwang, J. H. Lee, T. S. Kim, D. S. Yoon, and E. G. Yang, "Development of a peptide inhibitor-based cantilever sensor assay for cyclic adenosine monophosphate-dependent protein kinase" *Analytical Chimica Acta*, vol. 585, pp. 344–349, 2007.

[60] F. H. and E. G. A. Goldsztein, S. Babar, M. Voué , J. De Coninck , J. Conti , J. Marchand-Brynaert S. Devouge, "Gastric ATPase phosphorylation/dephosphorylation monitored by new FTIR-based BIA–ATR biosensors," *Spectroscopy*, vol. 24, pp. 257–260, 2010.

[61] E. Snir, E. Amit, A. Friedler, and S. Yitzchaik, "A highly sensitive square wave voltammetry based biosensor for kinase activity measurements" *Biopolymers*, 2015.

[62] S. Shiosaki, T. Nobori, T. Mori, R. Toita, Y. Nakamura, C. W. Kim, T. Yamamoto, T. Niidome, and Y. Katayama, "A protein kinase assay based on FRET between quantum dots and fluorescently-labeled peptides" *Chemical Communication,* vol. 49, no. 49, pp. 5592–4, 2013.

[63] R. Freeman, T. Finder, R. Gill, and I. Willner, "Probing protein kinase (CK2) and alkaline phosphatase with CdSe/ZnS quantum dots," *Nano Letters*, vol. 10, pp. 2192–2196, 2010.

[64] Y. Wang, L. Zhang, R. P. Liang, J. M. Bai, and J. D. Qiu, "Using graphene quantum dots as photoluminescent probes for protein kinase sensing," *Analytical Chemistry,* vol. 85, pp. 9148–9155, 2013.

[65] K. I. Macconaghy, C. I. Geary, J. L. Kaar, and M. P. Stoykovich, “Photonic crystal kinase biosensor,” *Journal of American Chemical Soceity*, vol. 136, pp. 6896–6899, 2014.

[66] K. I. MacConaghy, D. M. Chadly, M. P. Stoykovich, and J. L. Kaar, “Optically diffracting hydrogels for screening kinase activity in vitro and in cell lysate: impact of material and solution properties” *Analytical Chemistry*, vol. 87, no. 6, pp. 3467–75, 2015.

[67] A. Wieckowska, D. Li, R. Gill, and I. Willner, “Following protein kinase acivity by electrochemical means and contact angle measurements” *Chemical Communication* , no. 20, pp. 2376–8, 2008.

[68] O. I. Wilner, C. Guidotti, A. Wieckowska, R. Gill, and I. Willner, “Probing kinase activities by electrochemistry, contact-angle measurements, and molecular-force interactions,” *Chemistry - A Eur. Journal*, vol. 14, pp. 7774–7781, 2008.

[69] R. Freeman, R. Gill, and I. Willner, “Following a protein kinase activity using a field-effect transistor device” *Chemical Communication*, no. 33, pp. 3450–2, 2007.

[70] P. E. Nikhil Bhalla, Mirella Di Lorenzo, Giordano Pula, “Protein phosphorylation analysis based on proton release detection: Potential tools for drug discovery,” *Biosensensors and Bioelectronics*, vol. 54, no. 0, pp. 109–114, 2014.

[71] J. M. Rothberg, W. Hinz, T. M. Rearick, J. Schultz, W. Mileski, M. Davey, J. H. Leamon, K. Johnson, M. J. Milgrew, M. Edwards, J. Hoon, J. F. Simons, D. Marran, J. W. Myers, J. F. Davidson, A. Branting, J. R. Nobile, B. P. Puc, D. Light, T. A. Clark, M. Huber, J. T. Branciforte, I. B. Stoner, S. E. Cawley, M. Lyons, Y. Fu, N. Homer, M. Sedova, X. Miao, B. Reed, J. Sabina, E. Feierstein, M. Schorn, M. Alanjary, E. Dimalanta, D. Dressman, R. Kasinskas, T. Sokolsky, J. A. Fidanza, E. Namsaraev, K. J. McKernan, A. Williams, G. T.

Roth, and J. Bustillo, “An integrated semiconductor device enabling non-optical genome sequencing” *Nature*, vol. 475, no. 7356, pp. 348–52, 2011.

[72] “Ion Torrent,” 2011. [Online]. Available: lifetechnologies.com/iontorrent.

[73] S. Lindsay, “Biochemistry and semiconductor electronics--the next big hit for silicon?,” *Journal of Physics Condensed. Matter*, vol. 24, no. 16, p. 164201, 2012.

[74] J. N. Anker, W. P. Hall, O. Lyandres, N. C. Shah, J. Zhao, and R. P. Van Duyne, “Biosensing with plasmonic nanosensors” *Nature Materials*, vol. 7, pp. 442–453, 2008.

[75] H. Nordin, M. Jungnelius, R. Karlsson, and O. P. Karlsson, “Kinetic studies of small molecule interactions with protein kinases using biosensor technology,” *Analytical Biochemistry*, vol. 340, no. 2, pp. 359–368, 2005.

[76] M. Kristin, S. Albrecht, and A. Schaller. "Targeted Analysis of Protein Phosphorylation by 2D Electrophoresis." Plant Phosphoproteomics: Methods and Protocols (2015): 167-176.

[77] L. Sudarsanareddy, N.V. Kukushkin, and A. L. Goldberg. "cAMP-induced phosphorylation of 26S proteasomes on Rpn6/PSMD11 enhances their activity and the degradation of misfolded proteins." Proceedings of the National Academy of Sciences (2015): 201522332.

Chapter 3 Biochemistry, Biofunctionalisation and Sensor Characterisation

This chapter investigates the proteins and peptides used to study phosphorylation. It also describes the conventional biochemical assay, the western blot, performed to observe phosphorylation of proteins. The biofunctionalisation of silicon nitride surfaces for protein immobilization as well as pH variations on silicon nitride will be discussed. The silicon nitride substrates were silanised to create protein-binding groups on their surface and subsequently the protein or the enzyme was immobilised to enable the desired biochemical reaction. The chemical activity of glucose oxidase, i.e. oxidation of glucose by glucose oxidase, was quantified on Si_3N_4 by measuring the change in pH after the reaction. This reaction was performed to check whether experimental concerns over the efficiency of the different silanisation reagents, enzyme and protein immobilisation and the measurement technique were justified. Further pH measurements on silicon nitride using a range of pH buffers and the capacitance-voltage (CV) characteristics are presented. Colorimetric assays used to validate the experimental analysis are also demonstrated.

3.1 Myelin Basic Protein

In this study myelin basic protein (MBP) is used for phosphorylation studies. MBP is a membrane protein of the central nervous system that plays a crucial role in the myelination of nerves. Phosphorylation of MBP is essential for maintaining the physiological stability of the myelin sheath [1]. However, abnormal phosphorylation of MBP is associated with multiple sclerosis [2]. Phosphorylation of MBP is mediated by the enzyme called as Protein Kinase-C alpha (PKC-α) in the presence of PKC-α kinase activator [3]. Dephosphorylated MBP, purified from bovine brain using FPLC liquid chromatography, was purchased from Millipore. MBP has 170 amino acids (aa) with a molecular weight of around 19 kDa. Given below is the structure and sequence

of MBP. The sequence shows that there are 18 serine amino acids and 7 tyrosine amino acids available for the phosphorylation.

a)

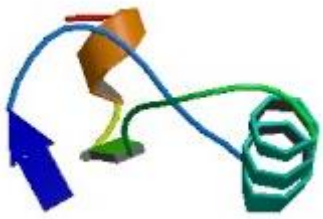

b)

10 20 30 40 50
AAQKRP**S**QR**S** KYLA**S**A**ST**MD HARHGFLPRH RD**T**GILD**S**LG RFFG**S**DRGAP
60 70 80 90 100
KRG**S**GKDGHH AAR**TT**HYG**S**L PQKAQGHRPQ DENPVVHFFK NIV**T**PR**T**PPP
110 120 130 140 150
SQGKGRGL**S**L **S**RF**S**WGAEGQ KPGFGYGGRA **S**DYK**S**AHKGL KGHDAQG**T**L**S**
160
KIFKLGGRD**S** R**S**G**S**PMARR

Figure 3-1 a) 3D structure of myelin basic protein (MBP); Source: ModBase b) sequence of MBP; Source: Uniprot.

3.2 Peptides

Protein phosphorylation studies were also done on peptides. A peptide is a smaller molecule than protein with 50 or fewer amino acids [4]. Two peptides were synthesised to study the kinase activity. Both peptide-1 (NH2-CRRRKGSFRRKK-COOH) and peptide-2 (NH2-RRRKGSFRRKK-COOH) were prepared with one phosphorylation site (serine amino acid). The only difference between peptide-1 and peptide-2 was the presence of an extra amino acid, cysteine, in peptide-1. The composition of both peptides was confirmed using mass spectroscopy studies. The purity levels of the prepared peptides were found to be above 85%, which was revealed by high performance liquid chromatography (HPLC).

3.3 Western blot

Western blot is an analytical technique commonly used by biochemists to determine the proteins within a sample. Phosphorylation of MBP was carried out in a buffer solution and was detected using this conventional immunoblot technique. This technique was mainly used to optimise the reaction conditions. For instance, the amount of kinase to be used and to identify a suitable buffer strength for the phosphorylation on the semiconductor structures. Optimising buffer strength was crucial for the experiments since the aim was to measure pH changes associated with phosphorylation on silicon nitride. When measuring pH changes associated with a biochemical process, a low strength of buffer is required so that the local pH changes occurring in the solution are not masked by the buffer.

Phosphorylation of MBP (in solution) was carried out in "complete reaction buffer" (1 mM Tris base, pH 7.4, 30 mM NaCl and 2 mM $MgCl_2$) and "low ionic strength buffer" (0.2 mM Tris base, pH 7.4, 6 mM NaCl and 0.4 mM $MgCl_2$). The entire reaction volume was fixed to 100 μl for all replicates and controls. 1 μM ATP and 4 units of PKC-α (1 unit per 25 μl) were subsequently added. To initiate the phosphorylation reaction, 5 μl of PKC lipid (1:20 of reaction volume) activator containing 0.5 mg/ml phosphatidylserine and 0.05 mg/ml diacyglycerol in 20 mM MOPS (pH 7.2), 25 mM β-glycerol phosphate, 1 mM sodium orthovanadate, 1 mM dithiothretiol and 1 mM $CaCl_2$, was added. Two sets of control reactions were performed, one without PKC lipid activator and the other with 0.1 μM PKC kinase inhibitor (GF 109203X), and were added before introducing the kinase activator.

Now 10 μl of reaction samples of phosphorylation and controls per lane were subjected to 12% acrylamide SDS-PAGE. The proteins were electrophoretically transferred to a polyvinylidene fluoride (PVDF) membrane. Washing and hydration of membrane was done using TBST buffer. Membranes were incubated at 4 ºC for 24 hours with phospho-(Ser) PKC substrate antibodies (1:1000) or 2 hours at room temperature with an anti-MBP antibody. A species-specific HRP-linked secondary antibody was then incubated for 45 minutes at room temperature. Enhanced chemiluminescence (ECL) method was used to detect the immunobands on the membranes. Stepwise procedure of the western blot is described in the following section Appendix-1.

3.3.1 Results of immunoblot detection

Figure 3-2 shows two gels that were run with six lanes each, with phosphorylation reaction and its control. Lanes 2 to 6 had 10 μl of complete phosphorylation reaction with MBP, kinase and its activator. The difference between the lanes was in the buffer strength and its composition: reaction in the lane 2 was done in 5 mM Tris base, pH 7.4, 150 mM NaCl and 10 mM MgCl2; lane 3 reaction buffer was identical to lane 2 except it had 5% of bovine serum albumin (BSA); lanes 4 and 5 differed from lane 2 and 3 by using 1/5 of the amount of each component. Therefore the only difference was that the phosphorylation reaction in lane 4 and 5 was carried in 1 mM Tris base, pH 7.4, 30 mM NaCl and 2 mM $MgCl_2$, with and without BSA. Lanes 1 and 6 had the control reactions: lane 1 was without kinase and lane 6 was without kinase activator. One gel was developed with phospho-tagged antibodies and other gel was developed with myelin basic protein antibodies. Figure 3-2 A shows the data for phosphorylation of MBP.

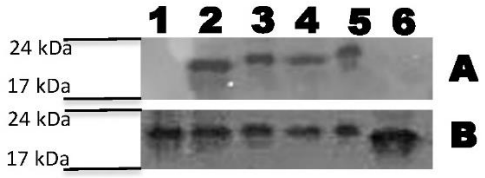

Figure 3-2 Western blot: A) phosphorylation reaction blot; B) protein check blot; lanes 1-6 differ only in the buffer composition and strength, 1: complete buffer without kinase, 2: complete buffer with complete reaction, 3: complete buffer + BSA with complete reaction, 4: low ionic strength buffer with complete reaction, 5: low ionic strength buffer + BSA with complete reaction, 6: complete buffer without kinase activator : complete buffer was composed of 150 mM NaCl, 5 mM Tris pH 7.4 and 10 mM MgCl2. low ionic strength buffer was composed of 30 mM NaCl, 1 mM Tris pH 7.4 and 2 mM MgCl2

Luminescent bands were observed between 17 and 24 kDa, since MBP has a molecular weight of 18.2 kDa. No luminescence was observed in lanes 1 and 6 as shown in figure 3-2 A. After removing phospho-specific antibodies from the same blot, it was run with MBP antibodies to check whether MBP was present in lanes 1 and 6. Western blot on figure 3-2 B shows that MBP was present in all lanes. These results are consistent with the fact that phosphorylation of MBP was due to PKC-α kinase. It also depicts that PKC-α lipid activator is essential for activating kinase. In

addition we concluded that our 'low ionic strength' buffer had the right composition to perform phosphorylation of proteins.

3.4 Silicon Nitride as a pH sensor

pH is defined as the amount of hydrogen ions present in the aqueous solution which determines its acidity or basicity. Mathematically it is the negative logarithmic of hydrogen ion concentration in a solution. A large number of chemical reactions involve a change in pH on completion. This creates a need of developing pH-sensitive materials for understanding various chemical and biological reactions that involve a change in pH. One such material is silicon nitride. Silicon nitride based sensors have been used extensively in the development of ion-sensitive field effect transistors [5]. In Si_3N_4 based ISFETs, the gate of the transistor is made up of Si_3N_4 which modulates the channel current depending upon the charge that imbibes on the surface at a particular pH.

In this research the pH is detected on the silicon nitride as a change in the depletion capacitance of an electrolyte-insulator semiconductor (figure 3-3). Silicon wafers with 50 nm of SiO_2 and 100 nm of Si_3N_4 deposited by plasma-enhanced chemical vapour deposition (PECVD) were obtained from the University of Cambridge. Prior to the use, wafers were cleaned using RCA cleaning and then aluminium was deposited as a back contact. The detailed steps of RCA cleaning are described in Appendix-1.

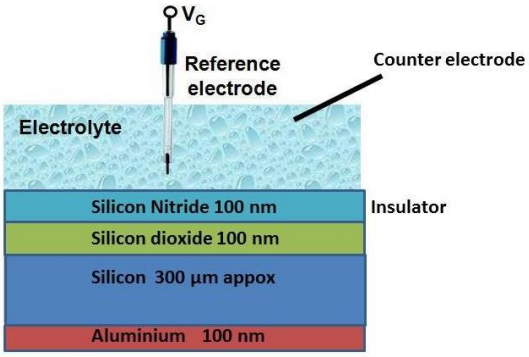

Figure 3-3 Electrolyte-insulator semiconductor (EIS) structure used for pH measurement.

After cleaning the silicon nitride surface becomes good for detecting pH changes. The detection mechanism is similar to the operation of field effect transistor (FET). The

difference lies in the removal of metal layer from the gate of FET and the dielectric layers under it come in direct contact with the electrolyte, whereby ions get adsorbed on the surface. This creates a conducting layer on the surface of the insulator and generates a similar effect to applying a gate voltage to a FET [6]. In particular, it can be explained by site binding theory, which relates solid-liquid interface potential to local pH changes in the solution [7] [8]. At the interface the Si_3N_4 surface has active sites in the form of neutral surface hydroxyl (SiOH) groups. The release of H^+ ions from a chemical reaction (for example upon phosphorylation of protein there is a release of a proton from every amino acid that gets phosphorylated) or the measure of H^+ ion in a solution of particular pH is captured by SiOH groups until thermodynamic equilibrium is established between SiOH and H^+ ions released in the bulk electrolyte solution, as shown by the reaction

$$SiOH_2^+ \leftrightarrow SiOH + H^+$$

After the hydrogen ion is captured by the silicon nitride, the surface potential of the structure changes. If this structure acts as the gate of the transistor, gate to source voltage of the transistor would also change. Equation 1.1 [9] below shows the dependence of the semiconductor surface potential (ϕ_s) on the hydrogen ion concentration:

$$\phi_s = -\frac{C_1}{C_h}(E_1 d_2 + E_2 d_2) + \phi_d + \frac{qN_{sil}}{C_h}\left\{\frac{[H_s^+]^2 - K_+K_-}{[H_s^+]^2 + K_+[H_s^+] + K_+K_-}\right\} + \frac{qN_{sil}}{C_h}\left\{\frac{[H_s^+]^2 - K_+K_-}{[H_s^+] + K_{N+}}\right\} \quad (1.1)$$

where C_1 is the accumulation capacitance due to the two dielectric layers, namely Si_3N_4 and SiO_2 in the structure that has been used (see Figure 3-3). $E_{1,2}$ and $d_{1,2}$ denote the electric field and thickness of each dielectric layer. C_h is the Helmholtz layer capacitance per unit area, N_{sil} is the number of silanol sites per unit area and $K_{+/-}$ is the dissociation constant for the chemical reaction at the insulator. It is apparent from the equation that a highly sensitive pH sensor would require a relatively large value of N_{sil}. The presence of two dielectric layers increases the pH sensitivity of the surface [10]. With two dielectric layers, as compared with a single insulator structure with the same concentration of H^+ ions on the surface, higher surface potential is achieved. Hence it is the increase in surface potential that decreases the threshold seen by the

channel at the transistor gate. As a result, at a given voltage the depletion charge increases at higher concentration of H^+ ions.

3.4.1 Capacitance Voltage Characterisation of ElS structure

The surface potential (ϕ_s) on the insulator of EIS structure is measured by capacitance voltage characterisation. In this technique a dc voltage superimposed with a small ac signal is applied across the EIS structure and capacitance of the structure is measured. Figure 3.4 below shows a typical CV curve for n-type silicon substrate. There are 3 distinct regions of the curve 1) inversion 2) depletion and accumulation. The inversion region is formed with minority charge carriers and the accumulation region is the majority carries in the bulk substrate. Ideally when a low frequency ac signal (less than 100 Hz) is applied the saturation values of inversion and accumulation coincide with each, thereby giving the maximum capacitance of the structure [11-14].

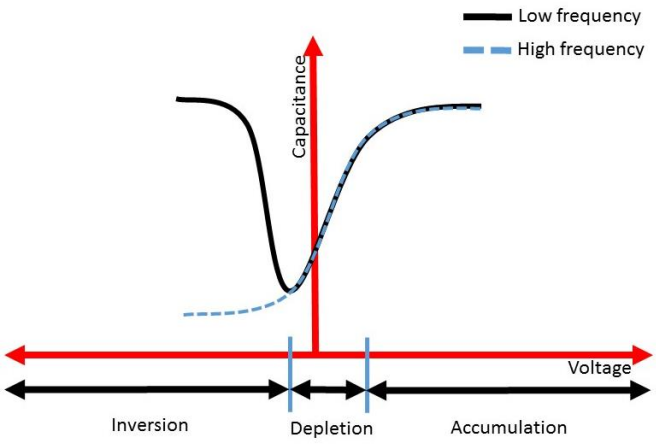

Figure 3-4 Capacitance Voltage characteristics of EIS structure with n-type semiconductor

On increasing the frequency, inversion capacitance decreases because at high frequencies (greater than 1 kHz), the generation rate is not fast enough to allow the formation of a minority carries at the insulator-semiconductor interface. However the accumulation and depletion capacitance remain same. Accumulation capacitance is the intrinsic capacitance of the structure (due to thickness of the insulator) that does get affected due to the small charge on the surface. Any charges on the surface for instance charge of a DNA or a pH change on the surface is reflected in the change of depletion region capacitance.

3.4. 2 Phosphate buffer pH studies on silicon nitride

The effect of phosphate buffer with different ionic strength, salt concentration and different pH was studied on a silicon nitride surface. The silicon nitride coated wafer was sandwiched between a Teflon well and a lower conductive copper plate, Figure 3-5, so that the aluminium coated side of the wafer sat on the lower conductive plate. This formed a planar Si_3N_4 well with 19.64 mm^2 interrogation area for the reaction defined by the size of the o-ring (5 mm diameter). The capacitance-voltage measurements were taken using a potentiostat with Ivium software.

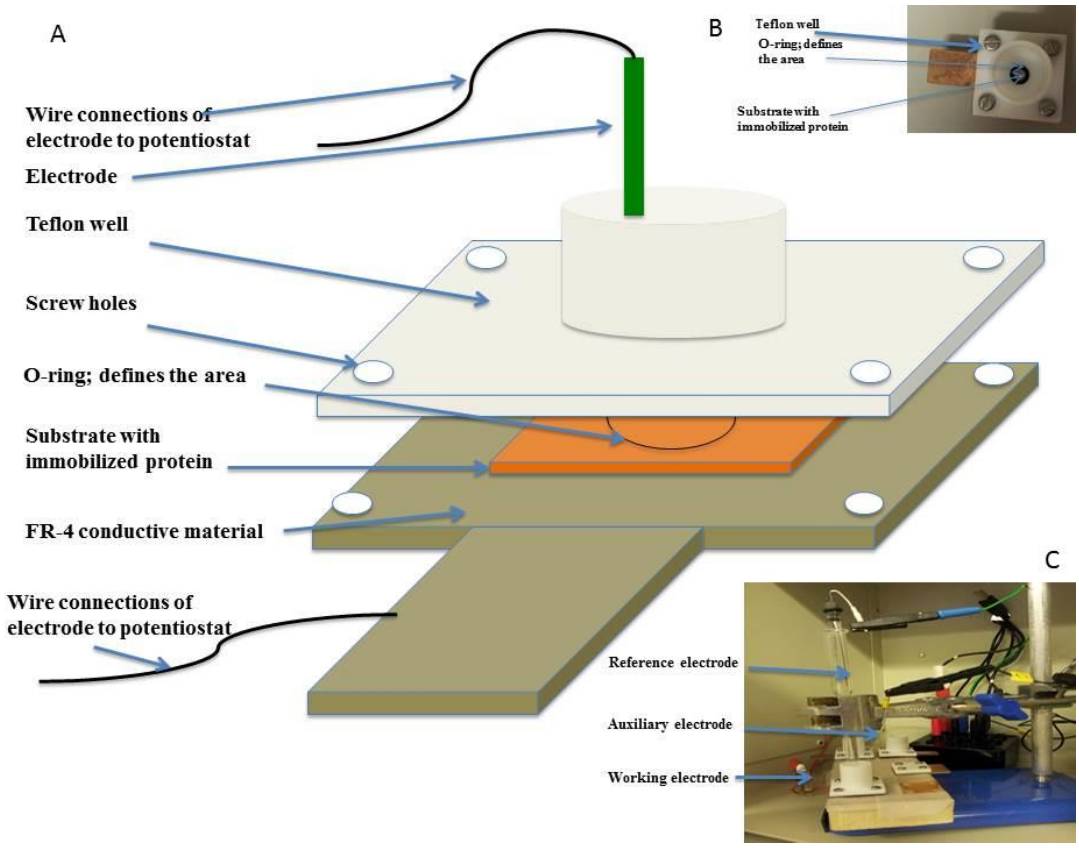

Figure 3-5 Scheme for pH measurement A) Cartoon showing detailed structure of a well (reaction cell) that sandwiches the wafer in a way that enables 3-electrode electrochemical measurement on it. B) top view of the well. C) 3-electrode electrochemical setup connections from potentiostat integrated with the well inside a faraday cage

To start with, phosphate buffers of decreasing pH 7.6, 7.0, 6.6 (10 mM) were used to study the capacitance changes on Si_3N_4 at 10, 100, 1000 Hz respectively. Buffers were prepared by mixing monobasic and dibasic solutions of phosphate in a certain ratio. It

was observed that the curves were more reproducible at 1000 Hz, so the measurements of the phosphorylation reactions are done at 1000 Hz in later stages of the project.

A)

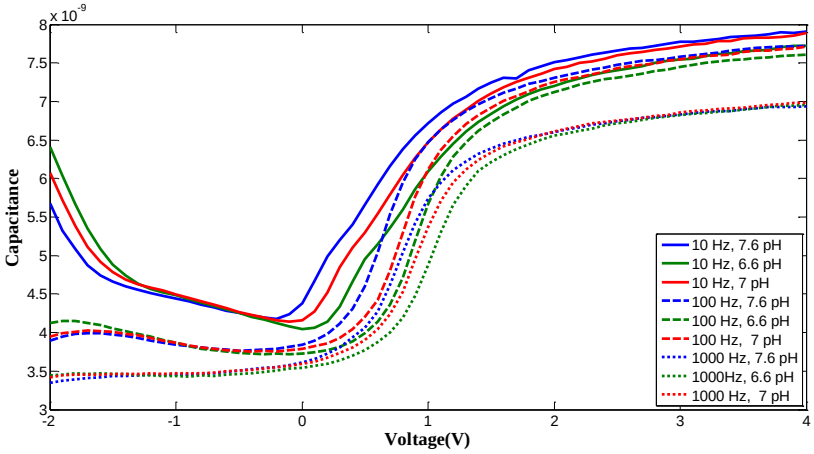

B)

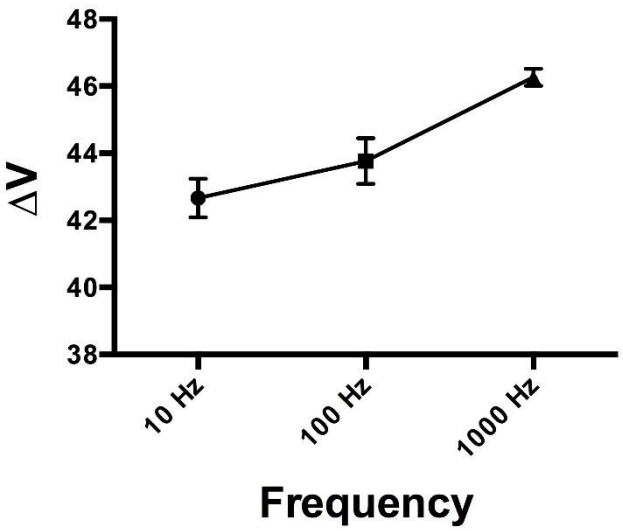

Figure 3-6 A) Curves at different pH (phosphate buffer 10 mM at 7.6, 7.0 and 6.6 and pH) and at different frequencies (10 Hz, 100 Hz and 1000Hz) B) Sensitivity of pH measurements at different frequencies i.e. Change in voltage per pH.

Figure 3-6 (A) shows curves at different pH and different frequencies. The pH sensitivity at 1000 Hz was around 46 mV/pH as compared to 44 mV/pH and 43 mV/pH at 10 Hz and 100 Hz, Figure 3-6 (B). Three successive readings were taken one after

another (e.g. at 6.6, 7.0, 7.6, 6.6, 7.0 and so on) to see the reproducibility and average values are reported here.

Another study was carried out to check the effect of ion-concentration on pH sensitivity of silicon nitride. Phosphate buffer of 5 mM, 10 mM and 20 mM concentrations, were prepared and it was observed that at low ionic strength the silicon nitride surface reveals slightly higher sensitivity. An increase of 4% sensitivity is seen with 5 mM phosphate buffers at different pH concentrations at 1000 Hz. Although the readings are repeatable in a single substrate, we found that our measurements were not very reproducible from substrate to substrate. This was attributed to the fact that the cleaning of the samples could vary from sample to sample which made the surface unstable.

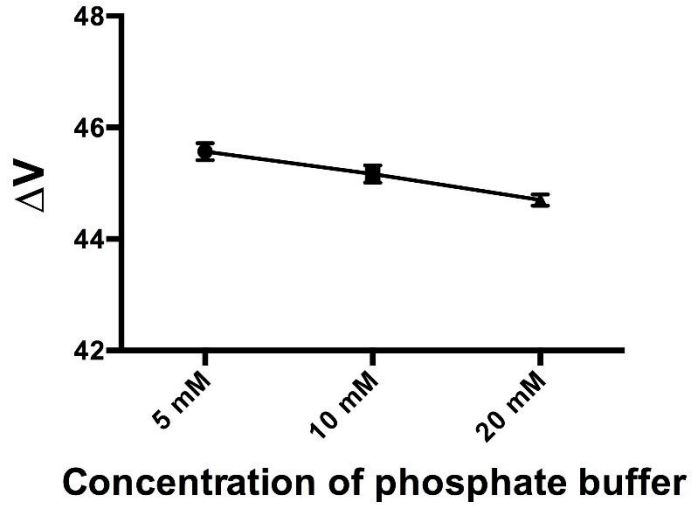

Figure 3-7 Sensitivity of silicon nitride with different molar strengths of phosphate buffer

To see whether stabilisation was an issue, pH was measured after silanising (section 3.5) the surface of silicon nitride with 3-Glycidyl-oxy-propyl-trimethoxy silane (GOPTS).

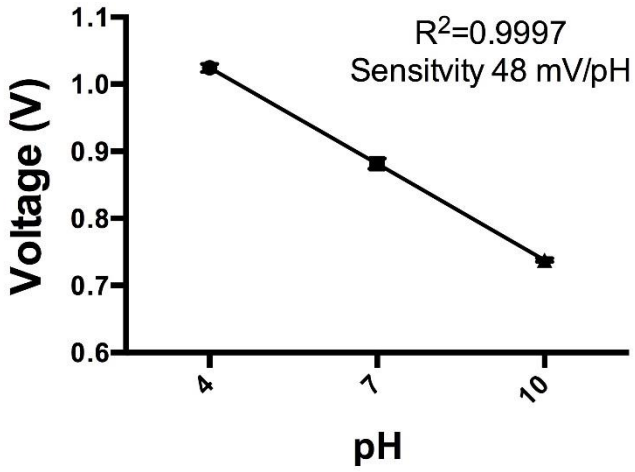

Figure 3-8 Sensitivity analysis for measured pH after silanising the surface of silicon nitride

An increase in pH sensitivity of the substrate was seen (see Figure 3-8 with 5mM phosphate buffer). In addition the reading was reproducible from one substrate to another.

3.4.3 Tris buffer pH studies on silicon nitride

Change in pH by using a range of Tris buffers was also measured on silicon nitride. The experimental setup was similar to the one followed for the pH studies with phosphate buffer (section 3.4.1). Tris buffer was prepared by using Tris HCl, $MgCl_2$ and NaCl with different concentrations of reagents. The buffer mentioned earlier in section 3.3, namely "low ionic strength buffer" was used for the pH studies. Since it was already confirmed that biofunctionalisation of silicon nitride stabilises the surface, GOPTS was used to silanise the surfaces before measuring voltage change caused by pH. The analysis for pH between 8.8 and 7.2 revealed a higher sensitivity between 52.72- 49.69 mV/pH as shown in Figure 3-13 as compared to 48 mV/pH achieved with phosphate buffer. The main reasons for this are the different ionic composition of the Tris buffer and lower buffer strength of 0.2 mM compared to 5 mM of phosphate buffer.

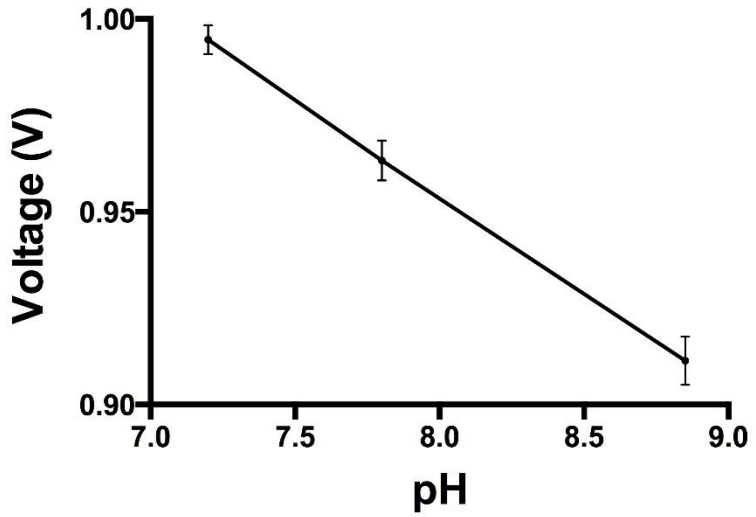

Figure 3-9 sensitive analysis for measured pH after silanising the surface of silicon nitride (pH measurement with Tris buffer)

3.5 Silanisation of Silicon Nitride

Silicon nitride was used for the measurement of pH change caused by the biochemical reaction. To avoid non-specific protein adsorption on Si_3N_4, silanisation that provides suitable covalent binding of proteins is performed on the surface of Si_3N_4. Therefore silanisation employs efficient binding of proteins on the sensing surface much like Si_3N_4. Biofunctionalisation of the Si_3N_4 surface was tested with 2 silane compounds (aminopropyltrimethoxysilane, APTES, and glycidoxypropyltrimethoxysilane, GOPTS) as well as hydrogen peroxide (H_2O_2). APTES is has a terminal amine group whereas GOPTS has an epoxy residue for further complex reactions.

Prior to silanisation, wafers were cleaned using RCA procedure described in Section 3.4. It is important to note that the RCA cleaning is avoided on the wafers with aluminium as a back contact. This is because HCl removes inorganics from the wafer and would remove the aluminium, possibly leading to contamination of the top surface (silicon nitride) of the wafer. Wafers with a metallic back contact were thoroughly rinsed with acetone and isopropanol (IPA) following a rinse in DI water. The substrate preparation and silanisation protocols for preparing Si_3N_4 surface for immobilisation of the protein are given in Appendix-1.

3.6 Confirming protein immobilisation TMB assay

Anti-protein A (antibody for protein A) were used to validate protein immobilisation using TMB (3,3´,5,5´-tetramentylbenzidine) assay. The samples are incubated with 0.25 μg μl^{-1} of antibody linked with horseradish peroxidase (HRP) and then washed with PBS. 200 μl of TMB, T-4444 (3,3´,5,5´-tetramentylbenzidine) solution is dispensed on the Si_3N_4 surface and the samples are incubated at room temperature for 20 minutes until a distinct and stabilised colour change (usually blue at Amax = 370nm and 652nm) is observed. If the reaction progresses quickly and the colour change does not stabilise after 10 minutes, it can be stopped by adding 50 μl of 2 M sulphuric acid. Absorbance should then be measured at 450 nm. A low-volume spectrophotometer was used (Genova Nano, Jenway Biotech, USA) to detect colour changes caused by horseradish peroxidase (HRP) activity.

3.7 Comparative protein immobilisation TMB assay

The protocols described above are the optimised methods for silanisation. However, varied numbers of experiments with different conditions (incubation time and concentration of reagents) were done to obtain the optimum conditions. This section will discuss the results and the experimental details of the analysis done to arrive at these optimised conditions.

Figure 3-10 shows the wavelength vs. absorbance characteristics of protein immobilised on the APTES/ glutaraldehyde (GA) modified silicon nitride surface. On treating the surface with TMB, the dye changed its colour from transparent to blue. Spectral analysis showed two peaks, one at 370 nm and the other at 650 nm, which confirmed the presence of HRP-linked antibody on the sample.

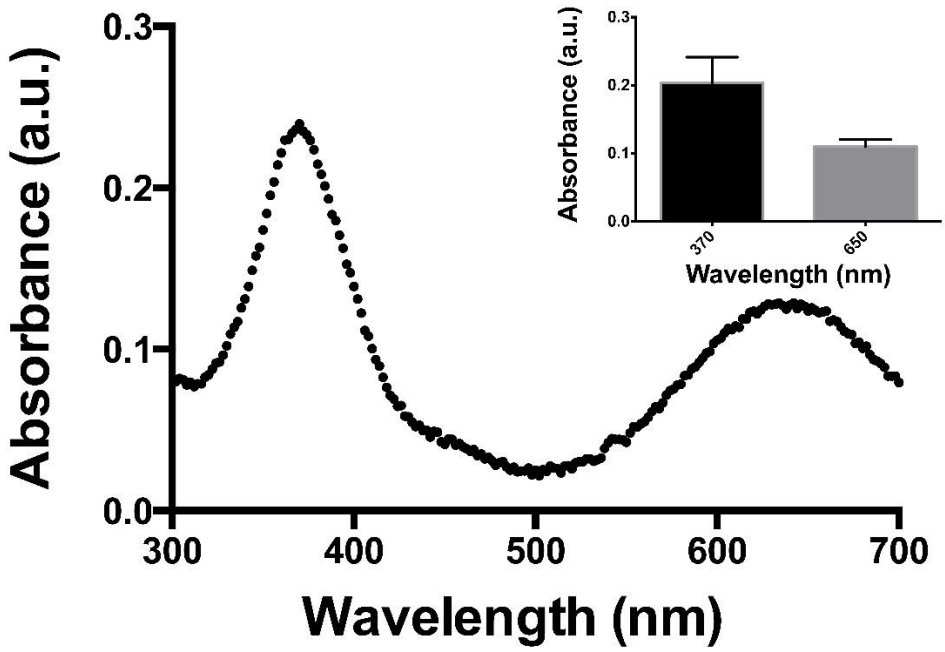

Figure 3-10 Absorbance vs. wavelength plot for protein immobilization on APTES/GA modified silicon nitride

To check, weather the HRP-linked antibodies were covalently attached to the self-assembled monolayer of APTES/GA, four control reactions were performed (Figure 3-11). The first control reaction was to block all sites of glutaraldehyde (GA) with 0.2 M ethanolamine for 30 minutes before adding protein. The second control was performed without APTES to see if GA binds non-specifically to the silicon nitride surface. The third was with similar conditions as the second except that it was done on a silicon surface to check if GA binds non-specifically to the silicon (since the

backside and the sides of the wafers were silicon). The fourth control was performed by immobilising proteins directly on the surface of the silicon nitride with APTES/GA.

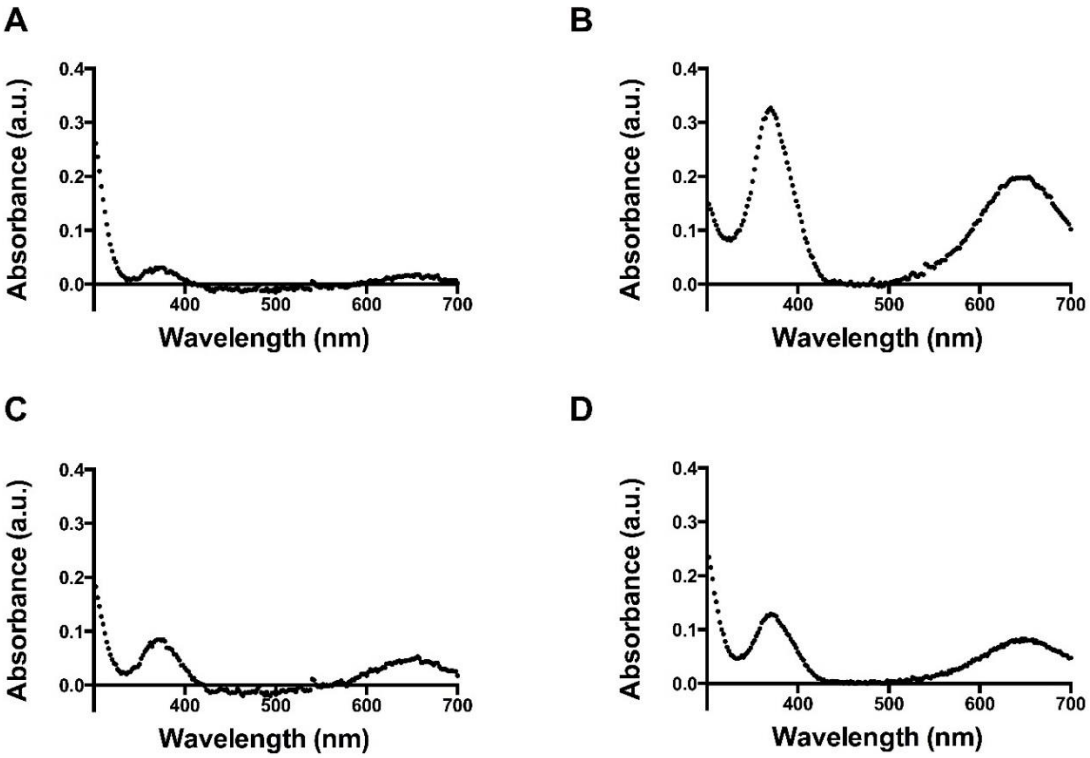

Figure 3-11 A) Control reaction where glutaraldehyde layer was blocked by 0.2 M ethanolamine for 30 minutes before adding protein B) non-specific binding of GA on silicon nitride C) non-specific binding of GA on silicon D) immobilizing proteins directly on the surface of the silicon nitride

Figure 3-11 A confirms that the peaks seen on Figure 3-10 were due to the presence of protein. It is also seen that there is some non-specific binding of GA and proteins on the silicon nitride surface which will be a critical issue in getting reproducible assembled monolayers of proteins. Figure 3-12 shows the results of protein immobilisation upon silanisation with GOPTS. The epoxy group on one end of GOPTS binds to the amine group of the protein.

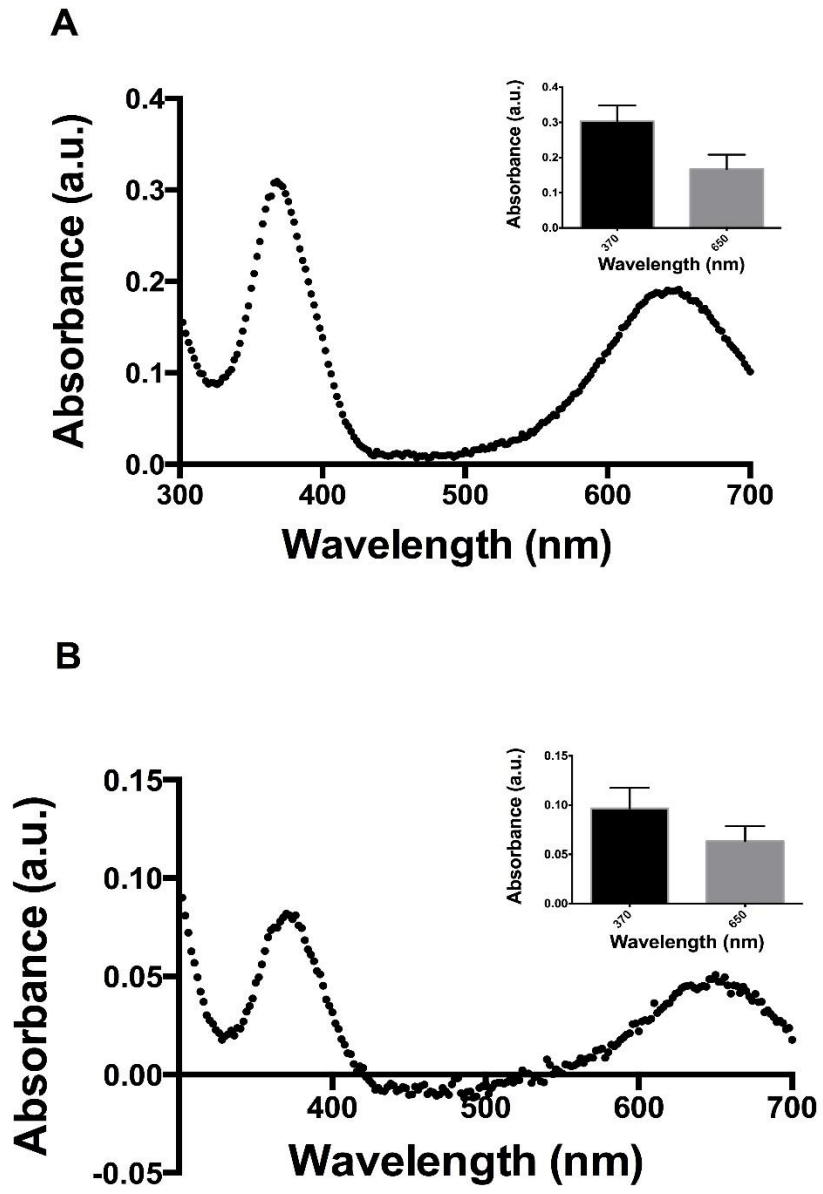

Figure 3-12 A) Protein immobilization on silicon nitride, 98% GOPTS in aqueous solution B) Protein immobilization on silicon nitride, 49% GOPTS aqueous solution.

As seen from the figure above, that higher the concentration of GOPTS (as seen in 98% concentration compared to 49% in aqueous solution), the greater the amount of protein that becomes immobilised on the surface of the silicon nitride. Almost twice the amount of absorbance is seen when the concentration of GOPTS in solution is doubled for silanising the silicon nitride surface. One advantage of using GOPTS over APTES for protein immobilisation is that it avoids the use of a cross-linking polymer like GA. This could possibly reduce the non-uniform distribution of proteins due to

non-specific binding of GA when APTES is used as silanisation compound. This is because it is also observed that protein immobilisation with GOPTS was slightly more reproducible than with APTES.

A control reaction, where the epoxide groups of GOPTS where subjected to alcohol to form an ether-based product was performed. After treating the sample with GOPTS, the surface was treated with ethanol and it was observed that protein A antibody linked with HRP did not bind to the substrate, Figure 3-13.

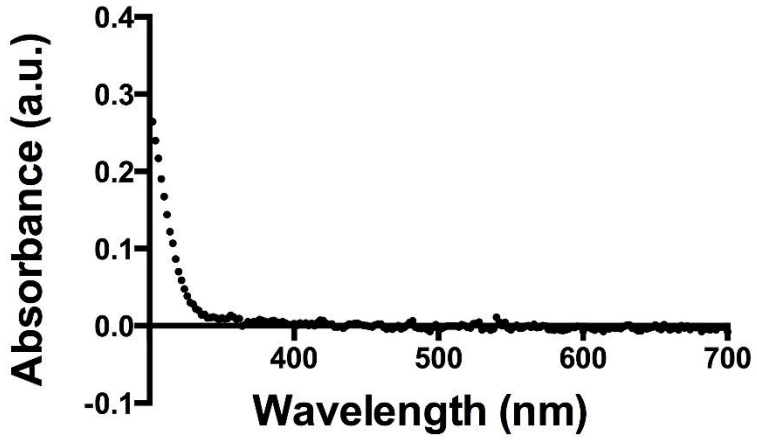

Figure 3-13 Protein immobilisation on silicon nitride after GOPTS was subjected to 20% ethanol

A new method of immobilising protein on silicon nitride surface by treating its surface with hydrogen peroxide was also explored. It was observed that by treating the silicon nitride with hydrogen peroxide there is a formation of primary amine groups on its surface, Figure 3-14. Ideally distinct peaks should be seen between 3700-3300 cm^{-1} with FTIR (Fourier transform infrared spectroscopy) analysis for primary amines. The results did not show any distinct peak corresponding to primary amine; but clusters of small peaks were observed between 3700-3300 cm^{-1}. In addition a lower amount of transmission in the same band was observed. One conclusion that can be made is that that a hydrogen ion has been added to the already present N-H groups in silicon nitride. Therefore the formation of primary groups, if any, absorbs greater amounts of light and hence transmission decreases after hydrogen peroxide treatment.

Silicon nitride forms primary amine groups on its surface in the presence of hydrogen source, and hydrogen peroxide undergoes a disproportionation reaction, i.e.

simultaneous reduction and oxidation. It is an excellent source of hydrogen both in reduced and as well as oxidised states.

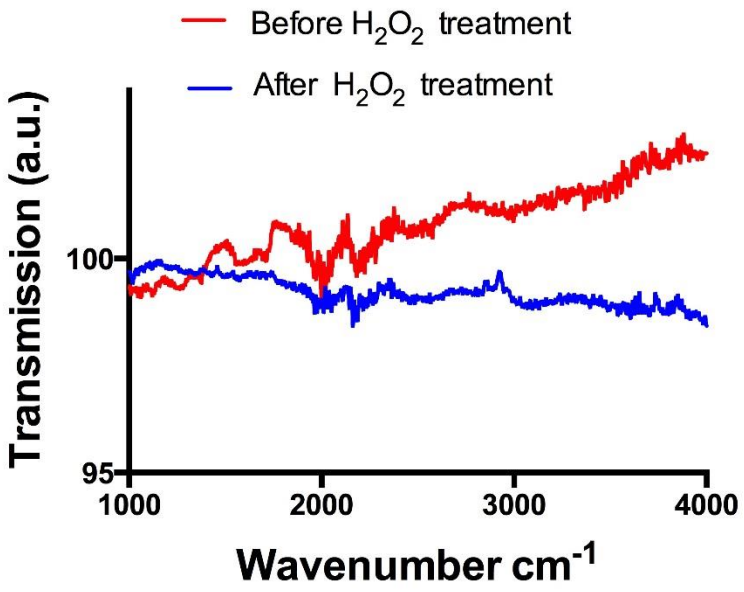

Figure 3-14 FTIR analysis of silicon nitride treated with hydrogen peroxide showing presence of amine groups

H_2O_2 undergoes disproportionation as follows.

- H_2O_2 as a reducing agent

$H_2O_2 \rightarrow 2H^+ + 2e^- + O_2$

- H_2O_2 as an oxidising agent

$H_2O_2 + 2H^+ + 2e^- \rightarrow 2H_2O$

The water formed after reduction of H_2O_2 is highly reactive and can undergo a further reaction with reduced silicon nitride as shown below

$Si_3N_4 + 2H_2O \rightarrow 2SiNH_2 + N_2 + SiO_2$

$2\ Si_3N_4 + 4\ H_2O \rightarrow 2SiNH_2 + 3N_2 + 4SiOH$

To immobilise proteins, the surface of the silicon nitride was treated with GA to form Schiff's base (N=C) and its aldehyde group subsequently immobilises the protein. Figure 3-15 and Table 3.1 shows the comparative absorbance characteristics after TMB assay of APTES, GOPTS and a H_2O_2 modified substrate.

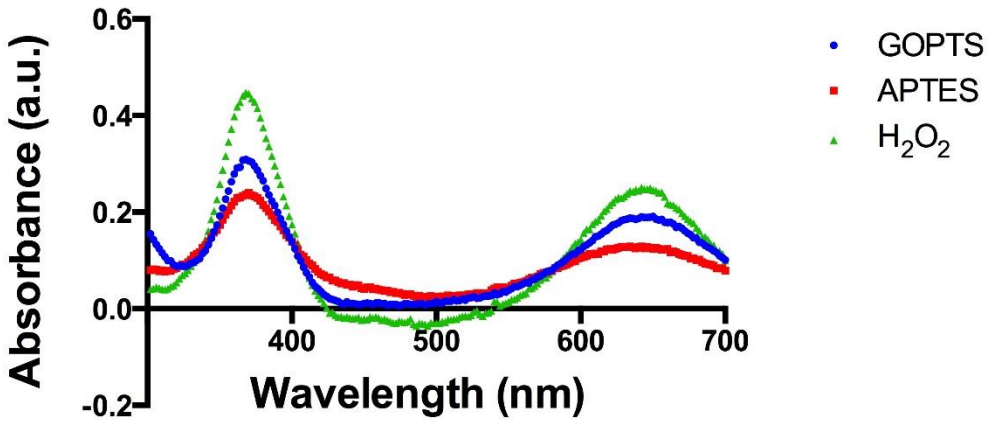

Figure 3-15 Comparison of absorbance characteristics after TMB assay on APTES, GOPTS and H_2O_2 modified silicon nitride for protein immobilisation.

Table 3-1 Average absorbance values (n≥ 3) characteristics after TMB assay on APTES, GOPTS and H_2O_2 modified silicon nitride for protein immobilisation.

Experiment	***Average absorbance***
APTES--Glutaraldehyde	0.148
APTES--Glutaraldehyde--Ethanolamine	0.021
Glutaraldehyde	0.327
Direct protein on Silicon Nitride	0.085
Si--APTES--Glutaraldehyde	0.129
GOPTS-49%	0.094
GOPTS-98%	0.250
GOPTS Control Rx. -98%	0.004
3 h Hydrogen Peroxide 8.25%	0.435
24h Hydrogen Peroxide 8.25%	0.030
24 h Hydrogen Peroxide 11.67%	0.083
24 h Hydrogen Peroxide 17.5%	-0.015
3 h Hydrogen Peroxide Control Rx.-8.25%	-0.020

From the table above it can be concluded that silicon nitride surfaces treated with hydrogen peroxide allows increased amounts of protein to be immobilised when

compared to APTES and GOPTS. In addition, it also shows that the formation of primary amines is time and concentration dependent. With higher concentrations of hydrogen peroxide, its time of exposure on silicon nitride should be reduced. If the sample is treated with higher concentrations of hydrogen peroxide for extended durations the surface becomes over-oxidised and results in the delamination of the nitride layer leaving a rough surface as shown in Figure 3-16.

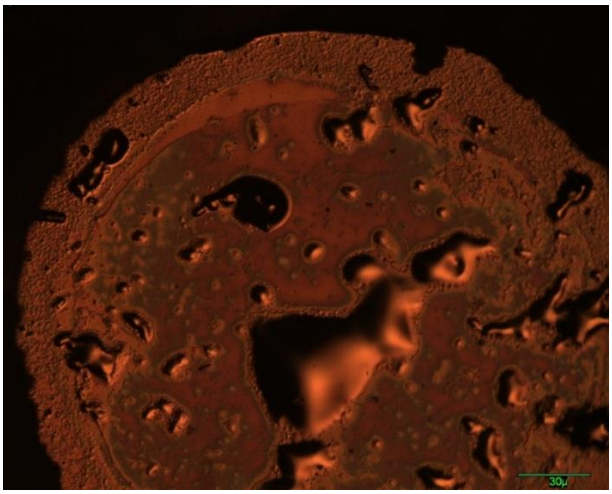

Figure 3-16 50 X silicon nitride surface after treating with 8.25% hydrogen peroxide for 24 hours in aqueous solution

3.8 pH change detection in biochemical reaction (a case study of glucose oxidase activity)

The oxidation of glucose into its metabolites is carried out by glucose oxidase. Glucose oxidase activity results in the breakdown of sugars into gluconic acid and hydrogen peroxide. After products are formed a decrease in overall pH of the reaction due to the formation of acidic molecules was expected. The reaction was performed in the same wells as described in previous sections. The glucose oxidase was immobilised on the silicon nitride surface and then glucose was added in solution to initiate the reaction. Prior to this reaction, an enzyme stability test was performed and the effect of pH change on the charge of enzyme was also studied. The enzyme stability test was done to check the stability of the silicon nitride surface after immobilising the enzyme. First the enzyme was immobilised using GOPTS and then measured pH of the solution at pH 7 PBS. A maximum change of 5 mV was observed in capacitance-voltage

measurements after the reaction was prolonged for 2 hours (Figure 3-17). This change was observed during the first 5 minutes of the reaction. From this experiment it was concluded that to measure a reliable reading from our sensor surface, one should wait for 5 minutes for the reaction to become stabilised before measuring any response from the sensor.

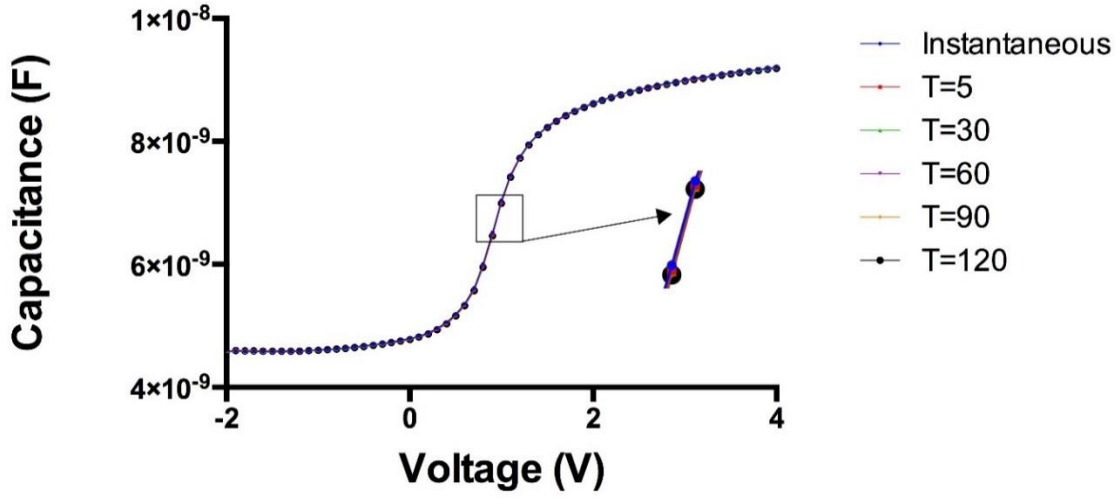

Figure 3-17 Glucose oxidase stability analysis on silicon nitride.

After performing the stability test, the silicon nitride was tested with a set of different pH solutions (at 6.6, 7.0, 7.4 pH PBS). The theoretical charge of the enzyme in this pH range, changes from 3.3 to -4.1 due to a very low sensitivity of the surface (27 mV/pH) after immobilising the enzyme, Figure 3-18.

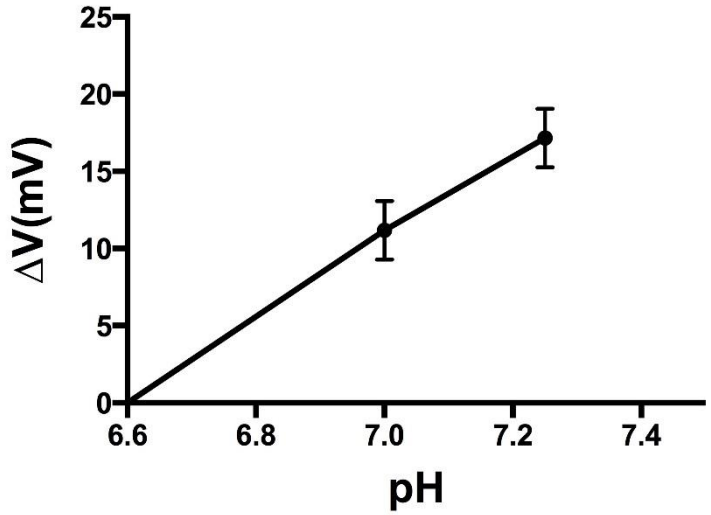

Figure 3-18 effect of change in charge of the enzyme due to change in pH

Finally oxidation of glucose by the glucose oxidase enzyme (8.5 units) with different concentrations of glucose was performed. It was observed that 8.5 enzyme units becomes completely consumed with a 20 mM enzyme concentration. The change in voltage is attributed to the change in pH. An increase in the depletion region voltage was seen while performing CV characterisation. Figure 3-19 shows the depletion voltage increasing with concentration of glucose.

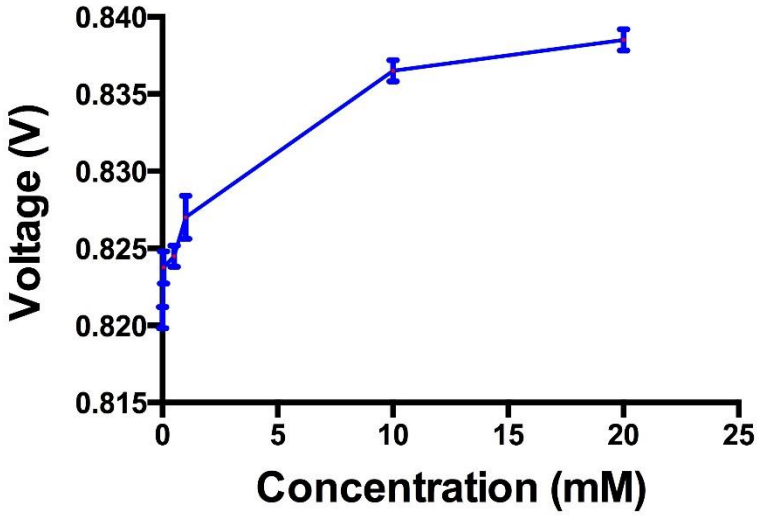

Figure 3-19 Change in depletion voltage with concentration of glucose

3.6 Conclusions

This chapter showed that pH changes associated with a chemical reaction on silicon nitride can be detected. The protein immobilisation techniques were experimentally validated. In general, the results served as a backbone for performing protein phosphorylation on EIS based structures. An interesting and exciting phenomenon witnessed was the way hydrogen peroxide assists protein immobilisation on silicon nitride. It is believed that understanding the detailed science behind the phenomenon is beyond the scope of this research, therefore we proceed further with protein phosphorylation reactions on silicon nitride.

References

[1] J. M. Boggs and J. M. Boggs, "Myelin basic protein: a multifunctional protein" *Cellular and Molecular Life Sciences*, vol. 63, pp. 1945–1961, 2006.

[2] J. K. Kim, F. G. Mastronardi, D. D. Wood, D. M. Lubman, R. Zand, and M. A. Moscarello, "Multiple sclerosis: an important role for post-translational modifications of myelin basic protein in pathogenesis" *Molecular Cell Proteomics* vol. 2, pp. 453–462, 2003.

[3] S. Nakashima, "Protein kinase C alpha (PKC alpha): regulation and biological function" *Journal of Biochemistry*, vol. 132, pp. 669–675, 2002.

[4] M. Aguilar, *TM HPLC of Peptides*, vol. 251, pp. 3–8, 2004.

[5] B. D. LIU, Y. K. SU, and S. C. CHEN, "Ion-sensitive field-effect transistor with silicon nitride gate for pH sensing," *International Journal of Electronics*, vol. 67. pp. 59–63, 1989.

[6] F. Yan, P. Estrela, Y. Mo, P. Migliorato, H. Maeda, S. Inoue, and T. Shimoda, "Polycrystalline silicon ion sensitive field effect transistors," *Applied Physics Letters*, vol. 8, pp. 053901 1-4, 2005.

[7] R. E. G. van Hal, J. C. T. Eijkel, and P. Bergveld, "A novel description of ISFET sensitivity with the buffer capacity and double-layer capacitance as key parameters," *Sensors and Actuators B: Chemical* vol. 24, pp. 201–205, 1995.

[8] M.-H. Wu, H.-W. Yang, M.-Y. Hua, Y.-B. Peng, and T.-M. Pan, "High-κ GdTixOy sensing membrane-based electrolyte-insulator-semiconductor with magnetic nanoparticles as enzyme carriers for protein contamination-free glucose biosensing" *Biosensors and Bioelectronics* vol. 47, pp. 99–105, 2013.

[9] A. V. Surmalyan, "Surface potential behavior in isfet based bio-(chemical) sensor," *Armenian Journal of Physics*, vol. 5, pp. 194–202, 2013.

[10] A. V. Surmalyan, "surface potntial behavior of ISFET based bio chemical sensors with two insulator layers in dark and under intensity modulated irradiation," *Armenian Journal of Physsics*, vol. 2, pp. 326–332, 2009.

[11] F, Clifford D., P W. Cheung, and W. H. Ko. "A generalized theory of an electrolyte-insulator-semiconductor field-effect transistor." Electron Devices, IEEE Transactions on 33.1 (1986): 8-18.

[12] O.J. Yong, H.J. Jang, W.J. Cho, and M. S. Islam. "Highly sensitive electrolyte-insulator-semiconductor pH sensors enabled by silicon nanowires with Al 2 O 3/SiO 2 sensing membrane." Sensors and Actuators B: Chemical 171 (2012): 238-24

[13] F. Jacob. "Chemical and Biological Sensors." Handbook of Modern Sensors. Springer International Publishing, 2016. 645-697.

[14] W.M. Hsien, C. H. Cheng, C.S. Lai, and T.M. Pan. "Structural properties and sensing performance of high-k Sm 2 O 3 membrane-based electrolyte–insulator–semiconductor for pH and urea detection." Sensors and Actuators B: Chemical 138.1 (2009): 221-227.

Chapter 4 Protein phosphorylation studies on silicon nitride surfaces

This chapter reports two combined methods to detect the phosphorylation of MBP by PKC-α kinase on silicon nitride. In one method, we employ the use of electrolyte–insulator–semiconductor (EIS) capacitor structures on silicon nitride, to detect the release of protons (H^+) associated with the phosphorylation. Protein phosphorylation is detected in terms of gate capacitance changes at the oxide-semiconductor interface of the EIS structure, as explained by theory in the previous chapters. The changes in pH are also measured using a commercial micro pH electrode to detect the phosphorylation of proteins [1]. The second method combines a localized surface plasmon resonance (LSPR) technique on silicon nitride in addition to the pH sensing [2].

4.1 pH changes associated with protein phosphorylation

Change in pH upon phosphorylation of proteins was studied with the use of adenosine tri-phosphate (ATP) as the source of phosphate. During phosphorylation of proteins, the phosphate group at the γ -position of the adenosine tri-phosphate (ATP) is transferred to the serine, threonine or tyrosine amino acids of the protein and the subsequent proton release was measured on the silicon nitride as shown on the scheme in Figure 4-1. This section will discuss in detail the materials and the experimental procedure.

4.1.1 Reagents

All chemicals were of analytical grade and were used as received, unless otherwise specified. All aqueous solutions were made with double de-ionised water, 18.2 MΩ cm, filtered with a Pyrogard filter (Millipore, USA). Tris base, $MgCl_2$, NaCl, acetone, NH_4OH, HCl, H_2O_2, 3-glycidoxypropyltrimethoxysilane (GOPTS), PKC-α kinase inhibitor GF 109203X, adenosine tri-phosphate (ATP) and 3,3´,5,5´-

tetramentylbenzidine (TMB) were all purchased from Sigma-Aldrich. Dephosphorylated myelin basic protein (MBP), purified from bovine brain using FPLC liquid chromatography, was purchased from Millipore. PKC-α human recombinant kinase produced in Sf9, was procured from ProSpec-Tany TechnoGene Ltd. The PKC lipid activator cocktail was obtained from Millipore. Polyclonal phospho-(Ser) PKC substrate antibody was purchased from Cell Signalling Technology.

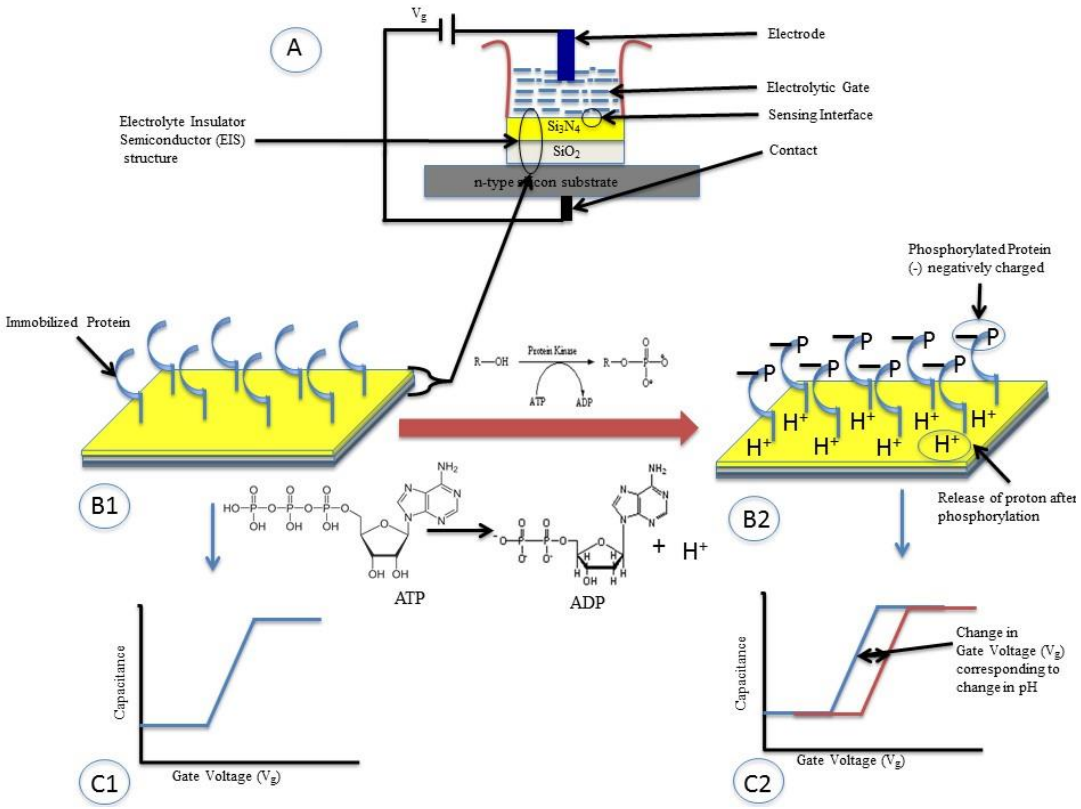

Figure 4-1 Scheme for analysis of protein phosphorylation: A) Field-effect device well for protein phosphorylation measurement; B1) Electrolytic insulator semiconductor (EIS) structure immobilised with protein; B2) Phosphorylated protein (negatively charged) and release of proton; C1) Capacitance vs. Gate Voltage characteristic curve of EIS; C2) Change in Gate Voltage corresponding to change in pH.

Horseradish peroxidase (HRP)-linked anti-rabbit IgG (NA934V) and anti-goat IgG (sc-2020) were purchased from GE Healthcare and Santa Cruz Biotechnology, respectively. MBP Antibody (C-16) goat polyclonal IgG 200 µg/ml (sc-139140) was purchased from Santa Cruz Biotechnology.

4.1.2 Biofunctionalization of Si_3N_4

The dried and acetone-vapour cleaned Si_3N_4 samples were silanised by incubation in 98% 3-glycidoxypropyltrimethoxysilane (GOPTS) in aqueous solution for 45 minutes. Five microliters of 156 μM myelin basic protein (MBP) was dispensed on the silanised Si_3N_4 surface using the Teflon well for 40 minutes, enabling the amino groups of the MBP to attach on the epoxide group of GOPTS. The unreacted GOPTS sites were blocked by incubating the sample in 20% ethanol for 30 minutes. The epoxide converts to ether when reacted with alcohol [3].

4.1.3 Protein phosphorylation on Si_3N_4

The phosphorylation reaction was performed on silicon nitride with the same concentrations as described for the phosphorylation in suspension of 100 μl of volume (Chapter 3). PKC-α activity was measured by analysing capacitance–voltage (*C–V*) characteristics of the $Si_3N_4/SiO_2/Si$ EIS structure. *C–V* measurements were performed using a CompactStat digital potentiostat (Ivium Technologies, The Netherlands). A conventional three-electrode electrochemical setup was employed with an Ag/AgCl reference electrode immersed in the electrolyte *via* a salt bridge, used to apply the gate voltage, and a platinum (Pt) counter electrode. During the measurements, the gate voltage (V_g) (applied between the reference electrode and the Al back-contact) was varied between -2.0 and +4.0 V, superimposed with a small 1 kHz ac signal with an amplitude of 10 mV. The first reaction measurement was taken after adding ATP and the kinase, before the start of phosphorylation process. After adding the kinase activator, the activity of the reaction was studied by recording the *C–V* characteristics every 2 minutes for 10 minutes. Finally the measurements were taken at 20, 40 and 60 minutes after the start of phosphorylation. In control reactions, *C–V* measurements were taken at the same time intervals. Each experiment was repeated at least 3 times and the reported data corresponds to the average values. The maximum observed value of the capacitance, C_{max}, which corresponds to $C_{dielectric}$ (capacitance of silicon nitride and silicon dioxide) does not vary more than 3% from curve to curve. Therefore the curves have been normalised for statistical comparison.

4.1.4 TMB assay

The MBP biofunctionalised Si_3N_4 surface was incubated with its antibody at a concentration of 0.5 μg μl^{-1} for 30 minutes. The surface was then rinsed with 1 mM Tris buffer, pH 7.4, to remove excess antibody. The unreacted sites of the protein were blocked with 5% BSA in de-ionised H_2O. The sample was then incubated with 0.25 μg μl^{-1} of secondary antibody linked with horseradish peroxidase (HRP) and then washed with 1 mM Tris buffer at pH 7.4. 200 μl of TMB, T-4444 (3,3´,5,5´-tetramentylbenzidine) solution was dispensed on the Si_3N_4 surface and the samples were incubated at room temperature for 20 minutes until a distinct colour change was observed. Finally the reaction was stopped by adding 50 μl of 2 M sulphuric acid and absorbance was measured at 450 nm using a low-volume spectrophotometer (Genova Nano, Jenway Biotech, USA).

4.2 Results of protein phosphorylation on silicon nitride

The immobilisation of MBP on the Si_3N_4 surfaces was demonstrated by adding an anti-MBP antibody followed by a HRP-modified secondary antibody. The TMB assay induces a colour change in the presence of HRP, which was detected using a spectrophotometer. Figure 4-2 shows a typical absorbance plot for the TMB assay where a peak was observed at 450 nm. The surface with immobilised MBP showed an absorbance 10 times higher than without MBP.

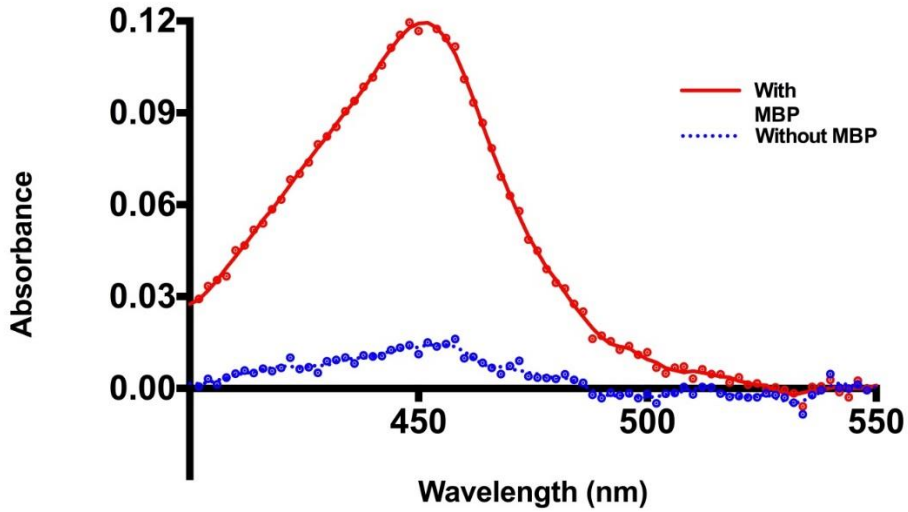

Figure 4-2 Immobilisation of myelin basic protein (MBP). The curve shows the absorbance peak at 450 nm for the TMB assay. The surface with immobilised MBP showed 10 times higher absorbance than the one without MBP. The lines are guides to the eye.

C–V characterisation of the EIS structures with MBP immobilised on the Si_3N_4 surface was also performed, achieving a pH sensitivity of 51.7 mV/pH (Figure 4-3), using 1 mM Tris buffer at pH 8.8, 7.8 and 7.2. The curves do not isolate the effect of any change in charge of the protein due to the pH. In theory, there is a charge change of 3.3 C between pH 7.2 to 8.8 for MBP [4]. In Figure 4-3, for a given voltage in the depletion region, an increase in capacitance is observed at a higher pH. This is attributed to the fact that at lower pH, the excess of H^+ ions on the Si_3N_4 surface decrease the threshold voltage of the structure. As a result, at higher pH the depletion region of the curve shifts to the left as shown in Figure 4-3. This shift indicates a change in the gate voltage, ΔV_g, which increases as pH decreases. This increase with pH was found to be linear with a regression coefficient of 0.99. The data inset on Figure 4-3 served as calibration curves for the change in gate potential due to the change in pH.

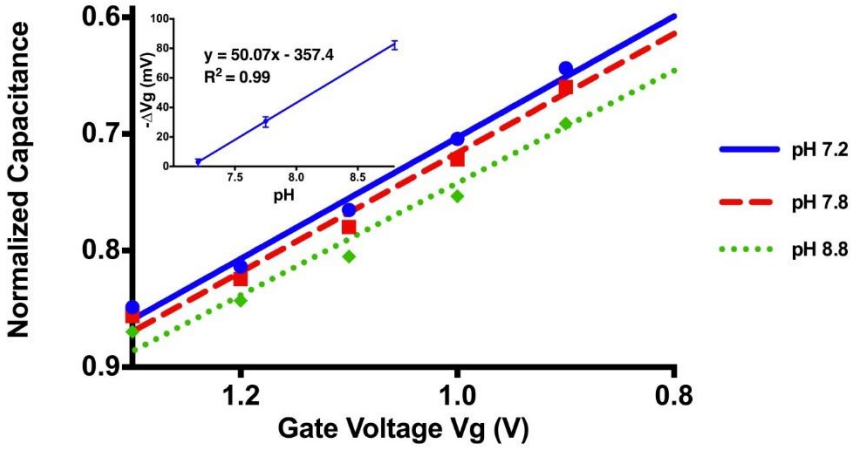

Figure 4-3 Capacitance–voltage (C–V) characterisation of the EIS structures with MBP immobilised on the Si_3N_4 surface was also performed, revealing a pH sensitivity of 51.7 mV/pH, using 1 mM Tris buffer at pH 8.8, 7.8 and 7.2. The curves have been normalised for statistical comparison since $C_{dielectric}$ (capacitance of silicon nitride and silicon dioxide) does not vary more than 3% from curve to curve.

Figure 4-4 A shows the changes in gate voltage, ΔV_g, upon treatment of immobilised MBP with PKC-α kinase (4 units), its activator and ATP, at different time intervals. As the time interval for the interaction of MBP with PKC-α/ATP is extended, the changes in ΔV_g increase, and stabilise after 13 minutes to a value of 37 mV. Experiments without PKC-α kinase activator, revealed a negligible change of 2.1 mV in gate potential (as seen in Figure 4-4 A). This implies that the kinase activator is essential to induce the chemical reaction on the biofunctionalised Si_3N_4 surface. The reaction with inhibitor did not show any significant changes in ΔV_g, which was 1.9 mV after 60 minutes.

Upon phosphorylation of MBP due to the kinase, each amino acid that undergoes phosphorylation releases a proton that is adsorbed on the surface of Si_3N_4. As a result, the threshold potential of the structure decreases and a change in potential is observed. As the reaction with kinase/ATP continues, phosphorylation increases, leading to higher V_g changes. The change in the threshold potential was inversely proportional to the amount of phosphorylation. The successful detection of the protein phosphorylation was then tested to assess the kinase activity. The Si_3N_4 surface immobilised with MBP was reacted with different concentrations of PKC-α kinase in the presence of ATP and the kinase activator for 40 minutes with a time interval of 2

minutes until 10 minutes and then at 20, 30 and 40 minutes after the start of the reaction.

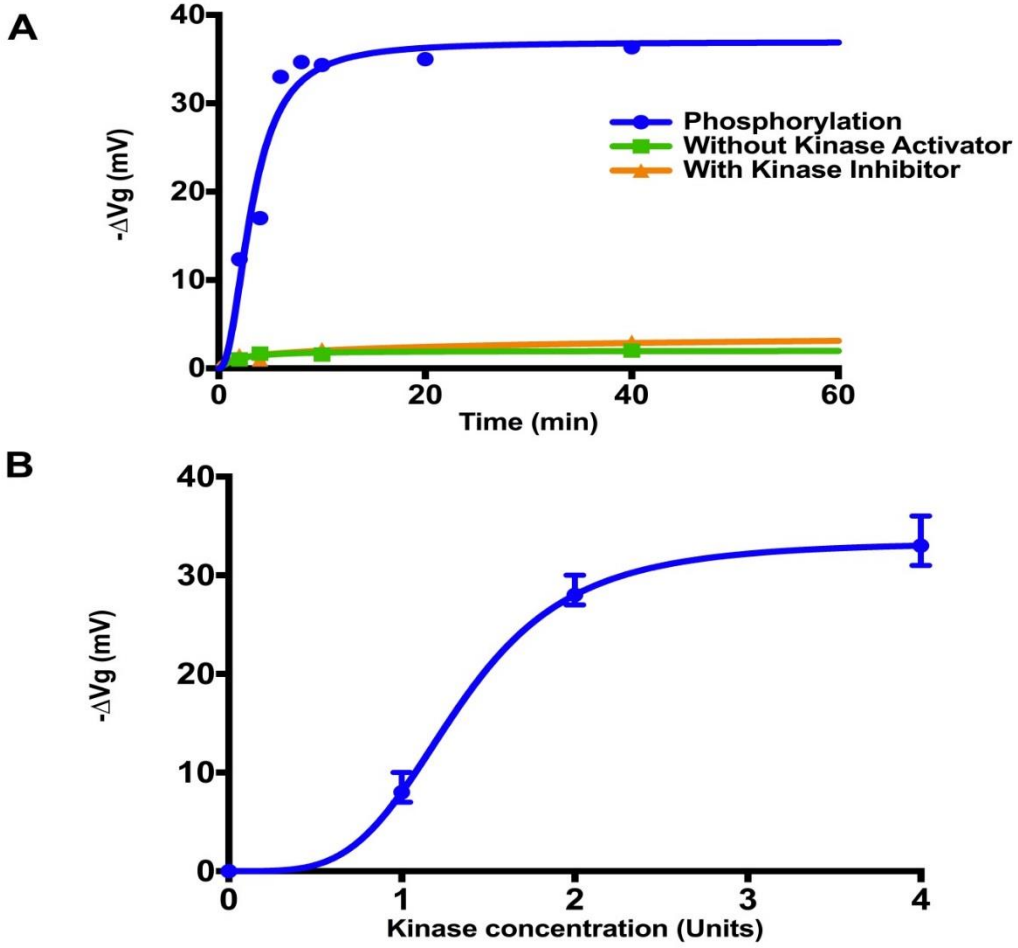

Figure 4-4 Protein phosphorylation on Si_3N_4: A) Time-dependent changes in gate potential upon (a) phosphorylation of MBP by PKC-α, (b) control reaction without kinase activator and (c) in the presence of kinase inhibitor; The points represent the mean values of replicates;. B) Kinase activity plot: phosphorylation with different kinase concentrations.

Fig 4-4 B shows the change in gate voltage, ΔV_g, after maximum kinase activity was observed with different kinase concentrations. The shape of curve depicts that a minimum of 0.5 units of kinase is necessary in order to observe any noticeable potential change. However 0.8 to 1.0 units of kinase are needed to yield a signal that distinguishes it from the controls (reactions with kinase inhibitor or without kinase activator) and confirm phosphorylation of protein.

4.3 Protein phosphorylation analysis using micro pH meters

For the direct pH measurements using the micro pH meter, the phosphorylation reactions and controls were carried out 'in solution' using similar concentrations of the different components as before. The volume of all reactants was kept at 100 µl for all replicates and controls. An In Lab Ultra Micro pH electrode with a S220 SevenCompact meter (Metter Toledo) was used to measure the pH of the reaction. This pH electrode had a tip of 3 mm diameter. The pH of the reaction was recorded every 2 minutes until 10 minutes and then at 20 minutes after the reaction. Each experiment was repeated three times and the average values are reported here.

4.3.1 Micro-pH electrode measurements

Figure 4-5 shows a pH change of 0.07 upon phosphorylation of MBP in solution, measured using a micro pH electrode. The pH of the reaction was found to be stable for 10 minutes before the start of the reaction i.e. after adding kinase, ATP and MBP in solution. As soon as the kinase activator was added there was an abrupt change in pH which stabilised after 2 minutes for the next 20 minutes. This change was not observed without kinase activator or with inhibitor of kinase. Therefore it is claimed that changes in pH were due to the phosphorylation of proteins and can be detected using a micro-pH electrode. Overall the total change in pH detection was very low, being of only 1.5 % to that observed on EIS sensors. This is attributed to the fact that the reaction is carried out in a buffer solution. The release of protons due to the phosphorylation reaction therefore disturbs only slightly the pH of the buffer. The pH value of 7.4 for the reaction was dictated by the need to retain the protein conformation and enable kinase activity. This indeed prevents high sensitivity responses. In addition, it was also apparent from the graph (Figure 4-5) that there was a long term drift and hysteresis losses in the sensor that result in slight pH changes when phosphorylation reaction is prolonged in order to check the stability. This accounts for the shape of the curve.

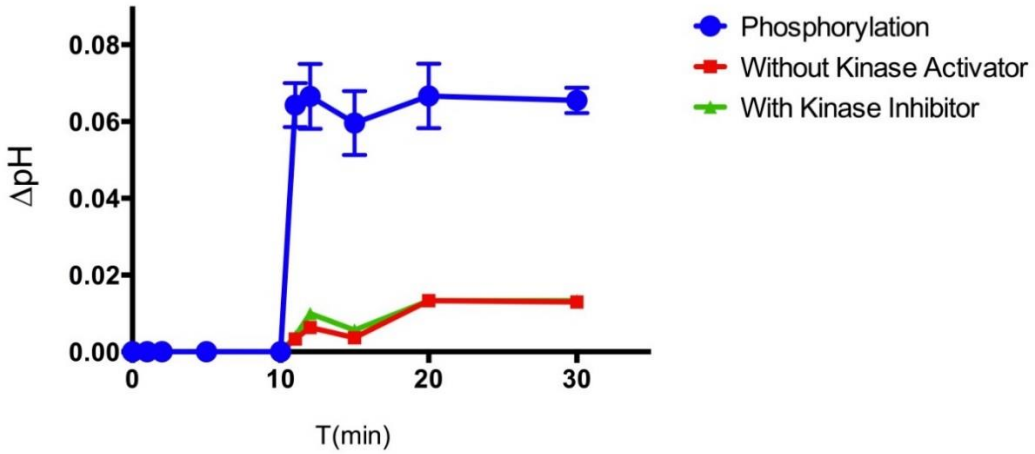

Figure 4-5 Protein phosphorylation measurement with a micro-pH electrode; 2-way ANOVA test where phosphorylation results are significant compared with the results of achieved without kinase activator and with kinase inhibitor within $p < 0.01$.

However, a 2-way ANOVA test revealed that phosphorylation results were significant when compared with controls (without kinase activator and with kinase inhibitor) within $p < 0.01$. So, nevertheless this methodology still proves to be a time and cost efficient in-laboratory technique that is able to distinguish between phosphorylated and non-phosphorylated substrates upon phosphorylation by kinase.

4.4 pH changes associated with thiophosphorylation

Thiophosphorylation of MBP by PKC-α was carried out in the presence of ATP-S. 3 sets of control reactions were performed: one without PKC lipid activator; second with the GF 109203X inhibitor, added before putting the kinase activator; and a third reaction where the protein phosphorylation was carried with ATP instead of ATP-S. Upon phosphorylation of MBP in the presence of ATP-S, the protein becomes thiolated. The thiophosphorylated proteins were then exposed to AuNPs (16 nm mean size), wherein the affinity between the thiol groups and Au resulted in the attachment of AuNPs to the thiophosphorylated substrates. Generally, the covalent attachment of quasi-spherical AuNPs to the thiol groups occurs at a fast rate so after 10 minutes the substrates were rigorously washed with the reaction buffer to remove electrostatically attached AuNPs. As a consequence the phosphorylated protein was labelled with AuNPs which enabled its detection by LSPR, alongside pH changes on the EIS

substrate. Thiophosphorylated samples showed a shift in the *C-V* characteristics, 30-35 mV higher than with the controls (Figure 4-6). It was also observed that the rate of transfer of γ-phosphate from ATP-S was slightly slower than from ATP, which is consistent with previous reports [5], [6].

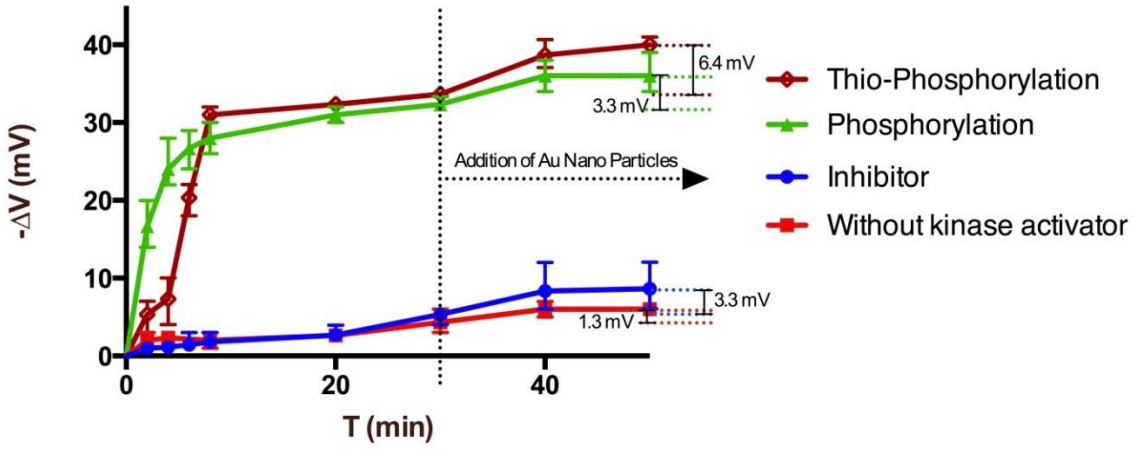

Figure 4-6 Kinase activity detected by measuring the release of proton associated with protein phosphorylation for the same samples where LSPR detection was performed.

However, after adding AuNPs, the amount of change in the voltage observed (6.4 mV in the case of thiophosphorylation) was small. This is attributed to the fact that the attachment of AuNPs slightly disrupts the outer Helmholtz plane (OHP) of the electric double layer in the Gouy-Chapman-Stern-Graham model of the EIS sensor. This disruption triggers the adsorption of ions from the OHP onto the electrode surface by constant Coulombic attractions forming the inner Helmholtz plane (IHP). This gives rise to the so-called surface complexation [7] whereby the affinity of attracting counter ions becomes higher and it is possible to form complex compounds on the surface from the buffer, thus bringing slight changes in the surface potential in that vicinity. Despite the small voltage changes observed after addition of nanoparticles the thiophosphorylated samples could still be distinguished from the controls (Figure 4-7).

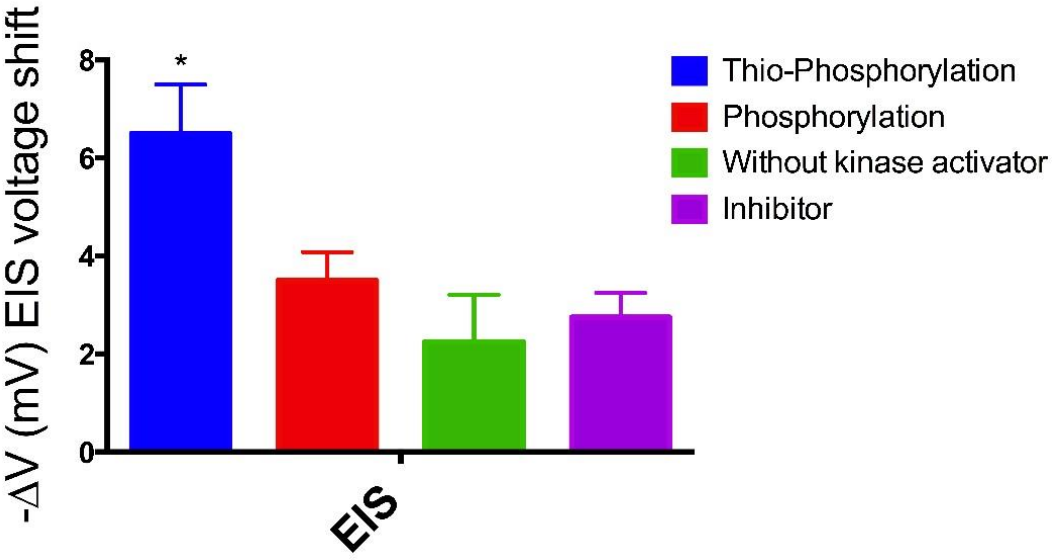

Figure 4-7 Statistical analysis of change in EIS signal upon AuNPs attachment. The thiophosphorylation was found to be significant when compared to other reactions. (= $p < 0.05$ n=3)*

4.5 LSPR detection of protein phosphorylation

The presence of AuNPs on the thiophosphorylated proteins enabled its detection by LSPR, alongside pH changes on the EIS substrate. The detection scheme is shown on Figure 4-8. Figure 4-9, thiophosphorylated sample, shows a red-shift of 31 nm in the absorption spectrum of silicon nitride as a background. The control reaction performed in the absence of kinase activator revealed < 10 nm of shift in the wavelength, confirming that the large redshift in the wavelength of thiophosphorylated sample was due to the covalent attachment of AuNPs to the sulphide group present on the γ-phosphate group transferred from ATP-S to the MBP. Secondly it emphasises that kinase activator is required to phosphorylate the MBP.

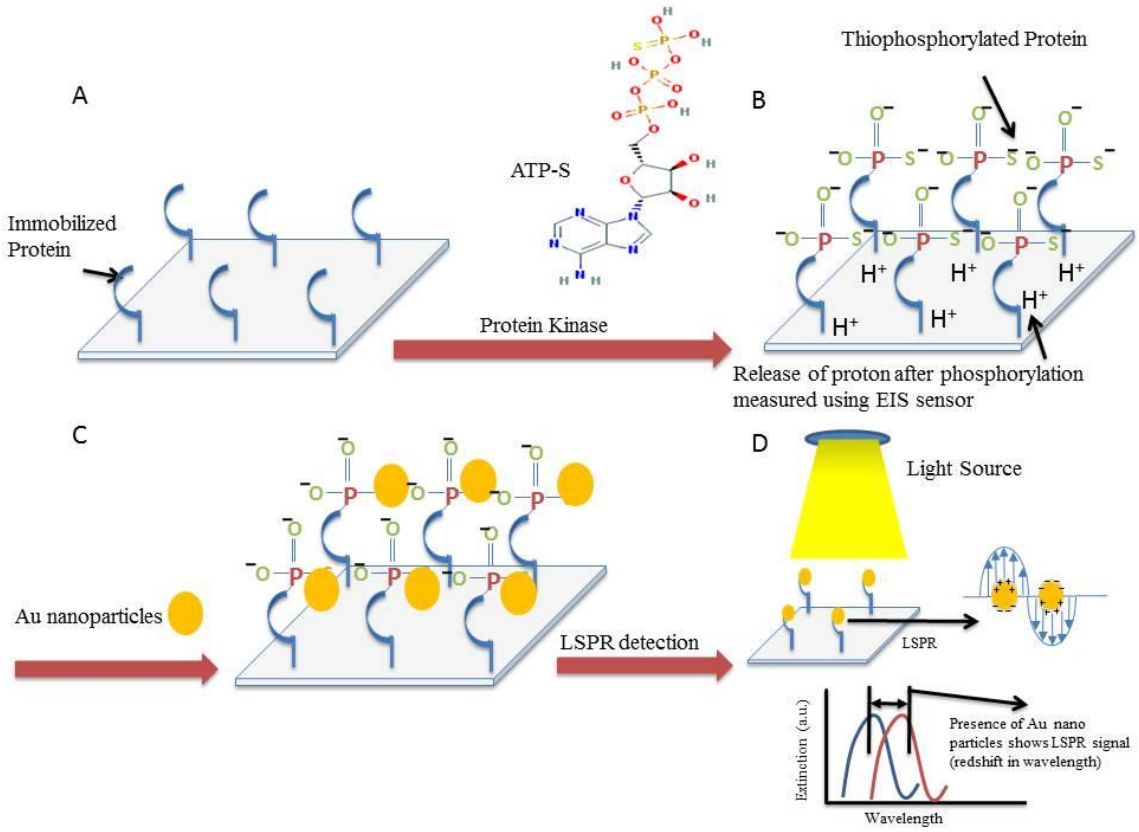

Figure 4-8 Schematic of working principle (A) immobilised protein on silicon nitride surface (B) Upon thiophosphorylation there is a release of proton and transfer of γ phosphate from ATP-S (C) covalent attachment of AuNPs to the sulphide group on thiophosphorylated protein (D) LSPR detection mechanism

There is also an increased absorbance observed in the thiophosphorylated samples which is due to the radiative decay of the enhanced electric near-field of the AuNPs that scatters light on silicon nitride, allowing it to absorb more energy in the far-field at the resonant frequency. The reaction where ATP-S was replaced by ATP, after phosphorylation, showed ~ 9 nm of average wavelength redshift. The reaction with a known inhibitor of kinase showed ~ 7 nm of redshift in the wavelength demonstrating

as a proof-of-concept, how new inhibitors could be screened for drug discovery using LSPR.

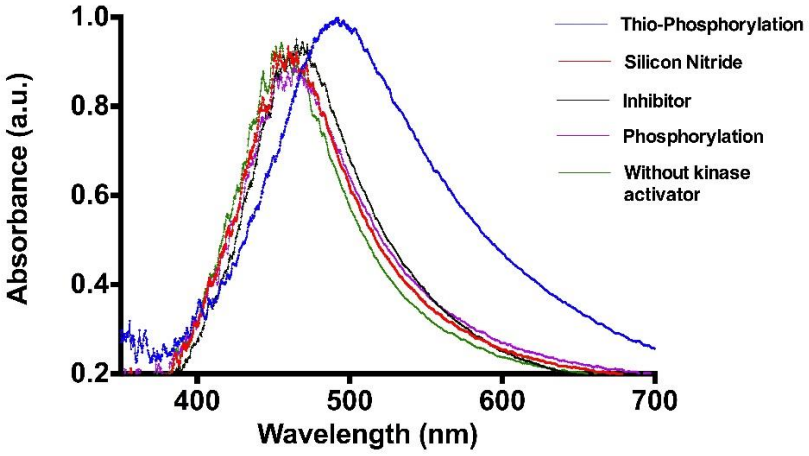

Figure 4-9 LSPR spectra in the absorption mode where thiophosphorylated substrates give significant LSPR shift in wavelength.

4.5.1 LSPR experimental setup

LSPR was done in reflection mode as shown in the schematic on figure 4-10. The instruments for LSPR namely, reflection probe (R400-7UV-VIS), halogen light source (LS-1-LL) and the spectroscope (USB4000-UV-VIS-ES) were purchased from Ocean Optics

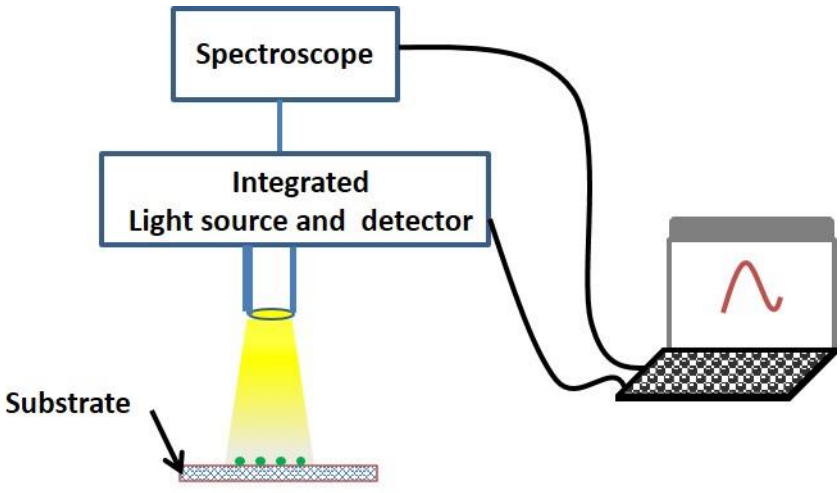

Figure 4-10 LSPR setup for reflection mode

. Before taking any signal from the scope, it was calibrated for dark and light spectrum modes. To get a light reference spectra 100 nm of aluminium deposition on a glass slide using thermal evaporation was used. The LSPR signal was then recorded in

absorption mode by observing the wavelength dependence of the light absorbed through by nanoparticles via Spectrasuite, cross-platform spectroscopy operating software from Ocean Optics. The schematic in figure 4.11 shows the dual mode setup for combined field effect and nanoplasmonic sensing.

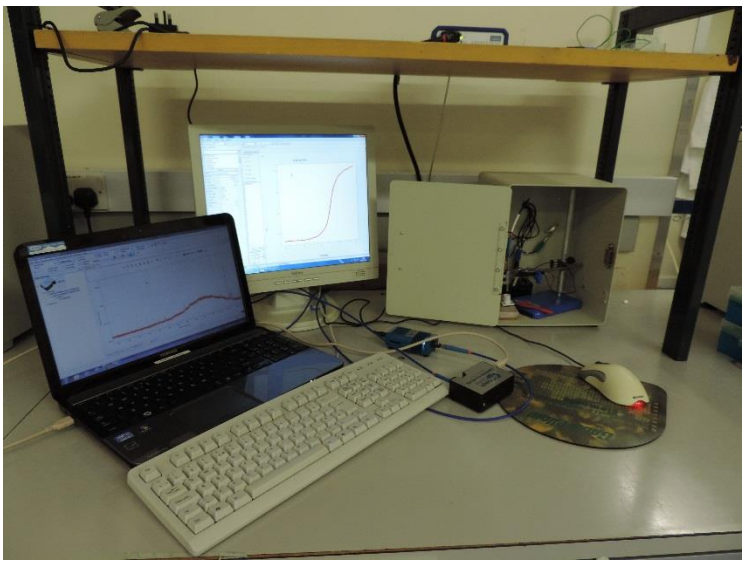

Figure 4-11 Dual mode setup LSRP + electrochemical field effect sensing

4.6 Dual mode sensing on silicon nitride

The signals obtained by both LSPR and electrochemical detection of proton release were significant for thiophosphorylation compared to negative controls (without kinase activator or in the presence of inhibitor, $p < 0.05$), Figure 4-12. Thiophosphorylation reaction in the presence of PKC inhibitor GF109203X did not elicit detection levels significantly higher than the control in the absence of kinase activator. Phosphorylation of MBP in the presence of ATP did not provide a significant signal in the LSPR experiments, while it did in the EIS-based measurements. The wavelength shift in thiophosphorylated samples is due to the plasmonic oscillations of electrons in the AuNPs.

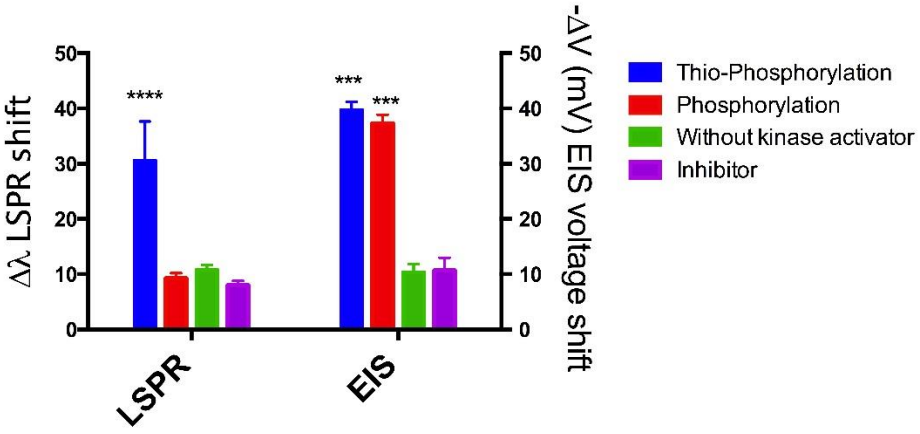

Figure 4-12 Statistical analysis of LSPR and EIS-based detection of thiophosphorylation.

4.6.1 Characterisation of AuNP distribution on Si_3N_4

As seen from the Figure 4-12, the variations in the LSPR response from sample to sample were larger in the case of thiophosphorylated samples than to the EIS signal. The variation in the LSPR signals are attributed to:

1) inconsistency in the shape and size of the nanoparticles
2) non-homogeneity of the nanoparticles
3) LSPR sensitivity to the varied densities of the AuNPs between samples

To analyse the first two attributes, electron microscopy studies were conducted. Transmission electron microscopy (TEM) was performed at 200,000x magnification with a JEOL JEM1200EXII transmission electron microscope with high contrast pole pieces. For TEM, 300-mesh nickel grids, coated with a fine layer of carbon, were used as substrates for the protein fractions in the microscope. MBP was immobilised in the same way as described in the above sections. TEM analysis of the thiophosphorylated substrates confirmed the irregularity in the shape and size of the nanoparticles in addition to variable density and heterogeneity among individual AuNPs in form of tetrahedral, cubic, octahedral and hexagonal phases that was apparent from the scans (Figure 4-13 A). The spatial diameter of the AuNPs in two dimensions, analysed using Image-J, varied from 10 nm to 25 nm in Gaussian distribution curve with average size of 16-17 nm (Figure 4-13 B).

A

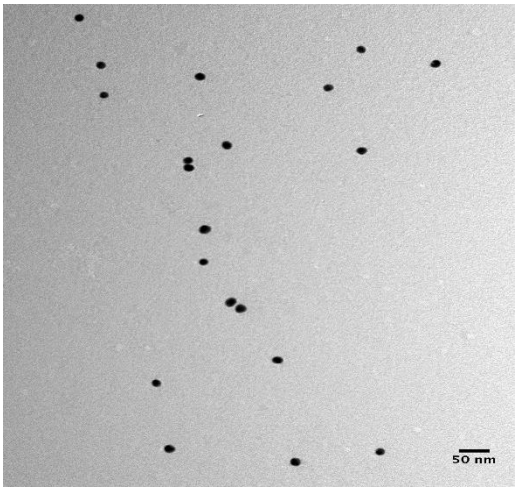

B

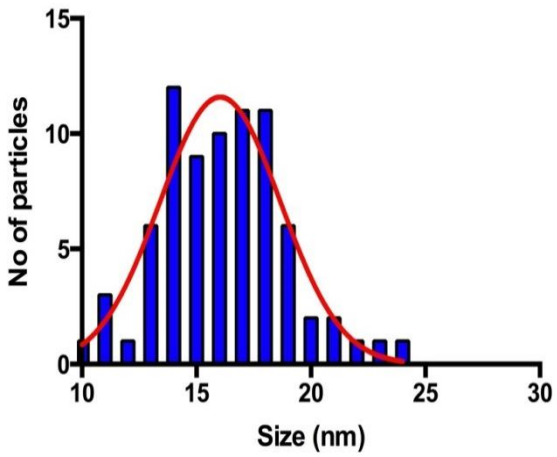

Figure 4-13 A) TEM image of thiophosphorylated sample. B) Size distribution of AuNPs, obtained by processing the TEM images of the AuNPs with Image-J software.

Producing AuNPs of consistent shape, size and homogeneity in bulk solution, is very difficult due to small variations in the equilibrium of the Gibbs free energy during the nucleation and growth of nanoparticles in solution. However, the variable density in the distribution of AuNPs, for instance random Au-Au couples that were observed in some areas, was ascribed to the formation of aggregates due to the increased affinity between the peptides and AuNPs in the presence of ATP-S [8] and the non-uniform distribution of the immobilised proteins that hinder the attachment of gold to all the thiophosphorylated sites. Additionally, pairs of AuNPs were observed at some sites, which are likely to form a 'plasmonic ruler' configuration. According to the equation

of the ‘plasmonic ruler’ for the Au particle pair [9] trapped in a protein medium, the corresponding LSPR shift should vary between 20 and 40 nm for the Au-Au distance given the size of particles observed under TEM.

The physical dimensions of the AuNPs are much larger than that of MBP. It was therefore possible that equal numbers of AuNPs attached for different amounts of thiophosphorylation, making it essential to control the density of the immobilised proteins. To control the distribution of proteins on the surface, self-assembled monolayers (SAMs) of 3-amino propyl triethoxy silane and allyl hydroxl silane (APTES/AHS) were tested. Concentrations of 0.01%, 0.1%, 1%, 10%, and 100% of APTES in AHS were tested. This lead to coatings with different densities and distributions of APTES. Since APTES allows immobilisation of the protein, the aforementioned setup was used to test the effect of protein density distribution on thiophosphorylation detection using the developed EIS/LSPR dual mode technology. In order to check the effectiveness of the APTES/AHS immobilisation, horseradish peroxidase (HRP) was used as a test protein. Levels of immobilisation were quantified by a TMB assay, Figure 4-14.

Higher concentrations of APTES led to a higher amounts of HRP to be immobilised on the silicon nitride surface. However, the linearity was low (regression coefficient < 0.97), especially at higher concentrations of APTES, possibly due to the linear mismatch in the orientation of SAM formation and the way proteins attach to the functionalised group on the SAM. An analysis on how LSPR and EIS based phosphorylation detection were affected by APTES concentration in the immobilisation of MBP was performed (Figure 4-15).

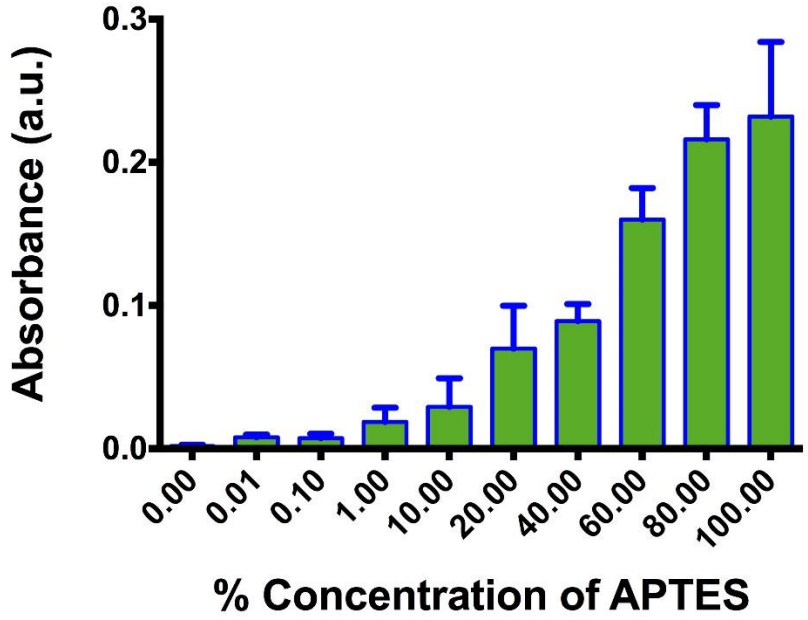

Figure 4-14 TMB assay for the conformation of protein immobilisation at varied concentration of APTES in APTES/AHS solution

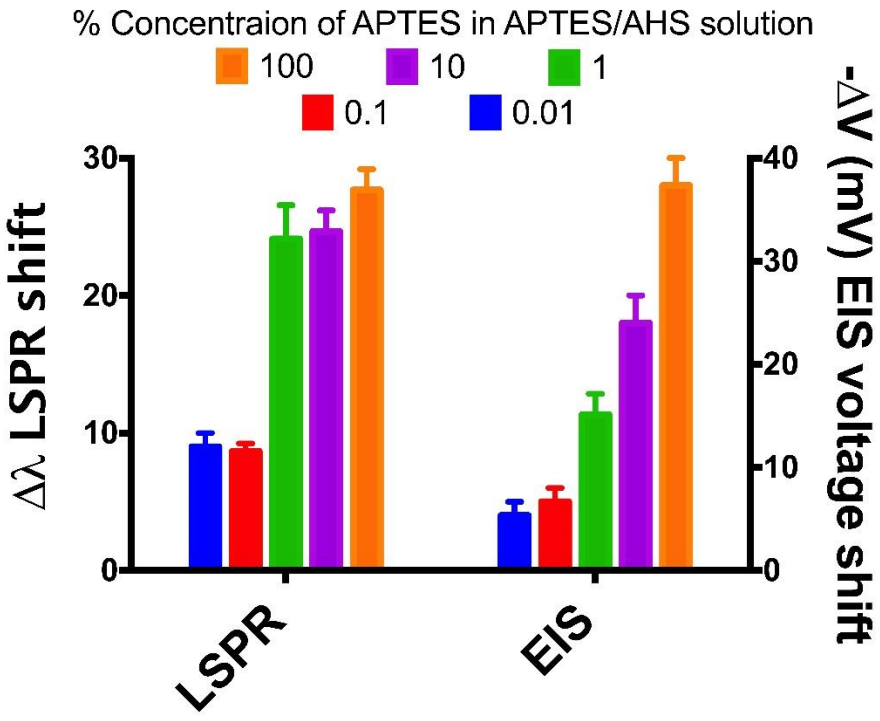

Figure 4-15 EIS and LSPR response at varied concentrations of APTES in APTES/AHS solution.

Our assumption that density of MBP can be controlled in as similar way as that of HRP was validated when the EIS signal was different at varied concentrations of APTES with optimal level only at 100% APTES, the LSPR signal at 1% 10% and

100% concentrations of APTES was found to be near-maximal. This might suggest that 1% concentrations of APTES is sufficient for maximal AuNP binding and saturation of the LSPR signal.

4.6.2 Effect of kinase concentration

The effect of varying concentrations of kinase on the assay efficiency was studied using both LSPR and EIS (see Figure 4-16). The response of LSPR was found to be marginally more sensitive than the EIS technique, which allowed the detection of a signal at lower concentrations of kinase. At 1 unit per 100 µl (10 mU/µl) the LSPR response is in fact maximal, whereas the EIS response is only around 30% of the maximum observed at 4 units of kinase. The EIS response is linear at low concentrations of kinase whereas the LSPR detection is typically dichotomic (i.e. on-off response, possibly suggesting saturation of binding sites for AuNPs at low thiophosphorylation levels).

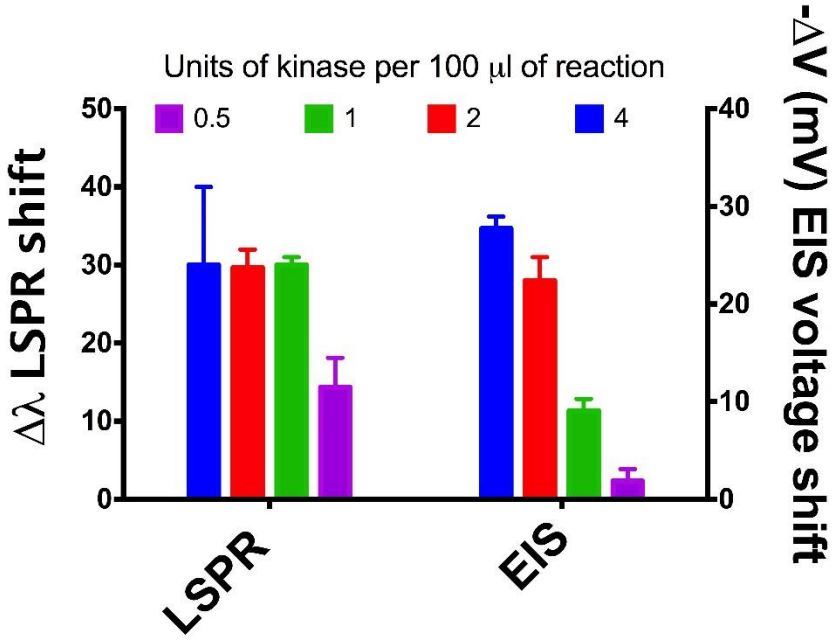

Figure 4-16 Comparison of assay efficiency at different kinase concentration on EIS and LSPR

4.6.3 Complementary response of EIS and LSPR

To validate the sensitivity of LSPR for the identification of kinase inhibitors, phosphorylation was conduction at 1 U kinase per 100 µl of reaction volume. The

experiments were conducted in the presence of PKC inhibitor (0.1 µM). The results were then compared with the EIS response (Figure 4-17).

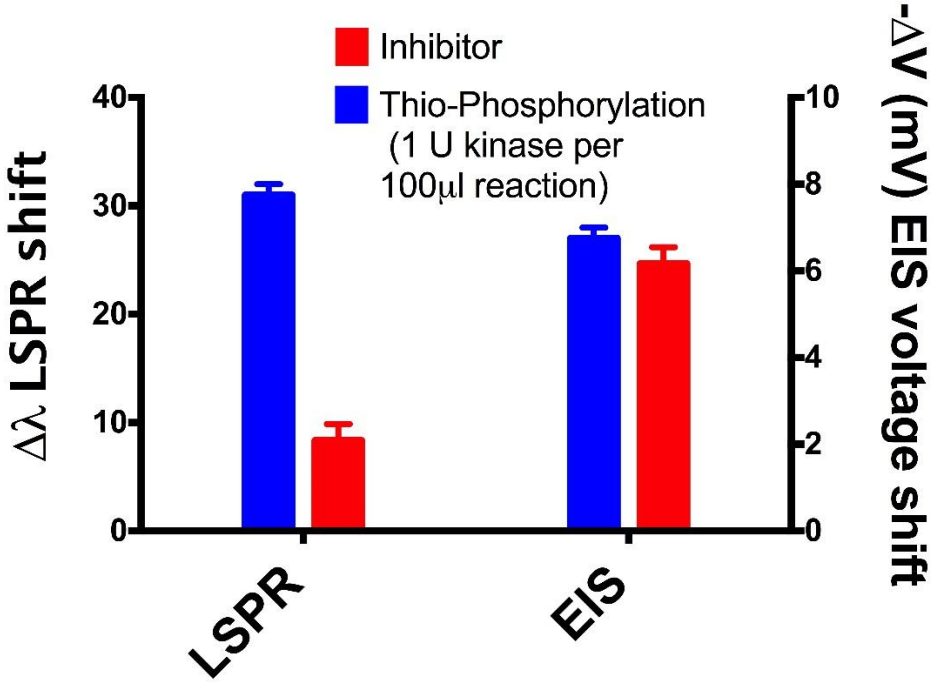

Figure 4-17 Thiophosphorylation vs. inhibition reaction at 10 mU/µl kinase (1U kinase per 100 µl reaction)

This response showed complementary sensing capabilities of EIS and LSPR. At lower concentrations of kinase or when low amount of phosphorylation happens, EIS will fail to distinguish signals from control although real-time signal response can be followed on EIS. On the other hand LSPR confirms the phosphorylation reaction with a digital response i.e. irrespective of the amount of phosphorylation. LSPR distinguishes controls from the reaction, provided at least 1 unit of kinase (10 mU/µl) per 100 µl is utilized in the reaction. The on/off signal response of LSPR can be observed in Figure 4-18. This figure plots LSPR and EIS data for the phosphorylation of MBP in the presence and absence of kinase inhibitor with different surface modification strategies.

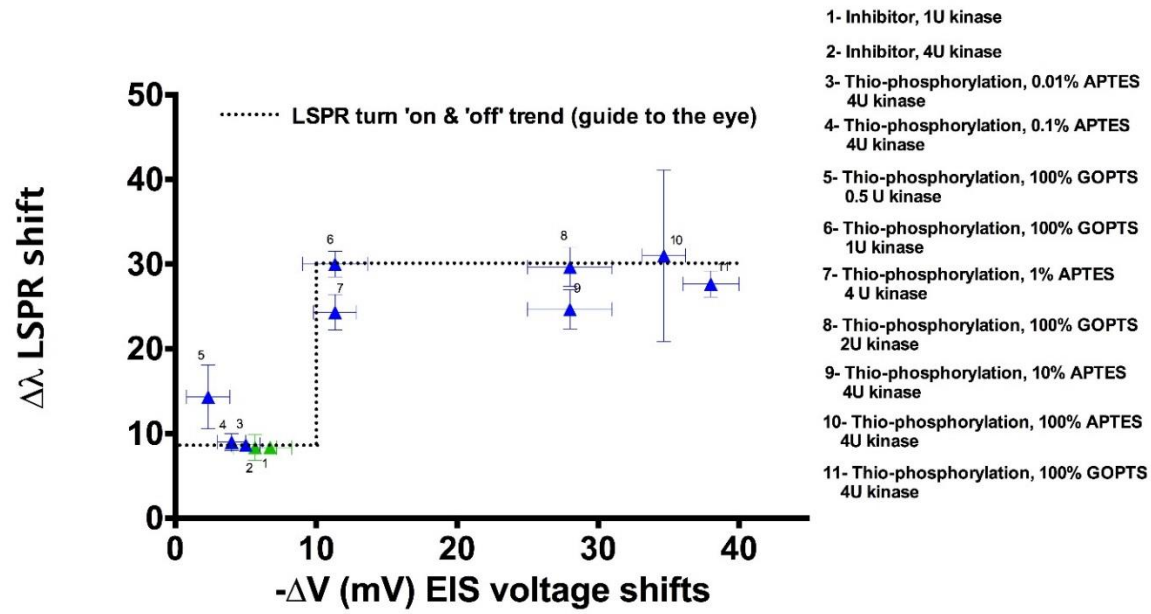

Figure 4-18 Comparison of assay efficiency at different kinase concentration on EIS and LSPR in the presence or absence of PKC inhibitor.

4.7 Thiophosphorylation studies using in-house synthesised peptides

Thiophosphorylation studies on in-house synthesised peptides was done to study the non-specific attachment of AuNPs to the cysteine amino acid. A large number of proteins have a cysteine amino acid as one of their components. AuNPs have a high affinity to the sulphur group present in the cysteine amino acid.

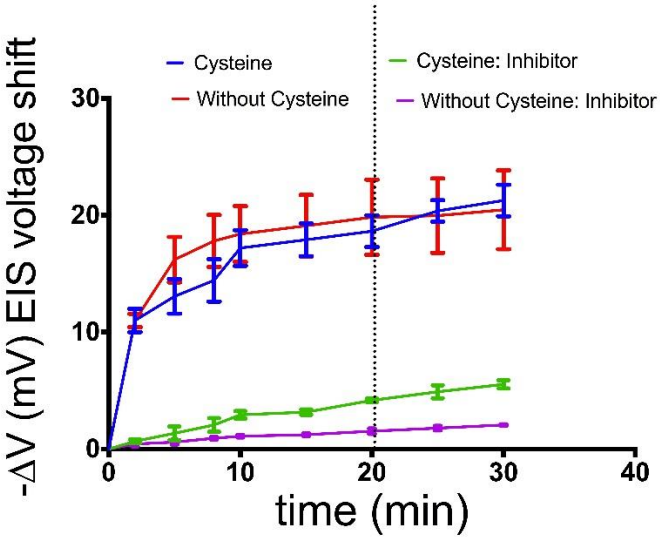

Figure 4-19 EIS response of thiophosphorylation of in-house synthesised peptides. The signal after the dotted line shows the changes after addition of AuNPs

Fortunately, MBP did not contain any cysteine, therefore it was necessary to study the interaction of AuNPs with the cysteine amino acid. Two peptides, described in Chapter 3, one with cysteine and another without cysteine obtained from Department of Pharmacy and Pharmacology, University of Bath. Peptides were immobilised on the surface of silicon nitride with GOPTS, similar to the MBP immobilisation described in the earlier sections. Figure 4-19 shows the EIS response of the peptides after thiophosphorylation. A mean value of 20 mV was observed after phosphorylation of both the peptides. In the presence of inhibitor, shifts < 5 mV in the EIS signal were observed. These shifts are attributed to the pH changes associated with the phosphorylation of peptides. LSPR redshifts of ~ 25 nm were observed upon attachment of AuNPs with the thiophosphorylated peptides (Figure 4-20).

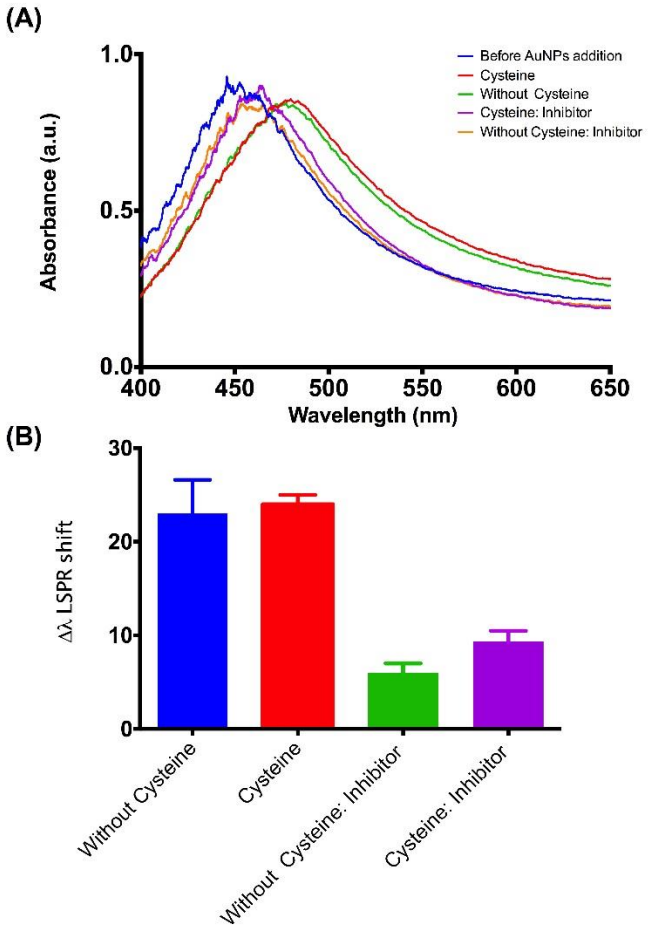

Figure 4-20 LSPR response of peptides upon thiophosphorylation (A) characteristic curves (B) statistics

The LSPR signal was comparatively more reproducible from the peptides with cysteine than that from the other peptide and MBP. This is due to the non-specific attachment of the AuNPs on the thiophosphorylated peptides. It is evident from Figure 4-20B that the non-specific attachment of the AuNPs do not contribute to the significant signal changes in the LSPR signal and the phosphorylation reaction can easily be distinguished from the inhibition reaction. The results suggested that the presence of a non-specific interaction may lead to periodicity in the distribution of AuNPs which contributes to less variation in the LSPR signal from sample to sample.

4.8 Optimisation of silicon nitride surfaces for dual mode sensing

This section studies the optical interactions of the various sizes of AuNPs on different thicknesses and compositions of Si_3N_4, while characterising the pH sensing properties of the surface. Table 4-1 summarizes the properties of 4 wafers with different sizes of Si_3N_4 layer that we studied.

Table 4-1 Properties of silicon nitride wafers used in the study

Wafer	*Average Thickness of Si_3N_4 and SiO_2 of on silicon wafer* (nm)	*Approximate N: O ratio in the top Si_3N_4 layer*	*FTIR peaks*	*Lattice spacing as seen from XRD* (angstrom, Å)	*Intensity of [321] peaks in XRD* (counts, a.u.)
1 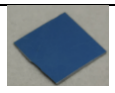	Si_3N_4: 400-410 SiO_2: 5-10	3:5	Si-H, Si-O, N-H, Si-N	d_{321} = 1.36	35
2 	Si_3N_4: 102-113 SiO_2: 45-50 nm	1:2	Si-H, Si-O, Si-N	d_{321} = 1.35 d_{101} = 2.70	160000

3 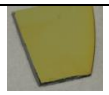	Si_3N_4: 160-170 SiO_2: 45-50	1:4	Si-H, Si-O, N-H, Si-N	d_{321} = 1.35 d_{101} = 2.71	53000
4 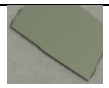	Si_3N_4: 100-115 SiO_2: 35-40	2:5	Si-H, Si-O, N-H, Si-N	d_{321} = 1.35 Å d_{101} = 2.70 Å	185000

Microscopy and spectroscopy scans to study the properties of the wafers are provided in Appendix-3. Four wafers have visibly different colours due to differences in their properties and thicknesses. Thicknesses of Si_3N_4 layers in all wafers were controlled during deposition process and the cross-section of the wafer was measured after the deposition using scanning electron microscopy (SEM). SEM was done using a JEOL SEM6480LV microscope. Energy dispersive x-ray analysis (EDX) was accomplished using high-sensitivity Oxford INCA X-Act SDD X-ray detector equipped with SEM. Fourier Transform Infrared Spectroscopy (FTIR) was performed directly over the surface of Si_3N_4 using a Perkin Elmer Frontier FTIR instrument in reflection mode, using a high-resolution MCT (mercury cadmium telluride) detector. X-ray diffraction (XRD) data was obtained using a BRUKER AXS D8 Adance, equipped with a Vante-1 detector using CuKα radiation (λ=1.5318 Å). EDX and FTIR spectroscopy studies revealed slight variations in the composition of the silicon nitride layer. These variations were due to different ratios of nitrogen and oxygen in the silicon nitride layer and mixed presence of Si-H, Si-O, N-H and Si-N bonds from sample to sample.

When Si_3N_4-based insulator-on-semiconductor (IOS) structures without AuNPs are exposed to light (250-2000 nm), there is a generation of excitons due to the radiative and non-radiative recombination of electron-hole pairs in the Si_3N_4 top layer [10]. This happens as a result of optical pumping of oxide-insulator interface (SiO_2-Si_3N_4) and insulator trapped charges in Si_3N_4 triggered by multiple reflections at the interface of the each layer in the wafer [11][12], [13]. The resultant extinction of this phenomenon gives rise to a (photoluminescence) PL peak in Si_3N_4[14]. It is this PL resonance peak of the Si_3N_4 that is enhanced by coupling LSPs in AuNPs immobilized on the top of

Si_3N_4. A strong dependence of PL peak and pH response of Si_3N_4 on the composition and structure of the Si_3N_4 is observed.

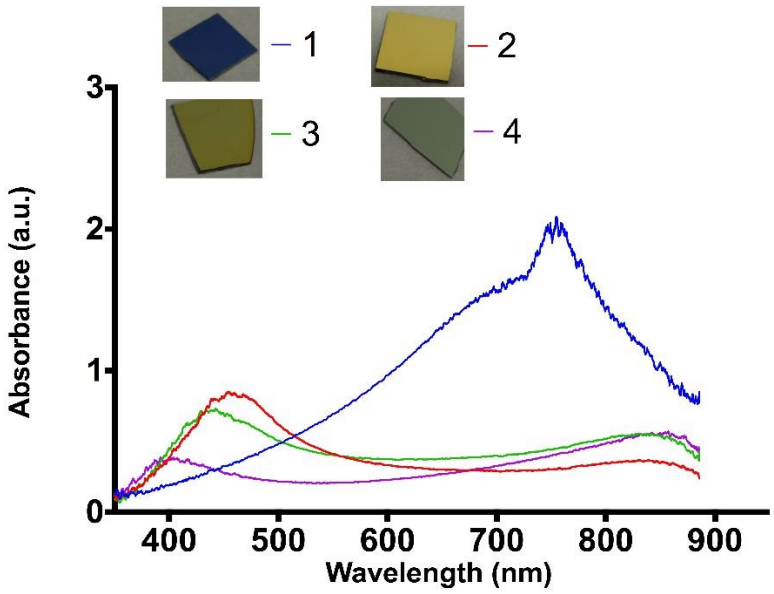

Figure 4-21 Optical response of the wafers; photoluminescence (PL) peaks of 4 different silicon nitride wafers

Figure 4-21 shows PL resonance peaks for all 4 wafers. There are 2 PL resonance peaks observed in the 3 wafers with a SiO_2 thicknesses of 35-50 nm and Si_3N_4 less between 100-200 nm. The first peak is between 400-450 nm and the second peak is around 820-830 nm. With an increase in the thickness of Si_3N_4 to 400 nm and decrease in the thickness of SiO_2 to 10nm there is only one PL resonance peak that is observed, at 750 nm. In addition, an increased amount of disorder in the grains and large lattice strain in Si_3N_4 is seen when its thickness is increased, relative to the other wafers from analysis of XRD scans. Evidently, it is the different structural properties and composition of Si_3N_4 that gives PL resonance peaks at different wavelengths. When the AuNPs are chemically attached on the surface there is an enhancement of the PL peak. Higher absorbance, widened full width half maximum (FWHM) and a redshift in the wavelength of PL peak is observed. Redshift in the PL peak is due to the Purcell effect [15] where the radiative recombination energies of the electron-hole pairs in Si_3N_4 are enhanced by the strong electromagnetic (EM) fields introduced by high-density mode LSPs in AuNPs [16-17]. Increased redshift was observed in the PL resonance peak with increase in the size of the nanoparticles, Figure 4-22. This is attributed to the following points:

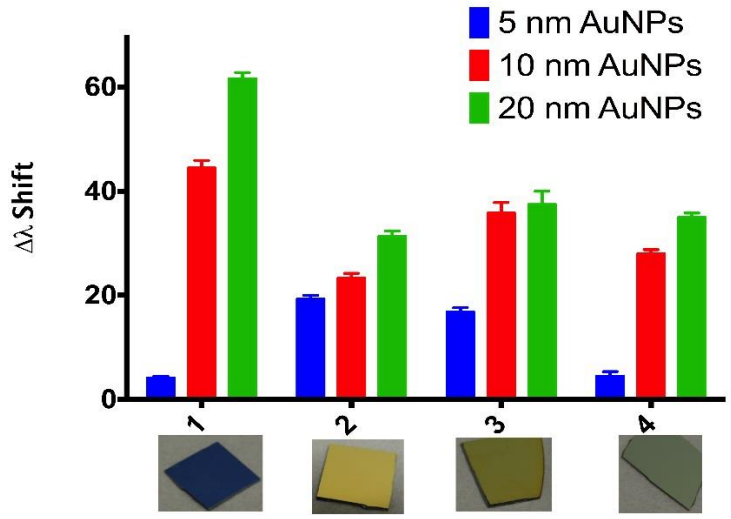

Figure 4-22) Changes in the wavelength (redshifts) of the PL peaks upon coupling with gold nanoparticles of varied sizes.

- larger diameter AuNPs decrease the distance between AuNPs and Si_3N_4 , indicating a strong interaction between them
- the density of LSPs modes increase with the size of AuNPs and confine stronger EM fields on the Si_3N_4 surface
- an enhancement in Purcell factor with an increase in the diameter of AuNPs that enhance the exciton-plamonic coupling.

Interestingly, the amount of redshifts were different for all wafers. This is due to the different compositions of Si_3N_4. With an increase in the thickness of Si_3N_4, the redshifts increases as seen from the Wafer-1 in Figure 4-22. This is associated with the fact that relatively higher amounts of radiative recombination would occur in a thick Si_3N_4 layer due to the presence of massed bulk Si_3N_4. However, we observe that the wavelength response to the size of the AuNPs is not linear for all wafer types. This is ascribed to the amount of nitrogen content in the wafers. The ionisation energy of a nitrogen atom is higher than that of oxygen atom. This means that nitrogen requires more energy relative to the oxygen for discharging an electron from its valence shell. This implies that the recombination energy of excitons from the nitrogen atoms is higher than that from oxygen atoms. Therefore Wafers 1 and 4, where relative content

of the nitrogen is higher than oxygen, the exciton-LSP coupling was not found to be effective when the nanoparticle in plane width decreases (in the case of 5 nm AuNPs).

While the composition and structural properties of the silicon nitride largely affects the optical response of the substrates, it is observed that the pH sensitivity of the substrates does not change drastically, Figure 4-23.

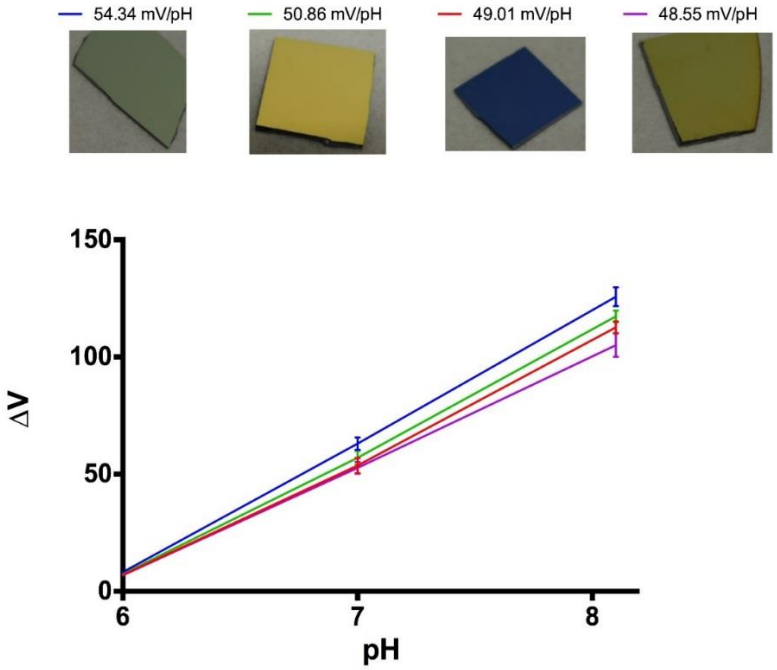

Figure 4-23 pH sensitivity of the different wafers used in the study

A difference of 10.5% between the most sensitive and the least sensitive Si_3N_4 is observed in comparison to 100 % changes in the PL enhancements between the samples with the best and the worst wavelength redshifts. This is primarily because the composition of Si_3N_4 does not extravagantly affect the hydration sites (dangling hydroxyl –OH bonds) on the nitride surface.

4.8.1 Recombination in silicon nitride

Recombination of the charge carriers was observed as a change in the inversion region capacitance upon shining light on the substrate. A 1 kHz frequency, 10 mV ac signal was superimposed on a dc sweep from -2.0 to 4.0 V. Without light, it is observed that there is a formation of inversion, depletion and accumulation region in the capacitance voltage characteristics of the EIS structure. Inversion capacitance is formed as the

minority carriers in the inversion region are not able to respond to the fast changes in the ac voltage. When light is shinned on the surface of the silicon nitride there is formation of excitons i.e. recombination of electrons and holes that takes place. Due to this effect there is an increase in the inversion capacitance of the structure (like a low-frequency response) Figure 4-24. A change in the threshold potential of the EIS device is also observed.

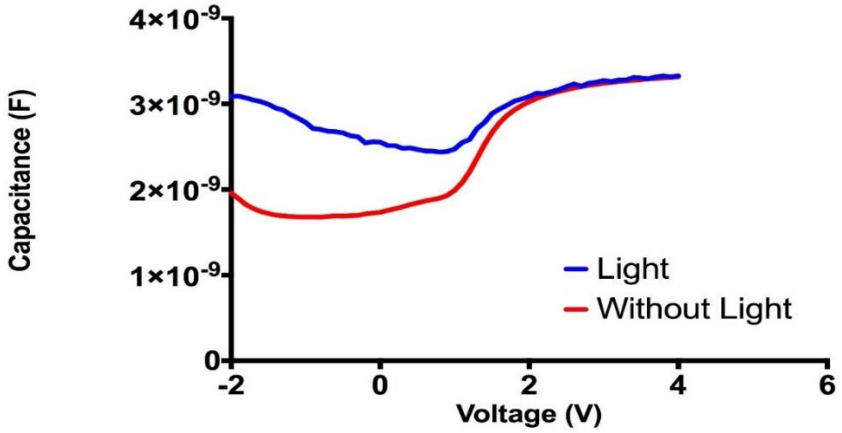

Figure 4-24 capacitance voltage characteristics of silicon nitride under light

4.8.2 Effect of cooling silicon nitride

This experiment was done to support the formation of excitons. When the wafer is super-cooled at a cryogenic temperature by dipping it in liquid nitrogen for 2 minutes, changes in the PL resonance are observed. The recombination rates of electron and holes changes when the temperature is changed. Once the wafers come back to the room temperature in 4 to 5 minutes, the PL peak also returns at its original PL resonance wavelength. This evidently demonstrates that the peaks PL peaks of silicon nitride are due to the formation of excitons, Figure 4.25.

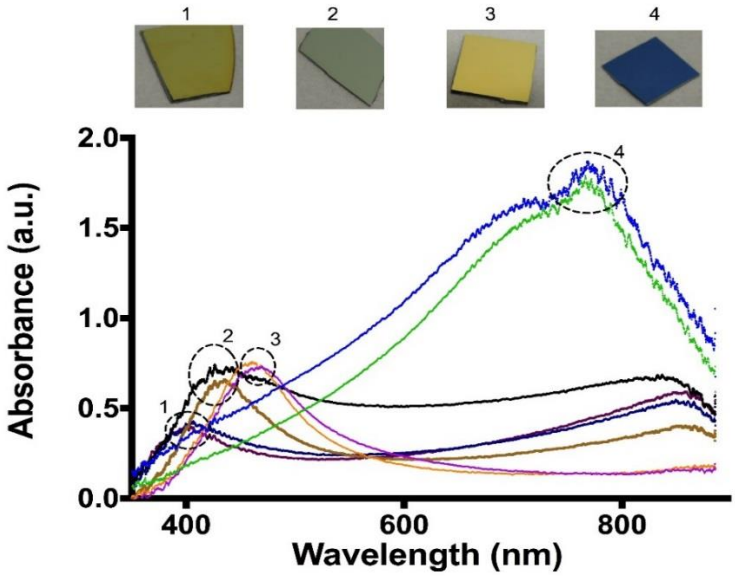

Figure 4-25 Effect of cooling wafer in liquid nitrogen

4.9 Conclusions

The chapter successfully demonstrated the detection of pH changes associated with the phosphorylation of proteins on pH-sensitive oxide semiconductor capacitors and with a commercial micro-pH electrode. A good correlation was observed between the hypothesis and the experimental results. Direct detection of pH variations is challenging due to the buffering capabilities of buffer solution and to the technological difficulties in developing micro-pH electrodes which are subjected to less hydration and ion-migration. Combination of pH sensing with LSPR detection revealed complementary biosensing capabilities of semiconductor materials, which is a step forward towards integrating multiple techniques on a single device for biosensing applications.

References

[1] N. Bhalla, M. Di Lorenzo, G. Pula, and P. Estrela, "Protein phosphorylation analysis based on proton release detection: potential tools for drug discovery," *Biosensors and Bioelectronics*, vol. 54, pp. 109–14, 2014.

[2] N. Bhalla, M. Di Lorenzo, G. Pula, and P. Estrela, "Protein phosphorylation detection using dual-mode field-effect devices and nanoplasmonic sensors," *Scientific Reports*, vol. 5, pp. 1-8, 2015.

[3] J. Piehler, a Brecht, R. Valiokas, B. Liedberg, and G. Gauglitz, "A high-density poly(ethylene glycol) polymer brush for immobilization on glass-type surfaces" *Biosensors and Bioelectronics*, vol. 15, no. 9–10, pp. 473–81, 2000.

[4] "Online Analysis Tools-Protein Chemistry." http://molbiol-tools.ca/Protein_Chemistry.htm.

[5] E. Kinoshita, E. Kinoshita-Kikuta, A. Shiba, K. Edahiro, Y. Inoue, K. Yamamoto, M. Yoshida, and T. Koike, "Profiling of protein thiophosphorylation by Phos-tag affinity electrophoresis: Evaluation of adenosine 5'-O-(3-thiotriphosphate) as a phosphoryl donor in protein kinase reactions" *Proteomics*, vol. 14, pp. 668–79, 2014.

[6] K. Horiuti, "Kinetics of contraction initiated by flash photolysis of caged adenosine triphosphate in tonic and phasic smooth muscles," *Journal of General Physiology*, vol. 94, pp. 769–781, 1989.

[7] M. Waleed Shinwari, M. Jamal Deen, and D. Landheer, "Study of the electrolyte-insulator-semiconductor field-effect transistor (EISFET) with applications in biosensor design," *Microelectronics. Reliability*, vol. 47, pp. 2025–2057, 2007.

[8] K. Kerman and H.-B. Kraatz, "Electrochemical detection of kinase-catalyzed thiophosphorylation using gold nanoparticles," *Chemical Communication*, pp. 5019–5021, 2007.

[9] P. K. Jain, W. Huang, and M. A. El-Sayed, "On the universal scaling behaviour of the distance decay of plasmon coupling in metal nanoparticle pairs: A plasmon ruler equation," *Nano Letters*, vol. 7, pp. 2080–2088, 2007.

[10] F. Wang, D. Li, D. Yang, and D. Que, "The coupling between localized surface plasmons and excitons via Purcell effect," *Nanoscale Research Lett*ers, vol. 7, pp. 669–674, 2012.

[11] J. C. Owicki, L. J. Bousse, D. G. Hafeman, G. L. Kirk, J. D. Olson, H. G. Wada, and J. W. Parce, "The light-addressable potentiometric sensor: principles and

biological applications" *Annual. Reviews of Biophysics and Bimolecular. Structure,* vol. 23, pp. 87–113, 1994.

[12] T. Yoshinobu, M. J. Schoning, R. Otto, K. Furuichi, Y. Mourzine, Y. Ermolenko, and H. Iwasaki, "Portable light-addressable potentiometric sensor (LAPS) for multisensor applications," in *Sensors and Actuators, B: Chemical*, vol. 95, pp. 352–356, 2003.

[13] T. Yoshinobu, H. Iwasaki, Y. Ui, K. Furuichi, Y. Ermolenko, Y. Mourzina, T. Wagner, N. Näther, and M. J. Schöning, "The light-addressable potentiometric sensor for multi-ion sensing and imaging," *Methods*, vol. 37. pp. 94–102, 2005.

[14] J. Kistner, X. Chen, Y. Weng, H. P. Strunk, M. B. Schubert, and J. H. Werner, "Photoluminescence from silicon nitride—no quantum effect," *Journal of Applied Physics*, vol. 110, pp. 023520 1-4, 2011.

[15] G. Sun, J. B. Khurgin, and R. A. Soref, "Practical enhancement of photoluminescence by metal nanoparticles," *Applied Physics Letters*, vol. 94, pp. 101103 1-3, 2009.

[16] L. Tsakalakos, J. Balch, J. Fronheiser, M.Y. Shih, S.F. LeBoeuf, M. Pietrzykowski, P.J. Codella, B.A. Korevaar, O.V. Sulima, J. Rand, A. Davuluru, 2007. Strong broadband optical absorption in silicon nanowire films. Journal of Nanophotonics, 1(1), pp.013552-013552.

[17] N.I. Zheludev Y.S. and Kivshar, 2012. From metamaterials to metadevices. Nature materials, 11(11), pp.917-924.

Chapter 5 Protein phosphorylation studies on gold surfaces

This chapter describes the charge changes associated with phosphorylation of proteins on gold (Au) surfaces. Electrolytic metal-insulator-semiconductor (MIS) capacitors with Au utilised as the sensing surface were used to detect changes in the charge associated with the phosphorylation of proteins. The charge sensing on the MIS capacitors was also combined with LSPR sensing with the use of gold nanoparticles. The results of MIS and LSPR techniques were validated using conventional surface plasmon resonance (SPR) and quartz crystal microbalance (QCM). This chapter also describes the plasmonic interactions on the Au surfaces visualised using finite element analysis software.

5.1 Protein immobilisation on gold surface

Self-assembled monolayers (SAMs) are chemical nanostructures (0.5-1.5 nm) that provide functionalisation of metals, insulators and semiconductor surfaces for the attachment of biomolecules such as proteins and DNA, [1]. Au surfaces have a high affinity to sulphur atoms (S) and forms a bond through chemisorption. This interaction allows thiol (R—SH) SAMs to be easily formed on Au surfaces [1–3]. Prior to the formation of SAMs, Au surfaces were stringently rinsed using acetone and then isopropanol. Solutions of 1 mM mercaptoundecanoic acid (MUA) and 1 mM 6-mercapto-1-hexanol (MCH) were prepared in ethanol and used to form the SAM by incubating in a 1:9 MUA and MCH mixture (MUA--MCH) for 18 hours. This is the optimised ratio that maximises the number of proteins attached by reducing effects like steric hindrance. It is the sulphur atom of the mercapto groups of MUA and MCH that attach to the Au surface. The other end of the MUA molecule has a carboxyl group that can be activated to allow later attachment of proteins. Likewise, MCH has a hydroxyl group on the other end that does not interact with the biomolecules but acts a spacer molecule between two MUA molecules. The carboxyl groups of MUA were converted to amine-reactive NHS esters for bio-conjugation using a 10 mM ethyl-

dimethylaminopropyl carbodiimide (EDC) and N-Hydroxysuccinimide (NHS) mixture (EDC—NHS) in a ratio of 4:1. The carboxylic group of MUA reacts with EDC to form an intermediate, o-Acylisourea, which is unstable in nature. o-Acylisourea forms a NHS ester in the presence of NHS to form stable conjugates with primary amines on the proteins. 156 µM myelin basic protein (MBP) was dispensed onto the Au surface and left for 15 minutes, enabling the amino groups of MBP to attach to the ester group of carboxyl EDC--NHS activated complex. The unreacted MUA sites were blocked by incubating the sample in 1 mM ethanolamine in Trisaminomethane (Tris) buffer, pH 7.5, for 10-12 minutes [4].

5.2 Dual mode sensing on Au surfaces

A technique combining both the field effect sensing (MIS) and optical sensing (LSPR) techniques was developed to study phosphorylation of proteins on the Au surfaces as shown in Figure 5-1 [5].

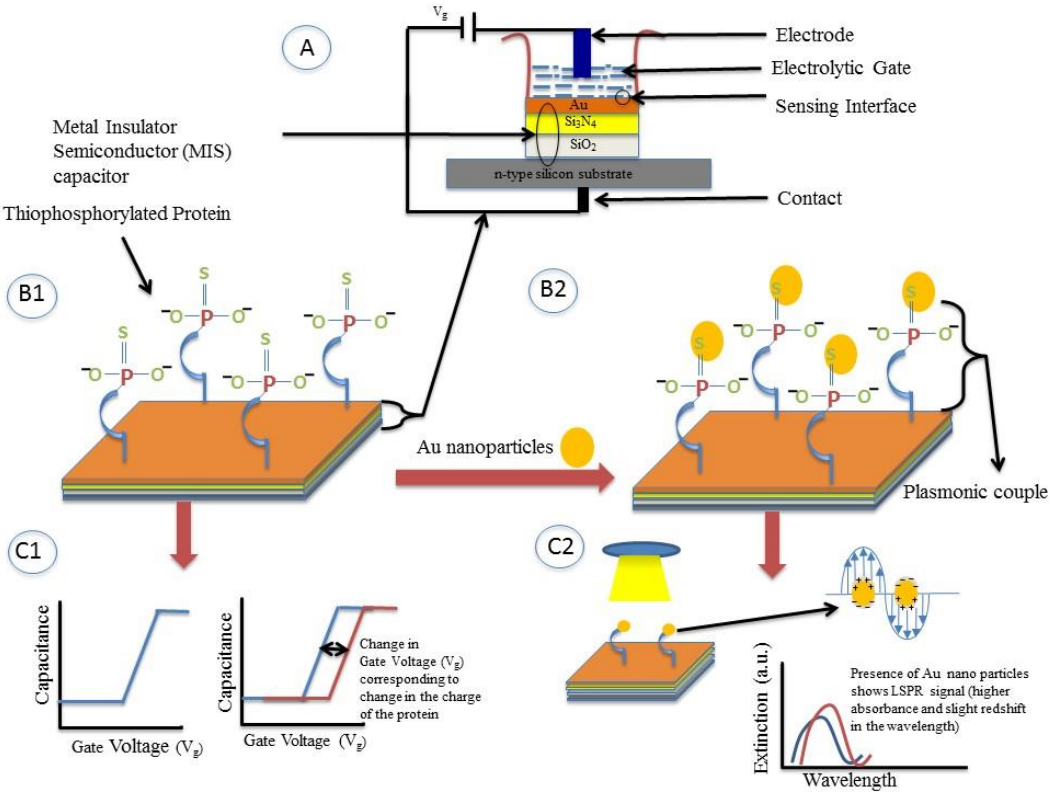

Figure 5-1 Scheme for protein phosphorylation analysis: (A) Field effect device for protein phosphorylation measurement; (B1) metal–insulator–semiconductor (MIS) capacitor structure with immobilised proteins after thiophosphorylation ; (B2) AuNPs attached to the thiol groups of thiophosphorylated proteins in 'plasmonic ruler' configuration; (C1) Capacitance vs. gate voltage

characteristic curves of MIS showing change in gate voltage corresponding to the charge on the phosphorylated proteins; (C2) LSPR measurement of plasmonic ruler.

To perform phosphorylation of the proteins, 5'-[γ-thio] triphosphate (ATP-S) was used a source of phosphate. This enables the attachment of gold nanoparticles (AuNPs) to the proteins which become thiophosphorylated on Au surfaces to form an AuNP–Au film plasmonic couple. The presence of this plasmonic couple was studied using LSPR. By combing two techniques a more reliable measurement is provided at reduced time and cost compared to other authentication methods.

MIS capacitance and LSPR were carried out on laboratory-prepared substrates. 10 nm of chromium was deposited by thermal evaporation on to the Si_3N_4 substrates, described in chapter 4, to act as an adhesion layer followed by 100 nm of gold. The final structure comprised of: Al—Si--SiO_2--Si_3N_4—Cr—Au. The wafer was sandwiched between a Teflon well with an o-ring and a conductive copper plate, such that the aluminium coated side of the wafer sat on the lower conductive plate.

5.2.1 MIS sensor studies

A conventional three-electrode electrochemical setup was employed with an Ag/AgCl reference electrode immersed in the electrolyte *via* a salt bridge used to apply the gate voltage and a Pt counter electrode. During the measurements, the gate voltage (V_g), was applied between the reference electrode and the Al back-contact and was varied between -2.0 and +2.0 V, superimposed with a small ac signal of 10.0 mV at 1 kHz. The first measurement for the reaction was taken after protein immobilisation, *i.e.* before the start of the phosphorylation process. After adding kinase, ATP and the kinase activator, the activity of the reaction was studied by recording the *C–V* characteristics every 2 minutes for 8 minutes and then a final measurement was taken at 20 minutes. Gold nanoparticles were then added and after 10 minutes a reading was taken before washing with the reaction buffer. After this, the sample was allowed to stabilise and two readings were taken at 10 minute intervals. In the control reactions, *C–V* measurements were taken at similar time intervals. Each experiment was repeated at least 6 times and the reported data corresponds to the average values.

Figure 5-2 shows the change in the gate voltage, ΔV_g, upon treatment of immobilised MBP with PKC-α kinase (4 units), its activator and ATP-S, at different time intervals. As the time interval for the interaction of MBP with PKC was extended, the changes in V_g increase until they stabilise after 10 minutes to a value of 12.0-13.5 mV.

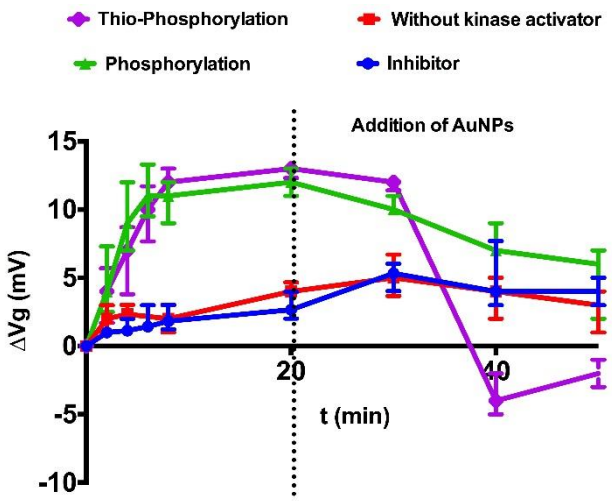

Figure 5-2 Protein phosphorylation on gold MIS capacitor structures: Time-dependent changes in gate potential upon: i) thiophosphorylation of MBP by PKC-α kinase in the presence of ATP-S; ii) phosphorylation of MBP by PKC-α kinase in the presence of ATP, iii) control reactions in the absence of kinase activator and iv) in the presence of kinase inhibitor;

Tests conducted with ATP instead of ATP-S also revealed similar values of voltage shifts between 12.0-13.0 mV. Experiments without PKC-α showed ≤4.0 mV shift, implying that kinase activator is essential to induce phosphorylation of MBP. The reaction where inhibitor was used showed a shift of ≤3.7 mV. Upon addition of phosphate or thiophosphate groups to the immobilised proteins there is a negative charge imparted on the surface of the sensor (Au), which is responsible for the shift in gate voltage and the MIS capacitor characteristics. The slight variations in gate voltage that are observed in the control reactions are ascribed to equilibrium changes in the buffer solution upon addition of kinase. To validate the thiophosphorylation process AuNPs were added to the reaction with Au covalently attaching to the thiol groups. After adding AuNPs, a significant shift in the voltage of -18.0 mV was observed in the thiophosphorylated samples. This is attributed to the fact that the AuNPs were covalently grafted to the thiophosphorylated proteins, thereby masking the negative charge imparted by the thiophosphoryl groups. All other experiments showed changes of < 5.0 mV. For instance, the reactions occurring in the presence of inhibitor and in

the absence of kinase activator showed changes < 1.5 mV. These small changes are due to non-specific interactions of the AuNPs with the proteins. In the reaction where phosphorylation was performed in the presence of ATP, the AuNPs interact slightly more than the other controls due to an apparent affinity of AuNPs to any charged molecules (phosphoryl groups transferred to the protein in this case). Most of these reactions have non-specific electrostatic interactions and are removed by stringent rinsing, leaving only the covalently bound or very strong electrostatically bound AuNPs on the surface [6]. The successful detection of the protein phosphorylation event was then assessed to study the kinase activity. The gold surface immobilised with MBP was reacted with different concentrations of PKC-α in the presence of ATP-S and kinase activator. Figure 5-3 shows ΔV_g after maximum kinase activity was observed with increasing kinase concentrations. It depicts that a minimum of 1-2 units of kinase per reaction (per 100 µl) is required to see any distinguishable change from the controls.

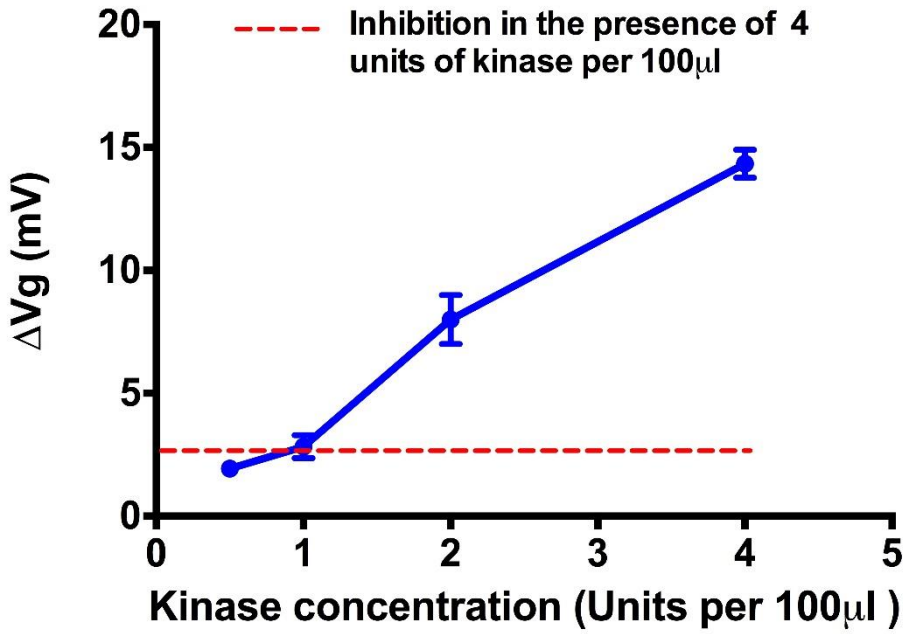

Figure 5-3 Variations in V_g observed upon thiophosphorylation with increasing kinase concentrations.

5.2.3 LSPR studies

LSPR measurements were performed on the same samples (on which MIS was measured) simultaneously at two instances, first after thiophosphorylation but before adding AuNPs and second, after adding the AuNPs. The readings were recorded using

SpectraSuite software *via* the LSPR system as described in the previous chapter. Figure 5-4 shows the measurement before adding gold nanoparticles. The resonance peak of the MIS structure with Au as the top layer was found to be 482 nm. These peaks are attributed to the surface plasmons formed on the surface of the gold when light shines on it. Shifts in this curve are monitored to analyse the binding of AuNPs to the gold surface.

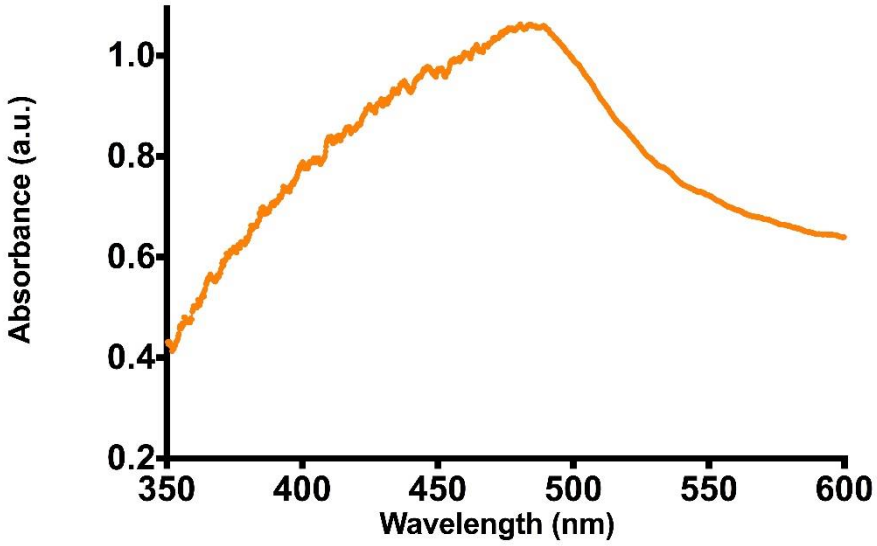

Figure 5-4 Resonance peak of gold.

Shifts in the wavelength were only seen in the thiophosphorylated reactions. An average red-shift of ~6 nm was observed in the thiophosphorylated samples, as compared to a small red-shift, ≤ 1.5 nm, in the controls (Figure 5-5 a,b,c). This increased spectral shift for the thiophosphorylated reactions is due to the formation of periodic 'plasmonic rulers', across the entire surface, whereby the plasmonic coupling results in a red-shift of the spectra. The surface distribution of the non-specifically attached AuNPs is non-periodic and therefore the shift was much smaller. In addition, the absorbance values of all the controls were found to be consistent and much smaller than the thiophosphorylated reactions (Figure 5-5 b). However, a blue-shift of 9.1 nm was observed in the thiophosphorylated reaction after stringent washing of the substrate with the reaction buffer.

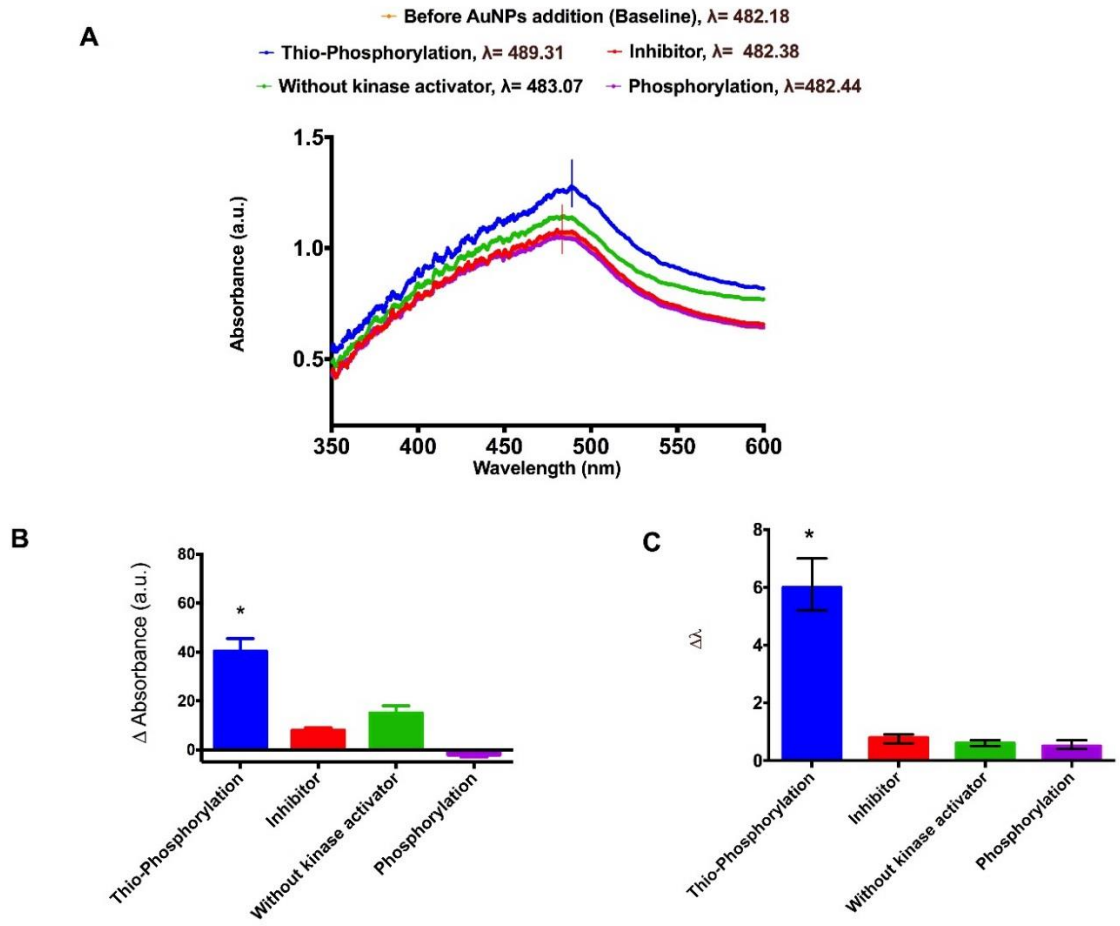

Figure 5-5 LSPR measurements for protein phosphorylation: (a) LSPR characteristic curve for thiophosphorylation , phosphorylation, controls in absence of kinase activator and presence of kinase inhibitor, and Au surface with immobilized proteins; (b) absolute absorbance change after adding AuNPs to thiophosphorylated , phosphorylated and control reaction samples; (c) LSPR wavelength shift after adding AuNPs to thiophosphorylated , phosphorylated and control reaction samples.

While there was a removal of non-specifically attached AuNPs from the controls, there was also a reduction of AuNPs from the thiophosphorylated sample. AuNPs usually have a tendency to cluster; therefore the NP aggregation around the covalently bound AuNPs was removed upon washing. The presence of higher absorbance signals is evidence of presence of covalently attached AuNPs from the thiophosphorylated proteins (Figure 5-6).

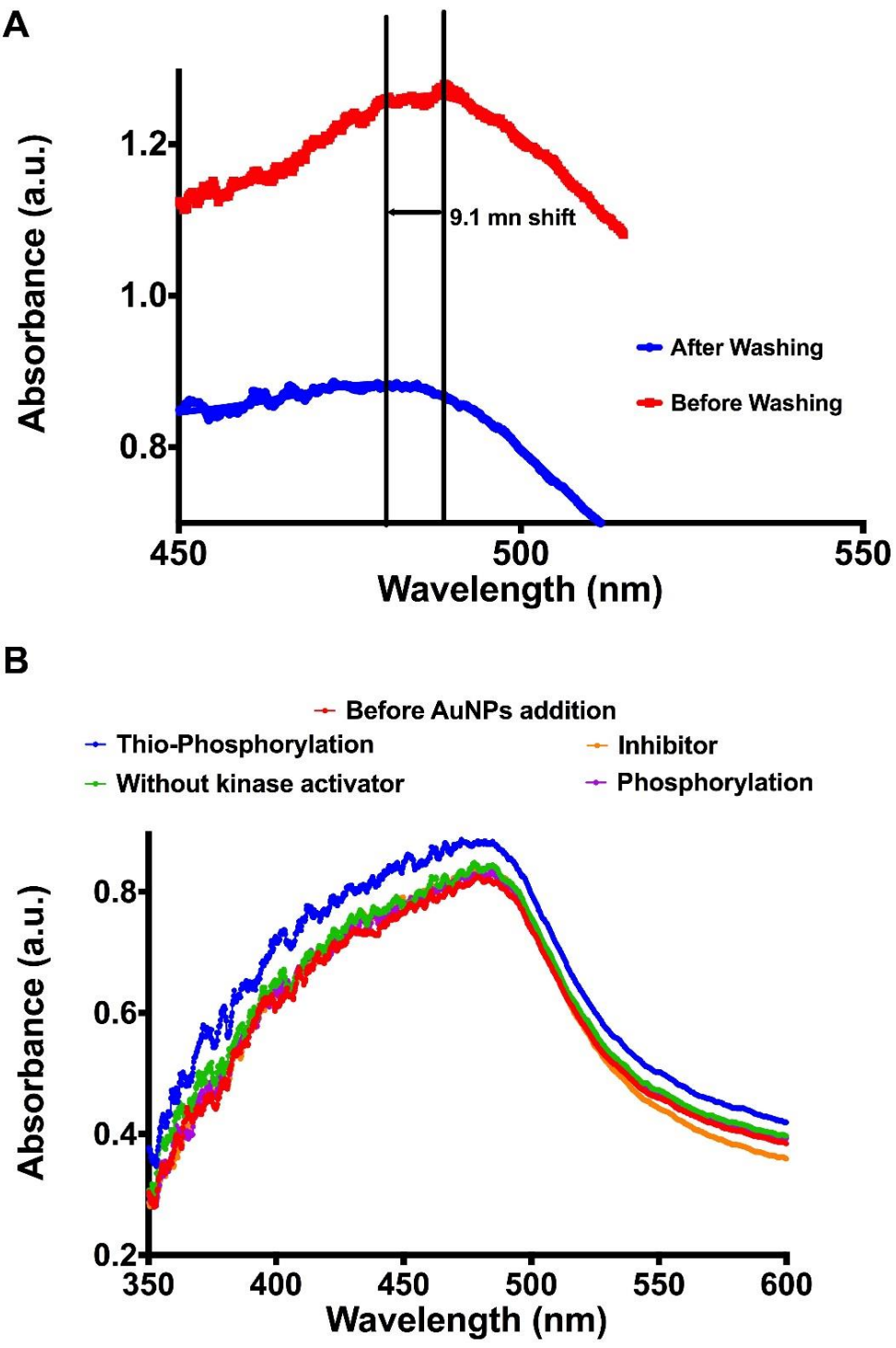

Figure 5-6 Effect of stringent washing (A) comparison of thiophosphorylation curve before and after washing (B) curves of all reactions after washing

An evaluation to cross-validate the removal of only aggregated AuNPs was done by comparing the full width at half maximum (FWHM) of the curves before and after washing. The change in the FWHM along with changes in the absorbance is associated

with the size of the plasmonic object. A broader peak indicates the presence of large range in size and shape (disorder in distribution) of the particles, whereas a decrease in the absolute absorbance indicates a decrease in the size distribution [7]. The FWHM of thiophosphorylated samples decreases by ~ 30 nm after washing, which is assigned to the decrease in the size of the plasmonic object (aggregated AuNPs), therefore asserting the fact that aggregated AuNPs are removed.

5.3 Finite element modelling

The electric field distribution in the plasmonic-coupled system was analysed using finite element modelling with COMSOL. COMSOL is a platform that allows users to visualise a physical effect dependent upon multiple factors that defines that phenomenon [8–10]. To visualise the plasmonic coupling effect, the MIS structure described previously (Al-Si-SiO_2-Si_3N_4-Cr-Au) was coupled with AuNP as shown by the geometry in Figure 5-7.

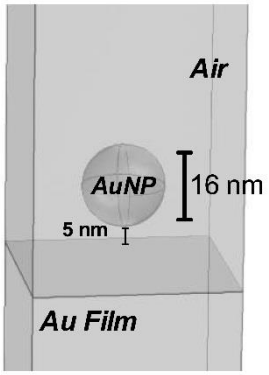

Figure 5-7 Geometry design of a plasmonic coupled system

Within the model, the AuNP and an Au film were separated by 5 nm. The size of the AuNP was chosen as 16 nm (the AuNPs have average size of 16 nm, discussed in Chapter 4). Below are the values of permittivity for the materials used to design the structure:

- Au at 564 THz : -3.54 -j2.58
- Si_3N_4: 7.5
- SiO_2: 2.25

- Cr: -9.84-j*23.21
- Si: 13.69

The other physical properties of the materials were extracted from the built-in materials library of COMSOL. Simulations were done using radio frequency module of COMSOL 4.4. The model was analysed in the frequency domain (emv) of the electromagnetic waves submodule using built-in Maxwell equations. A 'fine mesh' was used to obtain high-resolution analysis. COMSOL provides a number of default plots and the electric field distribution plot (Figure 5-8) was obtained to observe the plasmonic coupling integration between the Au-film and the AuNP.

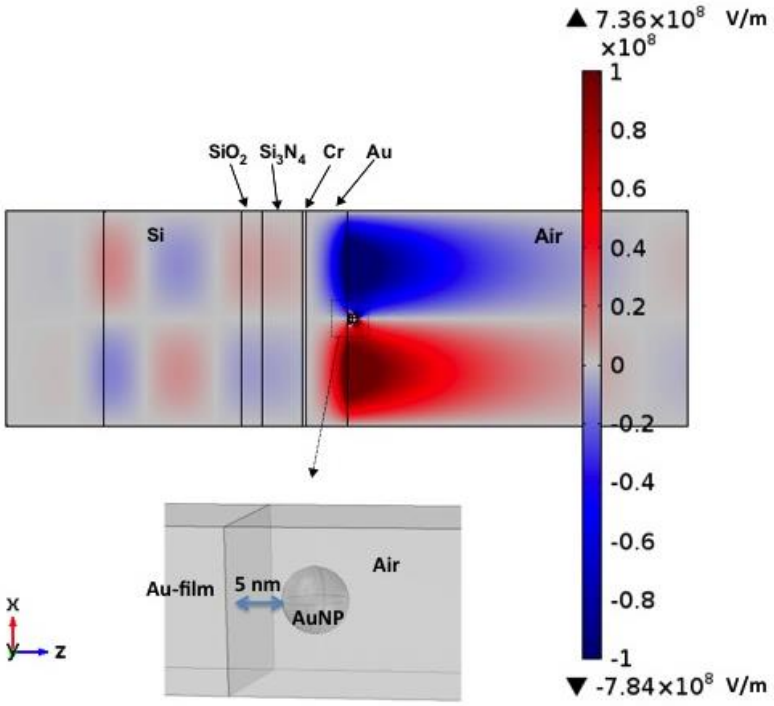

Figure 5-8 Electric field distribution of a plasmonic coupled system.

Simulations revealed that the plasmonic interaction between the Au-film and the AuNP had a resonance frequency of 485 nm (Figure 5-9).

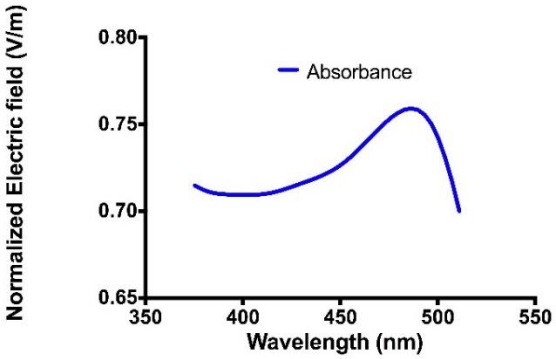

Figure 5-9 Absorbance of electric field distribution vs. wavelength

This is in agreement with the LSPR studies in the previous text (Section 5.2.3) where the Au-film and AuNP resonated around 480 nm. In addition it supports the experimental observation where a change in wavelength upon attachment of the AuNPs on Au film was seen.

5.3.1 Plasmonic ruler

The ability of 2 plasmons to quantify the distance between them gives rise to the formation of a 'plasmonic ruler'. When a surface plasmon (SP) or localised surface plasmon (LSP) resonating at its natural wavelength interacts with another plasmon (SP or LSP) there is a change in its resonant properties [11]. The shifts in wavelength that occur upon this interaction depend on the distance between the two plasmons [12]. In literature an empirical formula (Equation 5.1) was established by Jain *et al*. to quantify the 'plasmonic ruler' [13].

$$\frac{\Delta\lambda}{\lambda_o} = 0.18 \exp\left\{\frac{(-s/D)}{0.23}\right\} \quad (5.1)$$

where *s* is the inter particle separation, *D* is the diameter of nanoparticle (16 nm in this case) and λ_o is the resonance wavelength of substrate (480 nm in this case).

Figure 5-10 shows the change in wavelength versus the distance between the plasmons. According to the above empirical 'plasmonic ruler' equation the distance between the nanoparticle and the sensor film is estimated as 5.0 ±0.2 nm. This value

is calculated for a particle of 16 nm with a decay length of 0.12 nm that yields 5.0-6.5 nm of Δλ-shift on the LSPR signal.

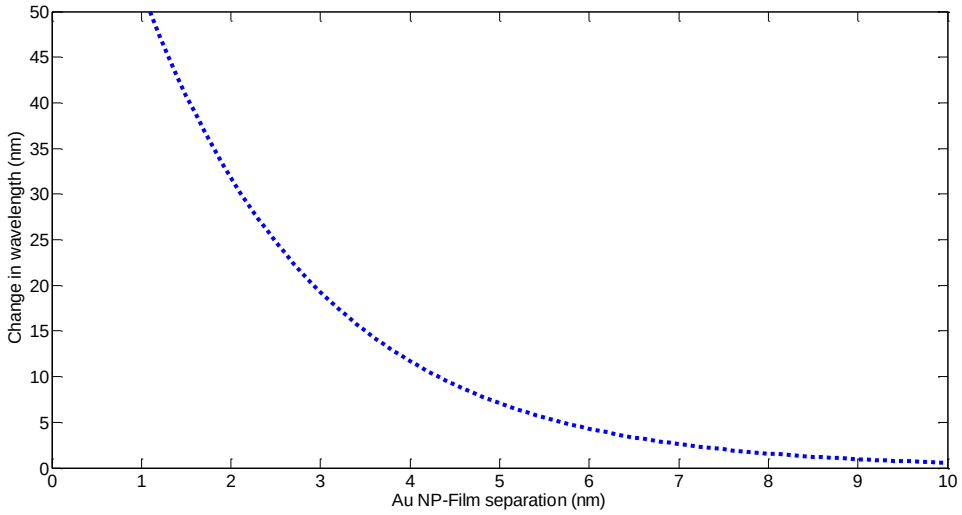

Figure 5-10 change in wavelength versus distance between the plasmons

This is in agreement with the approximate length of the bio-complex structure evaluated as approximately 5.0 nm (~1.5 nm for the MUA+EDC/NHS self-assembled monolayer and 3.0-4.0 nm for the protein).

5.4 SPR for phosphorylation of proteins

SPR measurements were carried out using a Reichert SPR 7000DC dual channel flow spectrometer at 25 °C. All reactions steps were validated on the Au chip. 50 nm Au-coated SPR gold chips, supplied from Reichert Technologies were used for studying the reaction with SPR. Prior to their use, these chips were cleaned using piranha solution (3:1, H_2SO_4:H_2O_2) and rinsed thoroughly with DI water. The concentrations of protein, kinase ATP-S, inhibitor and other biofunctionalisation reagents were as described in previous chapters. All buffers, namely Tris buffer and PBS 0.1 mM, pH 7.5 were filtered through 0.2 µm filters and degassed for 2 hours by sonication to avoid any bubble formation in the channels during SPR measurement. The MUA-MCH-modified Au chips were kept in running Tris buffer at a flow of 25 µl/min until a stable baseline was achieved. Then the surface was activated with EDC-NHS for 5 minutes and exposed to the proteins for 10 minutes. After this, ethanolamine was

injected for 10 minutes. Between each step washing of the surface was performed using the running Tris buffer. Following this, thiophosphorylation was performed in the presence of ATP-S, kinase activator and kinase and then the surface was washed with the running buffer after 15 minutes of incubation. The running buffer was then changed from Tris to 0.1 mM PBS (since the gold nanoparticles were prepared in 0.1 mM PBS) and the thiophosphorylated chips were kept in the new PBS running buffer at a flow rate of 35 µl/min until baseline stability was obtained. Finally gold nanoparticles were injected for 15 minutes followed by a washing step with the PBS buffer to remove unbound residues. The experiments were repeated 8 times to check the reproducibility and average values are reported in the next section of results.

5.4.1 SPR Analysis

Figure 5-11 shows the real-time SPR evaluation of all but one of the process steps performed to complete the thiophosphorylation assay. The only step that is not shown is the formation of the SAM using MUA and MCH along with its activation by EDC/NHS. A change of 1 µRIU on the instrument is approximately equivalent to a change of 1 pg/mm^2 protein surface coverage.

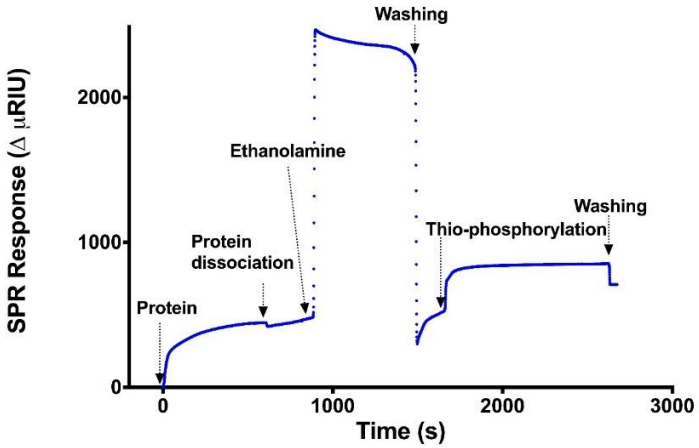

Figure 5-11 Real-time detection of the thiophosphorylation reaction using Reichert SPR 7000DC spectrometer

Upon immobilisation of MBP (19 kDa) on the SAM, a change of 393 µRIU was observed, which corresponds to approximately 0.002 nmol/cm^2 or 1.24×10^9 molecules/cm^2 of protein surface coverage. Similarly, after phosphorylation of proteins (*i.e.* addition of PO_3S^-, 111.04 g/mol) there was an addition of 0.075 nmol/cm^2 or 4.52×10^{10} molecules/cm^2. The total number of sites available for thiophosphorylation of MBP depends upon the number of amino acids capable of becoming phosphorylated. Assuming that roughly 25 sites are available for phosphorylation, around 9.92×10^{10} sites/ cm^2 are available for thiophosphorylation. In theory this corresponds to 145.6% thiophosphorylation. This is attributed to the overestimation of the assumption (µRIU =1 pg/mm^2) which is more valid for protein binding.

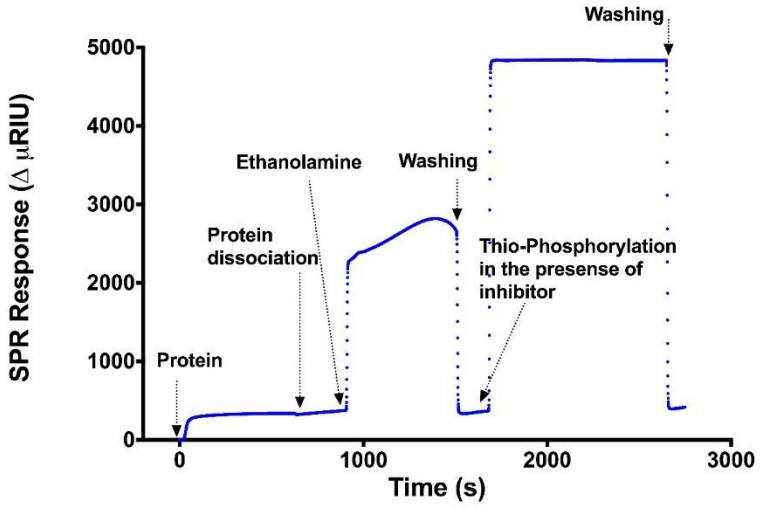

Figure 5-12 Real-time detection of thiophosphosphorylation inhibition reaction

Figure 5-12 shows a SPR plot whereby the thiophosphorylation reaction was inhibited by GF109203X. In the presence of the inhibitor there is an insignificant shift of 3.5 µRIU as compared to 86.6 µRIU after thiophosphorylation.

Figure 5-13 shows the binding of AuNPs to the thiophosphorylated sites yielded an average shift of 4999 µRIU, thereby, enhancing the sensitivity approximately 57 times as compared to 86.6 µRIU change observed after addition of thiophosphoryl groups. There are three effects that produce these shifts: 1) addition of mass on the Au surface upon attachment of the AuNPs; 2) interaction between the surface plasmon and the localised surface plasmons on the AuNPs; 3) significant change in the dielectric

properties of the multilayer biofilm upon AuNP attachment. All aforementioned reasons contribute to the changes in the refractive index of the SPR Au-film, thereby changing its sensitivity. The attachment of the nanoparticles on the inhibitor samples generates a change of 593 μRIU. These are mainly due to the non-specific attachment of the AuNPs on the surface of Au.

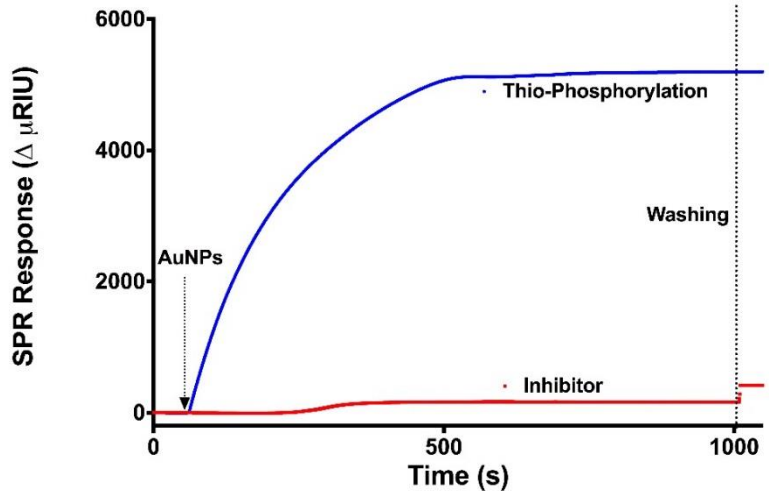

Figure 5-13 AuNPs attachement on thiophoshjorylated compared to the inhibition reaction.

Nevertheless, the thiophosphorylation reaction was easily distinguishable from the inhibitor as seen in Figure 5-13 and the statistical results in Figure 5-14

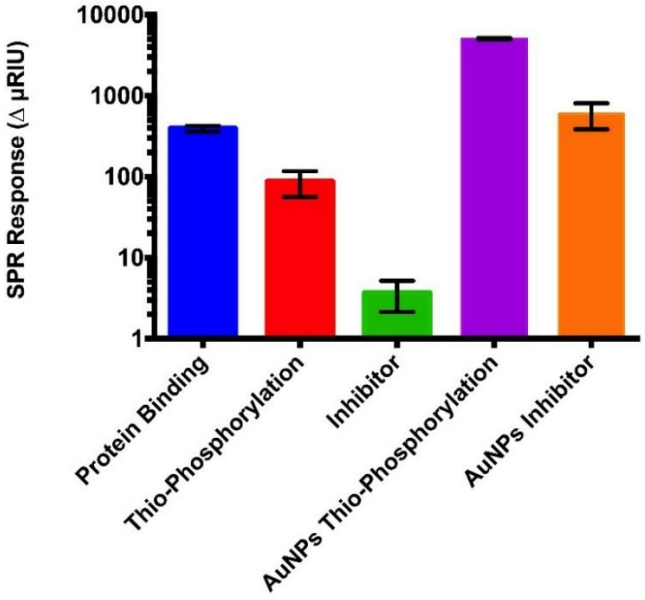

Figure 5-14 SPR response for the different positive and negative controls (the error bars indicate the standard deviation of 3 samples).

5.5 QCM analysis

The biofunctionalisation and thiophosphorylation on QCM was done on an AT-cut quartz crystal with 10 MHz resonant frequency with the same concentrations as those used for MIS and SPR measurements. The QCM was under quasi-static conditions where flow was introduced manually using a syringe, and sample solutions were injected at various steps, as described in Figure 5-15. The QCM crystals were purchased from JLM innovation and were given a stringent acetone wash before use.

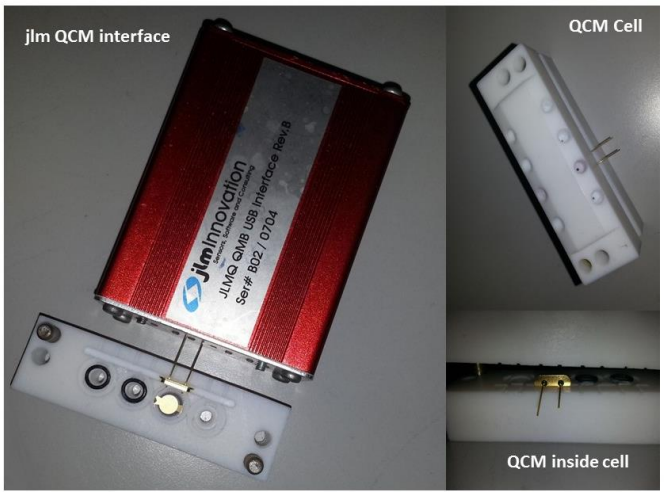

Figure 5-15 QCM cell integrated with 10 MHz crystal and an electronic interface.

The QCM response was quantified using the Sauerbrey equation (5.2) [14].

$$\Delta f = \frac{2 f_0^2}{A\sqrt{\mu_q p_q}} \Delta m \quad (5.2)$$

The variables of the equations are defined as follows: f_0 – resonant frequency; Δf – frequency change; Δm – mass change; A – piezoelectric active crystal area; p_q – density of quartz (2.648 g cm^{-3}); μ_q – shear modulus of quartz for AT cut crystal (2.947×10^{11} g cm^{-1} s^{-2});

Upon immobilisation of MBP a resonant frequency change of 130 Hz was observed as seen from Figure 5-16. This frequency change corresponds to 2.287×10^{12} protein molecules. Similarly for nanoparticle quantification, the QCM technique was implemented to calculate the total mass bound on the surface.

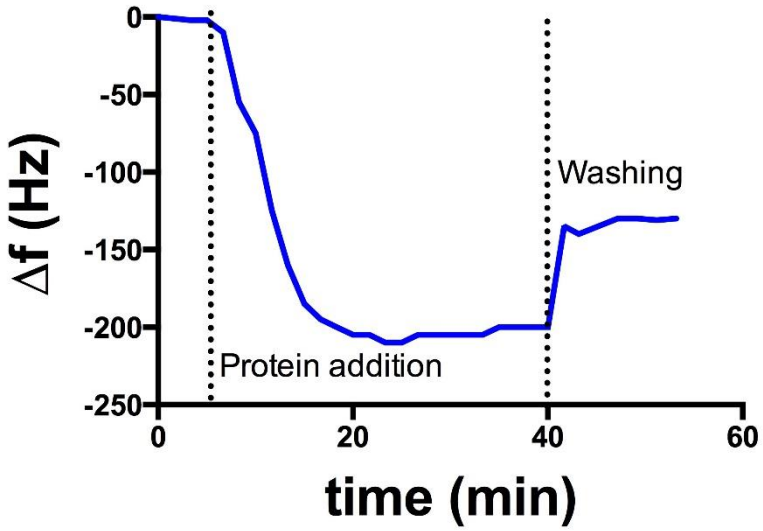

Figure 5-16 Quantification of portien using QCM.

A change of 170 Hz was observed upon AuNP addition (Figure 5-17). Using the Sauerbrey equation as a rough approximation of the mass loading (*i.e.* ignoring changes in viscosity in the system), this corresponds to an estimated AuNP mass of 480 ng/cm^2 or 1.45×10^9 NPs/cm^2 for 16 nm diameter AuNPs. This value is 10 times lower than the amount of thiophosphoryl groups estimated by SPR. Since the size of the nanoparticle is significantly larger than the size of the thiol group, not all phosphorylated sites are available for NP attachment.

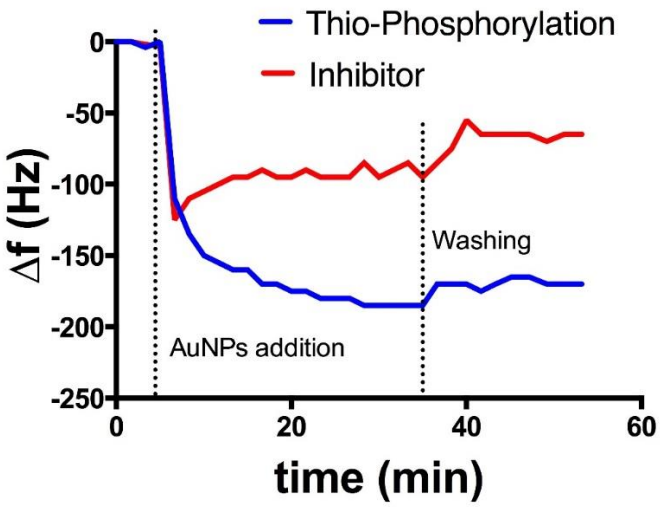

Figure 5-17 AuNPs quantification using gold nanoapartices.

However, this would mean that either the Sauerbrey equation has overestimated the mass of the AuNPs or/and the nanoparticles are clustered [15]. Since the NPs are suspended in a buffer, liquid entrapped could form a viscoelastic film that could then cause additional damping of the quartz oscillator leading to an overestimation of the mass by 10-20%.

References

[1] A. Ulman, "Formation and Structure of Self-Assembled Monolayers" *Chemical Reviews*, vol. 96, pp. 1533–1554, 1996.

[2] M. Godin, P. J. Williams, V. Tabard-Cossa, O. Laroche, L. Y. Beaulieu, R. B. Lennox, and P. Grütter, "Surface stress, kinetics, and structure of alkanethiol self-assembled monolayers," *Langmuir*, vol. 20, pp. 7090–7096, 2004.

[3] T. Wink, S. J. van Zuilen, A. Bult, and W. P. van Bennkom, "Self-assembled monolayers for biosensors" *Analyst*, vol. 122, pp. 43–50, 1997.

[4] H. Sellers, A. Ulman, Y. Shnidman, and J. E. Eilers, "Structure and binding of alkanethiolates on gold and silver surfaces: implications for self-assembled monolayers," *Journal of American Chemical Society*, vol. 115, pp. 9389–9401, 1993.

[5] N. Bhalla, N. Formisano, A. Miodek, A. Jain, M. Di Lorenzo, G. Pula, and P. Estrela, "Plasmonic ruler on field-effect devices for kinase drug discovery applications" *Biosensors and Bioelectronics*, vol. 71, pp. 121–128, 2015.

[6] K. Kerman and H.-B. Kraatz, "Electrochemical detection of protein tyrosine kinase-catalysed phosphorylation using gold nanoparticles" *Biosensors & Bioelectronics* vol. 24, no. 5, pp. 1484–1489, 2009.

[7] M. G. Blaber, A. I. Henry, J. M. Bingham, G. C. Schatz, and R. P. Van Duyne, "LSPR imaging of silver triangular nanoprisms: Correlating scattering with structure using electrodynamics for plasmon lifetime analysis," *Journal of Physcial. Chemistry C*, vol. 116, pp. 393–403, 2012.

[8] N. Bhalla, S.-S. Li, and D. W.-Y. Chung, “Finite element analysis of MEMS square piezoresistive accelerometer designs with low crosstalk,” in *CAS 2011 Proceedings of 2011 International Semiconductor Conference*, pp. 353–356, 2011.

[9] N. Bhalla, S. S. Li, D. Wen, and Y. Chung, “Simulations of MEMS based Piezoresistive Accelerometer Design in COMSOL,” *Proccedings of International COMSOL conference* pp. 2–5, 2011.

[10] N. Bhalla, S. S. Li, D. Wen, and Y. Chung, “Multi-Domain Analysis of Silicon Structures for MEMS based- sensors,” *Proccedings of International COMSOL conferenc* pp. 3–6,2011.

[11] R. T. Hill, J. J. Mock, A. Hucknall, S. D. Wolter, N. M. Jokerst, D. R. Smith, and A. Chilkoti, “Plasmon ruler with angstrom length resolution,” *ACS Nano*, vol. 6, pp. 9237–9246, 2012.

[12] C. Tabor, R. Murali, Mahmoud, and M. A. El-Sayed, “On the use of plasmonic nanoparticle pairs as a plasmon ruler: The dependence of the near-field dipole plasmon coupling on nanoparticle size and shape,” *Journal of Physcial Chemistry A*, vol. 113, pp. 1946–1953, 2009.

[13] P. K. Jain, W. Huang, and M. A. El-Sayed, “On the universal scaling behavior of the distance decay of plasmon coupling in metal nanoparticle pairs: A plasmon ruler equation,” *Nano Letters* vol. 7, pp. 2080–2088, 2007.

[14] N. Formisano, P. Jolly, N. Bhalla, M. Cromhout, S. P. Flanagan, R. Fogel, J. L. Limson, and P. Estrela, “Optimisation of an electrochemical impedance spectroscopy aptasensor by exploiting quartz crystal microbalance with dissipation signals,” *Sensors and Actuators B Chem* vol. 220, pp. 369–375, 2015.

[15] T. Hideaki, E.Kitamura, and Y. Seida. "Detection of AU (III) ions using a poly (N, N-dimethylacrylamide)-coated QCM sensor." Talanta146 (2016): 507-509.

Chapter 6 Phosphorylation studies on a CMOS chip and integration of microfluidics

This chapter extends the EIS sensing to MOSFET (metal—oxide—semiconductor field-effect transistor) devices for the detection of pH changes associated with the phosphorylation of proteins. The MOSFET gate was extended with nanoporous aluminium oxide (Al_2O_3) structures in order to study the pH variations. This chapter also discusses the integration of microfluidics with EIS structures for pH sensing applications.

6.1 MOSFET

The MOSFET is one of the most frequently used electronic devices in human life today. Although many may not realise it, but billions of MOSFETs are used in almost all electronic appliances where information must be stored or processed [1]. Sensing of biomolecules for disease diagnosis is an important application where MOSFETs have proved to be highly selective devices [2][3]. A MOSFET controls the electrical current flowing from one terminal known as the source, to another, known as the drain, through the application of an electrical voltage on the third terminal called the gate. A MOSFET is manufactured on the semiconductor material silicon, one of the most profuse materials found on earth [4]. The advantages of using silicon are:

1) Easy to modulate the conductivity of the material by controlled addition of impurity atoms
2) Charge carriers of different electrical signs (electrons: n-channel and holes: p-type) can be obtained depending on the type of impurities added
3) Allows creation of regions with different types of impurities on the same substrate

Charge of different signs can be isolated if a structure is manufactured with regions alternating with two types of impurities. For instance, an n-channel MOSFET consists of a source and a drain, two highly conducting n-channel semiconductor regions, doped with extrinsic impurities such as phosphorous on a p-type silicon substrate, Figure 6-1. The drain and source are isolated by the p-type substrate with reversed-biased p-n junctions. This creates a barrier between the two regions that prevent the charge to flow from one region to another [5].

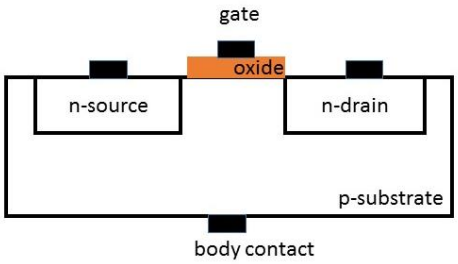

Figure 6-1 A simple n-channel MOSFET structure

The concept of the charge movement in a MOSFET is analogous to 2 tanks with different levels of water separated with a barrier as shown in Figure 6-2. When the barrier is lowered, the water flows from higher level to the lower.

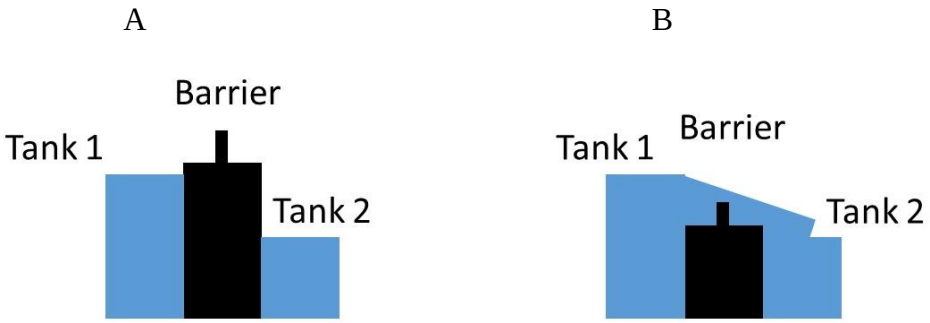

Figure 6-2 Concept of water flow when: A) barrier is closed (no flow); B) barrier is lowered and water moves from higher level to the lower.

Similarly, the barrier between the drain and the source in n-channel MOSFET is lowered by applying a voltage at the gate. The applied gate voltage induces a channel of electrons between the source and drain terminals. These electrons in the channel can be made to flow by applying a voltage across drain to source.

In a simple n-type MOSFET device the source terminal and the body of the device are grounded. The gate and drain voltages are applied with respect to the source. To induce

a conducting channel, the gate voltage (V_{gs}) should be greater than the threshold potential of the device (V_t). The threshold potential of the device is defined as the minimum potential required to create a conducting path between the source and the drain. When $V_{gs} > V_t$ and a potential is applied at the drain, i.e. $V_{ds} > 0$, current begins to flow through the induced channel. All electrons that leave the source exit through the drain. The presence of an insulator at the gate prevents the electrons passing through and hence the gate current is ideally zero ($I_g=0$). The conventional current that flows from the drain to source is denoted as I_d.

Increasing V_{gs} results in a high channel conductivity and therefore I_d increases. This process of increasing the induced channel conductivity by modulating the gate voltage is known as channel enhancement [6]. When $(V_{gs} - V_t) > V_{ds} > 0$, I_d is directly proportional to V_{ds}. In other words the induced channel behaves like a resistor. If V_{ds} is increased such that $(V_{gs} - V_t) < V_{ds}$ the channel no longer behaves like a resistor. There is a competition between the gate and drain to attract electrons from the p-substrate. Since the potential at the drain is higher than the gate, more electrons are attracted towards the drain and the concentration of electrons in the channel at the vicinity of the drain begins to decrease. The induced channel in this state is termed 'pinched-off'. In simple words, increasing V_{ds} results in decreased channel conductivity. However, I_d still continues to flow due to the potential difference between the drain and the source. The net effect on the device is that the change in the I_d decreases and becomes constant as V_{ds} is increased further.

The conditions described above allows the MOSFET device to operate in three modes [6]:

1) cut-off mode, $V_{gs}-V_t < 0$, no channel is created and the device;
2) triode mode, $V_{gs}-V_t > V_{ds} > 0$, the device acts as a variable source of current;
3) saturation mode, $0 < V_{gs}-V_t < V_{ds}$, the device acts as a constant source of current.

These modes are depicted in Figure 6-3

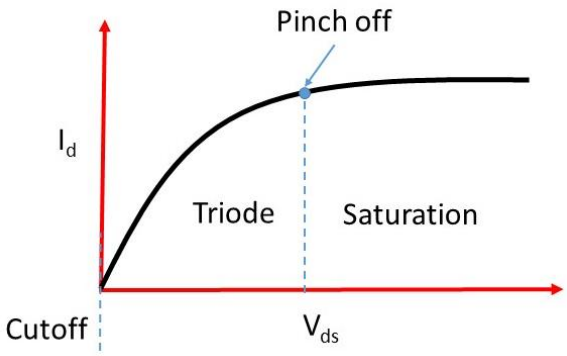

Figure 6-3 I_d-V_{ds} characteristic curve of MOSFET showing modes of operation

6.1.1 Extended gate MOSFET biosensor

The idea of extending the gate of the MOSFET is to integrate the micro-/nanostructures as transducers. Biocompatible micro-/nanostructures, such as zinc oxide nanorods, nanoporous Al_2O_3, and thin gold films, convert the chemical signal from biomolecules into an electrical signal, acting as effective biochemical transducers [7]. Figure 6-4 shows a schematic of an extended gate MOSFET device.

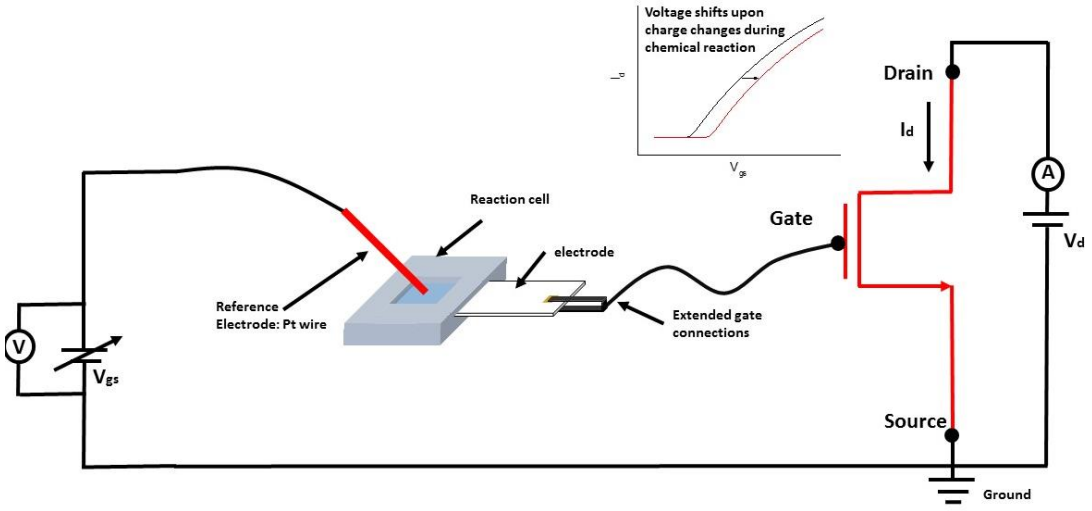

Figure 6-4 Schematic of an extended gate MOSFET

6.1.2 Experimental setup

The extended gate MOSFET sensor used in the experiments consisted of two parts: nanoporous Al_2O_3 electrodes, where protein was immobilised, and the MOSFET structure, which transduces the binding events at the Al_2O_3 electrode into electrical

signals. Nanoporous Al_2O_3 (60-100 nm diameter of the pore) electrodes were prepared using anodisation of 100 nm aluminium films. Anodisation is the process of oxidising the electrode. The electrode to be oxidised (aluminium in this case) acts as an anode and a suitable metal (for instance platinum) acts as the cathode. The anode and cathode are immersed in an electrolyte containing sulphuric acid. A voltage is applied across the anode and cathode and causes negatively charged anions to migrate to the anode and the oxygen in the anions combine with the aluminium to form Al_2O_3 [8].

The extended gate was fabricated by connecting the Al_2O_3 electrodes, fixed in a reaction cell, to the gate of the n-MOSFET device via a metal wire (Figure 6-4). n-MOSFETs were made using 0.8 µm AMS (Austrian Micro System) technology. The threshold voltage of the transistor was 0.82 V and transconductance was 69 µA/V. The length-by-width ratio of the transistor was 10:2 µm. The terminals of the transistor were provided with diode protection circuitry and were packaged in a standard CMOS chip. To operate the transistor, a voltage of 50 mV was applied between the drain and source (V_d or V_{ds}) and the gate-source voltage (V_{gs}) was swept from 0.0 to 5.0 V. These settings limited the current to less than 75 µA, avoiding any changes in V_{gs} by heating. All electrical measurements were done using an Agilent B1500A semiconductor device analyser. Figure 6-5 and 6-6 shows the I_d-V_{ds} and I_d-V_{gs} characteristics of the MOSFET respectively.

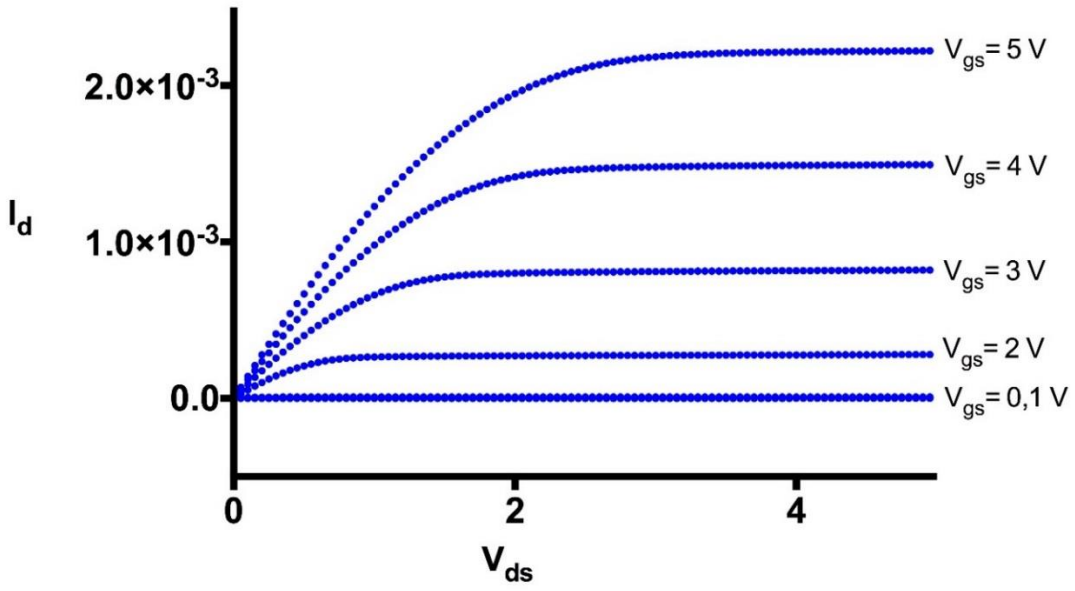

Figure 6-5 Drain characteristics of MOSFET

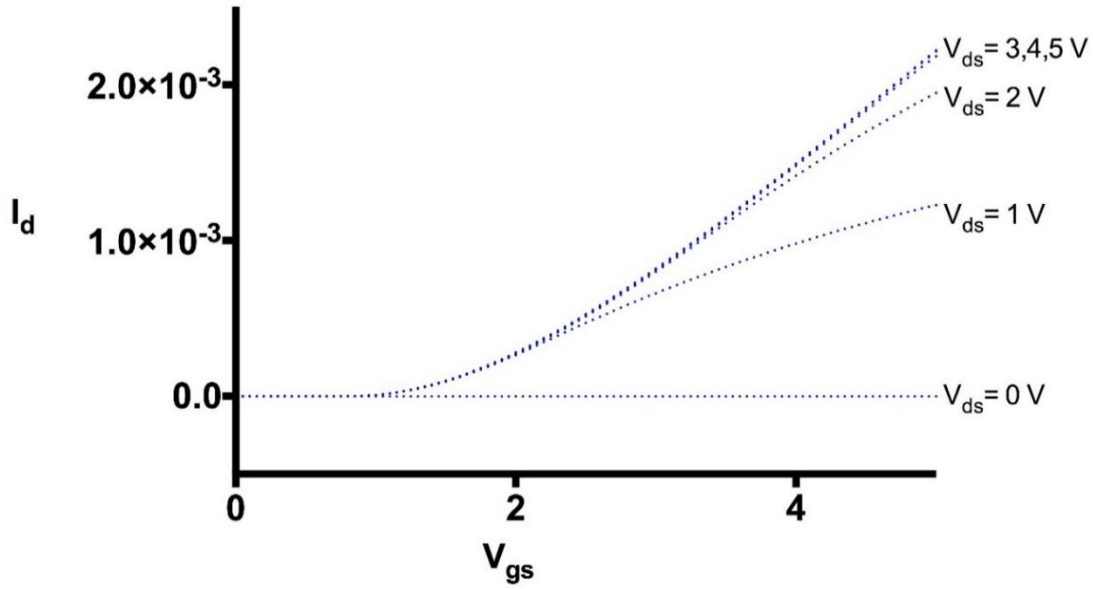

Figure 6-6 Transfer characteristics of MOSFET

6.1.3 pH measurement on Al_2O_3

The effect of pH changes on planar Al_2O_3 (100 nm thick) and nanoporous Al_2O_3 (60 nm pore) was measured using Tris buffer prepared in laboratory conditions (pH 6.6, 7.1 and 7.6). Phosphate buffers [Hanna instruments] (pH 4.0, 7.0 and 9.0) were also used to study pH variations. Figure 6-7 shows a picture of 60 nm Al_2O_3 prepared by anodisation of aluminium deposited on glass.

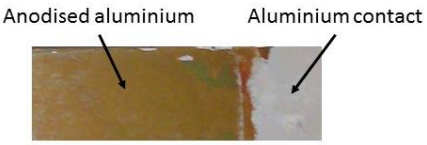

Figure 6-7 Physical appearance of 60 nm anodised structure in sulphuric acid

Figure 6-8 shows the changes in the I_d-V_{gs} characteristics of the MOSFET caused by variations in pH. An average (mean) sensitivity of 57 mV/pH was obtained on planar Al_2O_3 as compared to 23 mV/pH in 60 nm nanoporous Al_2O_3 structures.

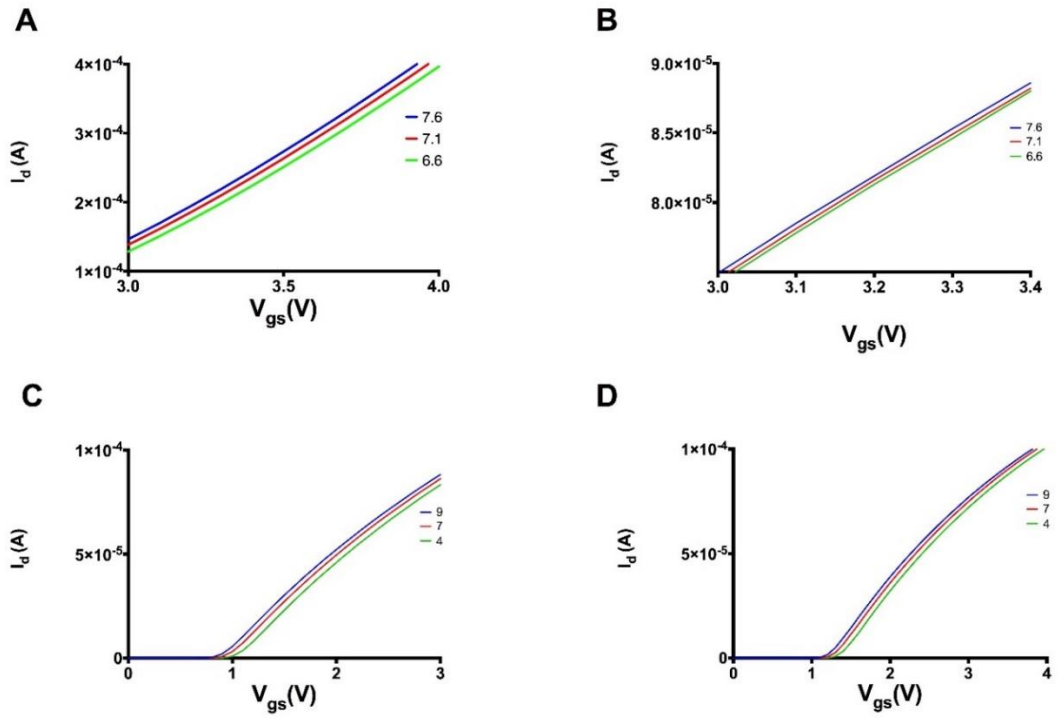

Figure 6-8 I_d-V_{gs} characteristics of the MOSFET due variations in pH on A) planar Al_2O_3 between 6.6-7.6 pH (Tris buffer) B) 60 nm porous Al_2O_3 6.6-7.6 pH (Tris buffer) C) 60 nm porous Al_2O_3 9-4 pH (phosphate buffer) after treating surface with H_2O_2 D) 60 nm porous Al_2O_3 9-4 pH (phosphate buffer) after treating surface with H_2O

The 60 nm size of the pores makes the surface more hydrophobic compared to the planar structures. The effect of this hydrophobicity is that it is not possible to saturate the ionic properties of the testing membrane [9]. This is one reason why the nanoporous structures have low pH-sensitivity. To saturate the ionic properties of the nanoporous Al_2O_3, the membrane was hydrated using 2 different methods. In the first approach, the sensing membrane was incubated in 35-37% hydrogen peroxide (H_2O_2) [10] for 1 hour and the second approach employed the use of DI water (H_2O with 18.2 MΩ resistance) t for 18 hours.

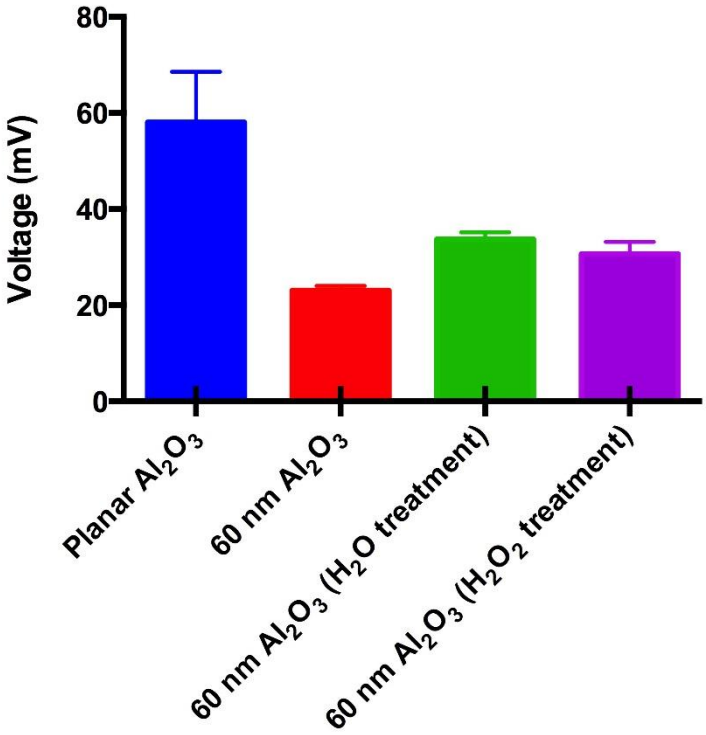

Figure 6-9 pH sensitivity of Al2O3 structures

After hydrating the sensing membrane, the pH sensitivity of the structures increased to between 30-31 mV/pH using H_2O_2 and between 32-34 mV/pH with DI H_2O. Statistical data of pH sensitivity for repeated measurements (n=3) is reported in Figure 6-9. Although the pH sensitivity of the nanoporous structures increased after hydrating the membrane, it was still lower than the sensitivity of planar structures. This is attributed to the properties of the interior sites of the porous membrane [8], [11]. The pores on the sensing membrane can be considered as periodically arranged defects that entrap ions existing in the test solution.

6.1.4 Protein immobilisation on Al_2O_3

Protein immobilisation studies were conducted using HRP as a model protein. A TMB assay was used to quantify the amount of HRP immobilised on the surface. A concentration of 156 µM HRP in pH 7.4 Tris buffer was used for immobilisation. The colour change induced by TMB assay in the presence of HRP was detected using a spectrophotometer. HRP was immobilised with two approaches:

1. Direct adsorption
2. Using 100 % GOPTS to fix HRP on the surface (protocol outlined in Section 3.5.2)

A control reaction for GOPTS functionalisation was performed by blocking the epoxide sites of the GOPTS with incubation of substrates in 20% ethanol.

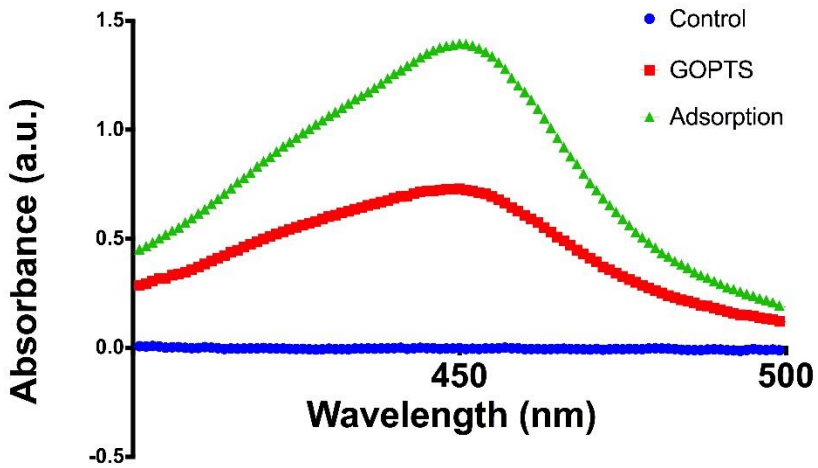

Figure 6-10 TMB assay: Immobilisation of HRP on 60 nm nanoporous Al_2O_3 structures

Figure 6-10 shows the data obtained after immobilisation of HRP on 60 nm nanoporous Al_2O_3 structures. Higher absorbance from the surfaces after adsorption of HRP was due to the entrapment of HRP molecules inside the pores. The adsorption of HRP is non-covalent and the molecules attach non-specifically with random distribution. This makes it difficult to remove the HRP as porous structures are hydrophobic in nature [12]. With the use of GOPTS controlled immobilisation of HRP was achieved as HRP binds covalently on the epoxide groups of GOPTS. This reduces non-specific binding due to adsorption and hence there is a low absorbance signal observed after HRP immobilisation using GOPTS. The control reaction where epoxide sites were blocked revealed insignificant changes.

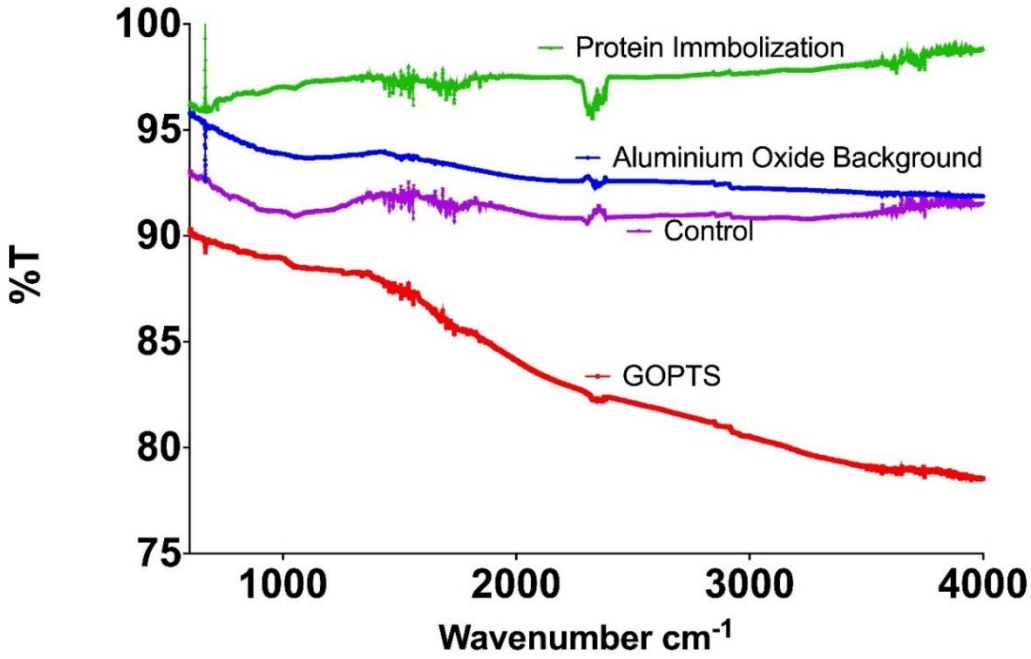

Figure 6-11 FTIR for HRP immobilisation on nanoporous Al_2O_3 using GOPTS

The immobilisation steps of HRP on nanoporous Al_2O_3 were also monitored using FTIR, Figure 6-11. After silanisation of Al_2O_3 with GOPTS, the peaks that appear between 1500-2000 show the presence of the epoxide group. There is an extension of these peaks when the epoxide ring opens and attaches molecules covalently. The extension of these peaks in the control reaction is due to the conversion of epoxide group into an ester upon exposure to ethanol. In the protein immobilisation reaction, these peaks appear due to the conversion of the epoxide group to an amine upon exposure to HRP. In addition, the existence of a strong peak between 2000-2500 shows the presence of HRP.

Figure 6-12 shows the data obtained after immobilisation of HRP on planar Al_2O_3 structures. It is evident from the curves on Figure 6-12 that similar to nanoporous structures, adsorption of HRP on the planar structures was higher than its immobilisation using GOPTS. Furthermore, the control reaction revealed insignificant changes compared to adsorption and GOPTS immobilisation.

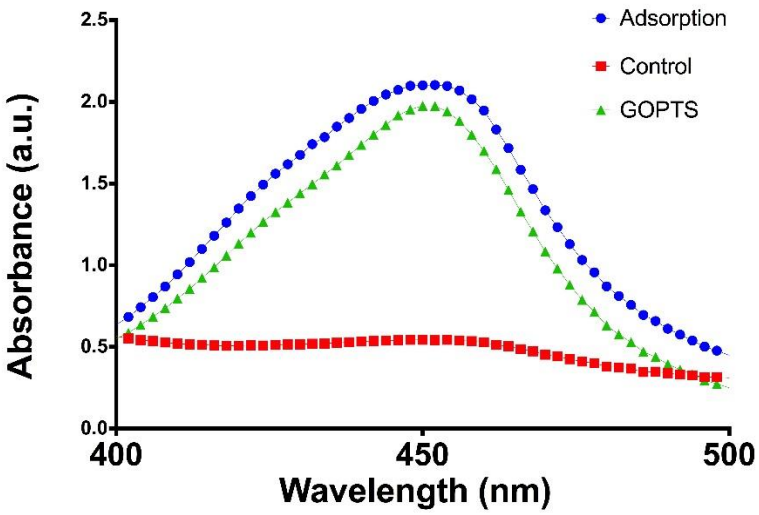

Figure 6-12 TMB assay: Immobilisation of HRP on planar Al_2O_3 structures

Statistical data of HRP immobilisation for repeated measurements (n=3) is reported in Figure 6-13.

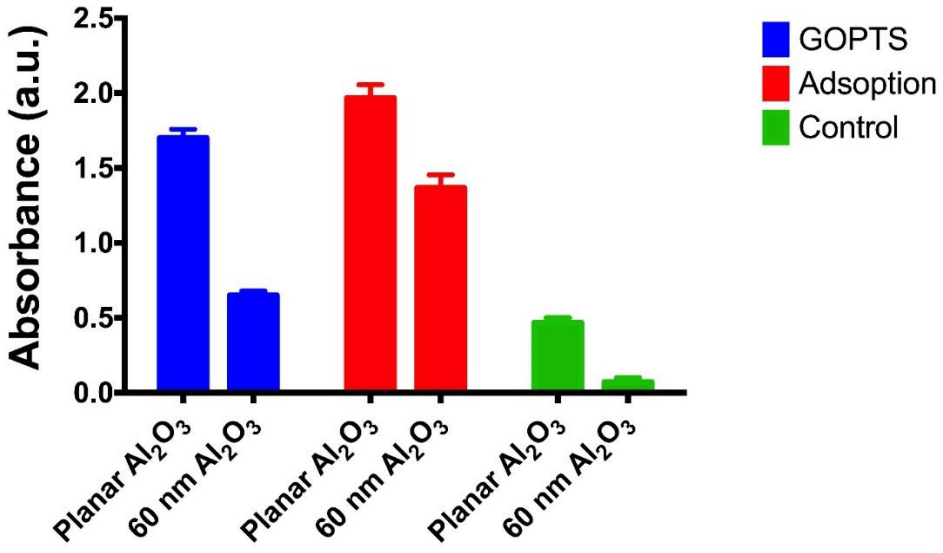

Figure 6-13 Absorbance of Al_2O_3 structures upon immobilisation of HRP

6.1.4 Protein phosphorylation on nanoporous Al_2O_3

After studying pH variations and testing immobilisation strategies on Al_2O_3, phosphorylation of protein was conducted on 60 nm nanoporous Al_2O_3 structures. The

release of proton associated with phosphorylation of MBP was measured by using a pH-sensitive Al_2O_3 structure as an extended gate of the MOSFET. MBP was immobilised using 100% GOPTS.

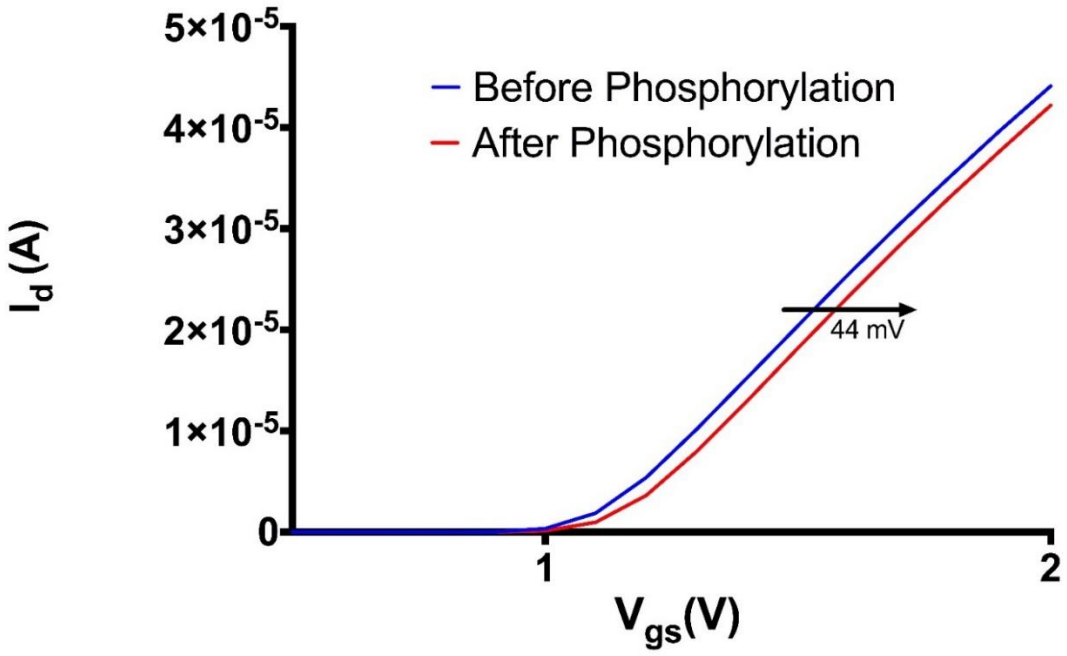

Figure 6-14 I_d-V_{gs} characteristics of the MOSFET showing voltage changes upon phosphorylation of proteins.

A change of 47 mV was observed just 2 minutes after the start of the phosphorylation reaction and stabilised at 44 mV after 10 minutes. Figure 6-16 shows the I_d-V_{gs} characteristics of the MOSFET demonstrating the change in the V_{gs} before and after the phosphorylation of proteins.

6.2 Microfluidics Integration

Microfluidics is the branch of engineering that studies the behaviour of fluids confined to dimensions less than 1 mm [13]. The advantages of having a microfluidic device are [14]:

1. The flow inside a microfluidic structure is laminar. It is easier to mathematically model laminar flow systems allowing prediction of the reaction environment.
2. Simple to fabricate.

3. Miniaturisation of device facilitates point-of-care high-throughput experiments.
4. Affordable.
5. Reduced volumes of samples and reagents.
6. Scale similarity to allow cell probing of subcellular phenomena

A microfluidic device integrated with a silicon nitride based EIS sensor, shown in Figure 6-15, was designed to study pH variations. The prototype was used to demonstrate the use of microfluidics with FETs, for instance the EIS sensor.

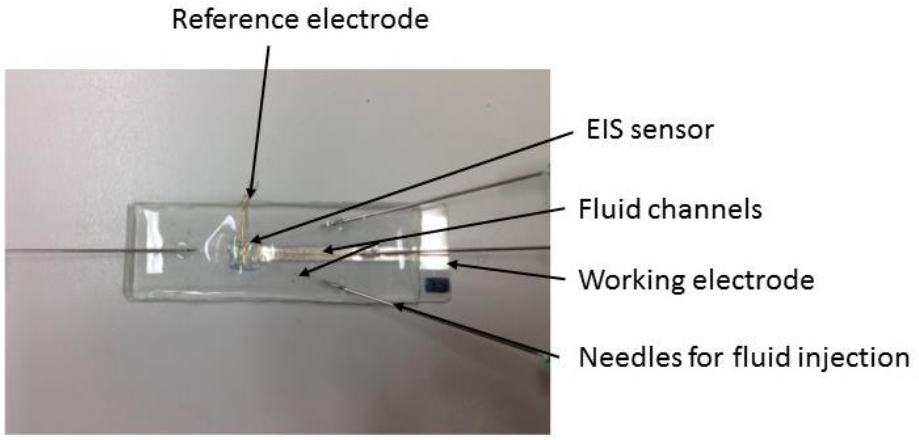

Figure 6-15 Integrated microfluidic and EIS sensor

6.2.1 Fabrication of microfluidic EIS sensor

The microfluidic device consists of channels made in polydimethylsiloxane (PDMS) on a glass substrate. Complete fabrication of the device was achieved without the use of a clean room nor photolithography. Shadow masks and aluminium moulds are shown in Figure 6-16 and were used to create different layers of the device.

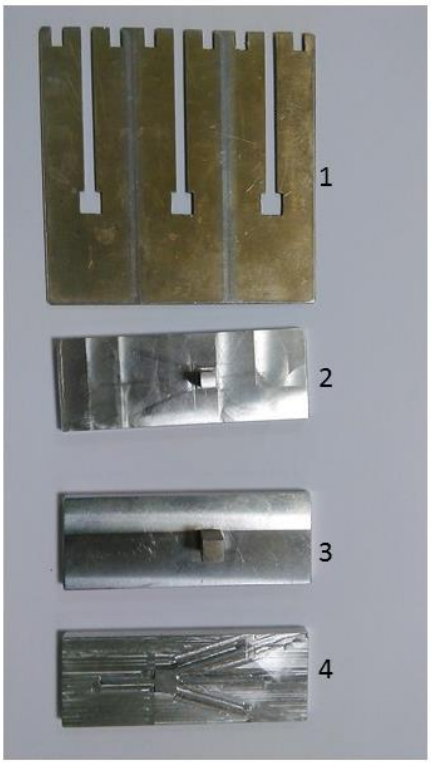

Figure 6-16 1: Shadow mask for the thermal deposition of aluminium on glass; 2, 3 & 4: moulds to create PDMS layers.

The first step in the fabrication was to deposit aluminium on the RCA-cleaned glass slides (protocol for RCA cleaning in Chapter 3, Section 3.4).

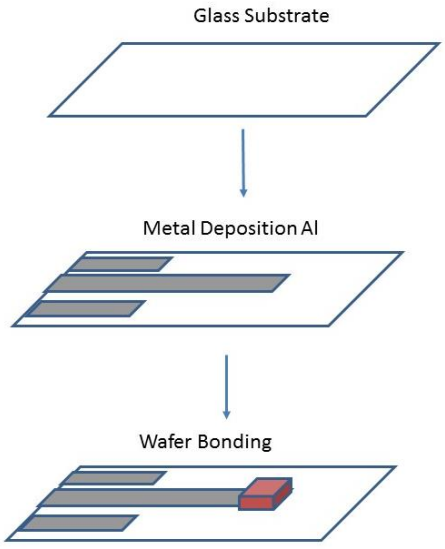

Figure 6-17 Aluminium deposition and silicon nitride adhesion on glass.

The deposited aluminium serves as a contact for the working electrode. Using the shadow mask shown in the Figure 6-16, 200 nm of aluminium was deposited on the glass by thermal evaporation. The silicon nitride EIS device was then placed on the aluminium and fixed with conducting silver paste. This electrically contacts the wafer to the aluminium contact pad. These steps are shown in Figure 1-17.

The next step involved the use of moulds 2, 3 and 4, shown in Figure 6-16, to develop a PDMS channel and ceiling of the device. These moulds were fabricated with aluminium using numerically controlled turning and milling machines. PDMS mixture [Sylgard® 184, Dow Corning] with silicone elastomer base and primer were mixed in a ratio of 10:1, desiccated to remove bubbles and poured on the moulds. PDMS was cured with a 30 minutes bake at 70 ºC. In order to bond the PDMS structure to the glass, both glass and PDMS were treated with oxygen plasma. The exposure to oxygen plasma creates silanol groups (Si-OH) on both the glass and PDMS. Silanol groups have a very high affinity to each other and form strong covalent bonds. Consequently, oxygen plasma treated glass and PDMS bond to each other when they are brought to a conformal contact.

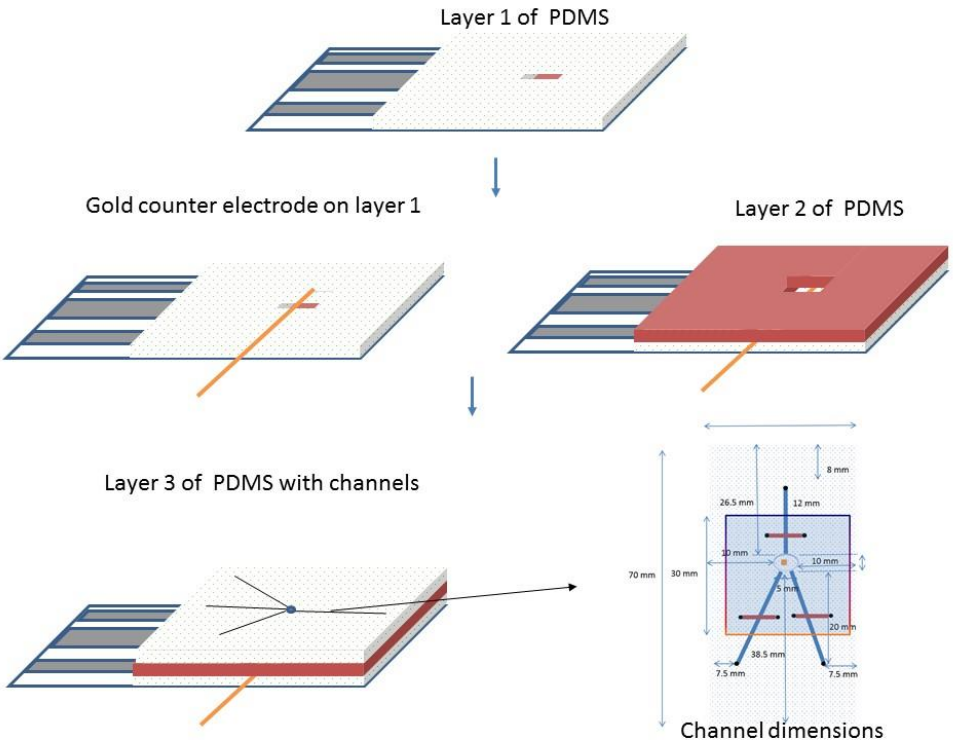

Figure 6-18 PDMS layers of the microfluidic device

The first PDMS layer that is bonded to the glass is made from mould 2 in Figure 6-16. The bonding of this layer on the glass acts to passivate the conducting aluminium rails. The second PDMS layer, made using mould 3, creates a well for the EIS sensor and the third layer, made with mould 4, forms the channels. A gold counter electrode was placed between the first and second PDMS layers, just above the EIS sensor. Pictorial representation of the PDMS layers is shown in Figure 6-18.

6.2.2 pH testing results

The microfluidic EIS device was tested with Tris buffer prepared in lab (pH 7.0, 8.0) to study the pH variations.

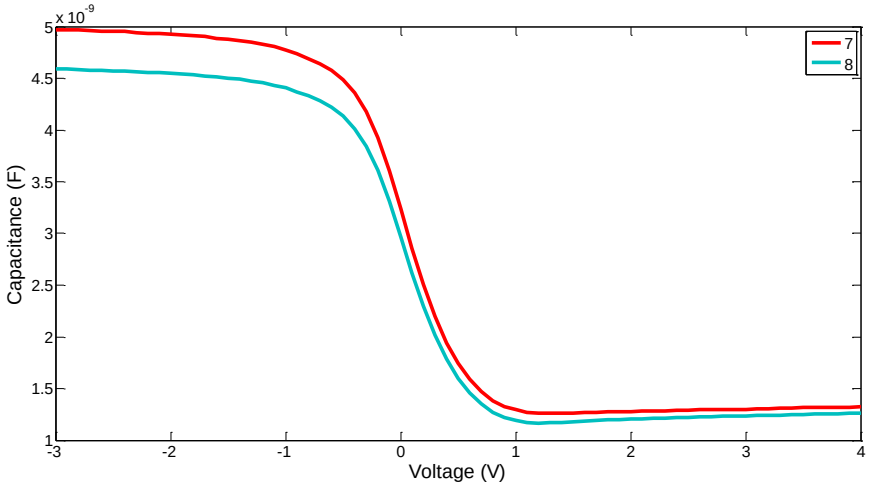

Figure 6-19 CV characteristics of EIS microfluidic pH sensor

Figure 6-19 shows a change of 65 mV between pH 7.0 and 8.0. However it can be seen that the accumulation region of then CV curve is not the same for pH 7.0 and pH 8.0 curves. This is due to the leakage of buffer solution outside the channels. This creates unwanted bubbles on the surface of the silicon nitride that alter the capacitance of the structure. The leakage is primarily due to the unconventional approach used to fabricate the device i.e. without using photolithography and clean room facilities to make the microfluidic structure. The next chapter gives a detailed discussion on why conventional techniques in making microfluidic structures haven't been used.

References

[1] B. L. Allen, P. D. Kichambare, and A. Star, "Carbon nanotube field-effect-transistor-based biosensors," *Advanced Mater*, vol. 19, pp. 1439–1451, 2007.

[2] T. Sharf, J. W. Kevek, and E. D. Minot, "Fabrication of low-noise carbon nanotube field-effect transistor biosensors," in *Proceedings of the IEEE Conference on Nanotechnology*, pp. 122–125, 2011.

[3] K. Maehashi, T. Katsura, K. Kerman, Y. Takamura, K. Matsumoto, and E. Tamiya, "Label-free protein biosensor based on aptamer-modified carbon nanotube field-effect transistors," *Analytical Chemistry*, vol. 79, pp. 782–787, 2007.

[4] A. C. Diebold, Handbook of silicon semiconductor metrology. 2001.

[5] G. J. Pridham, "Physics of Semiconductor Devices," Electronics and Power, vol. 16. p. 34, 1970.

[6] B. Razavi, Fundamentals of Microelectronics, vol. 13. 2008.

[7] S. K. Arya, C. C. Wong, Y. J. Jeon, T. Bansal, and M. K. Park, "Advances in Complementary-Metal-Oxide-Semiconductor-Based Integrated Biosensor Arrays" *Chemical Reviews*, vol. 115, pp. 5116–58, 2015.

[8] A. H. D. Graham, C. R. Bowen, J. Robbins, and J. Taylor, "Formation of a porous alumina electrode as a low-cost CMOS neuronal interface," *Sensors Actuators B Chemica*l, vol. 138, pp. 296–303, 2009.

[9] M. H. Wu, H. W. Yang, M. Y. Hua, Y. B. Peng, and T. M. Pan, "High-?? GdTixOy sensing membrane-based electrolyte-insulator-semiconductor with magnetic nanoparticles as enzyme carriers for protein contamination-free glucose biosensing," *Biosensors and Bioelectronics*, vol. 47, pp. 99–105, 2013.

[10] C.-C. Chen, H.-I. Chen, H.-Y. Liu, P.-C. Chou, J.-K. Liou, and W.-C. Liu, "On a GaN-based ion sensitive field-effect transistor (ISFET) with a hydrogen peroxide surface treatment," *Sensors Actuators B Chemical* vol. 209, pp. 658–663, 2015.

[11] H. Abe, M. Esashi, and T. Matsuo, "ISFET's using allows inorganic gate thin films," *IEEE Transactions Electron Devices*, vol. 26, 1979.

[12] J.-L. Lin, Y.-M. Chu, S.-H. Hsaio, Y.-L. Chin, and T.-P. Sun, "Structures of Anodized Aluminum Oxide Extended-Gate Field-Effect Transistors on pH Sensors," *Japanese Journal of Applied Physics*, vol. 45, pp. 7999–8004, 2006.

[13] G. M. Whitesides, "The origins and the future of microfluidics," *Nature*, vol. 442, pp. 368–373, 2006.

[14] H. Bruus, "Theoretical microfluidics," *Physics*, vol. 18, 2008.

Chapter 7 Conclusions and Outlook

In this thesis, it has been shown that field effect devices can be used for screening inhibitors of kinases. Kinases are enzymes that phosphorylate proteins in the presence of a phosphate source. Abnormal phosphorylation is often a cause of many diseases including cancer and thus it is necessary to develop tools that can screen inhibitors of kinase. Phosphorylation of MBP and peptides was carried out on EIS and MIS field effect devices. Field effect devices were also successfully integrated with LSPR detection of the phosphorylation of proteins.

The main results obtained from the work are summarized below:

1. Development of strategies to control immobilisation of protein on the silicon nitride using APTES, GOPTS and H_2O_2 as chemicals.
2. Control of the density of proteins on silicon nitride substrate using combination of APTES/AHS
3. Successful detection of the release of proton associated with phosphorylation of immobilised protein/peptide on EIS silicon nitride based substrates.
4. Successful detection of the release of proton associated with phosphorylation of proteins in solution using commercial micro-pH electrode.
5. Detection of phosphorylation of proteins using localised surface plasmon resonance
6. Detection of the negative charge imparted on the proteins upon their phosphorylation on gold MIS structures,
7. Demonstration of how new inhibitors of kinases (potential drugs) can be screened using the above mentioned system that was tested for phosphorylation.
8. Phosphorylation detection using SPR technique.
9. Quantification of phosphorylated proteins using QCM.
10. Modelling of plasmonic coupling phenomenon on gold MIS sensor using COMSOL

11. Characterisation of anodised nanoporous aluminium oxide for pH sensing applications
12. Use of extended MOSFET technology to detect phosphorylation of proteins
13. Demonstration of how EIS field effect devices can be integrated with microfluidics
14. Demonstration of the need of combining multiple technologies on a single platform to quantify a biochemical reaction
15. Demonstrated a proof of concept of a new drug discovery biosensor that combines electrochemical and nanoplasmonic techniques on a single platform

The EIS and MIS devices had a remarkable performance for the detection of phosphorylation of proteins. Buffer conditions, materials and surface chemistry was optimized for the phosphorylation studies on EIS and MIS. The integration of microfluidics on EIS devices was one area that was not optimized, since it was out of the timeframe of the work. In addition, limited budget of the project denied the use of clean room facilities that is necessary to fabricate sophisticated microfluidic devices. Furthermore, for similar reasons the use of MOSFET to detect phosphorylation was abandoned after preliminary detection of phosphorylation of MBP. The idea of using MOSFETs was to test the proof of concept developed on EIS device that was close to a commercial biosensor.

It is believed that the integration of microfluidics and the use of MOSFETs will be covered in the future scope of the work. Moreover integration of MOSFETs with microfluidics will ease the development of an automated device that can be used to screen the novel inhibitors of kinases. MOSFET technology can also be readily adopted for high-throughput applications. Using complementary metal oxide semiconductor (CMOS) and very large scale integration (VLSI) technology, an array of MOSFETs could be developed. Gate of each MOSFET of an array can then be addressed by biomolecules suspended in a buffer using appropriate microfluidic channels. For instance, proteins can be immobilised on all MOSFETs of an array. Phosphorylation of proteins can then be carried out in the presence of kinase inhibitors where each MOSFET is exposed to different inhibitors. In this way, multiple candidate

compounds for kinase inhibitors can be screened in one run, enabling fast discovery of new inhibitors.

The work also scrutinises directions for the use of nanoparticle in the future drug discovery technologies. Nanoparticles with unique properties can be used to enable detection techniques such as magnetic and plasmonic sensing. For example, in this study plasmonic properties of the gold nanoparticles have been exploited to enable LSPR detection of phosphorylated proteins. Similarly, other plasmonic nanoparticles such as silver can be used to quantify kinase activity. In addition magnetic particles, quantum dots and pigmented nanoparticles can engineered to quantify kinase activity using techniques like Hall sensing, fluorescence-based and colorimetric assays respectively.

Multiplexing of detection technologies is another area that this work provides interest for the future biosensing applications. Combing multiple detection technology on a single platform makes the system robust for detection of any biochemical species. It provides cost effective and time saving technique to confirm the activity of a chemical reaction in a single run. In addition, more than one parameter of the reaction for instance, association/dissociation constant, real-time kinetics, rate of product formation and structure of biolayer can be studied, when multiple technologies are integrated on a single biosensor.

The dual mode label free techniques developed in the work may create interest in the field of cell biology and cell signalling research to probe intracellular kinase activities. A classic example of using EIS device for future study of kinase activity would be to immobilise a proteins and a cell of interest. The cell can then be lysed to release kinases in the presence of a particular kinase and study the activity of kinase inhibitor.

The technology developed in this work i.e. combination of field effect devices and nanoplasmonic sensing has been coined as ‘PhosphoSense Technology’. The project aspires that the PhosphoSense Technology will represent an important innovation in future biomedical and drug discovery research.

Appendix 1

Detailed procedure of Western blot

1. Preparation of working solutions
    a. Solution A (acrylamide solution), 100 ml, 30 % (w/v) acrylamide, 0.8% (w/v) bis-acrylamide: Add 29.2 g acrylamide and 0.8 g bis-acrylamide in 100 ml of water and stir until they are completely dissolved.
    b. Solution B (4x separating gel buffer),100 ml: Mix, 75 ml 2 M Tris HCl (pH 8.8) i.e. 1.5 M final concentration with 4 ml 10 % SDS (0.4 %) and 21 ml of water (DI), together to make Solution B.
    c. Solution C (4x stacking gel buffer),100 ml: Mix, 50 ml 1 M Tris HCl (pH 8.8) i.e. 0.5 M final concentration with 4 ml 10 % SDS (0.4 %) and 46 ml of DI water, together to make Solution C.
    d. Running buffer or electrophoresis buffer, 1000 ml: Take 3 g Tris base i.e. final concentration 25 mM, 14.4 g glycine 192 M, 1 g SDS 0.1 % and mix in DI water to make 1000 ml. The final solution should be approximately pH 8.3.
    e. TBS-T: 10 mM Tris-HCl, pH 7.5, 150 mM NaCl, Tween 20 0.001 % V/v
    f. Transfer buffer 1 litre: 3.03 g Tris base, 14.4 g glycine in 800 ml of DI water and 200 ml methanol
    g. Solution 1: Mix together following reagents
        i. 100 ml 200 mM Tris, pH 8.5
        ii. 1 ml 250 mM luminol
        iii. 1 ml 40 mM p-Coumaric acid
    h. Solution 2
        i. 100 ml DI water
        ii. 60 µl 30% H_2O_2

    Store solutions 1 & 2 in dark glass/ plastic containers at 4 ºC
2. First a separating gel of 12 % is prepared as follows
    a. Preparation of running/separating gel for x% gel
        i. Solution A: x/3 ml
        ii. Solution B: 2.5 ml

iii. DI water: {7.5-(x/3)} ml
iv. 10% ammonium persulphate, APS,: 50 µl
v. TEMED: 5 µl (10 µl if x < 8%)

b. The sequence of adding is always water first, then solution B, solution A, APS and lastly TEMED
c. Pour the gel into an electrophoreses cassette.

3. Next a stacking gel was prepared (4 ml suitable for making 2 gels of size 6 cm × 8 cm × 0.75 mm) as follows and was poured on the top of the electrophoreses cassette.
    a. 2.3 ml DI water
    b. 0.67 ml Solution A
    c. 1 ml Solution C
    d. 30 µl 10% APS
    e. 5 µl TEMED
4. Put a comb on the top of the cassette to make wells
5. Allow the gels to polymerise for 1 hour. Remove the comb gently
6. Heat the protein sample at 90 ºC on a hot plate for 5 min
7. Pour into wells and run the gel between 60-100V with gel immersed in electrophoresis buffer.
8. Transfer of gel
    a. Soak the sponge pads and PVDF (Polyvinylidene fluoride) in methanol and transfer buffer.
    b. Stack the gel in between the sponges and plates as follows: positive plate - 3 sponge layer- PVDF paper- gel-PVDF paper- sponge- negative plate.
    c. Close the plates and immerse in the transfer buffer within the electrophoresis tank. Then run at 100 volts for 1 hour.
9. Once the proteins are transferred, hydrate the PVDF membrane in TBST solution for 10 minutes using a bag kept on a laboratory based see-saw.
10. Similarly, wash in BSA for 10 minutes to block the protein-free sites (to minimise non-specific biding of antibodies on the membrane)
11. Primary antibody wash (for identifying protein of interest), left overnight (~xx hours)
12. 45 minutes of TBST wash. Changing solution every 15 minutes

13. 30 minutes of TBST wash with 5% milk
14. 1 hour in secondary antibody linked with HRP (1/2000 anti-rabbit) in TBST with 5% milk
15. 1 hour wash in TBST. Change solution every 15 minutes
16. ECL (enhanced luminescence) western blot development
    a. Mix equal parts of solution 1 & 2
    b. Add to the blot and incubate for 1 minute with constant agitation
    c. Wrap in cling film and expose the film using the development machine

Protocol for changing antibodies on a blot

The phosphoantibody was ripped off and MBP antibodies were used to check the presence of MBP in all lanes. Protocol for changing the antibodies on a same blot is given below:

1. Hydrate the membranes for 45 minutes in TBST. Change TBST every 15 minutes
2. Place the blots in a plastic bag with 10 ml of restoring buffer at 37 ºC in a water bath for 10 minutes and then shake for 5 minutes at room temperature.
3. 1 hour wash in TBST. changing buffer every 15 minutes
4. 1 hour wash in TBST 5% milk
5. 1hour wash in TBST 5% milk with anti-MBP (1/1000)
6. 45 minute wash in TBST, changing solution every 15 minutes.
7. 30 minute wash in TBST 5% milk
8. 1 hour wash in TBST 5% milk 1/5000 anti-goat HRP
9. 45 minute TBST wash for 45 minutes. Change solution every 15 minutes.
10. Repeat ECL steps as in 4.2.2.1

RCA cleaning protocol

1. Cut Si_3N_4 wafer into dies of arbitrary shape having at least 5 mm of circular diameter.
2. Immerse the die into a solution of $NH_4OH:H_2O_2:H_2O$ (1:1:5) at 90 ºC for 5 to 10 minutes. This removes organic contaminants from the wafer.
3. Rinse the die with DI water at 18.2 MΩ,

4. Immerse the die into a solution of $HCl:H_2O_2:H_2O$ (1:1:6) at 90 ºC for 5 to 10 minutes. This removes inorganic contaminants from the wafer.
5. Rinse with de-ionized water at 18.2 MΩ, DI water.
6. Dry by passing nitrogen gas over the surface
7. 100 nm of aluminium was thermally deposited on the back side of the wafer (on the side with Si)
8. Sonicate in acetone for 10 minutes.
9. Rinse with IPA (Isopropyl alcohol)
10. Rise with DI water and dry with nitrogen gas.

Protein immobilisation with APTES

1. Immerse the wafer in 5% APTES in acetone for 6 hours at room temperature. Make sure that the petri dish in which experiment is performed is sealed with paraffin.
2. Rinse the substrate with acetone and DI water
3. Cure the substrate for 5 minutes on a hot plate at 90 ºC
4. Immerse the substrate in a solution of glutaraldehyde, GA, (15% in DI) for 3 hours
5. Rinse the substrate thoroughly with DI water or the buffer in which the protein (to be immobilised) solution is made.
6. Dispense the protein solution onto the sample
7. Rinse the unreacted protein with PBS
8. Block the unreacted aldehyde groups in 0.2 M ethanolamine for 30 minutes
9. Rinse thoroughly with DI water and store in Tris or PBS for further complex reaction.

Protein immobilisation with glycidoxypropyltrimethoxysilane (GOPTS)

1. Immerse the cleaned substrate in a GOPTS aqueous solution (5%, 10%, 49%, and 98%) for 45 minutes. 98% GOPTS in aqueous solution is most stable for protein immobilisation.
2. Remove the silanised substrate and dry with nitrogen gas
3. Cure the substrate for 5 minutes on a hot plate at 90 ºC
4. Add protein solution and incubate for 6 hours or overnight at room temperature

5. Rinse the protein-coated substrate with the same buffer in which the proteins were suspended
6. Add ethanol to block any unreacted GOPTS sites.
7. Rinse thoroughly with DI water and store in Tris or PBS for further complex reaction.

Protein immobilisation on Si_3N_4 with H_2O_2

1. Immerse Si_3N_4 substrate in H_2O_2 (8.25% in aqueous solution) for 3 hours
2. Rinse the substrate thoroughly with DI water
3. Dry the substrate with nitrogen gas
4. Immerse the substrate in a solution of glutaraldehyde (15% in DI) for 3 hours
5. Rinse the substrate thoroughly with DI water or the buffer in which the protein (to be immobilised) solution is made.
6. Dispense the protein solution onto the sample
7. Rinse the unreacted protein with PBS
8. Block the unreacted aldehyde group in 0.2 M ethanolamine for 30 minutes
9. Rinse thoroughly with DI water and store in Tris or PBS for further complex reaction

Details of the materials used in the project

Product	**Supplier**
PKC-alpha kinase, recombinant human	Prospec
Myelin Basic Protein, dephosphorylated	Millipore
PKC lipid activator	Millipore
ATP	Sigma Aldrich
ATP-S	Sigma Aldrich
Ethanol	Sigma Aldrich
Acetone	Sigma Aldrich
2-propanol	Sigma Aldrich
Hydrogen peroxide	Sigma Aldrich
APTES	Sigma Aldrich

GOPTS	Sigma Aldrich
MPTES	Sigma Aldrich
AHS	Sigma Aldrich
Gold Nanoparticles 5, 20 50 nm	Sigma Aldrich
Instrumentation	**Supplier**
Potentiostat, Compactstat	Ivium Technologies
LSPR homemade, fibre optics, USB 4000 spectroscope, halogen lamp and spectra suite	Ocean Optics
SPR	Reichert
OCM	JLM innovation
SEM	JEOL SEM6480LV
TEM	JEOL JEM1200EXII
XRD	Agilent
FTIR	Perkin Elmer
Semiconductor analyser	Agilent B1500

Appendix 2

In this appendix capacitance-voltage (*C-V*) curves of pH variations on silicon nitride surfaces and charge variations on gold surfaces is described.

Appendix figures 2.1 to 2.4 shows the pH tests on silicon nitride. It is observed that as the concentration of H^+ increase the threshold potential of the substrate also increases.

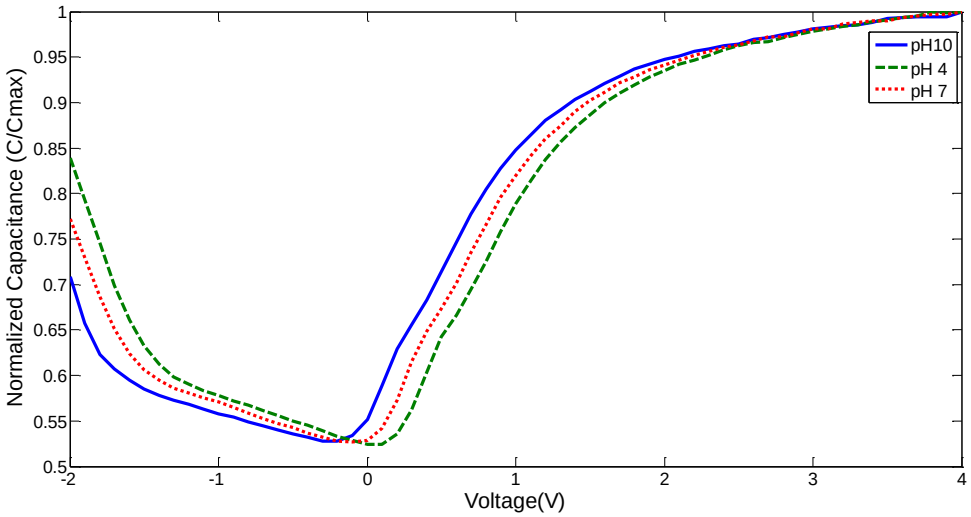

Appendix figure 2.1 pH variation on silicon nitride EIS sensor; Experimental conditions: -2V to 4V DC sweep superimposed with a 10 mV a.c. signal of 10 Hz; Buffer: 10 mM phosphate buffer

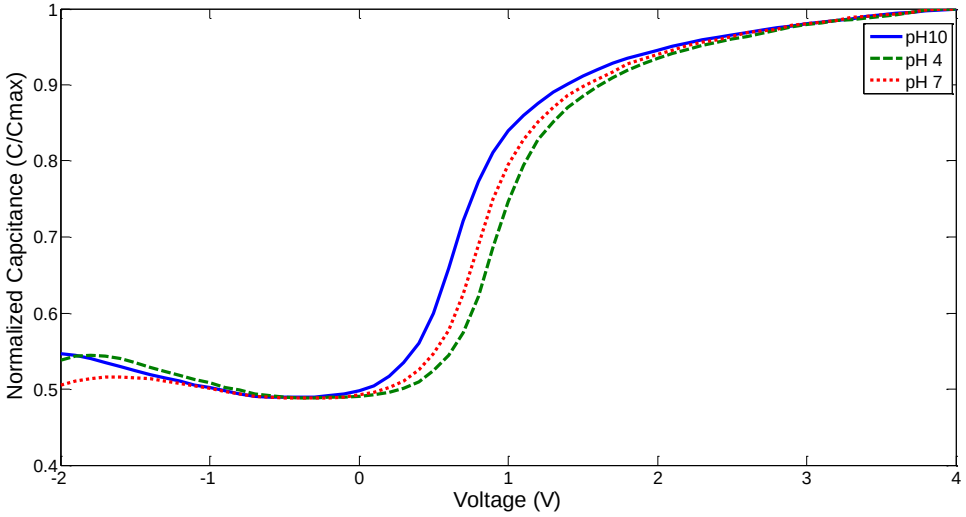

Appendix figure 2.2 pH variation on silicon nitride EIS sensor; Experimental conditions: -2V to 4V DC sweep superimposed with a 10 mV a.c. signal of 100 Hz; Buffer: 10 mM phosphate buffer

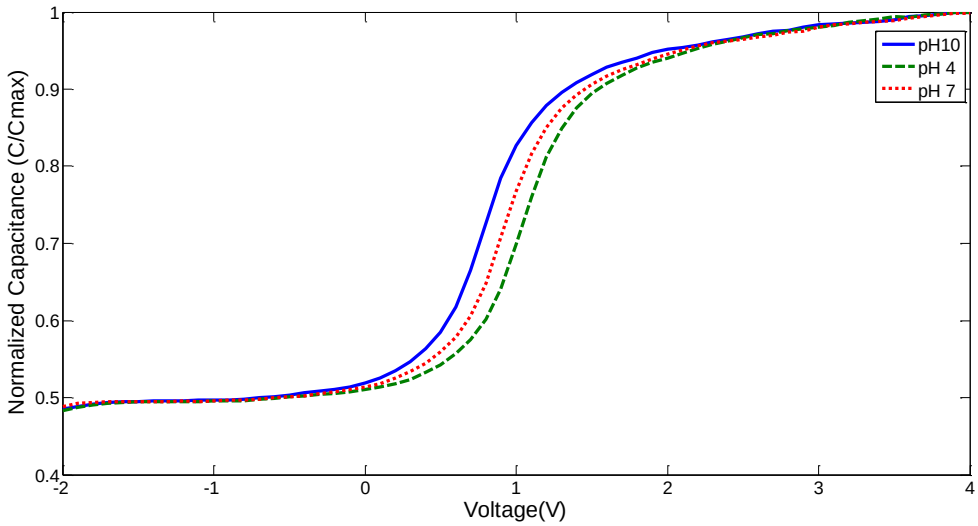

Appendix figure 2.3 pH variation on silicon nitride EIS sensor; Experimental conditions: -2V to 4V DC sweep superimposed with a 10 mV a.c. signal of 1000 Hz; Buffer: 10 mM phosphate buffer

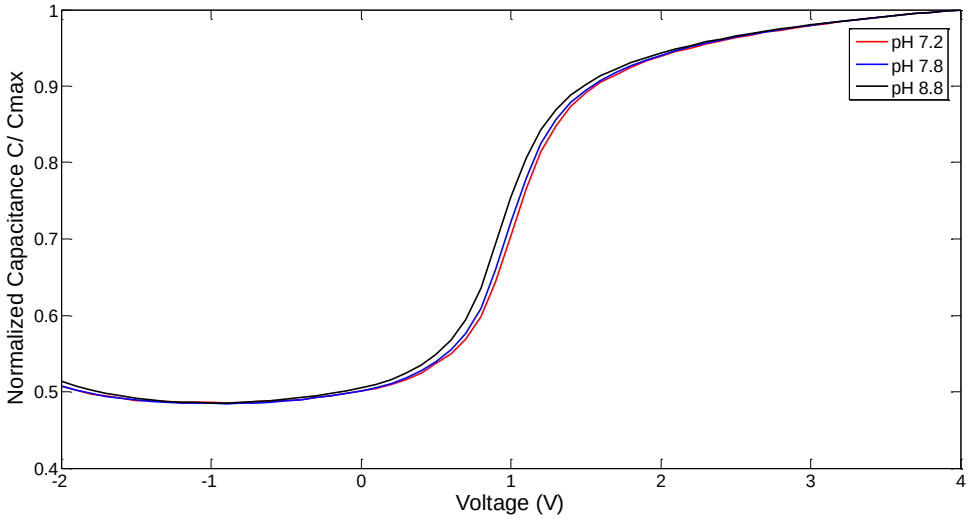

Appendix figure 2.4 pH variation on silicon nitride EIS sensor; Experimental conditions: -2V to 4V DC sweep superimposed with a 10 mV a.c. signal of 1000 Hz; Buffer: 0.2 mM Tris buffer

Appendix figure 2.5 below shows the changes in the surface potential of the silicon nitride upon oxidation of glucose by glucose oxidase enzyme.

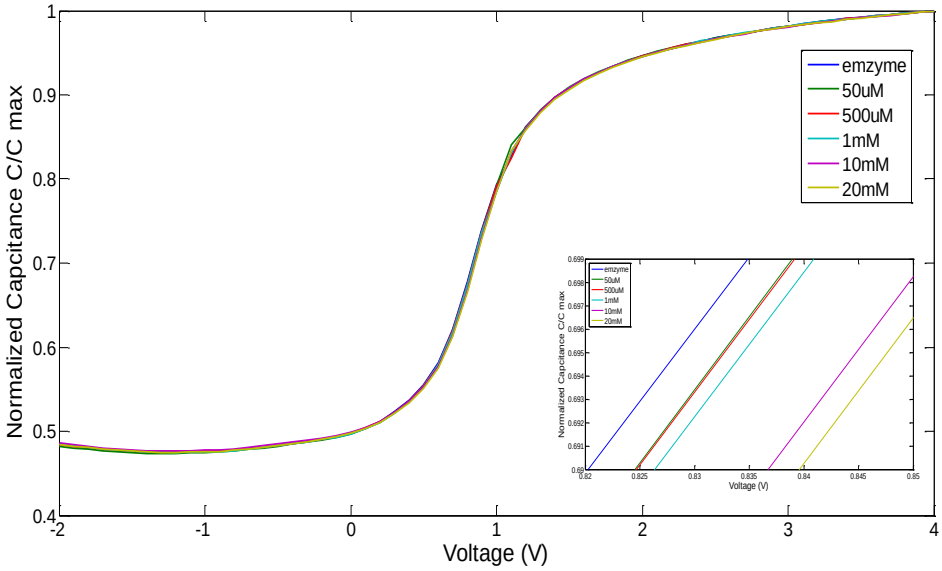

Appendix figure 2.5 pH variation on silicon nitride EIS sensor upon glucose oxidation; Experimental conditions: -2V to 4V DC sweep superimposed with a 10 mV a.c. signal of 1000 Hz; Buffer: 0.2 mM Tris buffer

Appendix figure 2.6 below shows the changes in the surface potential of the silicon nitride upon phosphorylation of MBP by PKC-α kinase.

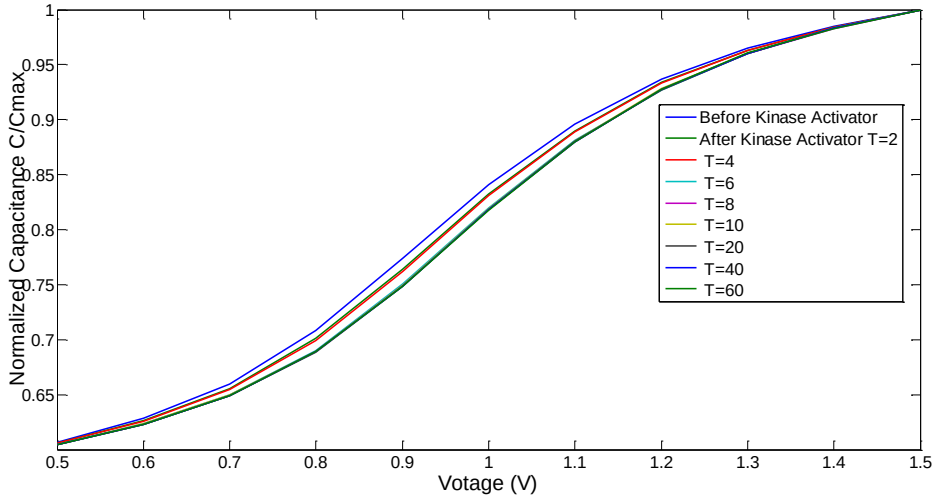

Appendix figure 2.5 pH variation on silicon nitride EIS sensor upon phosphorylation of MBP; Experimental conditions: 0.5V to 1.5V DC sweep superimposed with a 10 mV a.c. signal of 1000 Hz; Buffer: 0.2 mM Tris buffer

Appendix figure 2.7 below shows the changes in the surface potential of the silicon nitride upon inhibition of phosphorylation of MBP by PKC-α kinase.

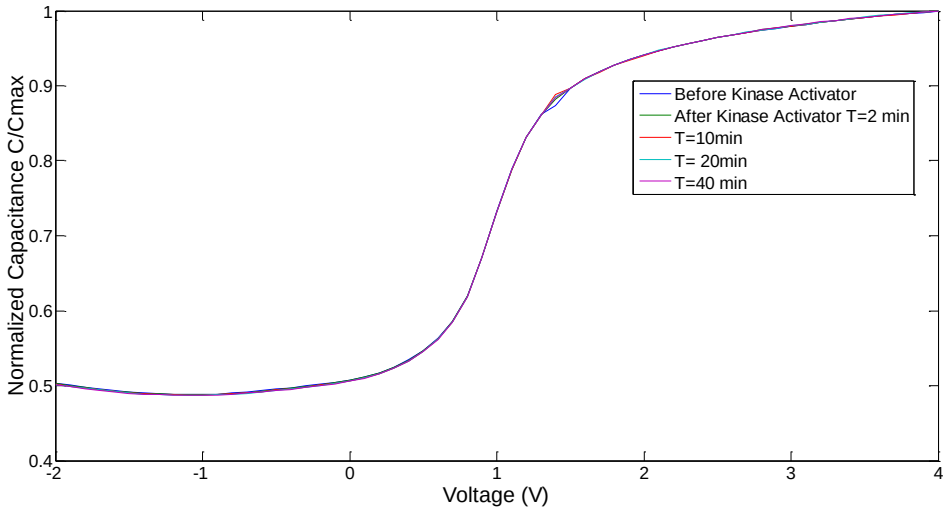

Appendix figure 2.6 pH variation on silicon nitride EIS sensor upon inhibition of MBP phosphorylation; Experimental conditions: -2V to 4V DC sweep superimposed with a 10 mV a.c. signal of 1000 Hz; Buffer: 0.2 mM Tris buffer

Appendix figure 2.8 below shows the changes in the surface potential of the silicon nitride surface upon when phosphorylation of MBP is carried out without activation of PKC-α kinase.

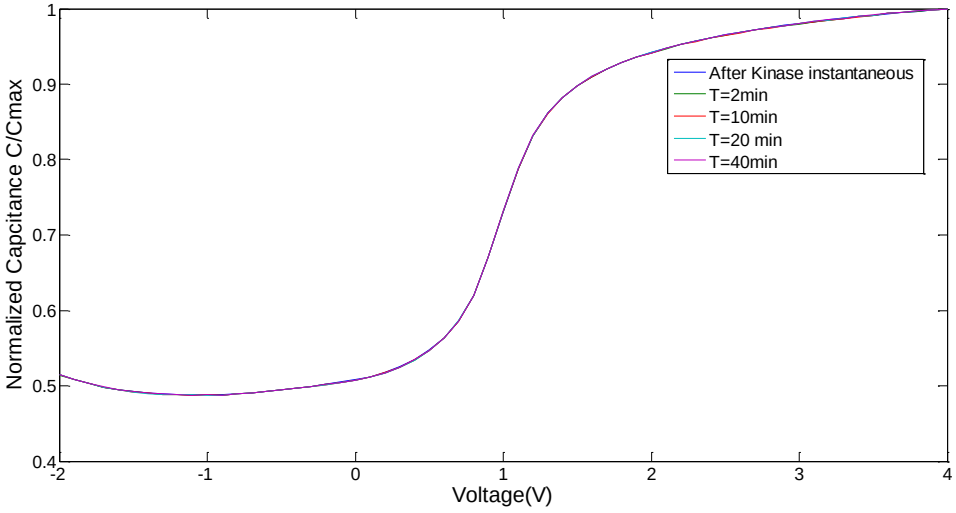

Appendix figure 2.7 pH variation on silicon nitride EIS sensor associated with control of MBP phosphorylation in the absence of kinase activator; Experimental conditions: -2V to 4V DC sweep superimposed with a 10 mV a.c. signal of 1000 Hz; Buffer: 0.2 mM Tris buffer

Appendix figure 2.9 below shows the changes in the surface potential of the silicon nitride upon thiophosphorylation of MBP by PKC-α kinase.

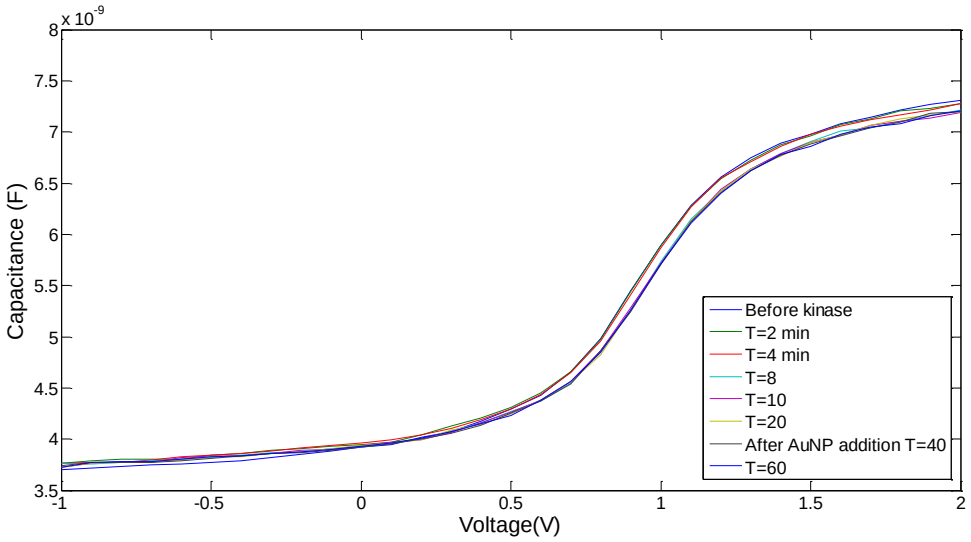

Appendix figure 2.8 pH variation on silicon nitride EIS sensor upon thiophosphorylation of MBP; Experimental conditions: -1V to 2V DC sweep superimposed with a 10 mV a.c. signal of 1000 Hz; Buffer: 0.2 mM Tris buffer

Appendix figure 2.10 below shows the changes in the surface potential of the silicon nitride upon inhibition of phosphorylation of MBP by PKC-α kinase.

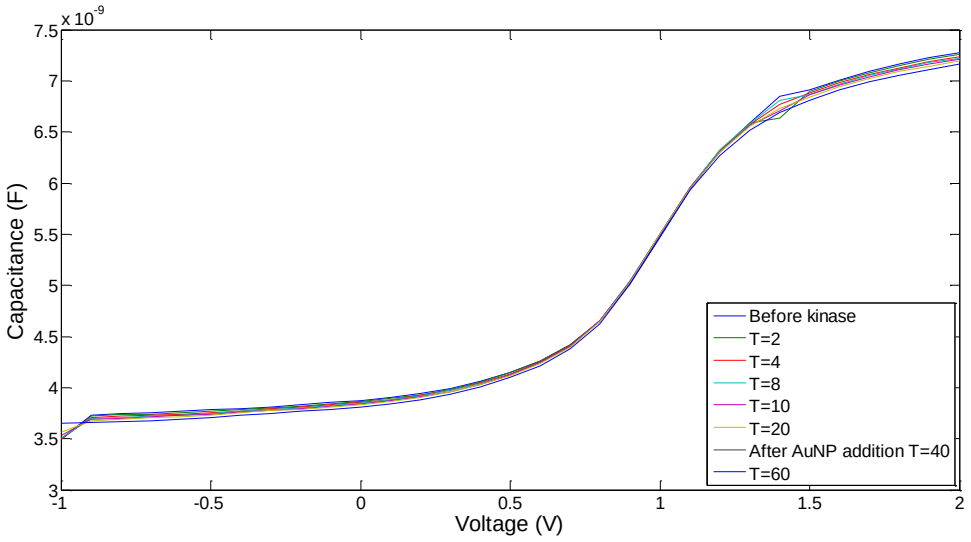

Appendix figure 2.9 pH variation on silicon nitride EIS sensor upon inhibition of MBP thiophosphorylation; Experimental conditions: -1V to 2 V DC sweep superimposed with a 10 mV a.c. signal of 1000 Hz; Buffer: 0.2 mM Tris buffer

Appendix figure 2.11 below shows the changes in the surface potential of the silicon nitride surface upon when phosphorylation of MBP is carried out without activation of PKC-α kinase.

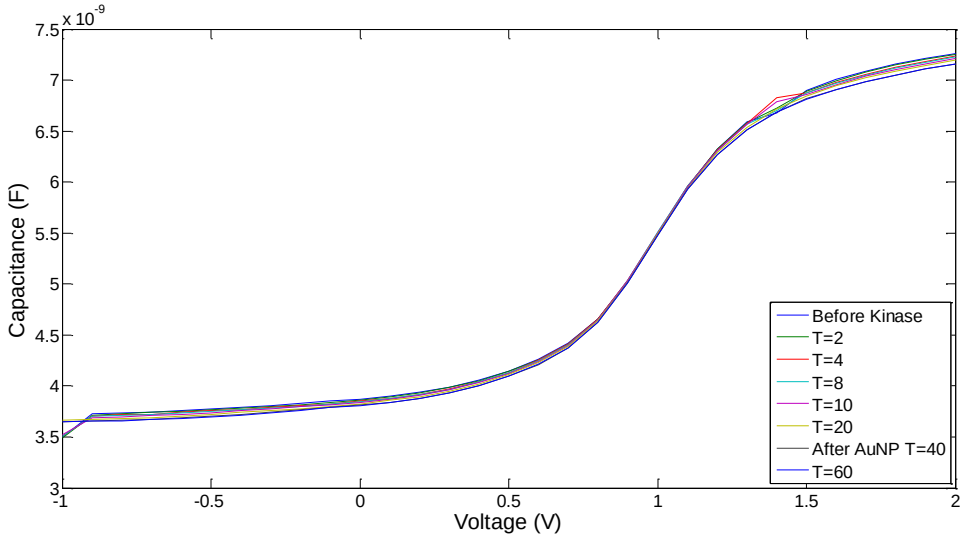

Appendix figure 2.10 pH variation on silicon nitride EIS sensor associated with control of MBP thiophosphorylation in the absence of kinase activator; Experimental conditions: -1V to 2V DC sweep superimposed with a 10 mV a.c. signal of 1000 Hz; Buffer: 0.2 mM Tris buffer

Appendix figure 2.12 below shows the changes in the surface potential of the silicon nitride surface upon phosphorylation of peptide-1 by PKC-α kinase.

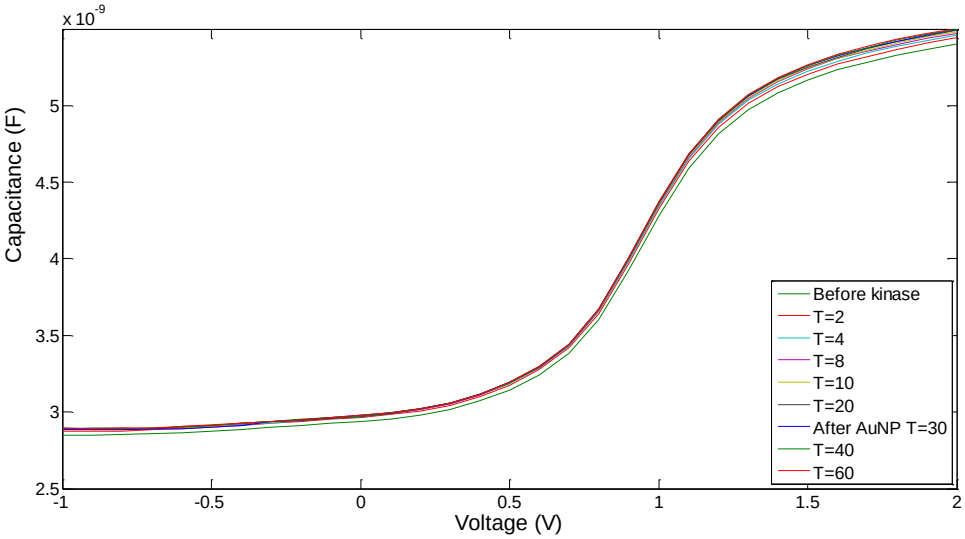

Appendix figure 2.11 pH variation on silicon nitride EIS sensor upon thiophosphorylation of peptide-1 (with cysteine); Experimental conditions: -1V to 2V DC sweep superimposed with a 10 mV a.c. signal of 1000 Hz; Buffer: 0.2 mM Tris buffer

Appendix figure 2.13 below shows the changes in the surface potential of the silicon nitride surface upon inhibition of phosphorylation of peptide-1 by PKC-α kinase.

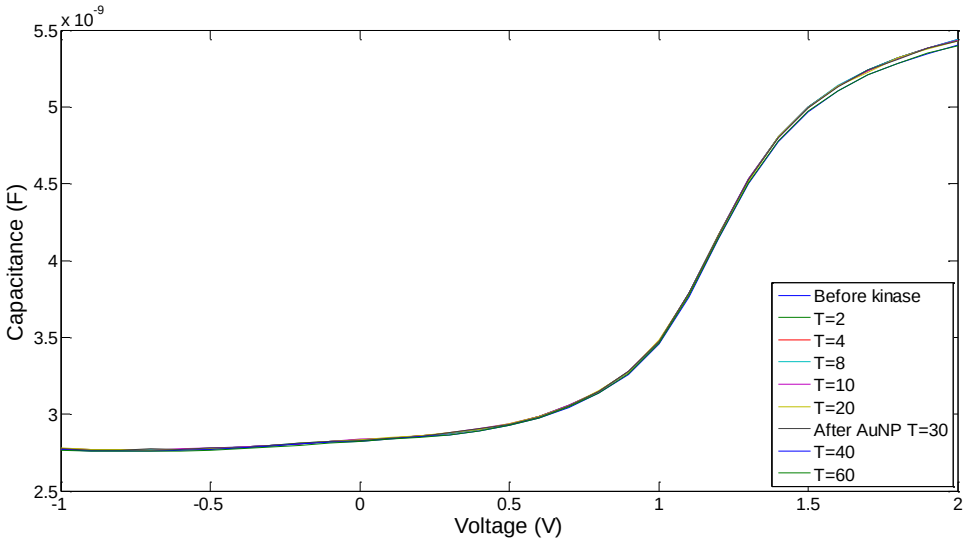

Appendix figure 2.12 pH variation on silicon nitride EIS sensor upon inhibition of thiophosphorylation of peptide-1 (with cysteine); Experimental conditions: -1V to 2V DC sweep superimposed with a 10 mV a.c. signal of 1000 Hz; Buffer: 0.2 mM Tris buffer

Appendix figure 2.14 below shows the changes in the surface potential of the silicon nitride surface phosphorylation of peptide-2 by PKC-α kinase.

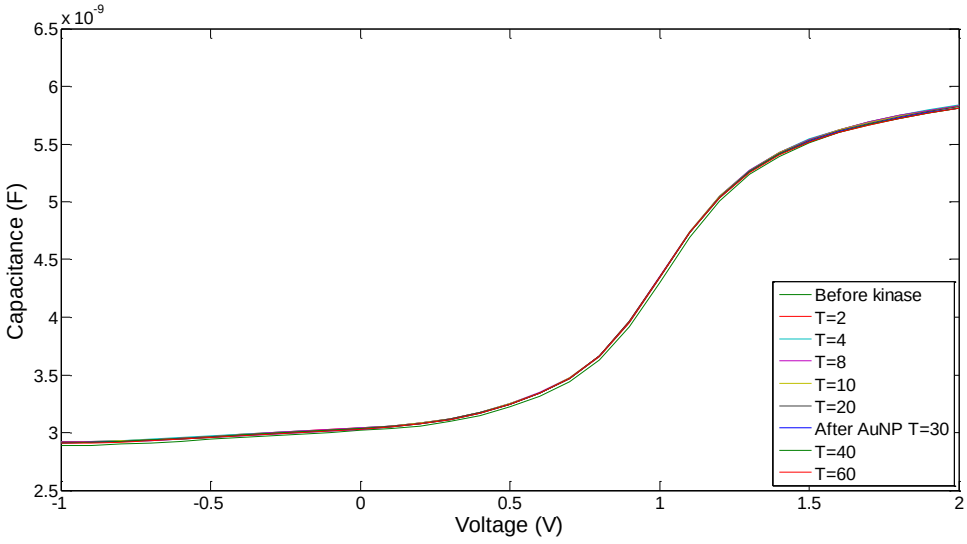

Appendix figure 2.13 pH variation on silicon nitride EIS sensor upon thiophosphorylation of peptide-2 (without cysteine); Experimental conditions: -1V to 2V DC sweep superimposed with a 10 mV a.c. signal of 1000 Hz; Buffer: 0.2 mM Tris buffer

Appendix figure 2.15 below shows the changes in the surface potential of the silicon nitride surface upon inhibition of phosphorylation of peptide-2 by PKC-α kinase.

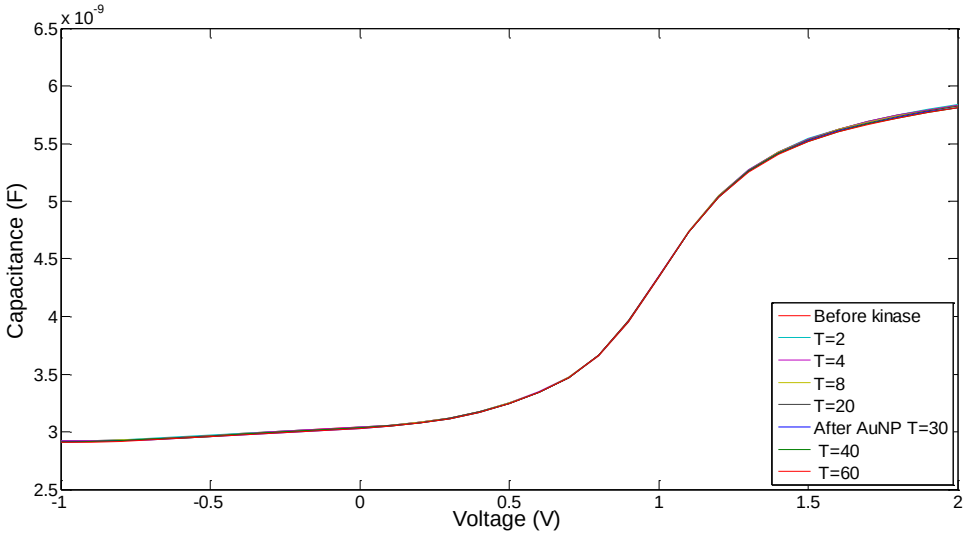

Appendix figure 2.14 pH variation on silicon nitride EIS sensor upon inhibition of thiophosphorylation of peptide-2 (without cysteine); Experimental conditions: -1V to 2V DC sweep superimposed with a 10 mV a.c. signal of 1000 Hz; Buffer: 0.2 mM Tris buffer

Appendix figure 2.16 below shows the changes in the surface potential of the gold based sensor upon thiophosphorylation of MBP by PKC-α kinase.

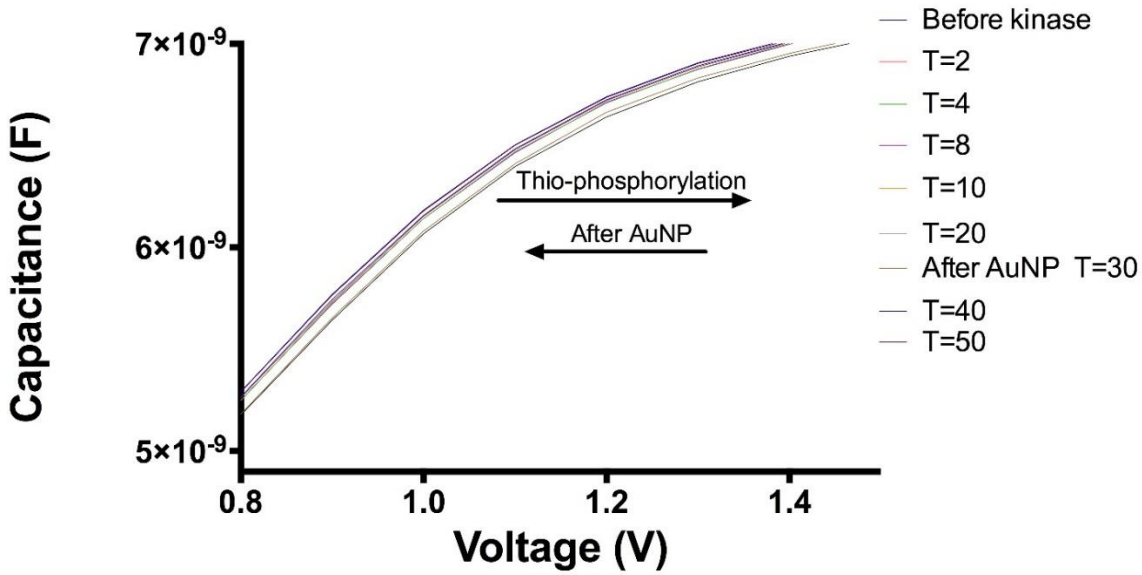

Appendix figure 2.15 Charge variation on gold MIS sensor upon thiophosphorylation of MBP; Experimental conditions: 0.5 V to 1V DC sweep superimposed with a 10 mV a.c. signal of 1000 Hz; Buffer: 0.2 mM Tris buffer

Appendix figure 2.17 below shows the changes in the surface potential of the gold based sensor upon phosphorylation of MBP by PKC-α kinase.

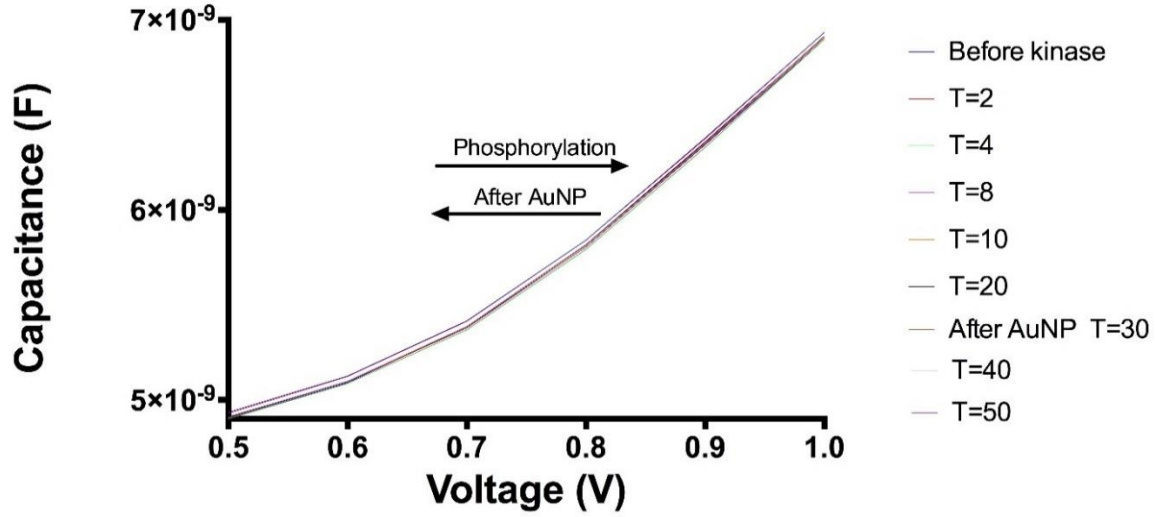

Appendix figure 2.16 Charge variation on gold MIS sensor upon phosphorylation of MBP; Experimental conditions: 0.5 V to 1V DC sweep superimposed with a 10 mV a.c. signal of 1000 Hz; Buffer: 0.2 mM Tris buffer

Appendix figure 2.18 below shows the changes in the surface potential of the gold based sensor upon inhibition of thiophosphorylation of MBP by PKC-α kinase.

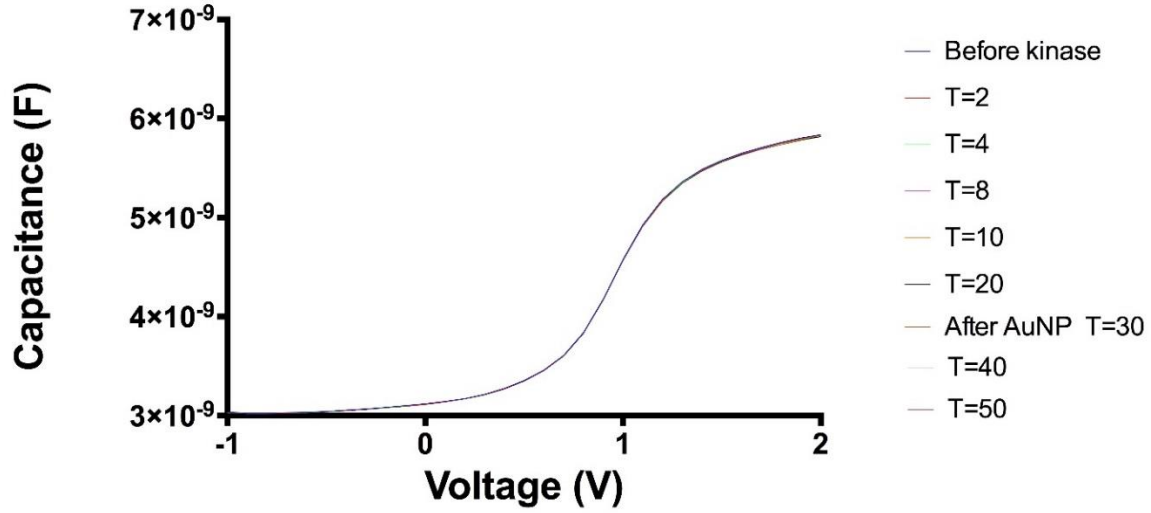

Appendix figure 2.17 Charge variation on gold MIS sensor upon inhibition of thiophosphorylation of MBP; Experimental conditions: -1V to 2V DC sweep superimposed with a 10 mV a.c. signal of 1000 Hz; Buffer: 0.2 mM Tris buffer

Appendix figure 2.19 below shows the changes in the surface potential of the gold based sensor upon thiophosphorylation of MBP with activating PKC-α kinase.

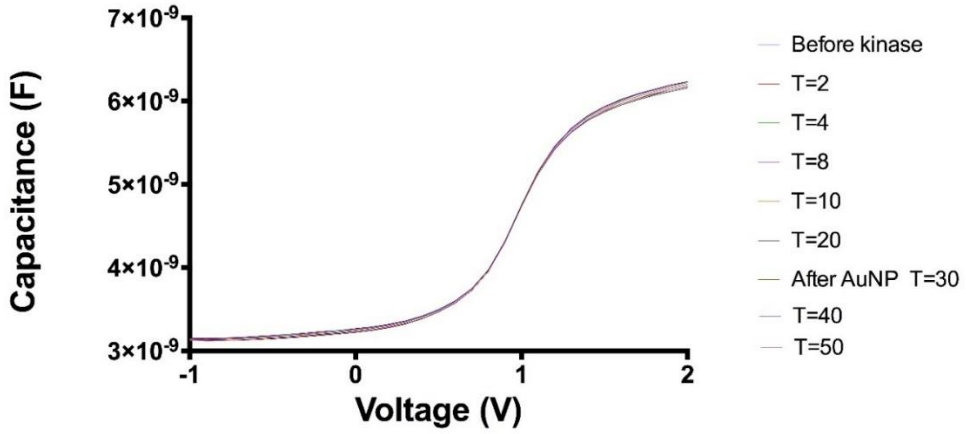

Appendix figure 2.18 Charge variations on gold MIS sensor after control of MBP phosphorylation in the absence of kinase activator; Experimental conditions: -1V to 2V DC sweep superimposed with a 10 mV a.c. signal of 1000 Hz; Buffer: 0.2 mM Tris buffer

Appendix figure 2.20 shows pH characterisation of 4 different silicon nitride films on Si wafers. The difference among them is in their composition and thickness of silicon nitride layer. Detailed characterisation of their structure and composition is in appendix 3.

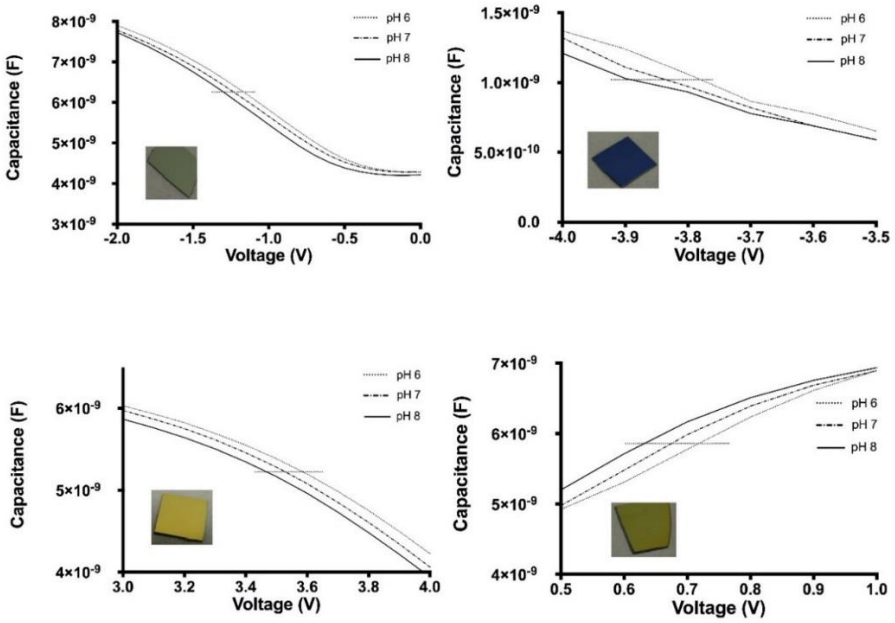

Appendix figure 2.19 pH characterisation of 4 different silicon nitride structures

Appendix 3

In this appendix electron microscopy data of 4 types if silicon nitride characterisation is presented. Discussion on properties of these wafer and how they influence biosensing is presented in chapter 4.

Wafer 1

Appendix figure 3.1 Physical appearance of wafer 1

The SEM image below shows the cross section of the wafer 1 with silicon nitride of around 110 nm thick.

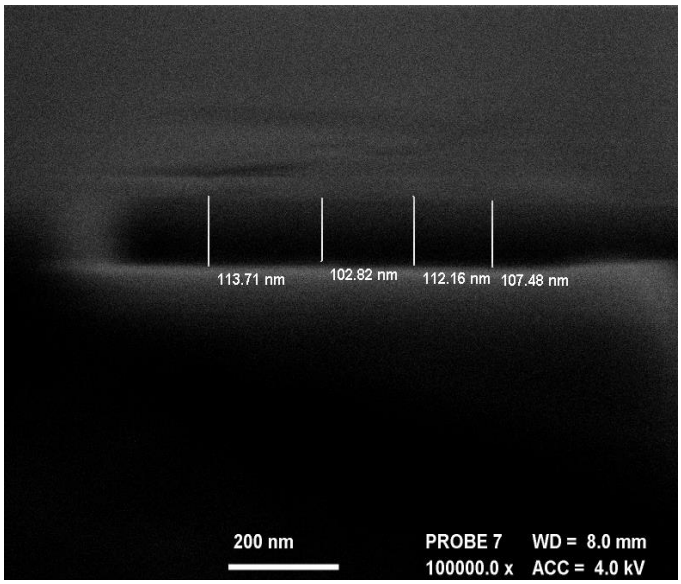

Appendix figure 3.2 SEM image: cross-section of wafer 1

The data in the figures Appendix figure 3.3 and 3.4 shows the EDX scan and amounts of SI, O and N in the scanned region.

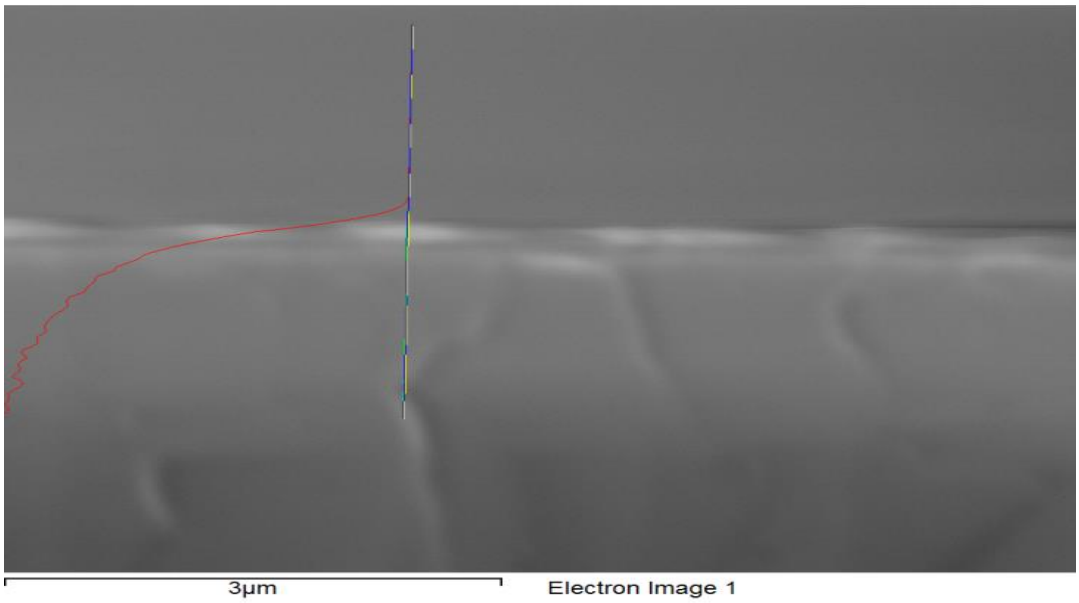

Appendix figure 3.3 EDX scan showing cross section of wafer 1

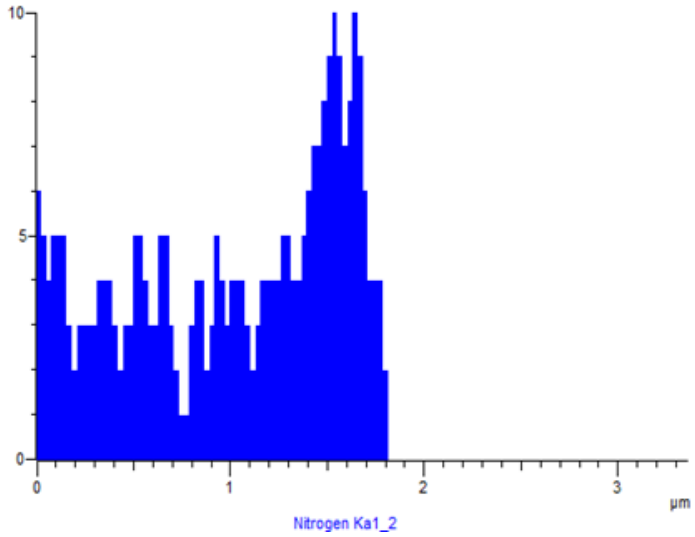

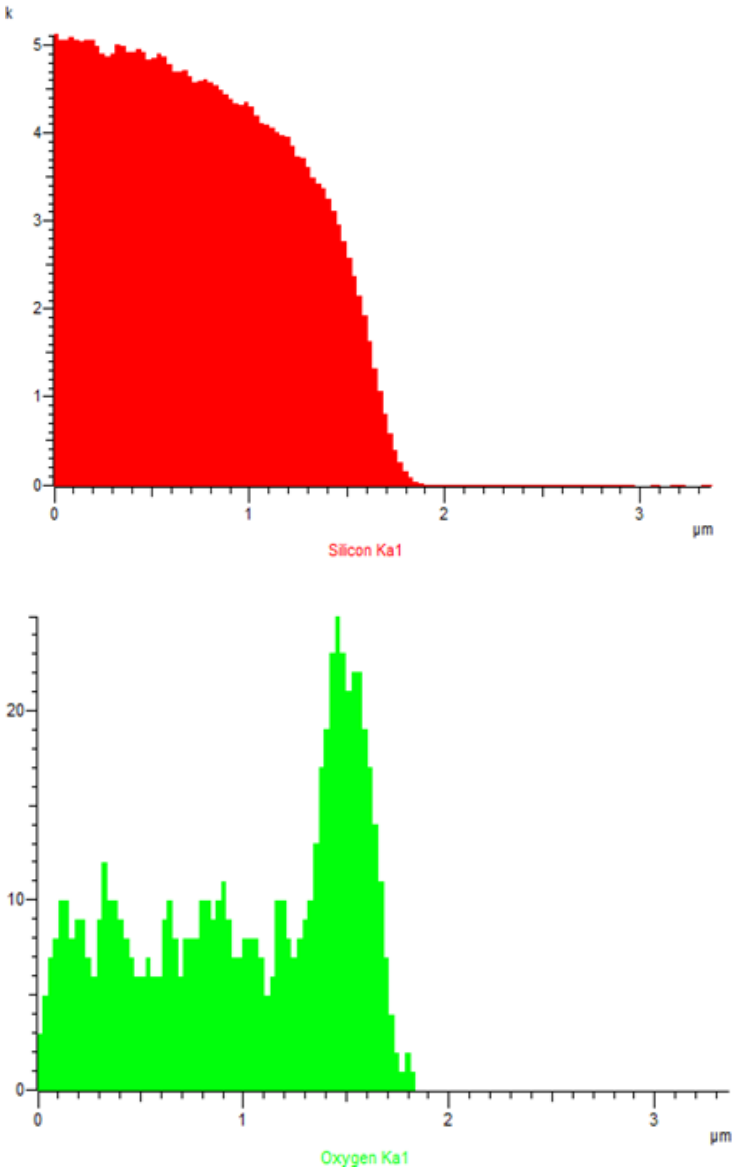

Appendix figure 3.4 Amounts of Si, O, N atoms in cross section of wafer 1

The figure below shows the XRD characterisation of the wafer 1 where strong peak is observed at 69.185^{o}

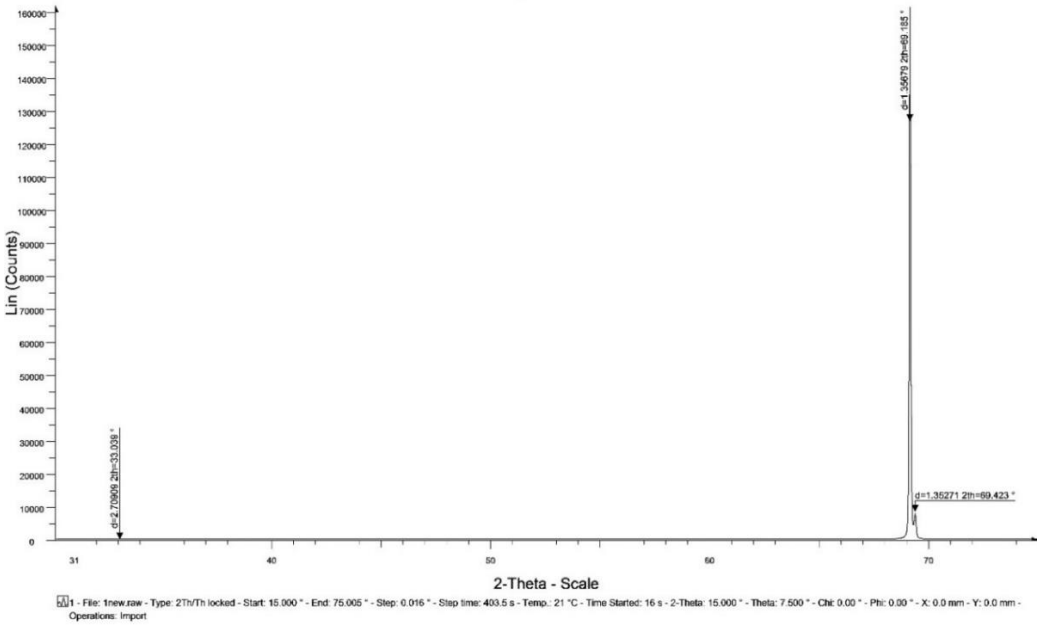

Appendix figure 3.5 XRD of wafer 1

Wafer 2

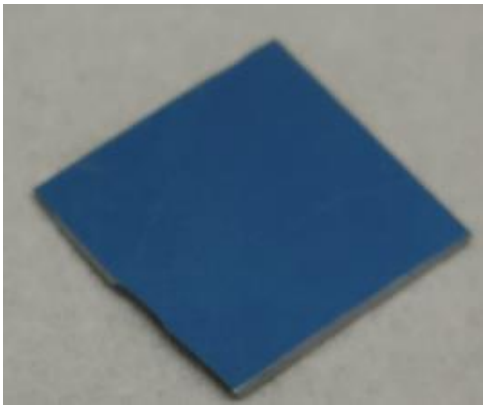

Appendix figure 3.6 Physical appearance of wafer 2

The SEM image below shows the cross section of the wafer 2 with silicon nitride of around 400 nm thick.

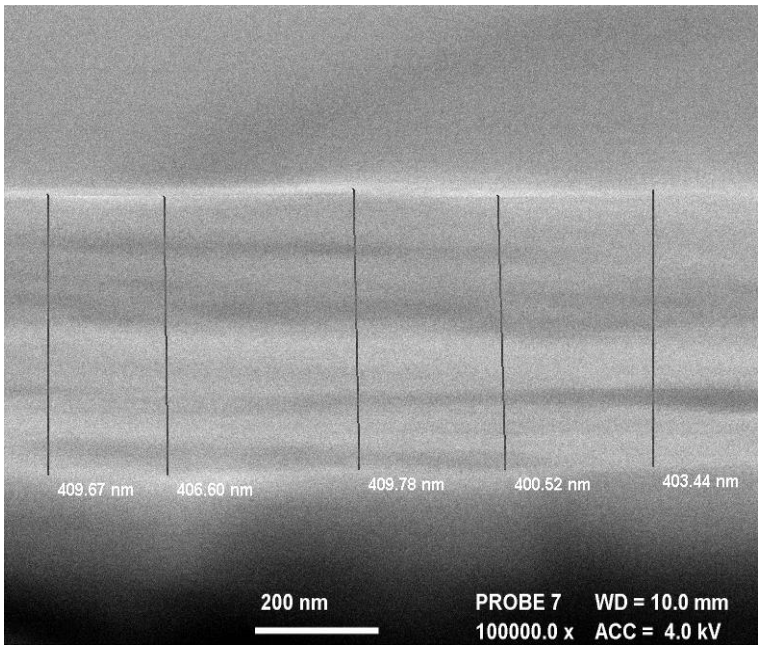

Appendix figure 3.7 SEM image: cross-section of wafer 2

The data in the figures Appendix figure 3.8 and 3.9 shows the EDX scan and amounts of SI, O and N in the scanned region.

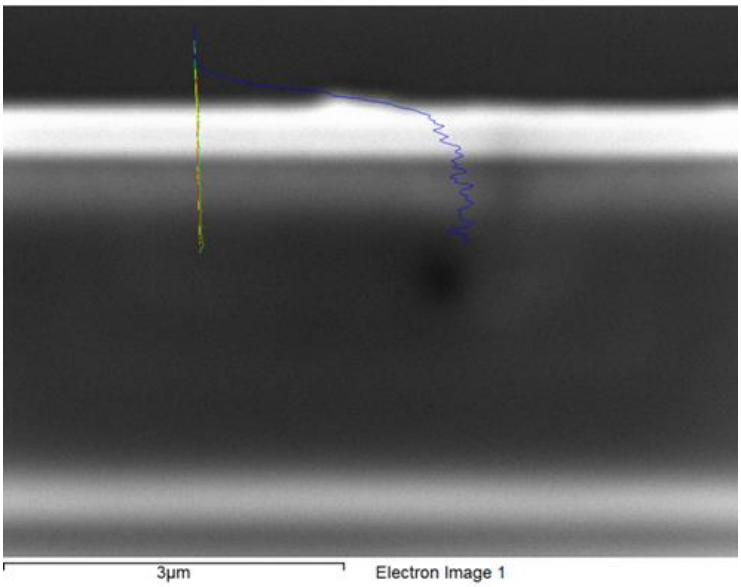

Appendix figure 3.8 EDX scan showing cross section of wafer 2

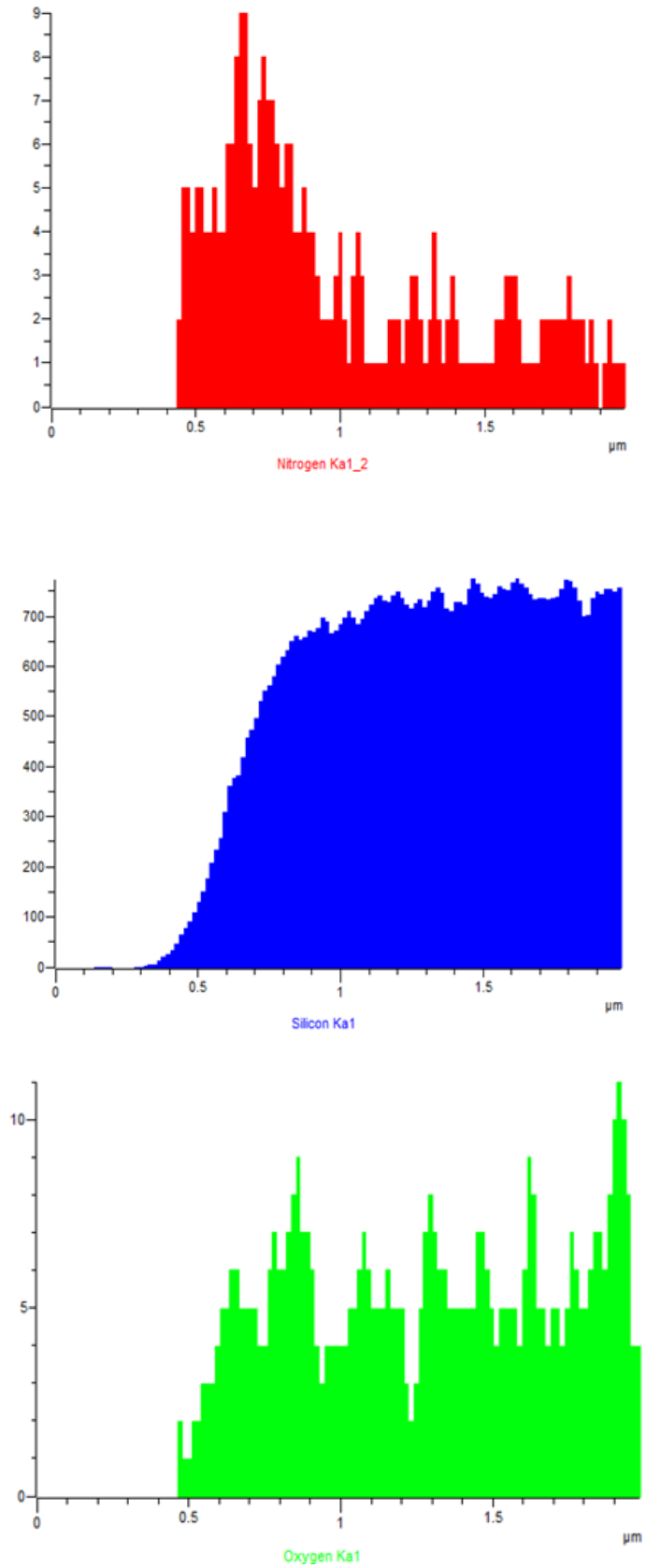

Appendix figure 3.9 Amounts of Si, O, N atoms in cross section of wafer 2

The figure below shows the XRD characterisation of the wafer 2 where a weak peak is observed at 68.845^{o}

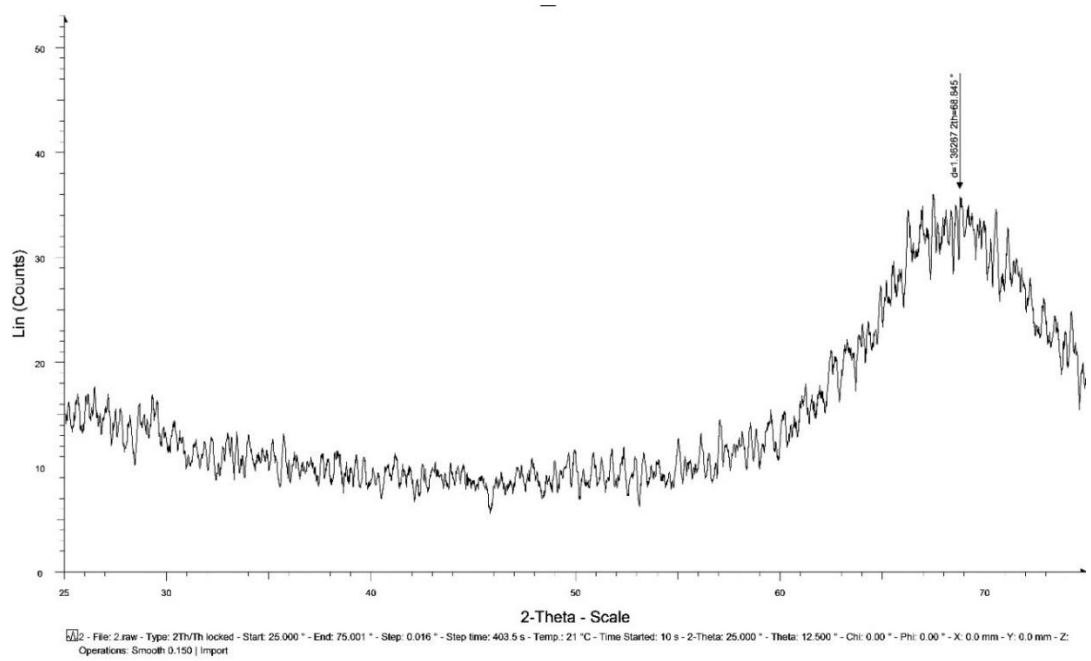

Appendix figure 3.10 XRD of wafer 2

Wafer 3

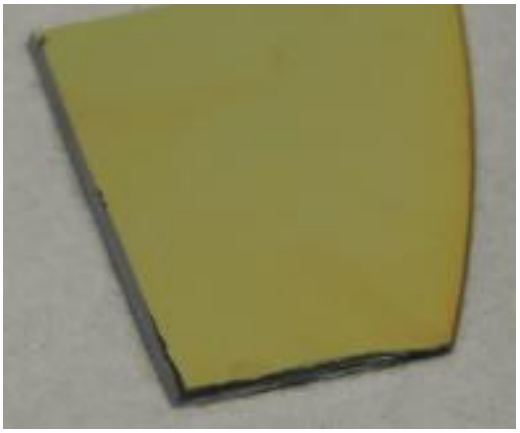

Appendix figure 3.11 Physical appearance of wafer 3

The SEM image below shows the cross section of the wafer 3 with silicon nitride of around 160 nm thick.

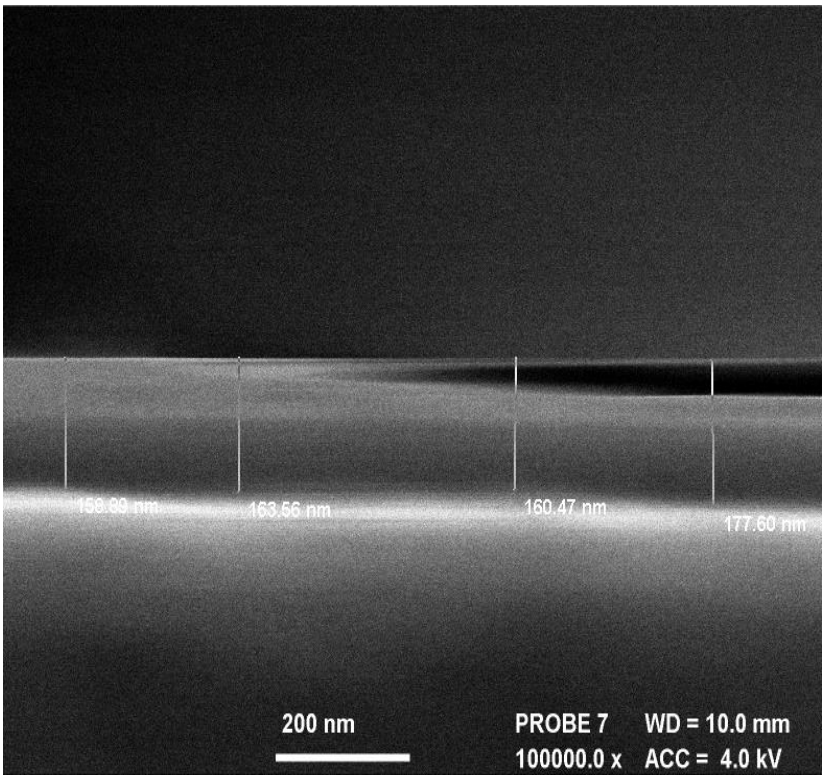

Appendix figure 3.12 SEM image: cross-section of wafer 3

The data in the figures Appendix figure 3.13 and 3.14 shows the EDX scan and amounts of SI, O and N in the scanned region.

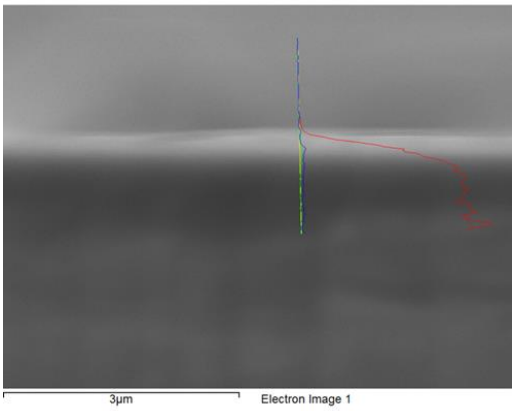

Appendix figure 3.13 EDX scan showing cross section of wafer 3

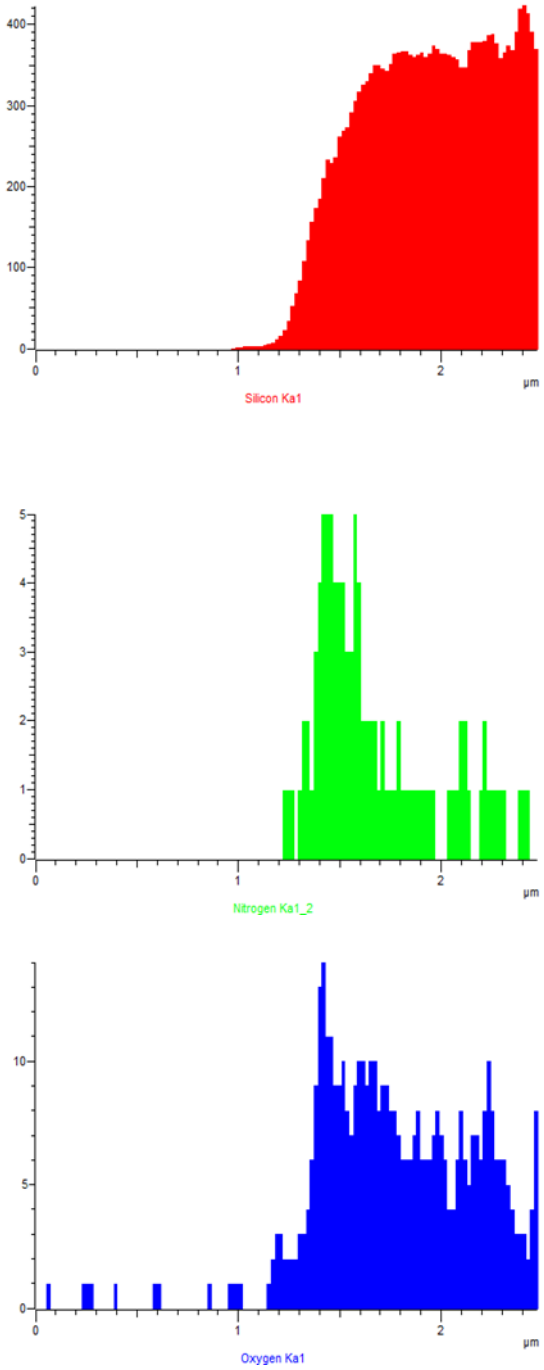

Appendix figure 3.14 Amounts of Si, O, N atoms in cross section of wafer 3

The figure below shows the XRD characterisation of the wafer 3 where a strong peak is observed at 69.188^{o}

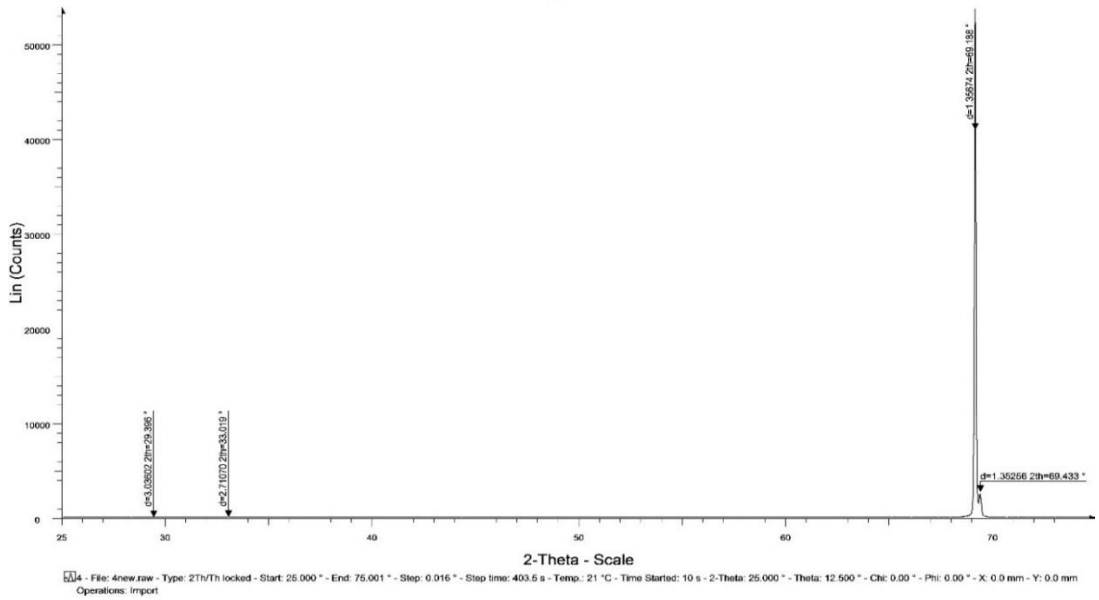

Appendix figure 3.15 XRD of wafer 3

Wafer 4

Appendix figure 3.16 Physical appearance of wafer 4

The SEM image below shows the cross section of the wafer 4 with silicon nitride of around 110 nm thick.

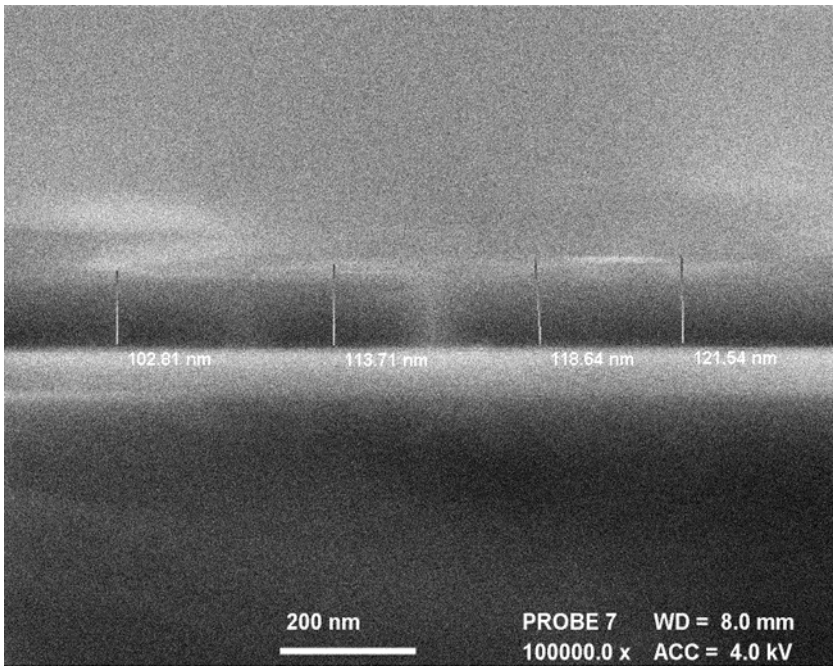

Appendix figure 3.17 SEM image: cross-section of wafer 4

The data in the figures Appendix figure 3.18 and 3.19 shows the EDX scan and amounts of SI, O and N in the scanned region.

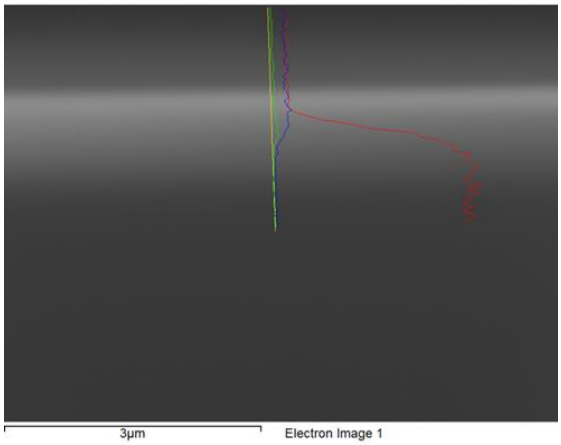

Appendix figure 3.18 EDX scan showing cross section of wafer 3

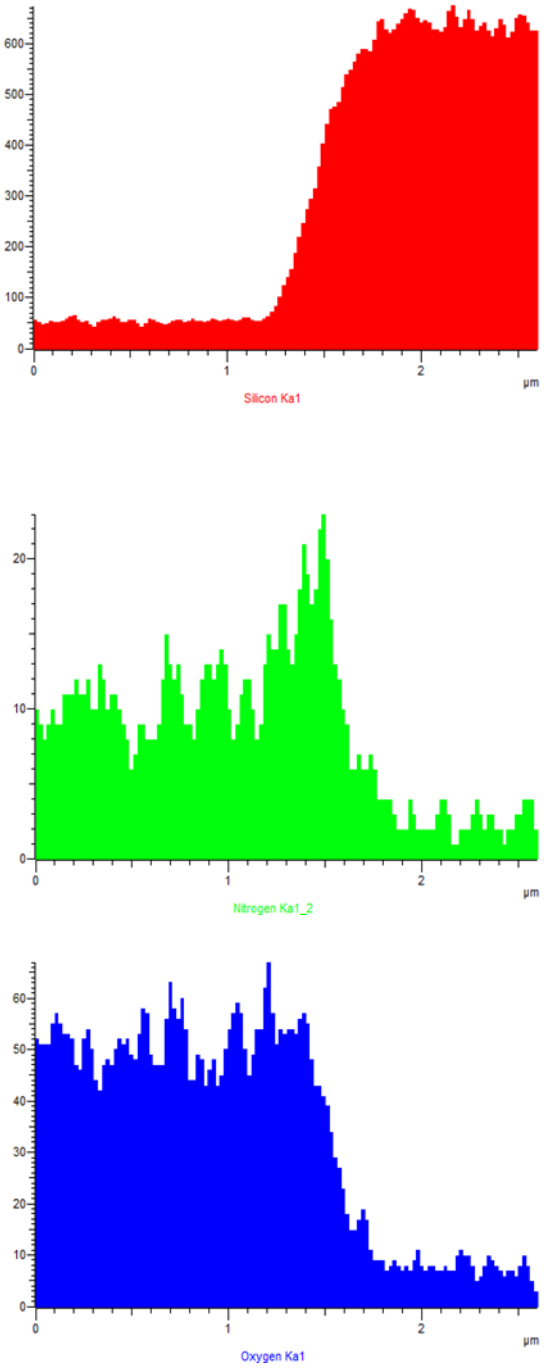

Appendix figure 3.19 Amounts of Si, O, N atoms in cross section of wafer 2

The figure below shows the XRD characterisation of the wafer 4 where a strong peak is observed at 69.188^{o}

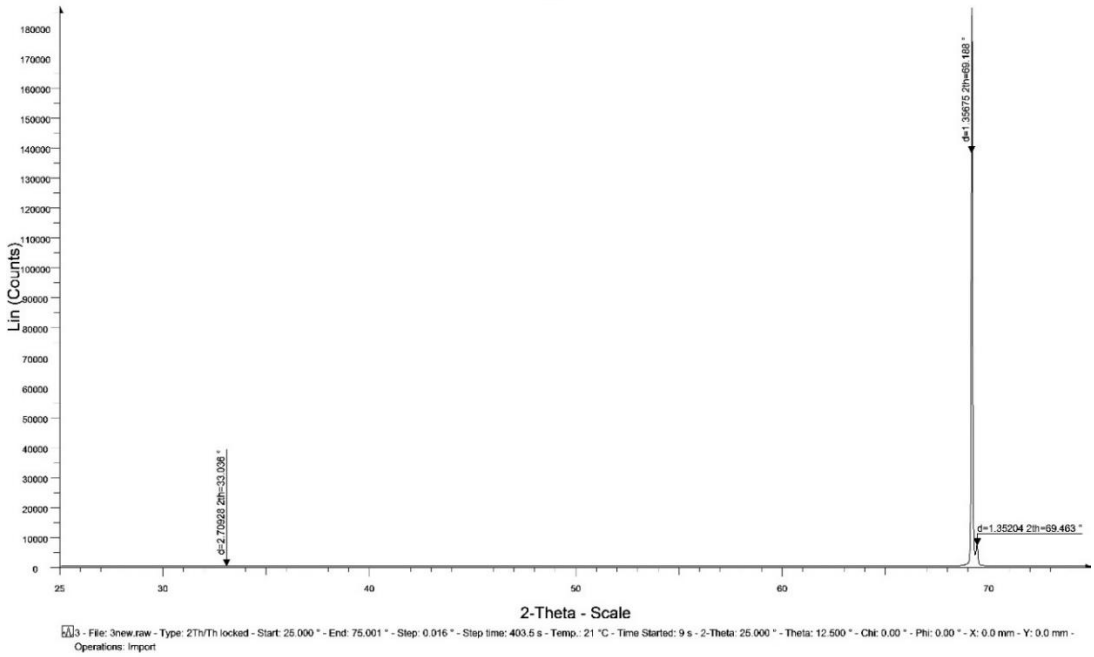

Appendix figure 3.20 XRD of wafer 4

FTIR characterization

The figure below shows the FTIR characterisation of all 4 wafers used in this study.

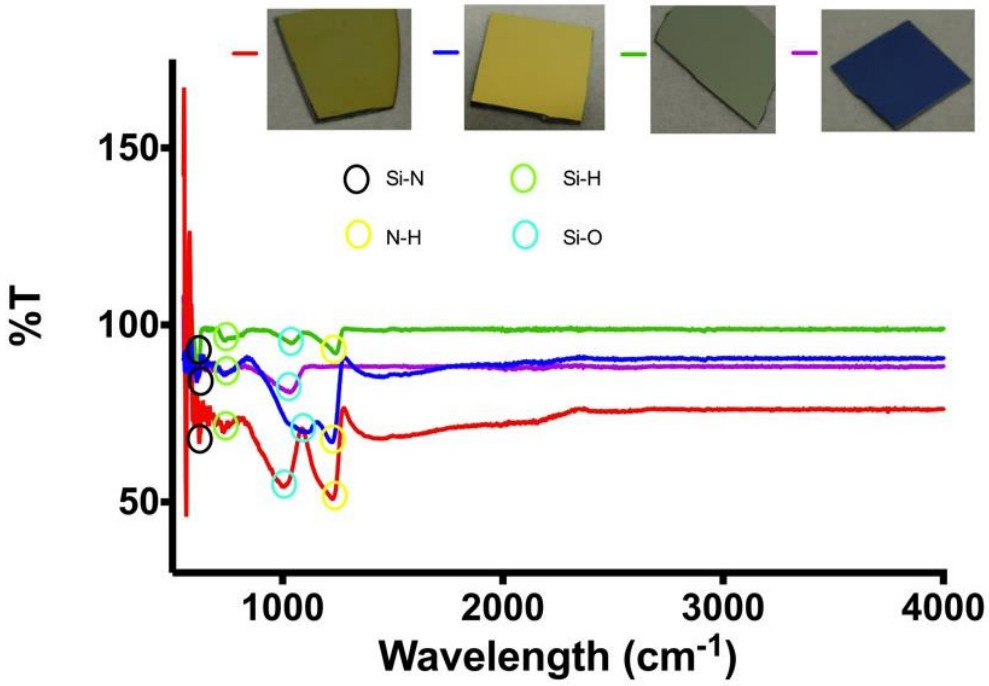

Appendix figure 3.21 FTIR of 4 wafers

Published Work

Publication related to the work described in this thesis:

A. Patent

1. **Nikhil Bhalla**, Mirella Di Lorenzo, Giordano Pula, Pedro Estrela, Materials and Methods for Analysing Phosphorylation of Target Protein. UK Patent application No. GB 1405954.7 filed 2 April 2014

B. Journal

Under preparation/submission

1. **Nikhil Bhalla** et al. Size and composition dependent localized surface plasmons and exciton coupling on pH sensitive silicon nitride nanofilms *In preparation*
2. **Nikhil Bhalla** et al. Review on kinase drug discovery technologies; *In preparation*

Published

1. **Nikhil Bhalla**, Nello Formisano, Anna Miodek, Aditya Jain, Mirella Di Lorenzo, Giordano Pula, Pedro Estrela; "Plasmonic ruler on field effect device for kinase drug discovery applications" *Biosensors and Bioelectronics*, 71,121-128. 2015
2. **Nikhil Bhalla**, Mirella Di Lorenzo, Giordano Pula, Pedro Estrela; "Protein phosphorylation detection using dual-mode field-effect devices and nanoplasmonic sensors" *Scientific Reports* 5, 8687. 2015
3. **Nikhil Bhalla**, Mirella Di Lorenzo, Giordano Pula, Pedro Estrela; "Protein phosphorylation analysis based on proton release detection: potential tools for drug discovery" *Biosensors and Bioelectronics,* 54, 109-114. 2014
4. Jules L Hammond, **Nikhil Bhalla**, Sarah D. Rafiee, Pedro Estrela; " Localized Surface Plasmon Resonance as a Biosensing Platform for Developing Countries" *Biosensors* ,4, no. 2: 172-188.2014 (Review paper on LSPR)

C. Conference Abstracts/Proceedings

1. **Nikhil Bhalla**, Shrey Pathak, CR Bowen, JT Taylor, M Di Lorenzo, G Pula, P Estrela ' Field-effect devices for kinase drug discovery' 4th *International Conference on Bio-Sensing Technologies*, Lisbon, Portugal, May 2015
2. **Nikhil Bhalla**, Nello Formisano, Anna Miodek, Mirella Di Lorenzo, Giordano Pula, Pedro Estrela 'Integrated nanoplasmonic and field-effect devices for kinase drug discovery' *2nd International Conference on Label-Free Technologies*, Boston, USA, March 2015
3. **Nikhil Bhalla**, Mirella Di Lorenzo, Giordano Pula, Pedro Estrela, Novel tools for protein phosphorylation analysis based on proton release detection, *World Congress on Biosensors* , Melbourne, Australia, May 2014

Other published work:

A. Journal

Under preparation/submission

1. Nello Formisano, **Nikhil Bhalla**, Mel Heeran, Juana Reyes Martinez, Amrita Sarkar, Maisem Laabei, Pawan Jolly, Chris R. Bowen, John T. Taylor, Sabine Flitsch, Pedro Estrela; 'Inexpensive and fast pathogenic bacteria screening using field-effect transistors' *In preparation*

Published

2. Anna Miodek, Edward MM. Regan, **Nikhil Bhalla**, Neal A.E. Hopkins, Sarah A. Goodchild, Pedro Estrela; "Optimization of anti-fouling ternary SAM layers for impedance-based aptasensors" *In Press*
3. *Nello Formisano, ***Nikhil Bhalla***, *Caleb Wong, Mirella Di Lorenzo, Giordano Pula, Pedro Estrela; "Multimodal electrochemical and nanoplasmonic biosensors using ferrocene crowned nanoparticles for kinase drug discovery applications" *Electrochemistry Communication* 57,70-73. 2015 (*Authors equally contributed to the work)
4. Nello Formisano, Pawan Jolly, **Nikhil Bhalla**, Mary Cromhout, Shane Flanagan, Ronen Fogel, Janice L Limson, Pedro Estrela; "Optimisation of an Electrochemical Impedance Spectroscopy aptasensor by exploiting Quartz

Crystal Microbalance with Dissipation Signals" *Sensors and Actuators B: Chemical* 220, 369-375. 2015

5. **Nikhil Bhalla**; Chung, Danny W.Y.; Chang, Yaw-Jen; Uy, Kimberly J.S.; Ye, Yi Y.; Chin, Ting-Yu; Yang, Hao C.; Pijanowska, Dorota G. "Microfluidic Platform for Enzyme-Linked and Magnetic Particle-Based Immunoassay." *Micromachines* 4, no. 2: 257-271. 2013

B. <u>Conference Abstracts/Proceedings</u>

1. Nello Formisano, **Nikhil Bhalla**, Caleb Wong, Pedro Estrela' Multi-mode electrochemical biosensing for kinase drug discovery applications using ferrocene crowned nanoparticles' 4th *International Conference on Bio-Sensing Technologies*, Lisbon, Portugal, May 2015
2. P Jolly, N Formisano, SD Rafiee, **Nikhil Bhalla,** A Miodek, R Dondi, DK Yang, LC Chen, P Kasak, J Tkac, MD Lloyd, I Eggleston, P Estrela, DNA aptamer-based approaches for detection of multiple prostate cancer biomarker *22nd Meeting of the EAU Section of Urological Research ESUR*, Glasgow, UK, October 2014
3. **Nikhil Bhalla,** Wen Yaw Danny Chung, Kerwin Wang, Teddy Lesmana, Pedro Estrela, Electrowetting enabled magnetic particle immunoassay with on-chip magnetic washing, *Proceedings of IEEE-SENSORS* , Baltimore, USA, November 2013
4. Teddy Lesmana, Wen-Yaw Chung, Nguyen-Tan Nhut Quang, **Nikhil Bhalla**, A Linear Current to Frequency Converter for Amperometric Glucose Sensing System, *BMES International Symposium of Biomedical Engineering*, Taiwan, November 2012
5. Danny Wen Yaw Chung, **Nikhil Bhalla**, Hsi-Wen Li, Yi Ying Ye, Hao Chun Yang, Dorota G. Pijanowska Hall's Effect Based Sensing Mechanism for Nano Super Paramagnetic Particle-Protein Complex Structure, *IEEE-Asia Pacific Conference on Transducers APCOT*, Nanjing, China, July 2012
6. **Nikhil Bhalla**, Danny Wen Yaw Chung, Kimberly Jane S. Uy, Dorota G. Pijanowska Nitrocellulose based Microfluidic Platform for Immunoassay, *IEEE-Asia Pacific Conference on Transducers APCOT*, Nanjing, China, July 2012

7. **Nikhil Bhalla**, Sheng Shian Li, Danny Wen-Yaw Chung Finite Element Analysis of MEMS Based Piezoresistive Accelerometer Designs. *IEEE-International Conference on Semiconductor CAS*, Romania, October 2011
8. **Nikhil Bhalla**, Sheng Shian Li, Danny Wen-Yaw Chung Multi- Domain analysis of MEMS Based Si structures, *COMSOL-International Conference*, USA, October 2011
9. **Nikhil Bhalla**, Sheng Shian Li, Danny Wen-Yaw Chung Simulations of MEMS based Piezoresistive Accelerometer Design in COMSOL, *COMSOL-International Conference* , USA, October 2011
10. **Nikhil Bhalla**, Danny Wen-Yaw Chung, Sundaram Sumaninathan Optical Detection of Cancer and Development of Feedback Assisted Surgical Scalpel, *BMES International Symposium of Biomedical Engineering*, Kaohsiung, Taiwan, December 2010-. (Awarded for one of best papers in the symposium)